Expected Repository Environments in Granite: Thermal Environment

Technical Report

October 1984

John D. Osnes, Glenda K. Coates,
Keith B. DeJong, Marc C. Loken, Ralph A. Wagner
of
RE/SPEC Inc.

prepared for

ACKNOWLEDGMENTS

ABSTRACT

This report was prepared for the Reference Repository Conditions - Interface Working Group and will be used to formulate a standardized description of repository conditions for use by the Civilian Radioactive Waste Management Program. A baseline repository in granite is defined and three waste types are considered: unreprocessed spent fuel, commercial high-level waste, and defense high-level waste. Three different scales of repository environment are described - the very-near field (near the waste canister), the near field (the room and pillar), and the far field (the entire repository and surroundings). Information was compiled from the literature and, in addition, a number of calculations were performed. The major emphasis is on describing the thermal environment although the ground-water flow and chemical and radiation environments are also described.

Preceding page blank

TABLE OF CONTENTS

Preceding page blank

TABLE OF CONTENTS

(Continued)

TABLE OF CONTENTS
(Concluded)

LIST OF FIGURES

LIST OF FIGURES

(Continued)

LIST OF FIGURES
(Continued)

LIST OF FIGURES
(Continued)

LIST OF FIGURES

(Continued)

LIST OF FIGURES

(Continued)

LIST OF FIGURES

(Concluded)

LIST OF TABLES

LIST OF TABLES
(Concluded)

EXECUTIVE SUMMARY

The objective of this report is to describe the environment expected in and around a repository located in granitic rock. The major emphasis is on describing the thermal environment, although the ground-water flow and chemical and radiation environments are also described. The expected reposi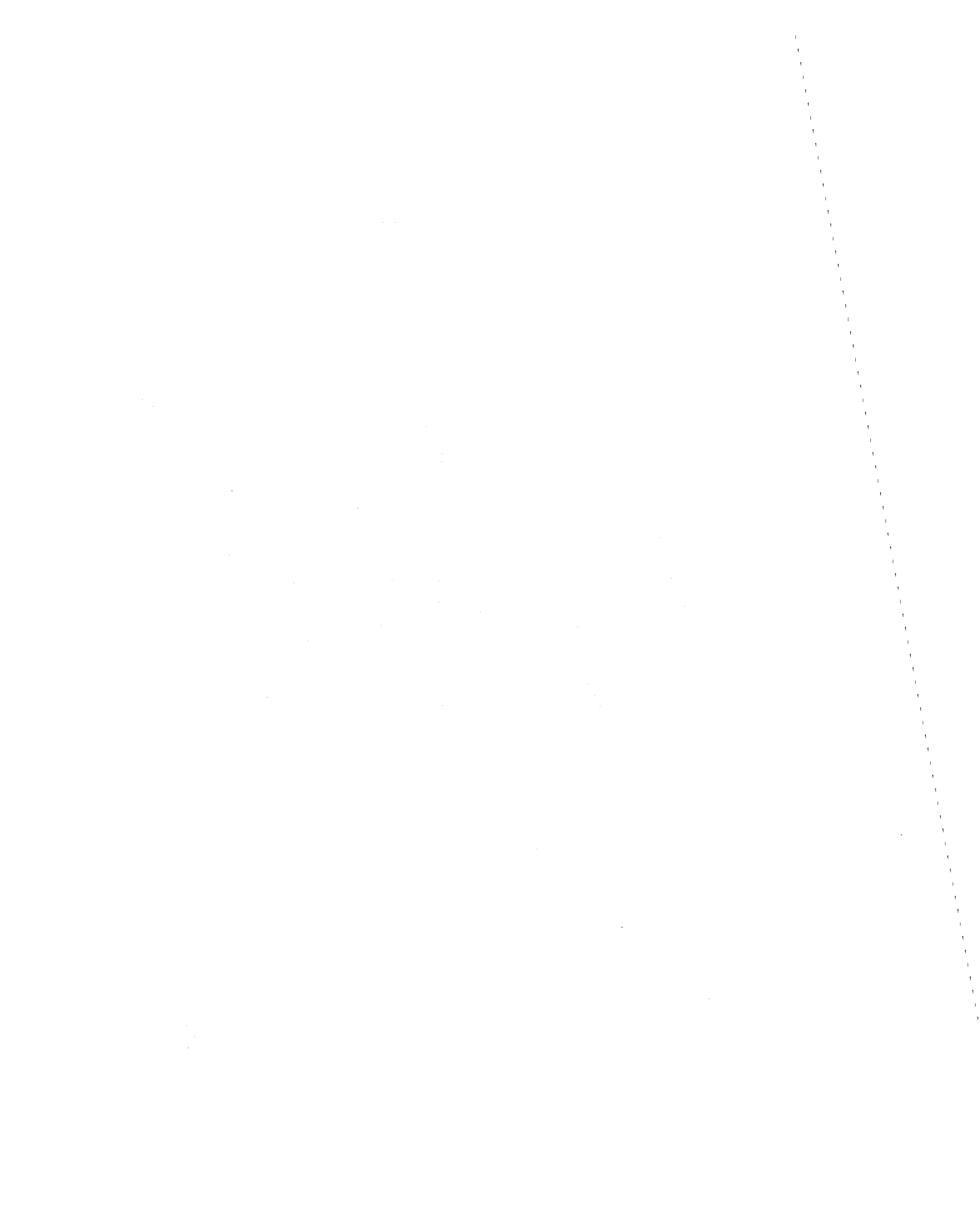tory environment was defined by reviewing available literature and by performing supplementary numerical analyses in those areas where information was not available. Modeling was generally carried out on three scales: the very-near field (near the waste canister), the near field (the storage room and pillar), and the far field (the entire repository and a large portion of the surrounding geologic formation). Three types of nuclear waste were considered: unreprocessed spent fuel (SF), commercial high-level waste (CHLW), and defense high-level waste (DHLW).

An extensive literature review was performed to determine the thermal, hydrogeological, and mechanical properties typical of granite. Table ES-1 lists the thermal and hydrogeological properties assumed for the generic granite in the numerical simulations performed in this study. Note that three values of thermal conductivity were assumed to assess the sensitivity of the thermal environment to this parameter. The properties assumed for the three waste types and for the other materials in the models are also listed in Table ES-1.

The repository design used in this report is based on a synthesis of conceptual and generic design studies which have been carried out throughout the world to date. The reference repository consists of a series of long, parallel tunnels on one horizontal level at a depth of 1,000 m, with the waste canisters emplaced into vertical drill holes in the tunnel floors. The rooms are spaced 30 m center-to-center and are 7.5 m wide by 7.0 m high, yielding an extraction ratio of 25 percent. One-, two-, and four-row layouts of canisters were modeled in this study, but the thermal response in the very-near-field and near-field regions were nearly identical for all three canister layouts. The diameter of the vertical drill hole is sufficiently large to allow a 0.1-m-wide annulus between the waste canister and the rock, and the drill hole is approximately 2.0 m deeper than the length of the canister. The annulus and the drill hole above the waste canister is backfilled with crushed granite immediately after waste emplacement.

Table ES-1. Thermal and Hydrogeological Properties Assumed for Materials in Thermal Environments Study

Material	Thermal Conductivity (W/m-K)	Specific Heat (J/kg-K)	Density (kg/m^3)	Porosity (%)	Permeability (m^2)
Granite	1.75 2.52 3.29	809.3	2650.	0.01	1.02 x 10^{-15}
Backfill (Crushed Granite)	0.266	809.3	1828.	31.0	N.A.[a]
Emplacement Room Air	75.[b]	1003.	1.3	N.A.[a]	N.A.[a]
Nuclear Waste SF[c]	1.21	837.4	2995.	N.A.[a]	N.A.[a]
CHLW	1.21	837.4	2995.	N.A.[a]	N.A.[a]
DHLW	1.35	1047.	2800.	N.A.[a]	N.A.[a]

(a) N.A. - Not Applicable.

(b) Internal details of SF canister not modeled. Internal temperatures calculated using predictions based on McCann [1980].

(c) Equivalent conductivity based on combined conduction-radiation heat transfer across room.

In plan view, the repository is square in shape with sides 1.87 km in length. The shaft pillar is located in the center of the repository in an inactive area containing maintenance shops and other facilities. The inactive area is 700 m square.

The operational sequence assumed for the reference repository is as follows:

(1) The waste is emplaced over a 20-year period;

(2) A five year "monitoring" period follows during which the repository is kept open so that the wastes can potentially be removed;

(3) The repository is "blast-cooled" for 100 days; and

(4) The repository is backfilled with crushed granite and decommissioned.

It is assumed that each room is filled with waste instantaneously. The entire repository is filled sequentially from the outermost edges in toward the shaft pillar over the 20-year emplacement period.

Areal thermal loadings of 20, 25, and 25 W/m^2 were considered for SF, CHLW, and DHLW repositories, respectively. The initial canister powers were 550 W for SF, 2100 W for CHLW, and 578.5 W for DHLW. It was necessary to reduce the initial canister power of CHLW to 700 W to obtain acceptable temperatures in and near the canister. With this change, the peak temperature rises predicted in the very-near field were similar for all three waste types and were approximately 180°C at the canister skin for a granite thermal conductivity of 2.52 W/m-K. These results were nearly independent of the canister layout considered. The peak temperatures consistently occurred at later times in the SF repository than in the CHLW and the DHLW repositories and these temperatures were sustained over a longer period of time. The higher concentration of long-lived isotopes in SF is responsible for this difference. Even though the areal thermal loading of SF was only 80 percent of CHLW, the peak temperature rise predicted on the repository midplane in the far-field models was approximately 93°C for both waste types. The effect of convective heat transfer by regional and thermally induced ground-water flow on the predicted far-field temperatures was negligible.

1 INTRODUCTION

The main objective of the U.S. Department of Energy's (DOE) Civilian Radioactive Waste Management (CRWM) Program is the safe disposal of commercially generated nuclear wastes. The CRWM Program is focusing on mined geologic disposal in deep underground formations. This report forms part of the Rock Mechanics Program which is one component of the overall CRWM Program [Neff, 1980]. To ensure proper coordination and communication amongst the many organizations which are involved, a number of Interface Control Boards (ICB) have been established. The work presented here was done under the guidance of the Reference Repository Conditions - Interface Working Group (RRC-IWG) which is an ad hoc Working Group established by the Isolation Interface Control Board.

The objective of this report is to describe the environment expected in and around a repository located in granitic rock. The report will be used by the RRC-IWG to formulate a standardized description of repository conditions which will serve as a guide for scientists conducting material performance tests; engineers preparing the design of repositories; scientists and engineers developing waste forms; and the technically conservative conditions to be used as a basis for DOE application for licenses.

A baseline repository design has been developed for use in this report based on existing studies. In the present design, storage rooms are mined in the granite 1,000 m below the surface of the earth, and cylindrical waste packages containing high-level waste in a solid matrix or spent fuel elements are emplaced in vertical holes in the floor of the storage rooms. The emplacement holes are backfilled immediately and the storage rooms are backfilled and sealed at some later time. Heat generated by the nuclear waste flows from the waste, through the waste package and backfill, through the surrounding geologic formation, and up to the surface of the earth, where it is eventually dissipated. The increased temperature associated with this heat flow is the main mechanism influencing the "expected environment" described in this report. A future report will deal with the mechanical effects associated with a repository.

The expected repository environment is described in terms of transient temperature fields and perturbations of ground-water flow. In addition, the granite and ground-water chemistry and the radiation fields are described. The rock properties of a generic granite have been assumed in the calculations and

three types of nuclear waste are considered: commercial high-level waste (CHLW), commercial unreprocessed spent fuel (SF), and defense high-level waste (DHLW).

The expected repository environments were defined by reviewing available literature and by performing supplementary numerical analyses in those areas where information was not available. A specific area which required additional analysis was the modeling of the ground-water flow, including thermally induced perturbations. In addition, parametric sensitivity analyses were performed in a number of areas where uncertainty existed. Modeling was generally carried out on three scales: the very-near field (near the waste canister), the near field (the storage room and pillar), and the far field (the entire repository and a large portion of the surrounding geologic formation).

Areal thermal loadings of 20, 25, and 25 W/m^2 were considered for SF, CHLW, and DHLW repositories, respectively, in granite. It was necessary to reduce the initial canister power of CHLW from 2,100 W to 700 W to obtain acceptable temperatures in and near the canister. With this change, the peak temperature rises predicted in the very-near field were similar for all three waste types and were approximately 180°C at the canister skin for a granite thermal conductivity of 2.52 W/m-K. These results were nearly independent of the canister layout considered. The peak temperatures consistently occurred at later times in the SF repository than in the CHLW and the DHLW repositories and these temperatures were sustained over a longer period of time. The higher concentration of long-lived isotopes in SF is responsible for this difference. Even though the areal thermal loading of SF was only 80 percent of CHLW, the peak temperature rise predicted on the repository midplane in the far-field models was approximately 93°C for both waste types. The effect of convective heat transfer by regional and thermally induced ground-water flow on the predicted far-field temperatures was negligible.

In the following section, the thermal, hydrogeological, and mechanical properties of granite are reviewed based on an extensive literature survey. In Section 3, the characteristics of a nuclear waste repository in granite are discussed and reference repositories for SF, CHLW, and DHLW are defined. The thermal response in the very-near field, near field, and far field is analyzed in Section 4. Section 5 deals with the chemical and radiation environments expected in nuclear waste repositories in granite. The results of this study are summarized in Section 6.

2 MATERIAL PROPERTIES

A literature survey was conducted to determine the properties of granitic rock and the in situ conditions in a granitic rock mass. A compilation of the thermal, mechanical, and hydrogeological properties collected from the literature appears in Appendix A. The following sections discuss each condition or property separately and identify the value or range of values used in this study. Data which seemed unreliable because of test procedures or lack of detail concerning their procurement were omitted.

2.1 ROCK MASS PROPERTIES

Granite is a hard, crystalline, silicate rock originating at great depths and at high temperature and pressure. Granite was selected for consideration as a possible host rock for a repository because of its occurrence in large, relatively uniform masses in the earth's crust, high mechanical strength, chemical stability, and small economic value. The granitic rock mass will serve as a natural barrier around the canister, retarding or preventing radioactive nuclides from reaching the biosphere via the ground water and providing strong mechanical isolation.

Most of the data found in the literature are from laboratory tests on intact rock. Intact rock refers to samples which do not contain the large structural features of the in situ rock mass such as joints and major discontinuities. Data from in situ rock tests may vary appreciably from data obtained from laboratory rock tests. One example of this is Young's modulus. Tests show that the modulus of the rock mass is always lower than the modulus determined from intact rock samples. Barton [1973] states that small laboratory samples (a few centimeters) may overestimate the actual rock strength of the in situ rock, but that this scale effect is less at a depth of several kilometers because cracks tend to close at depth.

The importance of in situ testing can be seen from the above discussion, and tests of this nature are recommended for the evaluation of potential repository sites.

2.1.1 In Situ Temperature

The in situ temperature at repository depth in granitic rock depends on the mean annual surface temperature and the rate of increase of temperature with depth (geothermal gradient), factors which vary with geographic location. The geothermal gradient in the Canadian Shield has been well studied [Cermak and Jessop, 1971; Sass and Lachenbruch, 1971] and generally lies between 10 and 15°C/km. The Central Stable Region and Sierra Nevada heat flow provinces also have geothermal gradients in this range [Roy et al, 1968]. The New England and the Basin and Range provinces have higher gradients with approximate ranges of 15-25°C/km and 25-35°C/km, respectively [Roy et al, 1968]. In this study an intermediate geothermal gradient of 20°C/km was assumed.

2.1.2 In Situ Stress

Measurements indicate that the in situ vertical stress is approximately equal to the weight of the overburden [Herget, 1973]. The horizontal in situ stress is frequently greater than the in situ vertical stress, probably because unloading by erosion reduces the vertical stress without relieving the horizontal stress. The relationship between the horizontal and the vertical in situ stresses is often expressed as the coefficient of lateral earth pressure, K_o, which is defined by the following equation:

$$K_o = \frac{\sigma_h}{\sigma_v} \tag{2-1}$$

where:

σ_h = in situ horizontal stress

σ_v = in situ vertical stress.

Based on in situ stress measurements from throughout the world, Brown and Hoek [1978] and Hast [1965] suggest that K_o be expressed as a function of depth in the following functional form:

$$K_0 = \frac{a}{z} + b \qquad\qquad (2\text{-}2)$$

where:

z = depth

a, b = constants.

Data reported by Herget [1973] for in situ vertical and horizontal stress are consistent with this functional form for K_0 [Osnes and Brandshaug, 1980]. Figure 2-1 shows the K_0 functions calculated by Brown and Hoek [1978] and by Hast [1965]. The K_0 function derived by Osnes and Brandshaug [1980] based on Herget's data for in situ stresses in Canadian Shield granite is also shown in this figure and is intermediate between the minimum values of Hast and the maximum values of Brown and Hoek.

The determination of in situ stress in rock is complicated by topography and tectonic stress. In areas with rugged terrain, measurements taken close to the surface are affected by local topography [Ranalli and Chandler, 1975]. A report by Hooker et al [1972] shows that additional stress due to mountainous topography is calculated to be 11.8 percent of the stress due to the overburden. Corrections for topographic factors are site specific, and no general correction exists to determine the influence of topography on in situ stress. Therefore, in situ stress determinations are best made in areas far from the surface and with relatively low topographical relief.

Tectonic stresses are due to either current forces in the earth's crust (active) or tectonic events (passive) that have stored elastic strain in the rock during a past episode of deformation [Ranalli and Chandler, 1975]. In rocks displaying excessive folding and uplift, residual stresses can create horizontal stresses that exceed the overburden pressure. Jaeger and Cook [1969] present several methods of calculating tectonic stress in simple geologic situations.

2.1.3 Discontinuities

Granites are massive rock formations characterized by primary and secondary structural features. These features can exert profound influences on a body of

COEFFICIENT OF LATERAL EARTH PRESSURE (K$_o$)
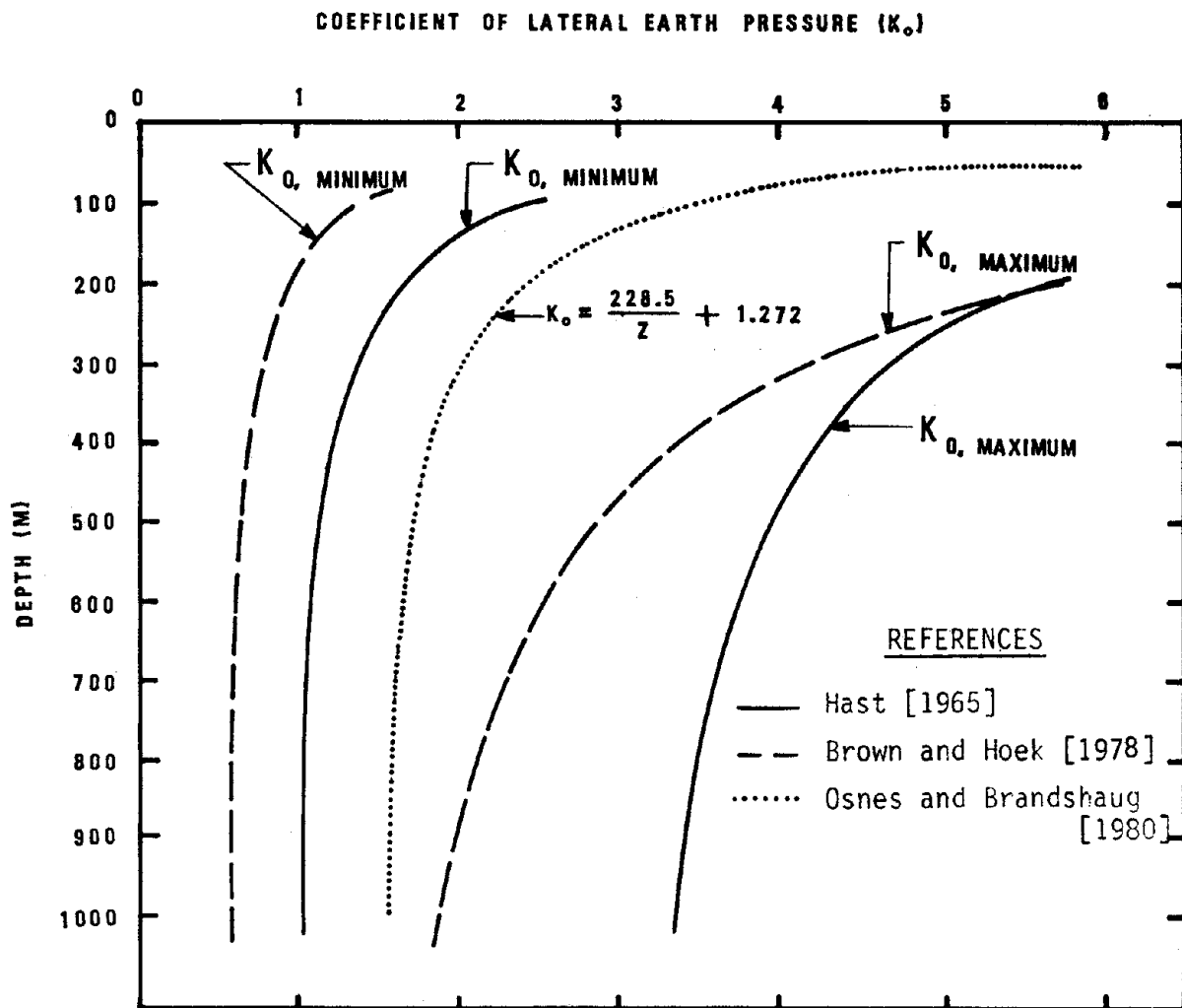
Figure 2-1.   Ratio Between Horizontal and Vertical In Situ Stress as a
              Function of Depth.

rock. In this study, a general description of the rock mass structure of a granitic rock located at depth is given.

Features of a rock mass which were developed at the time the rock originated are called primary structures. The most fundamental primary features of an igneous granite are texture and mineral content. Although primary features are fundamental in identifying the origin of granitic rock masses, it is the secondary features which are important in the study of the rock mass properties of the repository environment.

The major secondary structural features in a granitic rock mass are faults and joints. Faults are fractures along which rocks have been displaced relatively. Displacements along faults may be several miles or only a few inches. Faults tend to divide granite masses into large blocks extending hundreds of meters in depth and width [Kärnbränslesäkerhet, 1978b; Brown et al, 1975].

Joints are fractures along which no relative displacement has taken place. A joint plane may range in length from approximately a meter to several hundred meters. Spacing between joints may be only a few centimeters to tens of meters [Port-Keller and Gnirk, 1981]. The aperture width and frequency of joints tend to decrease with depth in a rock mass [Brown et al, 1975]. Materials such as clay or calcite may fill joints, depending on whether or not the joints have undergone secondary mineralization or hydrothermal alterations.

A repository site should be selected where there is little or no influence exerted by major faults. Jointing should be analyzed with respect to frequency and size since joints will probably be the main pathway for water movement in the repository rock. A host rock suitable for a repository is one in which the joints have little interconnection with respect to the total area.

2.2 THERMAL PROPERTIES

2.2.1 Thermal Conductivity

Thermal conductivity represents the ability of rock to conduct heat. Table 2-1 lists values taken from the literature for granite at temperatures from 291 to 298 K.

Quartz, one of the main constituents of granitic rock, is one of the most highly conducting rock-forming minerals. Work by Beck and Beck [1965]

Table 2-1. Thermal Properties of Granite[a]

Property	Units	Mean Value ± 1 Standard Deviation	Sources
Thermal Conductivity	W/m-K	2.52 ± 0.77	6 sources (15 data pts.)
Specific Heat	J/kg-K	809.3 ± 158.0	5 sources (11 data pts.)
Density	kg/m^3	2,650. ± 60.	17 sources (44 data pts.)

(a) Nominally at ambient temperature at 1,000 m depth (291 K to 298 K).

Table 2-2. Summary of Thermal Conductivities and Quartz
Content of Granite [After Beck and Beck, 1965]

Quartz Content (% by Weight)	Thermal Conductivity (W/m-K)
40.5 - 51.2	4.14 - 4.48
29.9 - 38.5	3.72 - 4.06
17.0 - 34.7	3.18 - 3.52
15.1 - 18.0	2.76 - 3.01

(Figure 2-2 and Table 2-2) shows that as the weight percent of quartz increases in coarse-grained granite specimens, the thermal conductivity increases.

Data from Geller [1970] and Dmitriyev et al [1969] (Figure 2-3) show a relationship between thermal conductivity and temperature. Although thermal conductivity generally decreases with increasing temperature for a particular rock specimen, the wide range of values for thermal conductivity at elevated temperatures does not allow a direct correlation between temperature and thermal conductivity for a typical granitic rock. For this study, three values for thermal conductivity have been used: the mean value shown in Table 2-1 and the mean value plus or minus one standard deviation (2.52, 3.29, and 1.75 W/m-K).

2.2.2 Specific Heat

Specific heat is a measure of a rock's capacity for absorbing thermal energy. Table 2-1 shows the mean value and standard deviation of values from the literature at temperatures from 291 to 298 K. For this study, the mean value of 809.3 J/kg-K has been used.

Specific heat increases as temperature increases [Birch et al, 1942; Dmitriyev et al, 1969; Lindroth and Krawza, 1971]. This is shown graphically in Figure 2-4.

2.2.3 Thermal Diffusivity

Thermal diffusivity is the ratio of a rock's thermal conductivity to its volumetric heat capacity. Thermal diffusivity can be calculated using the following relationship:

$$\alpha = \frac{k}{C_p \rho} \qquad (2-3)$$
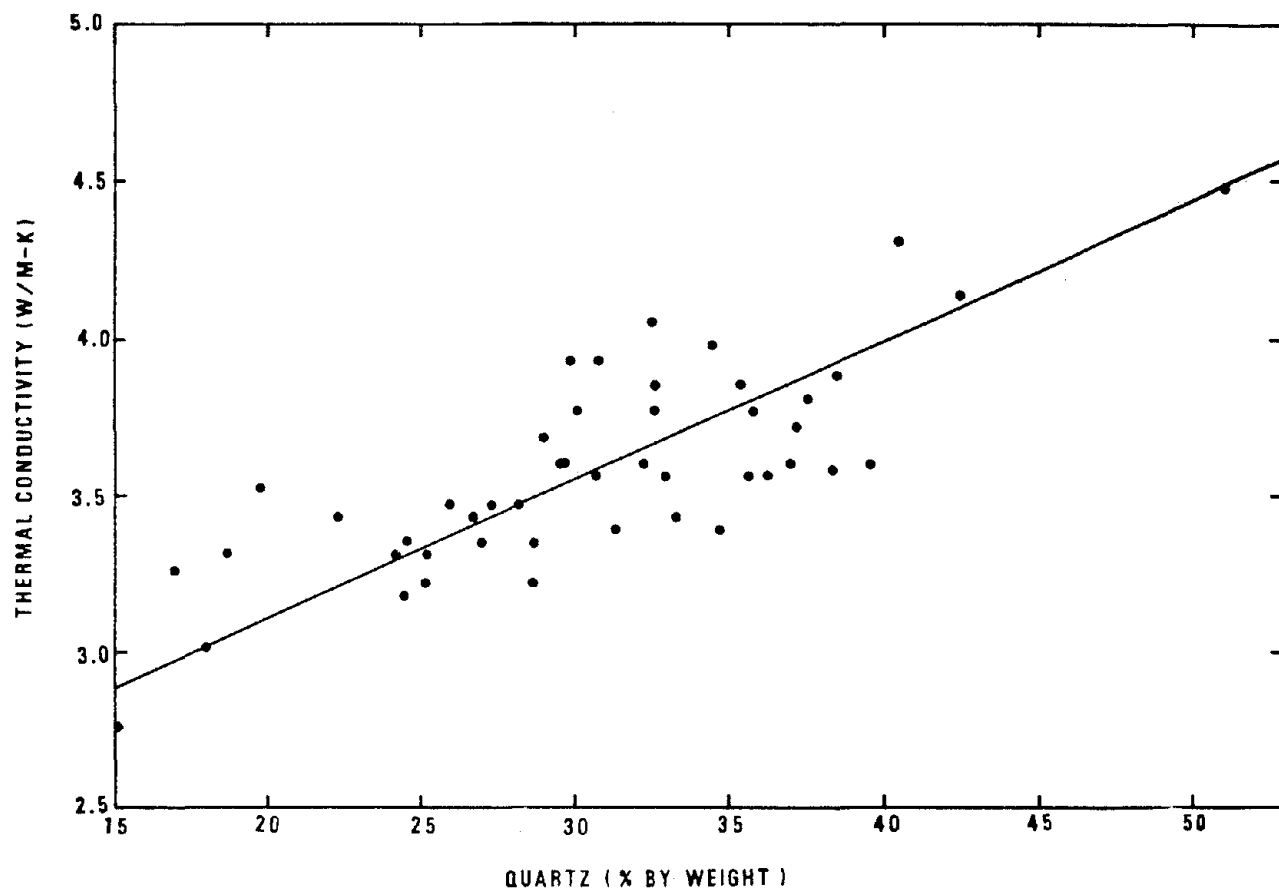
Figure 2-2. Thermal Conductivity of Granite as a Function of Quartz
Content [After Beck and Beck, 1965].
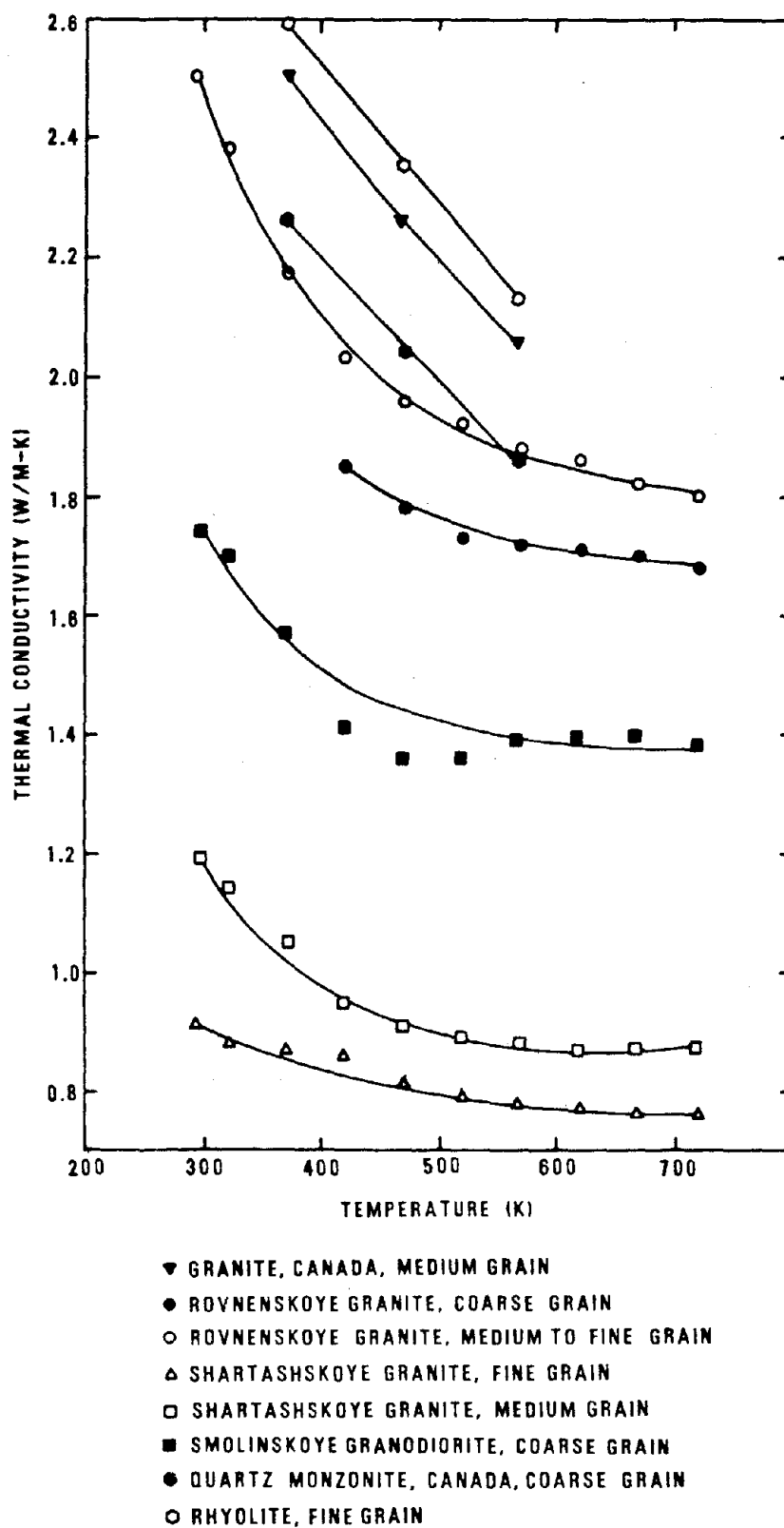
Figure 2-3.   Thermal Conductivity as a Function of Temperature.
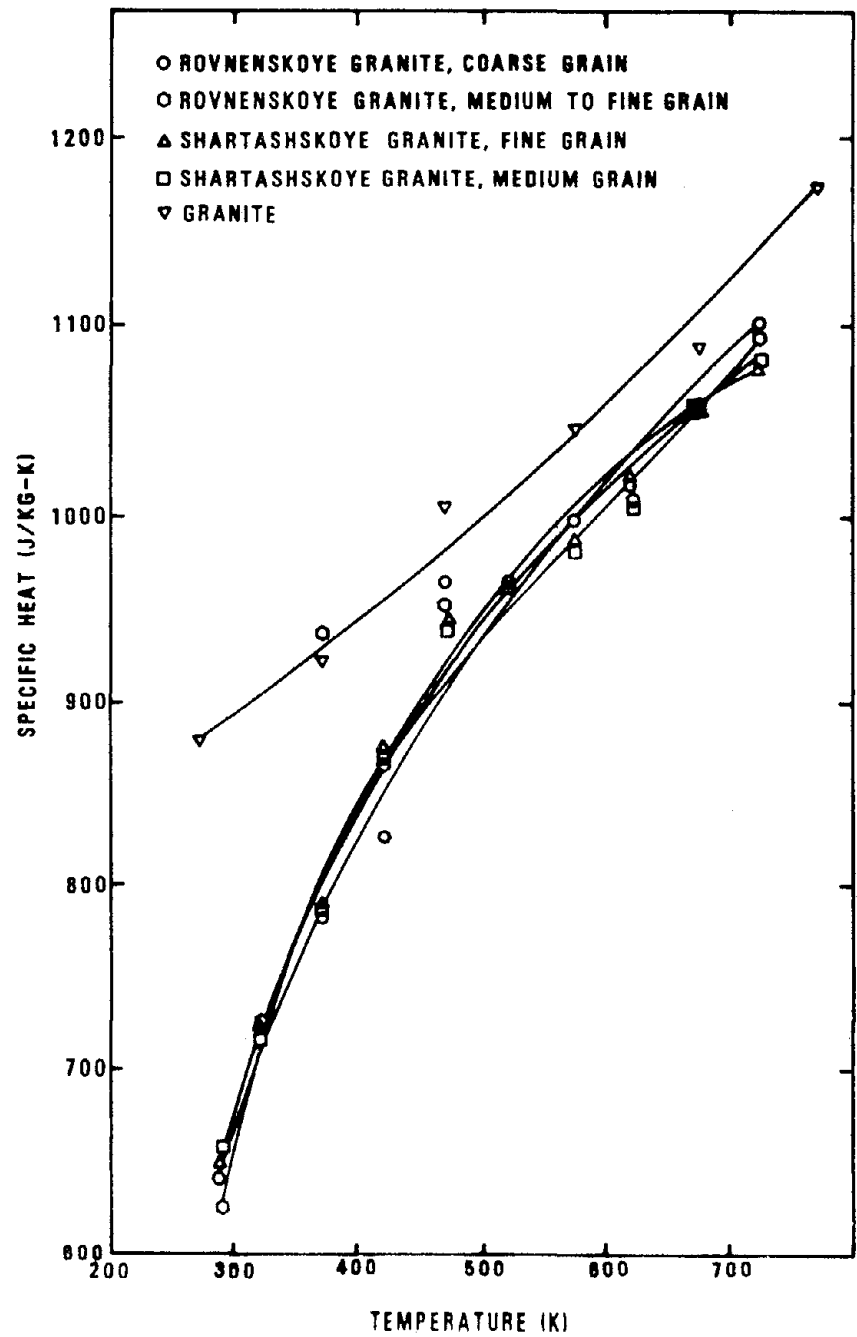
Figure 2-4. Specific Heat as a Function of Temperature.

where:

α = thermal diffusivity (m^2/s)

k = thermal conductivity (W/m-K)

C_p = specific heat (J/kg-K)

ρ = density (kg/m^3).

Data reported in the literature [Geller, 1970; Dmitriyev et al, 1969] indicate that the thermal diffusivity decreases with increasing temperature. In the temperature ranges being considered in this study, this effect is not considered important. Figure 2-5 presents this data graphically.

When the mean values from Table 2-1 are substituted into the above relationship, a value of approximately $1.17(10^{-6})$ m^2/s is obtained for the thermal diffusivity of a generic granite. This value is within the range of values found in the literature.

2.3 MECHANICAL PROPERTIES

The Expected Repository Environments in Granite (ERE-G) Study is currently concerned only with the thermal aspects of the repository. Future studies will also address the mechanical aspects. The following subsections discuss each of the mechanical properties thought to be important for modeling and selection of a generic granite for use as an underground radioactive waste disposal facility. In the tables of granitic rock properties in Appendix A, spaces left blank indicate areas where no data were available. Most of the references represent data obtained from laboratory tests on intact rock specimens. In situ testing is indicated in the "description" column. The data in Table 2-3 were compiled for tests at approximately ambient temperature at 1,000 m depth (293 to 298 K) and represent mean values and standard deviations of mechanical properties for a typical granitic rock.
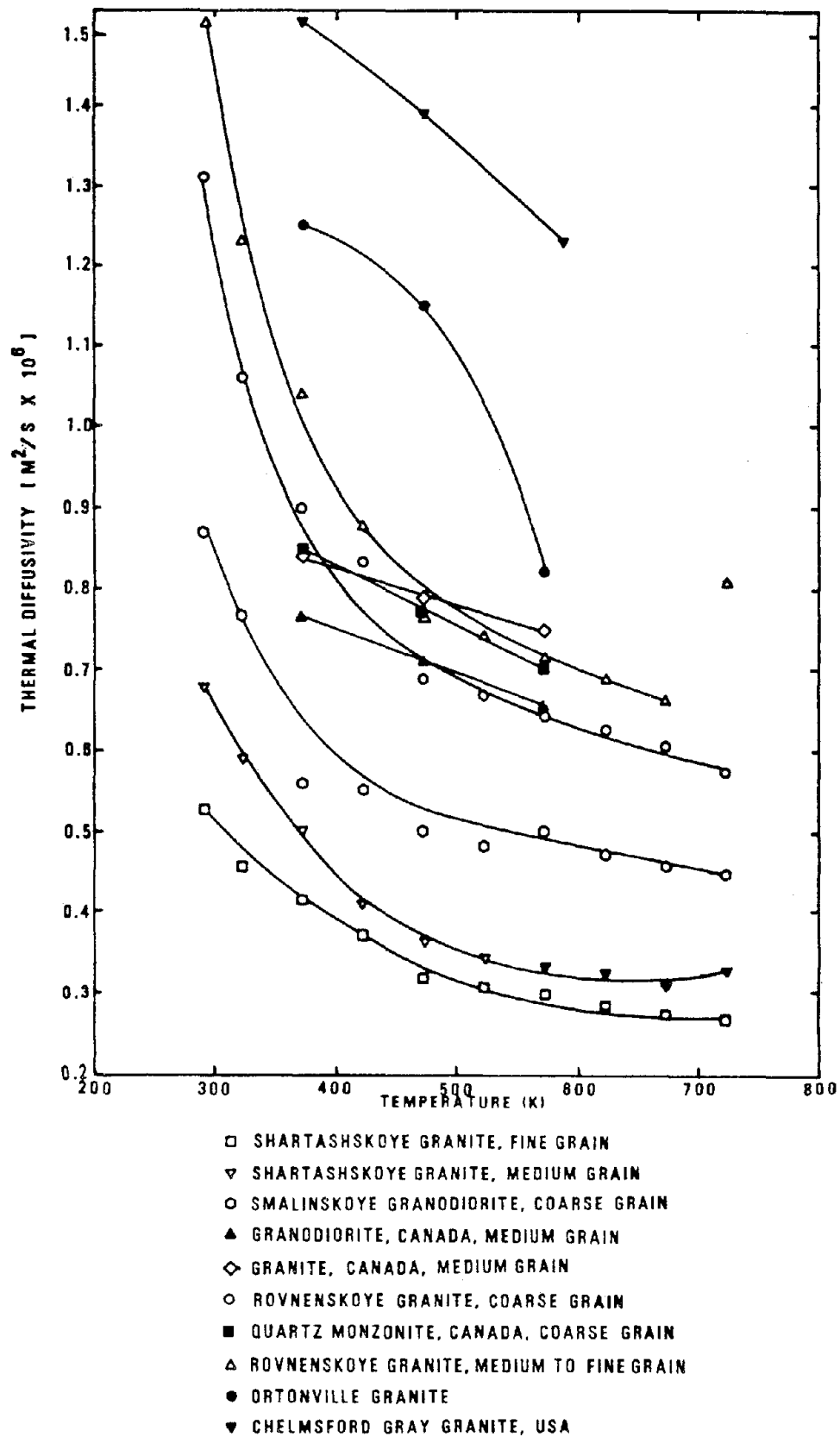
Figure 2-5. Variation of Thermal Diffusivity With Temperature.

Table 2-3. Mechanical Properties of Granite[a]

Property	Units	Mean Value ± 1 Standard Deviation	Sources
Modulus of Elasticity	GPa	49.9 ± 18.5	13 sources (64 data pts.)
Poisson's Ratio	-	0.21 ± 0.08	12 sources (42 data pts.)
Unconfined Compressive Strength	MPa	213.87 ± 68.68	17 sources (49 data pts.)
Tensile Strength	MPa	8.32 ± 3.48	7 sources (18 data pts.)
Thermal Expansion	10^{-6}/K	7.80 ± 1.36	3 sources (10 data pts.)
Density	kg/m^3	2,650. ± 60.	17 sources (44 data pts.)

[a] Nominally at ambient temperature at 1,000 m depth (293 to 298 K).

2.3.1 Density

Density is defined as mass per unit volume. Published density values for granitic rock lie within a narrow range. Table 2-3 lists the mean, standard deviation, and number of sources used in computing the generic density value. For this study, the mean density value of 2650 kg/m^3 has been used.

2.3.2 Young's Modulus

Young's modulus of elasticity is the ratio of the stress applied to a material to the resulting elastic strain. Most of the values found in the literature for Young's modulus of elasticity are based on laboratory tests of intact rock specimens. Structural features such as faults and joints which affect elastic properties and rock strengths on a large-scale basis are not taken into account in the data in Table 2-3. As compressive stress increases, discontinuities in the rock tend to close, causing the modulus to increase.

Experiments by Russian researchers [Dmitriyev et al, 1969] on granite at elevated temperatures (273 to 773 K) show that the elastic modulus decreases linearly with increasing temperature. This is due to a change in the individual crystal composition of the rock and relaxation processes occurring at the crystal interfaces. In Wingquist's investigation [1969], increasing temperature caused the elastic modulus to decrease.

The effect that temperature has on the elastic properties of rocks has not been studied extensively. Data for granite from two sources [Wingquist, 1969; Dmitriyev et al, 1969] plotted in Figure 2-6 indicate a sharp reduction in Young's modulus with increasing temperature. However, in the temperature range considered within the repository, the effect of temperature on Young's modulus is small.

2.3.3 Unconfined Compressive and Tensile Strengths

Unconfined compressive strength and tensile strength are defined as the maximum compressive and tensile stresses, respectively, applied uniaxially that a material can withstand without failure. Sufficient data were found in the
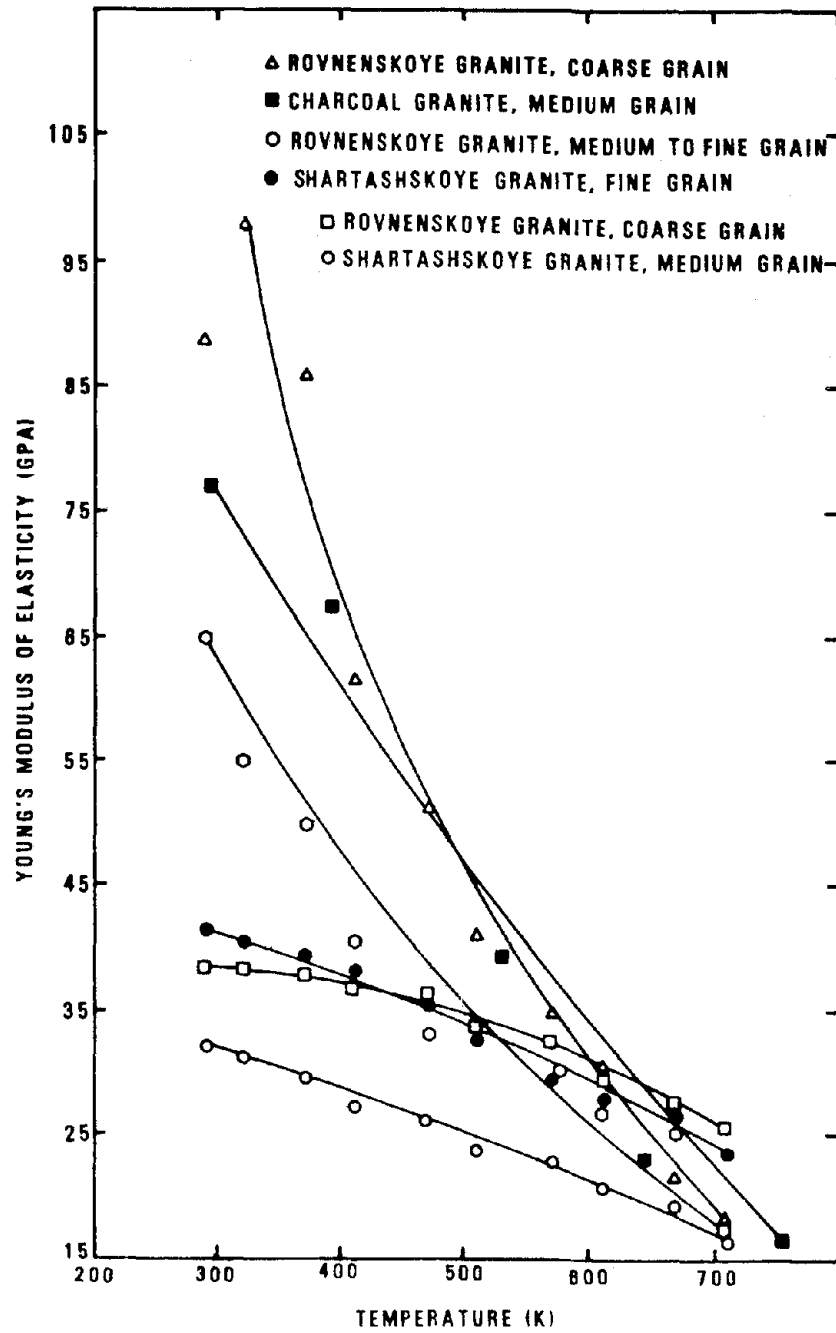
Figure 2-6. Young's Modulus of Elasticity as a Function of Temperature.

literature to establish a fairly wide range of strength values. Table 2-3 lists the values selected for a typical granitic rock. Figure 2-7 shows a slight decrease in unconfined compressive strength when temperature is increased. Few authors deal with the dependence of these properties on temperature. These data are not all-inclusive, and site-specific data should be obtained prior to the selection of a repository site.

2.3.4 Linear Thermal Expansion Coefficient

The linear thermal expansion coefficient represents the change in thermal strain of a material per unit change in temperature. Values from the literature [Dmitriyev et al, 1969; Geller, 1970] for the linear thermal expansion coefficient of granite are shown in Table 2-3. The variation of this coefficient with temperature is illustrated in Figure 2-8.

2.3.5 Shear Strength

The Mohr-Coulomb failure criterion is often used to define the shear strength of hard rock like granite, either within the intact rock itself or along structural discontinuities within the rock mass. This criterion specifies that the shear stress which tends to cause failure along a plane is resisted by the cohesion of the material plus a constant multiplied by the normal stress across the plane [Jaeger and Cook, 1969]. This relationship is given by:

$$\tau = S_0 + \sigma_n \tan \phi \qquad (2-4)$$

where:

τ = shear strength

S_0 = shear strength at zero normal stress (cohesion)

σ_n = normal stress on the failure plane (compression assumed positive)

ϕ = angle of internal friction.
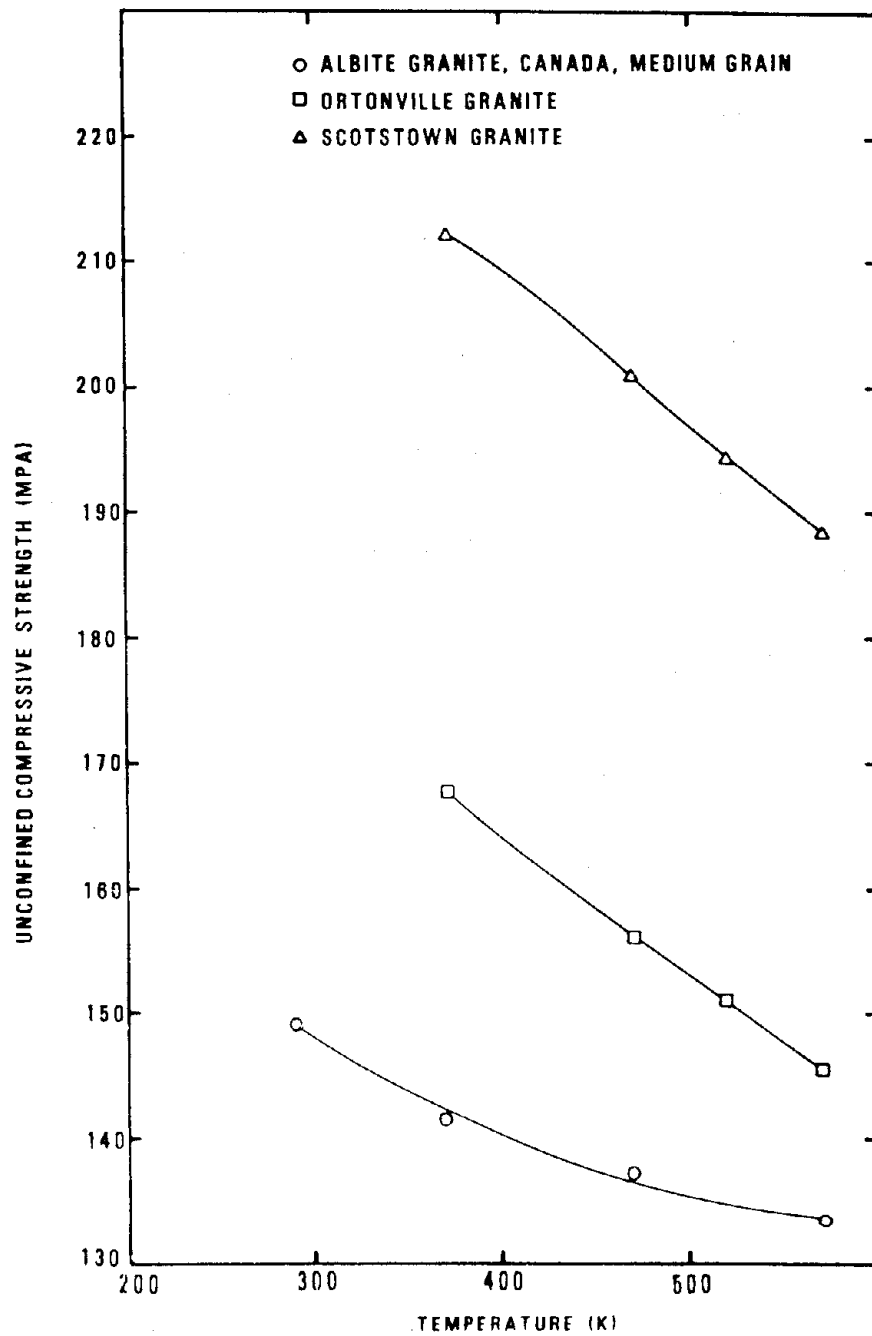
Figure 2-7. Unconfined Compressive Strength as a Function of Temper
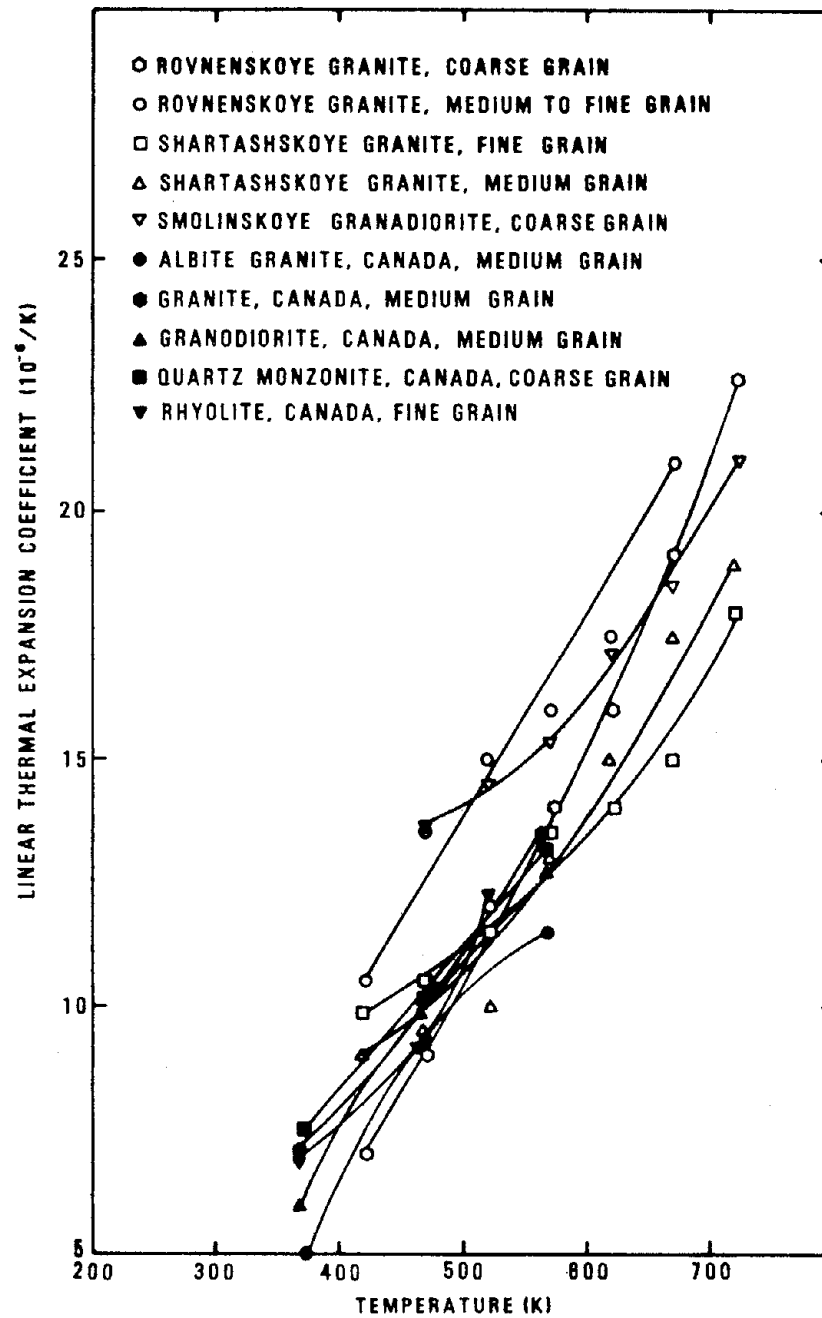
Figure 2-8. Linear Thermal Expansion Coefficient as a Function of Temperature.

The surface of a discontinuity, either smooth or rough, continuous or discontinuous, will affect the shear strength of the granitic mass. If the discontinuities are filled with formation debris or clay, the friction angle may be lower than if no alteration has occurred [Acres Consulting Services Limited et al, 1978].

Extensive literature searches in the past have revealed limited data for the angle of internal friction for granitic rock. Work by Kulhawy [1975] represents an extensive literature search for rock properties under triaxial test conditions. Based on work by Kulhawy and others [Acres Consulting Services Limited et al, 1978; Callahan, 1981; Swan, 1977; Office of Waste Isolation, 1978c], a range of values for the angle of internal friction is 20° to 58°, with an estimate for generic granite of 30°.

2.3.6 Other Mechanical Properties

The literature survey to determine the mechanical properties of a generic granitic rock revealed additional properties found in varying frequency. These properties include modulus of rigidity, compressibility, shear wave velocity, impact toughness, Shore scleroscope hardness, longitudinal wave velocity, and modulus of rupture. A discussion of these properties is not within the scope of this report, but Appendix A includes their values under the "Additional Properties" heading.

2.4 HYDROGEOLOGICAL PROPERTIES

2.4.1 Permeability and Hydraulic Conductivity

The terms "permeability" and "hydraulic conductivity" are often used interchangeably. Both terms refer to the ability of a rock to transmit fluid, but permeability is an intrinsic rock property while hydraulic conductivity is also a function of the fluid properties. Usually the hydraulic conductivity is given for a standard fluid (water) at standard conditions (20°C). Consequently, the two terms can be related to each other. Davis and DeWiest [1966] give this relationship as:

$$k_h = \frac{\kappa \rho g}{\mu} \qquad\qquad (2\text{-}5)$$

where:

k_h = hydraulic conductivity (m/s)

κ = permeability (m^2)

ρ = fluid density (kg/m^3)

g = gravitational acceleration (m/s^2)

μ = viscosity (kg/m-s).

For water at 20°C, Davis and DeWiest [1966] show the following equivalency between hydraulic conductivity and permeability:

$$k_h = 1.0 \text{ m/s} \sim \kappa = 1.02 \times 10^{-7} \text{ m}^2 \qquad\qquad (2\text{-}6)$$

where:

$\sim$ means "equivalent to".

The literature survey revealed few references to permeability studies conducted in situ at the depths similar to repository conditions. The mining and petroleum industries are responsible for most of the existing data.

The reader is referred to Appendix A where all permeability and hydraulic conductivity values found in the literature are listed in tabular form. A discussion of key references citing values for permeability of in situ granite follows.

Actual drill hole tests by Swedish researchers [Kärnbränslesäkerhet, 1978b] in granitic rock at the Krakemala, Finnsjö, and Karlshamn areas show zones of transmissive and nontransmissive rock at great depths. The nontransmissive areas have hydraulic conductivity measurements of less than 10^{-9} m/s. Hydraulic conductivity values for the transmissive rock are greater than 10^{-8} m/s.

Investigations were conducted by Carlsson and Olsson [1977] on five types of Swedish granite in order to determine the dependence of hydraulic conductivity on depth. The actual tests were conducted at depths down to only about 250 m,

and the data appears widely scattered. Carlsson and Olsson [1977] fit a line to their measured data using data from Snow [1968] to derive the following equation for the dependence of hydraulic conductivity on depth:

$$\log (k_h) = - (2.5 \log(z)+ 2.5) \qquad (2-7)$$

where:

k_h = hydraulic conductivity (m/s)

z = depth (m).

For a depth of 1,000 m, this equation gives a hydraulic conductivity of 10^{-10} m/s.

Kärnbränslesäkerhet [1978b] also reports that at depths greater than a few hundred meters in tested granite, an increasing number of zones with very low permeability exist. At these depths, zones of impervious rock divided by water-bearing fracture zones are found. The nontransmissive sections show hydraulic conductivities of less than 10^{-9} m/s. At depths greater than 900 m, there is little water movement between the water-bearing and impervious zones. Water age and chemical composition support these observations.

Appendix A lists values for permeability and hydraulic conductivity. In this study, the values assumed for permeability and hydraulic conductivity are 1.02×10^{-15} m^2 and 10^{-8} m/s, respectively. It is also assumed that the permeability is isotropic, acknowledging that this is a simplification.

2.4.2 Porosity

Porosity is defined as the fraction of the total volume of a rock that consists of pore spaces. When considering the hydraulic characteristics of a granitic rock, both primary (intact rock) and secondary (rock mass with fractures) porosity may be considered. Secondary porosity is defined as the ratio of the fracture volume to the total volume of rock and is a function of the spacing and aperture of the fractures. In an unweathered granite, intergranular spaces are negligible compared to fracture openings [Office of Waste Isolation, 1978a]. Consequently, most ground-water movement through a granite mass at depth will be through the discontinuities in the rock mass.

Brace and Orange [1968] note a strong correlation between electrical resistivity and porosity. By using measured bedrock resistivities from Swedish boreholes and the equation given by Brace and Orange [1968] for crystalline rock with low porosity, Swedish researchers [Kärnbränslesäkerhet, 1978b] calculated porosity values of around 0.005 for transmissive and nontransmissive rock zones. The relationship is:

$$\Theta^m = \frac{\rho_o}{\rho_s} \qquad (2\text{-}8)$$

where:

Θ = porosity

ρ_o = resistivity of the fluid in the pores

ρ_s = resistivity of the bedrock

m = a constant with values close to 2 for crystalline rock. In parallel fracture zones, $m = 1$.

The porosity of granitic rock mass has been assumed, for the purpose of this study, to be 0.01 percent. Values of porosity for intact granite are tabulated in Appendix A.

2.4.3 Hydraulic Gradient

The hydraulic gradient is defined as the change in hydrostatic head per unit of distance in a given direction [Brown et al, 1975]. In this study, the topography of the land overlying the repository is assumed to be reasonably flat so that the hydraulic gradient, which affects the movement of ground water, will only be minimally affected by local topographical considerations. Thus, it is assumed that local recharge and discharge zones are negligible and that the ground-water system consists of a regional flow which is assumed to be horizontal with a hydraulic gradient of 0.1, (1 m H_2O/km).

2.5 BACKFILL THERMAL PROPERTIES

The annulus between the drill hole and the canister is assumed to be back-filled with dry, crushed granite, a product of the repository mining operation. The size distribution of the particles is based on a standard ASTM sieve analysis [Portland Cement Association, 1968]. Aggregates which give a smooth grading curve and contain neither an excess or deficiency of any one size give the best density results [Marcuson and Bieganousky, 1977; Coates and Yu, 1969]. For this study, the aggregate was assumed to range in size from 0.025-cm-diameter fines to 0.65-cm-diameter fines.

The porosity and void ratio for the crushed granite annulus were estimated from data for typical aggregates in a natural state [Perloff and Baron, 1976]. A porosity of 31 percent is estimated for the crushed aggregate. Based on the definition of porosity as the voids between particles, the following relationship is used to calculate the void ratio of the dry, crushed granite:

$$\text{Void ratio} = \frac{V_v}{V_g} \tag{2-9}$$

where:

V_v = percent of total volume occupied by voids

V_g = percent of total volume occupied by crushed granite.

For a porosity of 31 percent, the void ratio is 0.45.

The density of the backfill can be calculated from the density of the bulk material by the relationship:

$$\rho_{bf} = (1 - \theta) \, \rho_b$$

$$= (1 - 0.31) \, 2650 \, \frac{kg}{m^3} \tag{2-10}$$

$$\rho_{bf} = 1828 \, \frac{kg}{m^3}$$

where:

ρ_{bf} = density of backfill

ρ_b = density of bulk material (granite)

θ = porosity of backfill.

Because the mass of the dry, crushed aggregate backfill is attributed primarily to the mass of the bulk material in it, the heat capacity of the backfill is approximately equal to the heat capacity of the bulk material. Therefore, the specific heat of the crushed granite backfill is assumed to be the same as the specific heat of granite (809.3 J/kg-K).

The thermal conductivity of the backfill is an important parameter for calculating the temperature field about the canister. The size distribution of crushed granite particles makes heat transfer calculations difficult. Estimates of thermal conductivity based on consolidated or ordered arrays of even-sized particles have frequently been made [Yagi and Kunii, 1957; Kunii and Smith, 1960; Woodside and Messmer, 1961]. These models take into account the combined effects of radiation, solid conduction, and convection and are based on a liquid-filled medium. A review by Crane et al [1977] of theoretical correlations of thermal conductivity of granular materials compares these correlations with experimental results. Based on this review, it appears an appropriate expression for the thermal conductivity of the backfill is the Hengst-Kaganer equation, which is a combination of Kaganer's [1966] and Hengst's [1934] expressions for the effective thermal conductivity of granular systems. The Hengst-Kaganer equation is written as:

$$\frac{k_{bf}}{k_v} = 5.8 \ (1-\theta)^2 \ \frac{k_b}{k_b - k_v} \left[\frac{k_b}{k_b - k_v} \ \ln \frac{k_b}{k_v} - 1 \right] + (1 - \frac{\pi}{4}) \qquad (2\text{-}11)$$

where:

k_{bf} = thermal conductivity of granulated material

k_v = thermal conductivity of voids (air, 0.0257 W/m-K)

k_b = thermal conductivity of bulk material (granite)

θ = porosity.

Using the mean value from the literature survey for granite's conductivity (2.52 W/m-K), the conductivity of the backfill calculated from Equation (2-11) is 0.266 W/m-K.

Table 2-4 summarizes the thermal properties assumed for the backfill material (dry, crushed granite) in this study.

2.6 NUCLEAR WASTE THERMAL PROPERTIES

Table 2-5 lists the values of thermal conductivity, specific heat, and density used for spent fuel (SF), commercial high-level waste (CHLW), and defense high-level waste (DHLW). In all cases in this report, the internal designs of the waste packages were ignored and the canisters were treated as uniform bodies with the properties listed in Table 2-5.

Table 2-4. Thermal Properties of Backfill Material
(Dry, Crushed Granite)

Property	Units	Value
Porosity	%	31.0
Thermal Conductivity	W/m-K	0.266
Specific Heat	J/kg-K	809.3
Density	kg/m^3	1,828.

Table 2-5. Thermal Properties of the Nuclear Waste

Property	Units	CHLW and SF	DHLW
Thermal Conductivity	W/m-K	1.21	1.35
Specific Heat Capacity	J/kg-K	837.4	1,047.
Density	kg/m^3	2,995.	2,800.

3 REFERENCE REPOSITORY IN GRANITE

3.1 SUMMARY OF PREVIOUS STUDIES

The repository design used in this report is based on a synthesis of conceptual and generic repository design studies which have been carried out throughout the world to date. The four main studies which provided useful information concerning repositories in granitic rock were: the U.S. Department of Energy's Generic Environmental Impact Statement [Office of Waste Isolation 1978a; 1978b; 1978c]; the International Fuel Cycle Evaluation Study [INFCE, 1979]; the Canadian studies carried out by the Atomic Energy of Canada Limited [Acres Consulting Services Ltd. et al, 1980a; 1980b]; and the studies undertaken in Sweden by Kärnbränslesäkerhet (KBS) [Saint Goubain Techniques Nouvelles, 1977; Finne and Engelbrektson, 1977]. A summary of the data from these studies is presented in Table 3-1. The repository concepts being proposed by the British [Griffin et al, 1979] were also reviewed but have not been included in this report because they do not meet some of the requirements, such as retrievability, which are felt to be necessary in the United States.

An inspection of Table 3-1 shows that the waste form is quite variable, as would be expected since each country operates different types of reactors. However, the repositories are very similar in design. They all consist of long tunnels located on one horizontal level within the rock mass with cylindrical waste packages emplaced into vertical boreholes in the tunnel floors. The major difference between the designs is not in their configurations but in the amount of heat initially contained, with the initial areal thermal loading varying from 6 to 47 W/m^2. The depth of the repositories varies from 500 to 1,000 m.

3.2 REFERENCE REPOSITORY DESCRIPTION

3.2.1 Waste Package

Three types of waste are considered in this report:

Table 3-1. Summary of Generic Repository Designs in Granite

	Geis USA		INFCE International		KBS Sweden	AECL Canada	
Canister							
Type of Waste	SF (PWR)	HLW	SF (PWR)	HLW	HLW	SF (HWR)	HLW
Waste Form	Bundle with Lead Backfill	Vitreous	Bundle	Vitreous	Vitreous	Bundle	Vitreous
Age (years)	10	10	10	10	10	10	10
Can Heat Load (W)	550	1700	550	500	1140	269	269
Can Material	Sch'l 30 Pipe	Sch'l 40S Pipe	Stainless Steel		Titanium	N.S.	N.S.
Diameter (m)	0.386	0.324	.35	0.22	0.612	0.91	0.457
Length (m)	4.9	3.0	4.9	3.0	1.8	1.5	3.03
Drill hole							
Cans/Hole	1	1	1	1	1	1	1
Diameter (m)	0.61	0.51	1.0	0.62	1.0	N.A.	0.6
Depth (m)	7.62	6.10	7.9	5.0	5.0	N.A.	4.75
Sleeve Material	Mild Steel		None	None	None	N.A.	None
Room							
Width (m)	5.5	5.5	3.7	3.7	3.5	7.5	7.5
Height (m)	7.6	6.1	4.5	3.5	3.5	6.15	5.0
Length (m)	85-170	85-170	500	188	188		
Cans Across Room	2	1	1	1	1	4	4
Spacing (m)	1.8	N.A.	N.A.	N.A.	N.A.	1.5	1.5
Pitch (m)	1.8	3.05	3.5	3.5	4.0	2.5	1.5
Room Thermal Loading (W/m^2)	111.	102.	42	39	81.4	57.4	95.6
Backfill	Crushed Granite		Sand/Bentonite		85% Sand 15% Bentonite	Crushed Granite & Clay	
Panel							
Extraction Ratio	42%	23%	15%	15%	14%	25%	25%
Pillar Width (m)	7.6	18.3	21.3	21.3	21.5	22.5	22.5
Panel Thermal Loading (W/m^2)	46.7	23.4	6.3	5.7	11.4	24.0	14.4
Repository							
Levels	1	1	1	1	1	1	1
Depth (m)	610	610	500	500	500	1000	1000

(1) Spent Fuel (SF). The reference SF canister contains a pressurized water reactor (PWR) fuel bundle structurally fixed inside a canister with helium filling the remaining canister volume. The canister material is carbon steel.

(2) Commercial High-Level Waste (CHLW). The reference CHLW canister contains vitrified waste from the reprocessing of spent fuel from light water nuclear power plants. The canister material is stainless steel.

(3) Defense High-Level Waste (DHLW). The reference DHLW canister contains vitrified nuclear waste which has been generated by the nation's defense program. The waste characteristics are based on the type of waste produced at the Savannah River Plant, South Carolina. The canister material is stainless steel.

SF and CHLW are assumed to be emplaced in the repository ten years after removal from the reactor, and DHLW is assumed to be 15 years old at emplacement. The waste package geometries and their initial heat generation rate are described in Table 3-2. The rate of decay of the heat generation rate is shown in Figure 3-1 where it is seen that the rate of decay is considerably slower for spent fuel than it is for CHLW or DHLW.

3.2.2 Repository

The reference repository consists of a long series of tunnels on one horizontal level at a depth of 1,000 m with the waste canisters emplaced into vertical boreholes in the tunnel floors. The room layout and dimensions are illustrated in Figure 3-2, where it is seen that the number of canisters across a tunnel was varied in this study. The diameter of the vertical borehole is sufficiently large to allow a 0.1-m-wide annulus between the waste canister and the rock. This annulus is backfilled with crushed granite.

In plan view, the repository is square in shape with sides 1.87 km in length. A square shaft pillar with no waste emplaced in it is located in the center of the repository with sides 700 m long. The areal thermal loading is 20, 25, and 25 W/m^2 for the SF, CHLW, and DHLW repositories, respectively.

Table 3-2. Waste Characteristics

Characteristic	SF	CHLW	DHLW
Initial Heat Generation Rate (W)	550	700 and 2,100	578.5
Canister Radius (m)	0.178	0.162	0.305
Canister Length (m)	4.673	3.048	2.997
Canister "Active" Length (m)	3.658	2.438	2.140
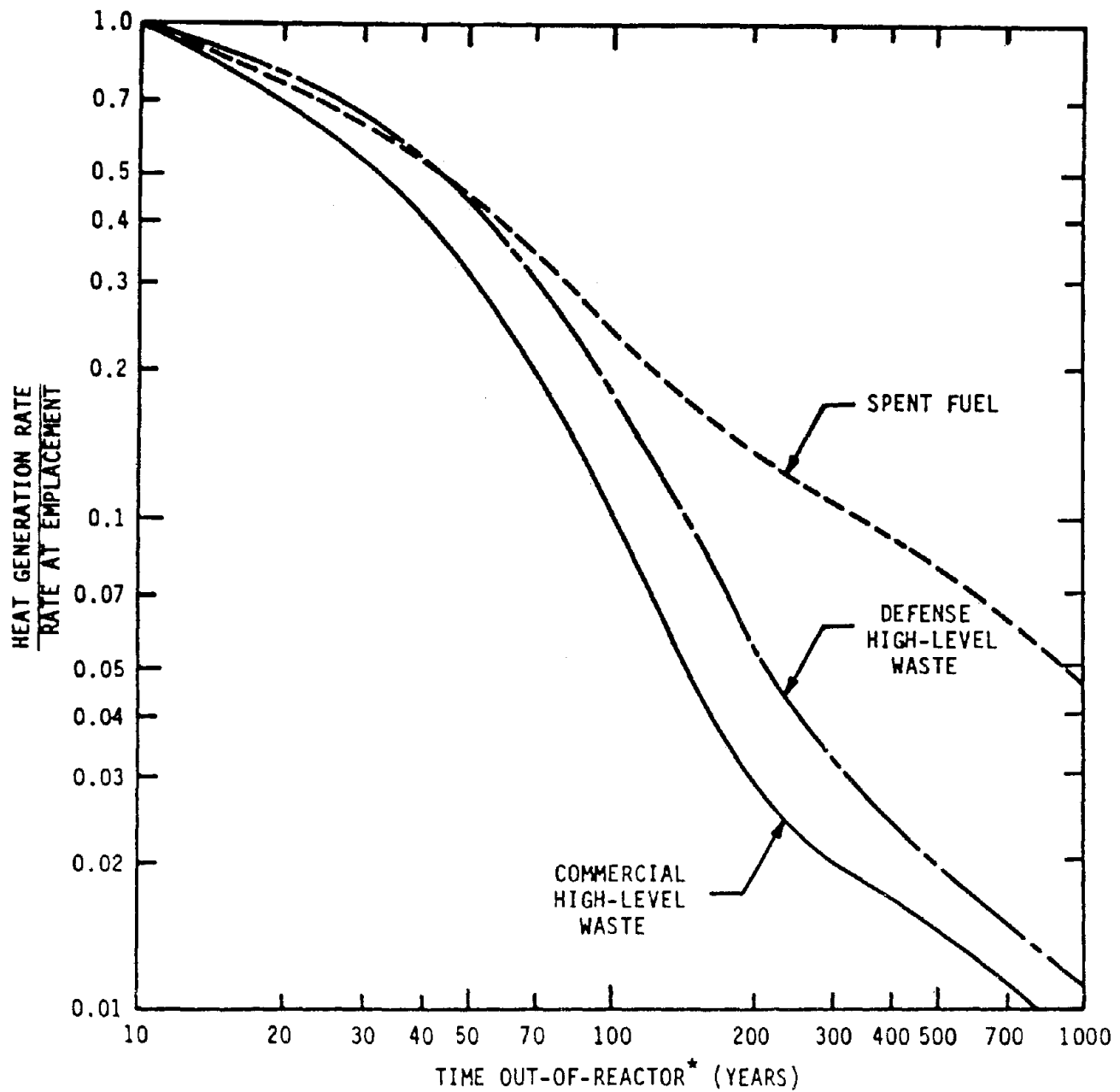
Figure 3-1. Decay Characteristics for Nuclear Waste Types (*Reference Time
           for DHLW is Time-of-Processing).

1 KM DEEP

EXTRACTION RATIO 25%

7.0 M

7.5 M ← 22.5 M → 7.5 M ← 22.5 M → 7.5 M

2 CANISTER LAYOUT

4 CANISTER LAYOUT

7.0 M

2.0 M

3 X 2.5 M

7.0 M

2.0 M

5 X 1.5 M

DRILLHOLE
  DEPTH - CAN LENGTH + 2 M
  DIAM - CAN DIAM + 0.2 M
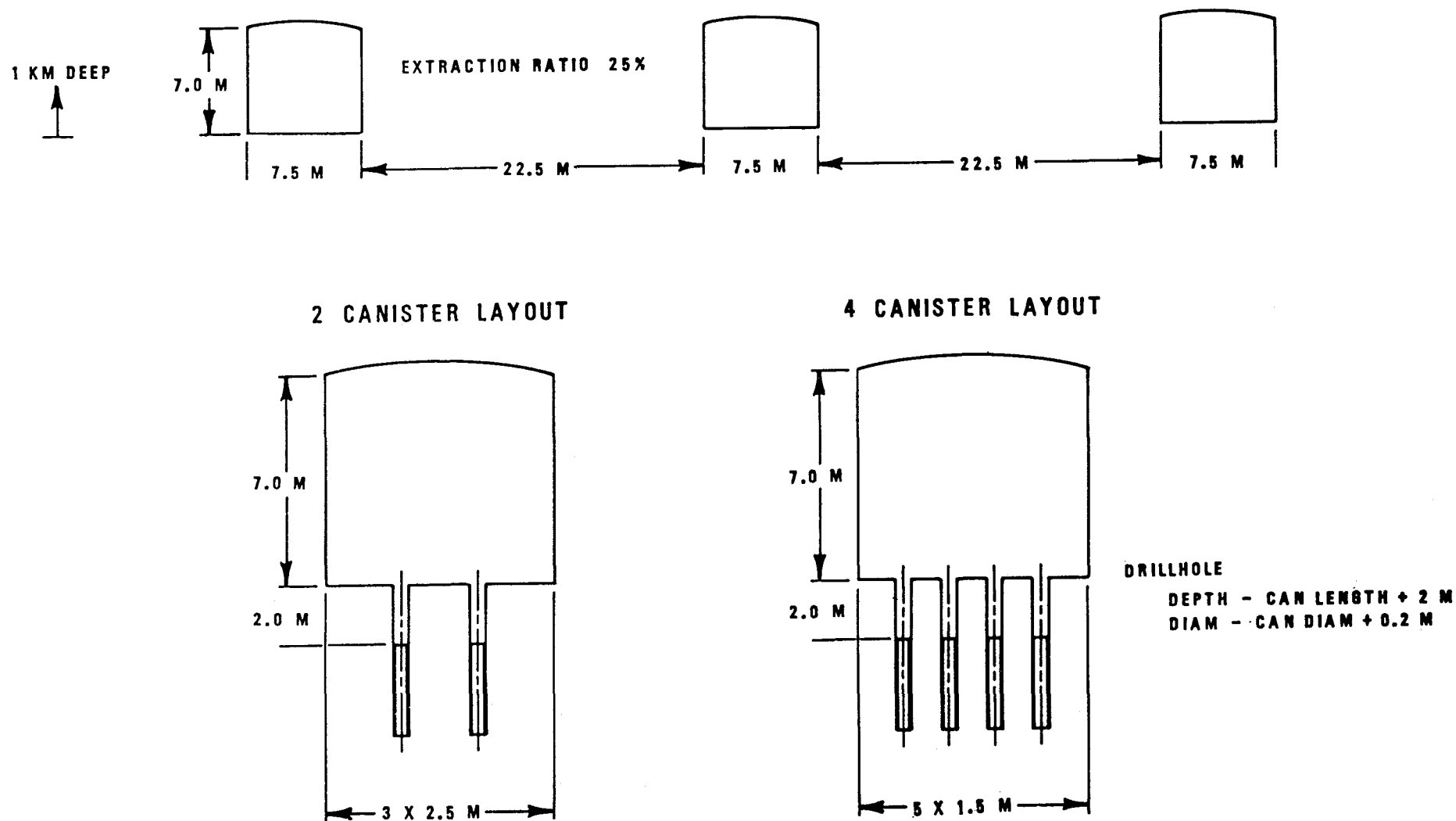
Figure 3-2. Reference Repository Layout for Expected Repository Environments in Granite.

3.3 OPERATIONAL SEQUENCE

The sequence of operations in the reference repository is as follows:

(1) The wastes are emplaced over a 20 year period;

(2) A five-year "monitoring" period follows during which the repository is kept open so that the wastes can potentially be removed;

(3) The repository is "blast-cooled" for 100 days; and

(4) The repository is backfilled with crushed granite and decommissioned.

It is assumed that each room is filled with wastes instantaneously. The entire repository is filled sequentially from the outermost edges in toward the shaft pillar at a rate which corresponds to the estimated arrival rates of the nuclear waste [Office of Waste Isolation, 1978a; 1978b; 1978c; 1978d].

4 THERMAL ANALYSES

A study of the long-term containment of radioactive waste requires investigations of the thermal response of the repository site at three scales: the very-near field (VNF), the near field (NF), and the far field (FF). The very-near-field analysis considers the waste package, the emplacement hole, and the rock within one-room diameter of the canister. The near-field analyses ignore the details of the waste package by treating the waste as a rectangular source of heat, but the rock mass in the pillar and one or two pillar widths above and below the disposal room are included in the analyses. The far-field analysis treats the repository as a horizontal heat-generating disk and examines the heat transfer and ground-water flow to great distances around the repository. Each analysis involves a different set of assumptions and modeling methods. The following sections discuss the modeling methods and the results for each region modeled.

4.1 VERY-NEAR-FIELD ANALYSES OF HEAT TRANSFER

4.1.1 Very-Near-Field Modeling Methods

The material properties in the reference repository are assumed to be temperature independent (see Section 2.2). Therefore, superposition techniques may be used to predict the temperature distribution produced by an array of waste canisters emplaced in one or more rows along the repository-room length. The superposition technique adds the contribution of single canisters to obtain the total thermal field. The superposition technique used to perform this analysis has been used in very-near-field analyses reported by Ratigan and Wagner [1978] and Ratigan [1980]. The results obtained using the superposition technique agree very closely with three-dimensional model results [Waldman, 1980].

The first step in the superposition technique is to obtain the temperature distribution about a single waste canister in an infinite medium. With the proper choice of model dimensions and boundary conditions, the solution for a single waste canister in an infinite medium can be obtained using a finite element axisymmetric model. The physical situation is depicted in Figure 4-1. The

(a)

(b)
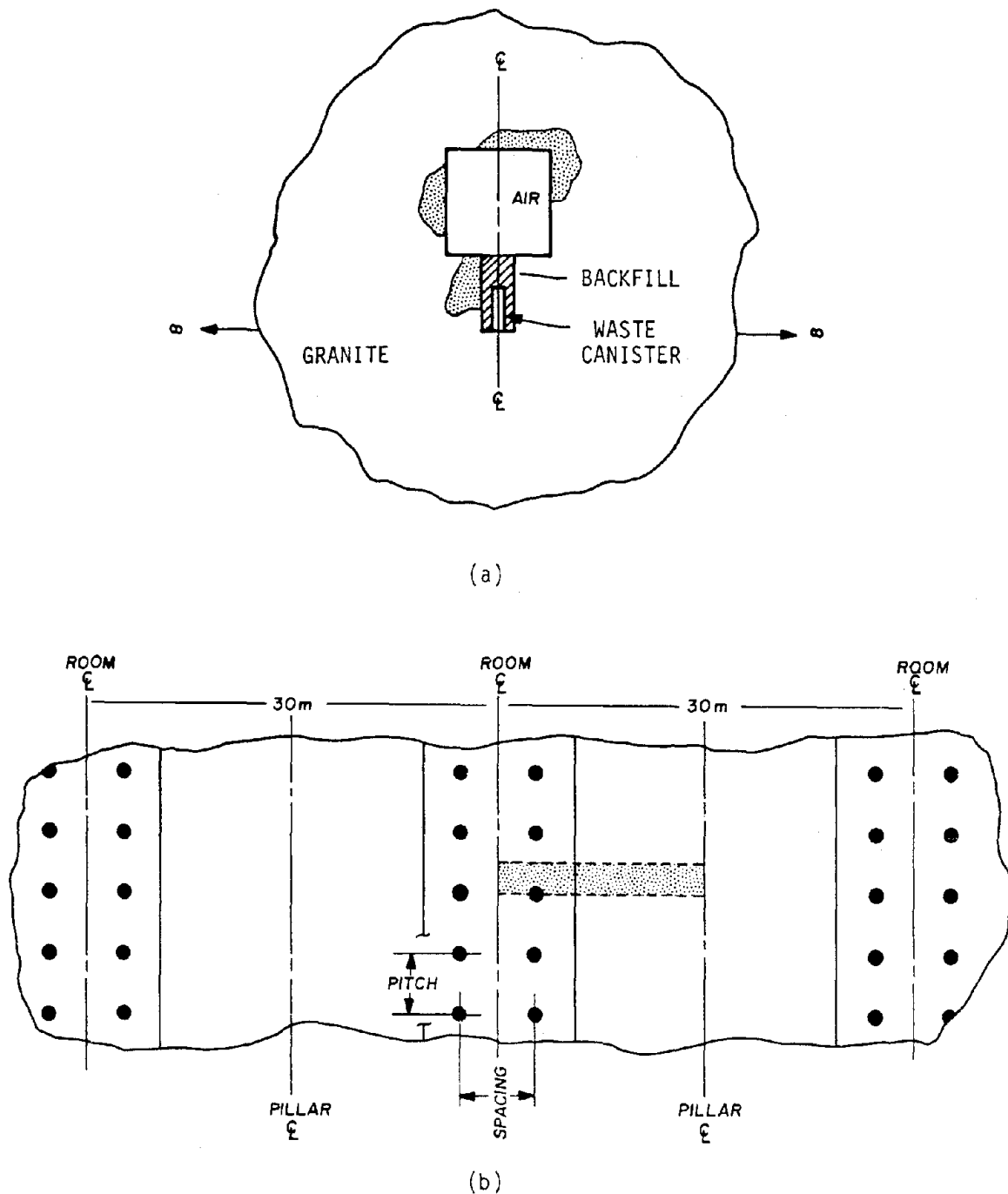
Figure 4-1. (a) Axisymmetric Model of a Waste Canister and Room in an
            Infinite Granitic Rock Mass. (b) Plan View of Several
            Adjacent Rooms Through Canister Midplane. Shaded Portion
            Represents Unit Cell in Which Temperature Distribution is
            Predicted by Superposition Technique.

dimensions for the canister and drill hole vary with the actual size of the containers of different waste types (see Figure 4-2).

The disposal room is actually rectangular, so the axisymmetric model approximates the rectangular room as a cylindrical room with a volume equivalent to a square room surrounding the waste canister. The height of the cylindrical cell is held constant and equal to the height of the disposal room (7.0 m). The radius of the cell is adjusted for each waste type to yield the appropriate volume according to the following equation:

$$r^2 = \frac{(Q_0)\ (W_r)}{\pi\ (ATL)\ (L_{R-R})} \tag{4-1}$$

where:

r = disposal room radius for unit cell

Q_0 = canister heat generation at emplacement

W_R = room width

ATL = areal thermal loading

L_{R-R} = centerline-to-centerline distance between adjacent rooms.

The second step in the superposition technique is the systematic summation of the contributions of each canister in the repository to obtain the temperature at a specific point of interest. Of course, the magnitude of the contribution from a single canister decreases as the distance between the canister and the region of interest increases. Canisters located far away have negligible effect on the temperatures in the region of interest. A plane through the midheight of the canisters is generally the region of primary interest since the highest temperatures occur in this plane. A representative portion of this plan section is illustrated in Figure 4-1. The summation process involved in superposing the effects of individual canisters is performed by computer program SPECTROM-42. Additional details of the superposition technique may be found in a report by Waldman [1980].

The internal details of the spent fuel canister are not modeled in this study when calculating temperatures external to the canister. Instead, the

ROOM
(AIR)

INFINITE
GRANITE
MEDIUM

BACKFILL

AIR

WASTE
CANISTER

(a)

(b)

CONSTANT DIMENSIONS FOR SF, CHLW, AND DHLW LAYOUT	
MODEL HEIGHT	= 500.0 m
MODEL WIDTH	= 250.0 m
ROOM HEIGHT	= 7.0 m
BACKFILL ABOVE CANISTER	= 2.0 m
NUMBER OF ELEMENTS	= 264
NUMBER OF NODES	= 861
ALL ELEMENTS 8 NODED	
ALL BOUNDARIES ADIABATIC	

VARYING DIMENSIONS FOR SF, CHLW, AND DHLW LAYOUTS	
ROOM RADIUS	
SF	= 1.479 m
CHLW 700 W	= 1.493 m
CHLW 2100 W	= 2.585 m
DHLW	= 1.354 m

Figure 4-2. (a) VNF Finite Element Mesh (FEM). (b) Close up of VNF FEM at the Room and Drill Hole.
(c) Dimensions for FEM.

canister is modeled as a heat generating solid with the thermal properties given in Section 2.2. This method does not affect the accuracy of the temperature distributions predicted on the surface of the canister and outside the canister. However, the internal temperatures cannot be accurately predicted without accounting for the combined heat transfer modes within the canister. The temperature difference between the spent fuel cladding and the canister wall was calculated using HYDRA-1 [McCann, 1980], a computer program which models the combined heat transfer modes within the canister. A graph (Figure 4-3) of the temperature difference as a function of canister wall temperature, filler material (helium), and heat generation rate is used to determine the temperature of the spent fuel cladding.

Only a fraction of the overall length of the waste canister actually contains heat generating waste. The active length of the waste within the canisters, along with the overall canister length, is listed in Table 3-2. The remaining length is modeled as air. Since radiative and convective heat transfer may be expected to be the predominant modes of heat transfer through the air, the air is modeled as a highly conductive medium with essentially zero heat capacity.

Temperatures in the very-near field were calculated for three waste types: SF, CHLW, and DHLW. Three thermal conductivities for granite (1.75, 2.52, and 3.29 W/m-K) were used. The backfill is assumed to be crushed granite. Based on Equation (2-11), the thermal conductivity of the backfill material in the SF models was adjusted to correspond to each of the granite conductivities (0.24, 0.26, and 0.28 W/m-K, respectively). The results of these models demonstrated that the influence of these small changes in backfill conductivity was negligible, so that only one backfill conductivity (0.26 W/m-K) was used in the CHLW and DHLW models. Three canister arrangements (one row, two rows, and four rows) were considered for certain combinations of waste types and granite thermal conductivity. The areal thermal loading (ATL) was 20 W/m^2 for SF and 25 W/m^2 for CHLW and DHLW. Results are presented in the form of graphs and tables of the temperature rise at three points: the canister centerline (cladding), canister skin, and drill hole edge. These points are of interest because they are locations where the repository design may be constrained because of adverse effects of temperature.
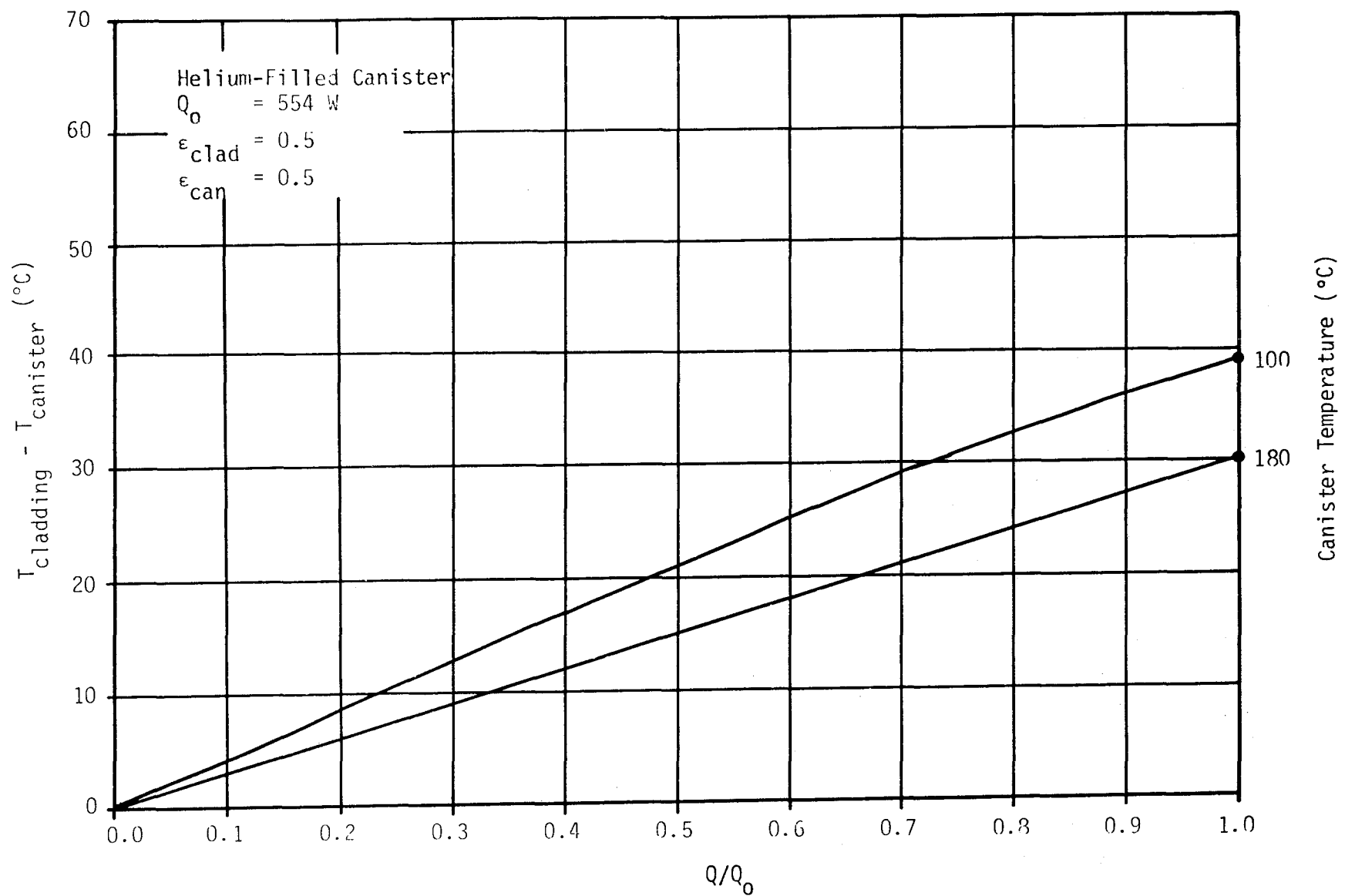
Figure 4-3. Steady-State Thermal Response of a PWR Spent Fuel Assembly in a Single Canister as Calculated by HYDRA-1 [After McCann, 1980].

4.1.2 Very-Near-Field Thermal Environments in a SF Repository

Two-row and four-row layouts of SF waste canisters are compared in the SF thermal analysis. The pitch for two rows of SF waste canisters is 1.83 m and twice that (3.67 m) for four rows.

The VNF thermal response as a function of time for a SF repository with two rows (Figure 4-4) and four rows (Figure 4-5) of canisters shows that maximum temperature rises are almost identical in the two-row and four-row layouts (see also Table 4-1) because the ATL was held constant. The room spacing was constant, but the canister row spacing changed from 2.5 m for the two-row layout to 1.5 m for the four-row layout. Similar results were also noted between a one-row layout and a two-row layout in the CHLW 2,100 W canister analysis (see Figures 4-10 and 4-11 and Table 4-4). A previous study (see Appendix E) noted similar temperature rises between one-row and three-row layouts with canister spacings similar to those in this analysis. Because the canister-row layout does not make an appreciable temperature difference in the temperature distribution, only two rows of waste canisters are studied in the CHLW and the DHLW analyses.

The temperature-rise peaks in SF (Figures 4-4 and 4-5) occur at approximately 15 years at the canister centerline (cladding), 20 years at the canister skin, and 30 years at the drill hole edge.

Three backfill conductivities (0.24, 0.26, and 0.28 W/m-K) and three granite thermal conductivities were considered in the SF analysis. Table 4-2 shows the temperature drop across the backfill for the three values of backfill conductivity. The maximum temperature difference caused by changing the backfill conductivity from 0.24 to 0.28 W/m-K is approximately 6°C at 0.1 year after emplacement. This difference is approximately 7 percent of the temperature rise at the canister skin of a SF waste canister at 0.1 year. This small difference is inconsequential and, therefore, the median value of 0.26 W/m-K is the only backfill conductivity value used in the CHLW and DHLW studies.

Temperature rise isotherms (Figures 4-6 and 4-7) based on a conductivity of 2.52 W/m-K show a large temperature gradient near the waste canister (see also Table 4-3). At 1.5 m from the canister centerline, the temperature is less than 15 percent of the temperature at the canister centerline. Away from the near vicinity of the canister, the majority of the thermal influence is from many canisters rather than any single canister.

Figure 4-4.   VNF Thermal Response as a Function of Time for a SF Repository.
               Two-Row Layout.
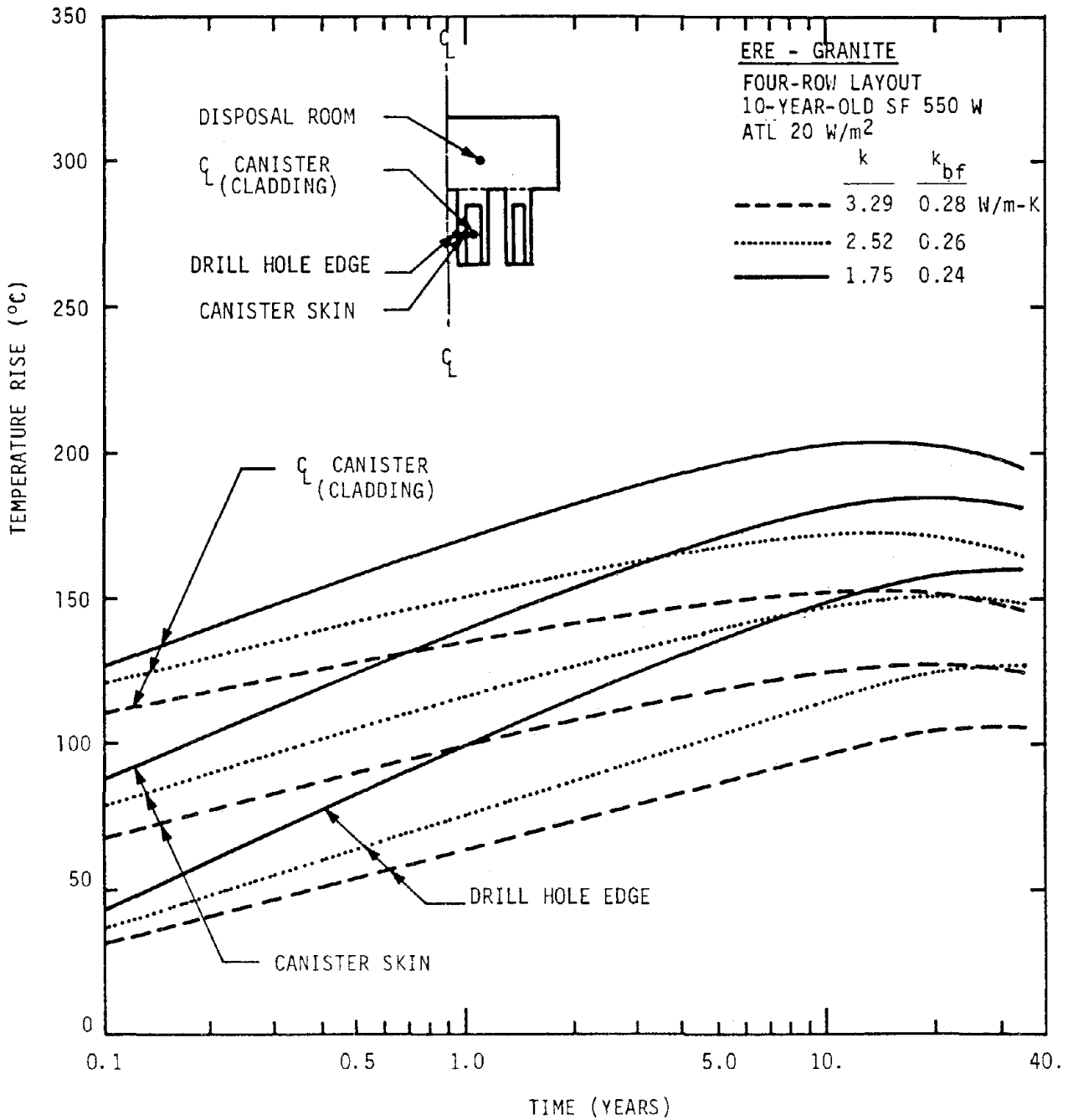
Figure 4-5. VNF Thermal Response as a Function of Time for a SF Repository.
Four-Row Layout.
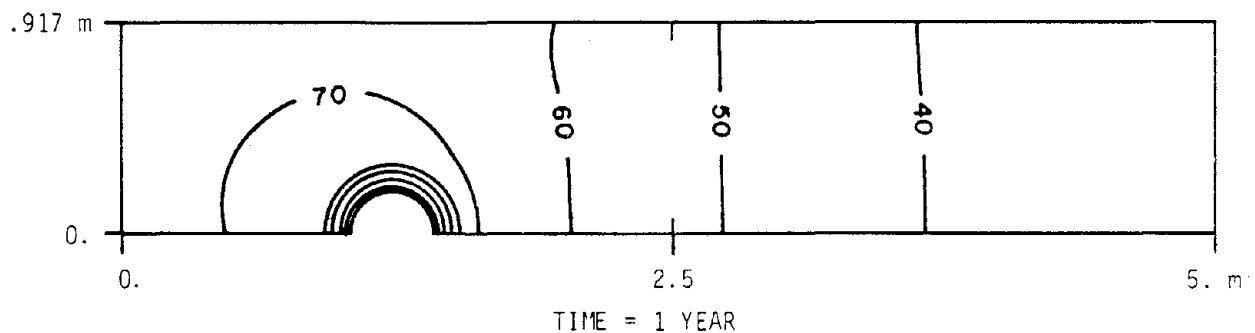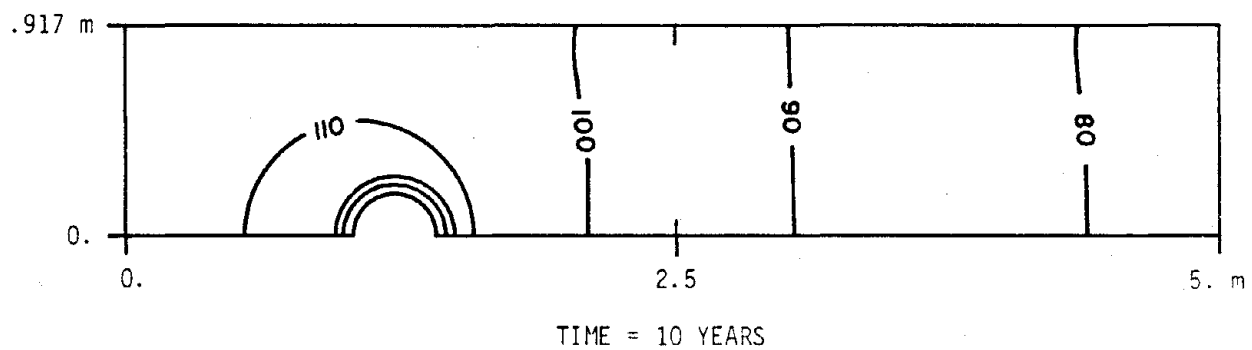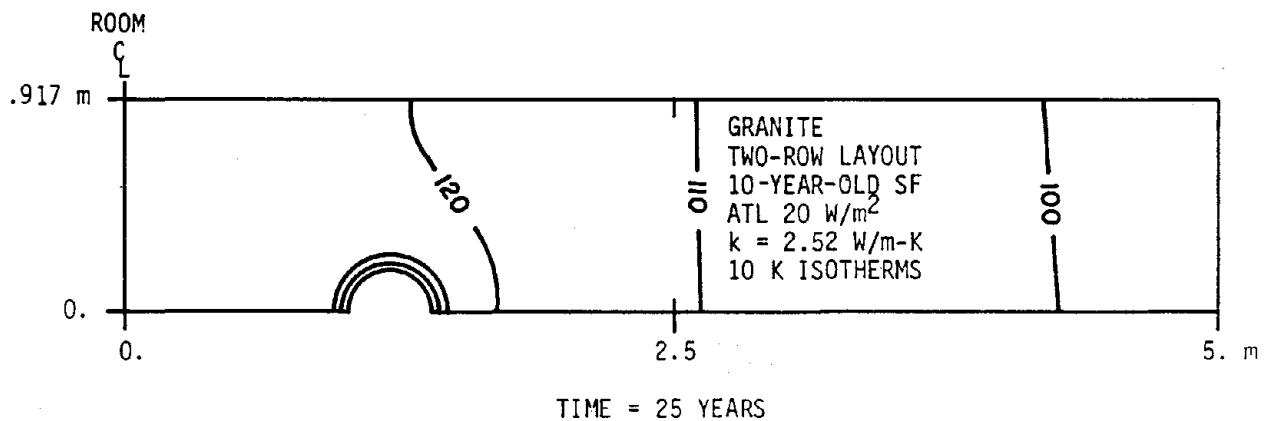
Figure 4-6. Temperature Rise Isotherms (°C) in VNF Region of a SF Repository in Granite. Two-Row Layout.

ROOM

GRANITE
FOUR-ROW LAYOUT
10-YEAR-OLD SF
ATL 20 W/m^2
k = 2.52 W/m-K
10 K ISOTHERMS

TIME = 25 YEARS

TIME = 10 YEARS

TIME = 1 YEAR
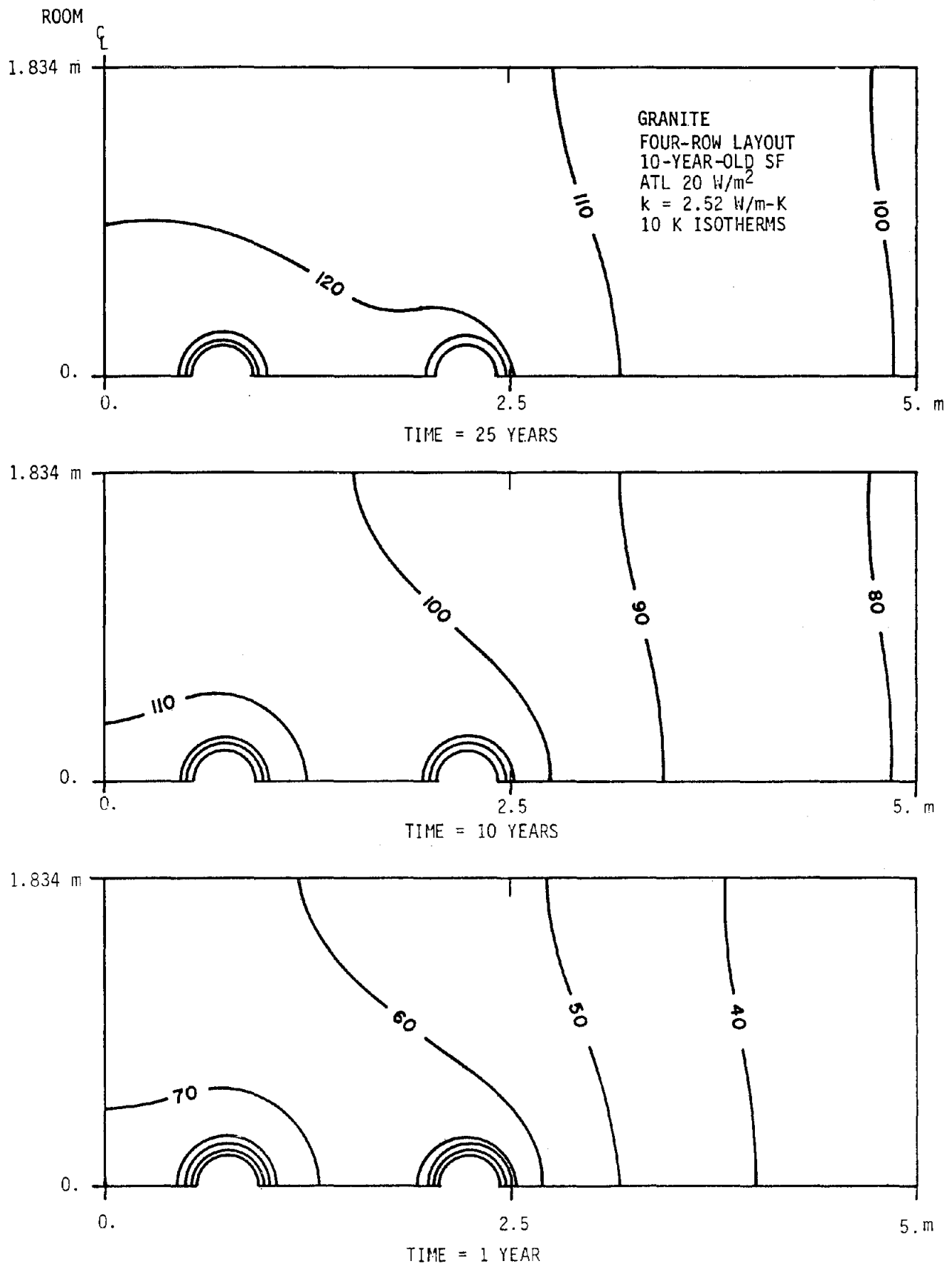
Figure 4-7. Temperature Rise Isotherms (°C) in VNF Region of a SF
            Repository in Granite. Four-Row Layout.

Table 4-1. Temperature Rises in VNF Region of a SF Repository (ATL = 20 W/m^2, Ambient Temperature = 20°C)

Granite Thermal Conductivity (W/m-K)	Drill Hole Edge		Canister Skin		Canister Centerline (Cladding)	
	Temp. Rise (°C)	Time (yrs)	Temp. Rise (°C)	Time (yrs)	Temp. Rise (°C)	Time (yrs)
Two-Row Layout						
1.75	101	1	143	1	175	1
	148	10	181	10	203	10
	160	25	185	25	201	25
2.52	77	1	116	1	152	1
	114	10	145	10	171	10
	125	25	149	25	169	25
3.29	63	1	99	1	137	1
	96	10	124	10	152	10
	106	25	127	25	150	25
Four-Row Layout						
1.75	101	1	143	1	175	1
	148	10	181	10	203	10
	160	25	185	25	201	25
2.52	77	1	117	1	153	1
	115	10	146	10	172	10
	127	25	151	25	170	25
3.29	63	1	99	1	137	1
	96	10	124	10	152	10
	106	25	127	25	150	25

Table 4-2. Temperature Difference Across Backfill in SF Repository With ATL = 20 W/m^2

Time (Years)	k_{bf} = .24 (W/m-K) 2 Rows ΔTemp.[a] (°C)	k_{bf} = .26 (W/m-K) 2 Rows ΔTemp.[a] (°C)	k_{bf} = .28 (W/m-K) 2 Rows ΔTemp.[a] (°C)
0.1	37.3	41.4	43.5
0.4	36.8	40.8	42.6
0.7	36.3	40.2	42.0
1.0	35.8	39.7	41.4
4.0	32.2	35.7	37.3
7.0	29.9	33.1	34.6
10.0	28.1	31.1	32.5
25.0	21.4	23.7	24.7
35.0	18.3	20.2	21.1

[a] Temperature increase from emplacement hole wall to canister surface.

Table 4-3. Temperature Rise as a Function of Distance From a Single Waste Canister
in a Large Granitic Mass With k = 2.52 W/m-K

Horizontal Distance	SF Temperature Rise (°C)		CHLW (700 W) Temperature Rise (°C)		DHLW Temperature Rise (°C)	
	1 Year	25 Years	1 Year	25 Years	1 Year	25 Years
Canister Centerline	72.06	43.86	131.98	64.50	81.94	50.02
Canister Skin	62.30	38.03	113.75	55.87	67.31	41.24
Drill Hole Edge	22.10	14.01	36.11	18.29	25.64	16.21
0.750 m	13.39	8.79	19.31	10.15	16.73	10.86
1.500	7.94	5.54	10.46	5.86	8.89	6.15
2.585	4.55	3.50	5.60	3.51	4.73	3.65
3.168	2.81	2.90	4.26	2.86	3.60	2.96
3.750	1.03	2.45	3.33	2.40	2.81	2.48
6.875	0.40	1.33	1.19	1.31	1.00	1.34
10.000	0.04	0.86	0.44	0.88	0.37	0.89
20.000	0.01	0.37	0.02	0.40	0.02	0.39
30.000	0.00	0.20	0.01	0.22	0.01	0.21
45.000	0.00	0.08	0.00	0.10	0.00	0.09
60.000	0.00	0.04	0.00	0.04	0.00	0.04
80.000	0.00	0.01	0.00	0.01	0.00	0.01
100.000	0.00	0.00	0.00	0.00	0.00	0.00

When the temperature rise profiles for the two-row configuration are compared for the 1.75 W/m-K and 3.29 W/m-K conductivities (Figure 4-8), it is clear that the lower conductivity causes significantly higher temperatures in the rock. On the other hand, the two-row layout produces nearly the same temperature rise as the four-row layout if the pitch is adjusted to give the same ATL (Figure 4-9). The outside canisters in the four-row layout are about 4 percent cooler than the inside canisters (Figure 4-9).

4.1.3 Very-Near-Field Thermal Environments in a CHLW Repository

The initial CHLW analysis considered 2,100 W waste canisters with an ATL of 25 W/m^2. Figures 4-10 and 4-11 show the thermal response as a function of time at the canister centerline, canister skin, and drill hole edge at the canister midplane. Some of the data is summarized in Table 4-4. The three granite thermal conductivities were 1.75, 2.52, and 3.29 W/m-K and the backfill thermal conductivity was 0.26 W/m-K. Figures 4-10 and 4-11 show the temperature rises for one row and two rows of waste canisters, respectively, while Figure 4-12 shows the temperature rises of a single waste canister in a large granitic mass. As with SF, the waste canister layouts (Figures 4-10 and 4-11) produce approximately the same temperature rises for a given thermal conductivity.

The temperature rises (Figures 4-10 and 4-11) range between 362°C and 456°C at the canister skin, depending on the granite thermal conductivity. The ambient temperature in the repository is 20°C, which would raise the canister skin temperature to a minimum of 382°C. Since this temperature would probably be excessive, design options which could reduce the temperature were examined.

One option for reducing the temperature rise would be to reduce the ATL by increasing the pitch between the waste canisters. This would reduce the temperature by a few degrees, but not by a large amount. The temperature rise for an individual canister without interaction from any other canisters is 325°C at the canister skin for the 3.29 W/m-K conductivity case (see Figure 4-12). This is only 37°C lower than the temperature rise for the one-row and two-row layouts. Therefore, for a canister loading of 2,100 W, most of the temperature rise at the canister skin is caused by the individual canister and not by the surrounding canisters. Other design options such as using a more conductive backfill material or increasing the diameter of the CHLW canister could reduce the temperatures in a 2,100 W canister.

Figure 4-?. Temperature Rise for a 550 W SF Canister as a Function of Distance From the Disposal Room Centerline at the Canister Midplane   Two-Row Layout.

Figure 4-9. Temperature Rise for a 550 W SF Canister as a Function of Distance From the Disposal Room Centerline at the Canister Midplane. Two-Row and Four-Row Layouts.
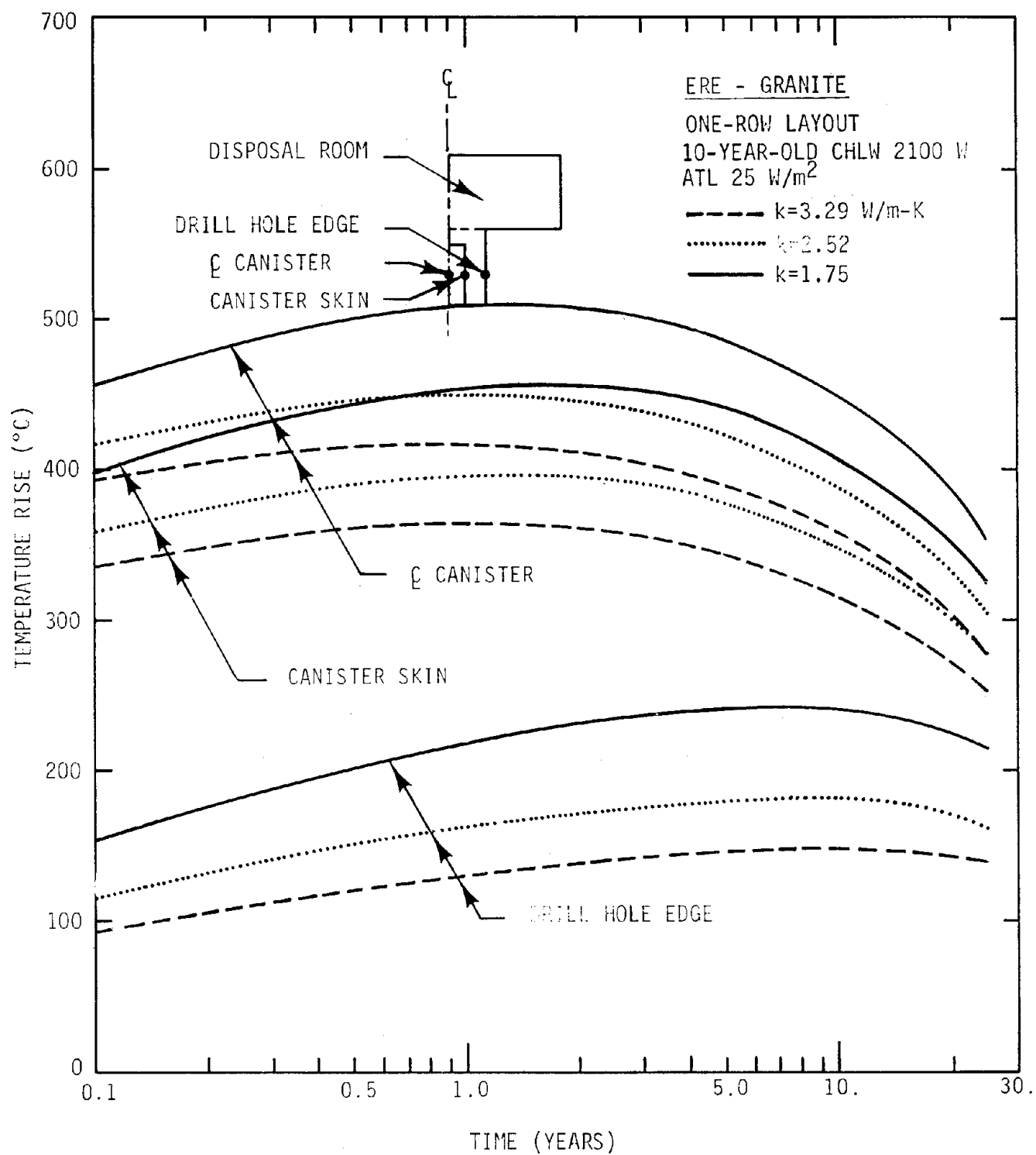
Figure 4-10.   VNF Thermal Response as a Function of Time for a CHLW Repository.
              One-Row Layout.
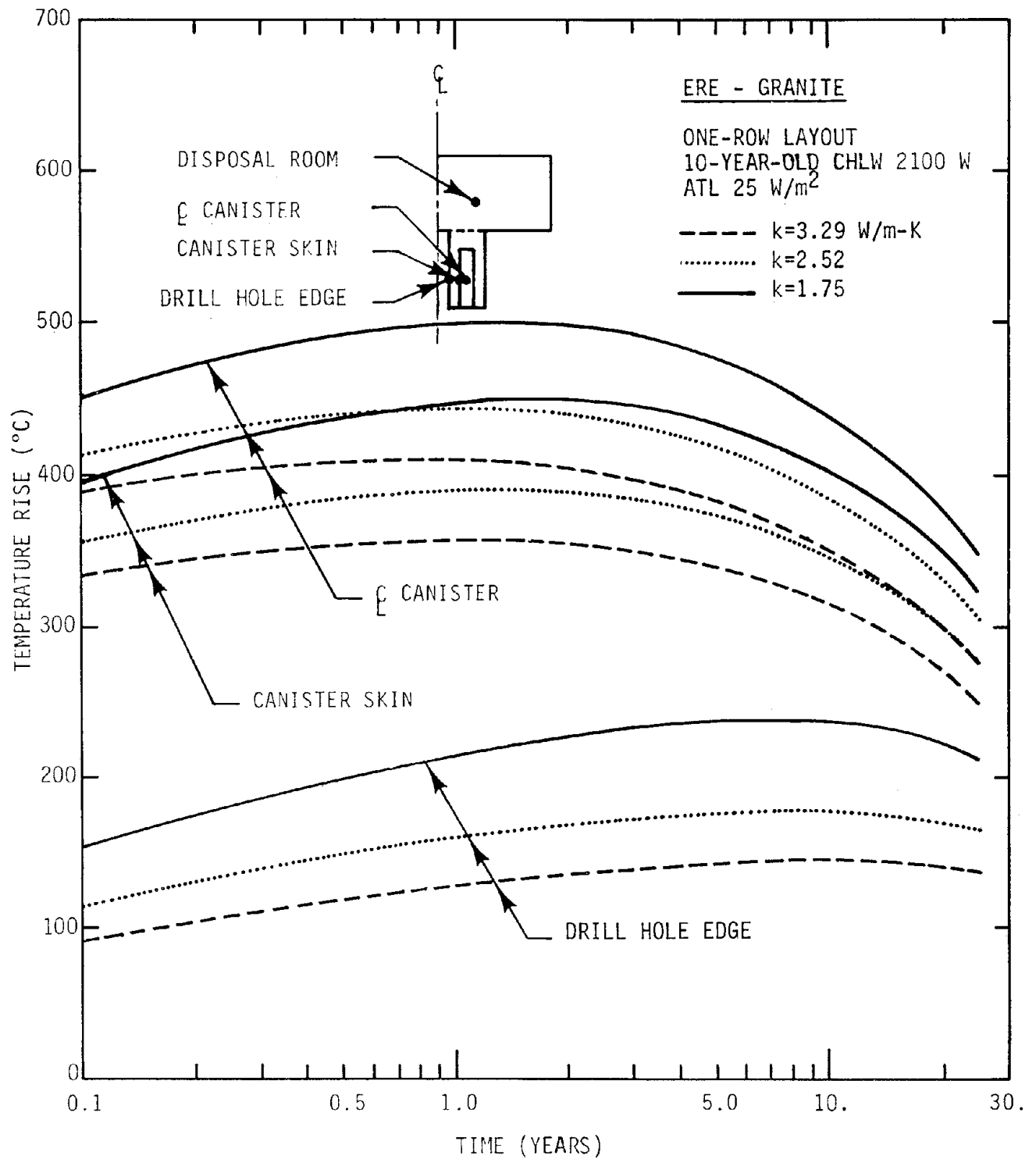
Figure 4-11.   VNF Thermal Response as a Function of Time for a CHLW Repository.
Two-Row Layout.
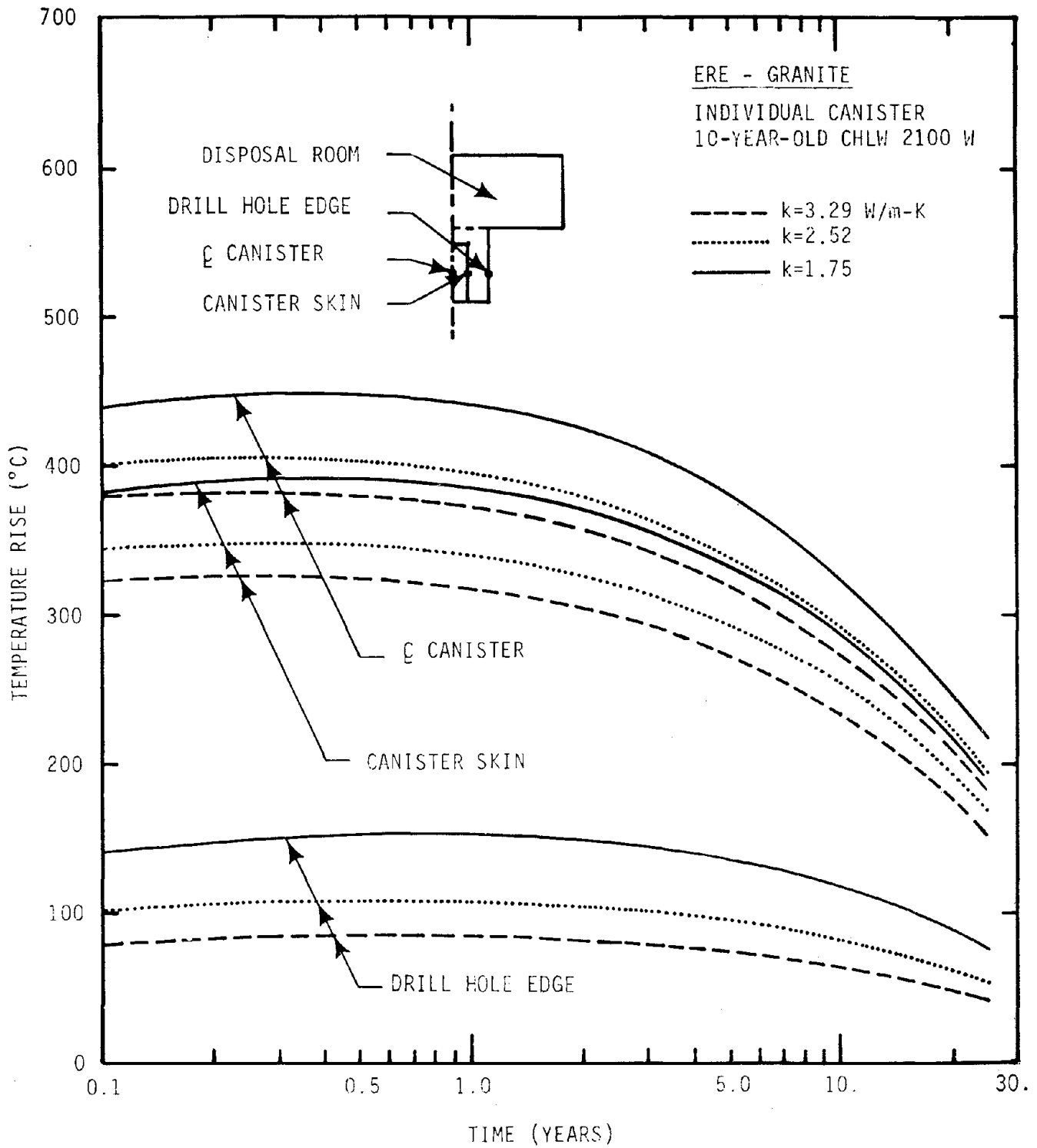
Figure 4-12. VNF Thermal Response as a Function of Time for an Individual Canister in a Large Granitic Mass.

Table 4-4. Temperature Rises in the VNF Region for CHLW and DHLW Repositories (ATL = 25 W/m^2, Ambient Temperature = 20° C)

	Granite Thermal Conductivity (W/m-K)	Drill Hole Edge		Canister Skin		Canister Centerline	
		Temp. Rise (°C)	Time (yrs)	Temp. Rise (°C)	Time (yrs)	Temp. Rise (°C)	Time (yrs)
CHLW 2,100 W Canister	2.52 (Two-Row Layout)	160.06	1	391.78	1	444.54	1
		179.15	10	348.15	10	386.63	10
		165.16	25	277.35	25	302.89	25
	2.52 (One-Row Layout)	163.06	1	396.08	1	450.86	1
		181.21	10	351.14	10	391.08	10
		166.51	25	279.32	25	305.84	25
CHLW 700 W Canister Two-Row Layout	1.75	133.41	1	210.46	1	228.47	1
		174.71	10	230.90	10	244.04	10
		171.19	25	208.50	25	217.22	25
	2.52	100.63	1	178.00	1	196.10	1
		135.82	10	192.24	10	205.44	10
		136.14	25	173.60	25	182.36	25
	3.29	81.62	1	159.16	1	177.30	1
		113.55	10	170.09	10	183.32	10
		115.48	25	153.02	25	161.80	25
DHLW 575.8 W Canister Two-Row Layout	1.75	128.18	1	168.60	1	180.10	1
		190.22	10	223.33	10	232.70	10
		202.47	25	226.73	25	233.60	25
	2.52	96.38	1	138.43	1	150.93	1
		148.34	10	181.97	10	192.21	10
		161.29	25	185.94	25	193.44	25
	3.29	79.38	1	120.77	1	133.83	1
		124.21	10	158.12	10	168.82	10
		137.00	25	161.86	25	169.70	25

Another way to reduce the canister-skin temperature is to lower the canister thermal loading by diluting the waste in a canister. A thermal analysis was conducted using a 700 W canister thermal loading and an ATL of 25 W/m^2. This canister loading and ATL results in temperature peaks similar to DHLW and SF. Figures 4-13 and 4-14 show the thermal response as a function of time for 700 W CHLW canisters at the three observation points. Comparing the results of a two-row layout (Figure 4-13) with the results for a single canister (Figure 4-14) shows that with the 700 W canister, the surrounding canisters contribute a much higher percentage of the total temperature rise. These results are similar to the SF and DHLW analyses, but not to the CHLW 2,100 W analysis.

Temperature in a CHLW waste package also peaks earlier than those in SF and DHLW (Figure 4-13) and the temperature peaks are narrower. The canister center-line peak temperature for CHLW occurs at approximately 5 years, the canister skin at approximately 8 years, and the drill hole edge at approximately 17 years; compared to 15, 20, and 30 years, respectively, for SF; and 17, 20, and 27 years, respectively, for DHLW at the same observation points. The maximum temperature rises at the three observation points again vary slightly due to the different conductivity values.

The temperature rise contours (Figure 4-15) for a 700 W CHLW canister for a conductivity of 2.52 W/m-K illustrate the steep temperature gradient near the canister. Plots of temperature rise versus horizontal distance from the room centerline (Figures 4-16 and 4-17) show that the temperature gradients are very high in the backfill and considerably lower in the rock.

4.1.4   Very-Near-Field Thermal Environments in a DHLW Repository

Figure 4-18 illustrates the thermal response as a function of time for three granite conductivities and two rows of DHLW canisters. Some of the data are also summarized in Table 4-4. The backfill conductivity is 0.26 W/m-K and the canister midheight temperature rises shown are at the canister centerline, canister skin, and drill hole edge. The temperature rise peaks at these observation points occur at approximately 17, 20, and 27 years, respectively, and show the sustained temperature rise peaks that were also noted for SF.

The temperature rise contours (Figure 4-19) show the progression of the isotherms at 1, 10, and 25 years for a conductivity of 2.52 W/m-K. The contours
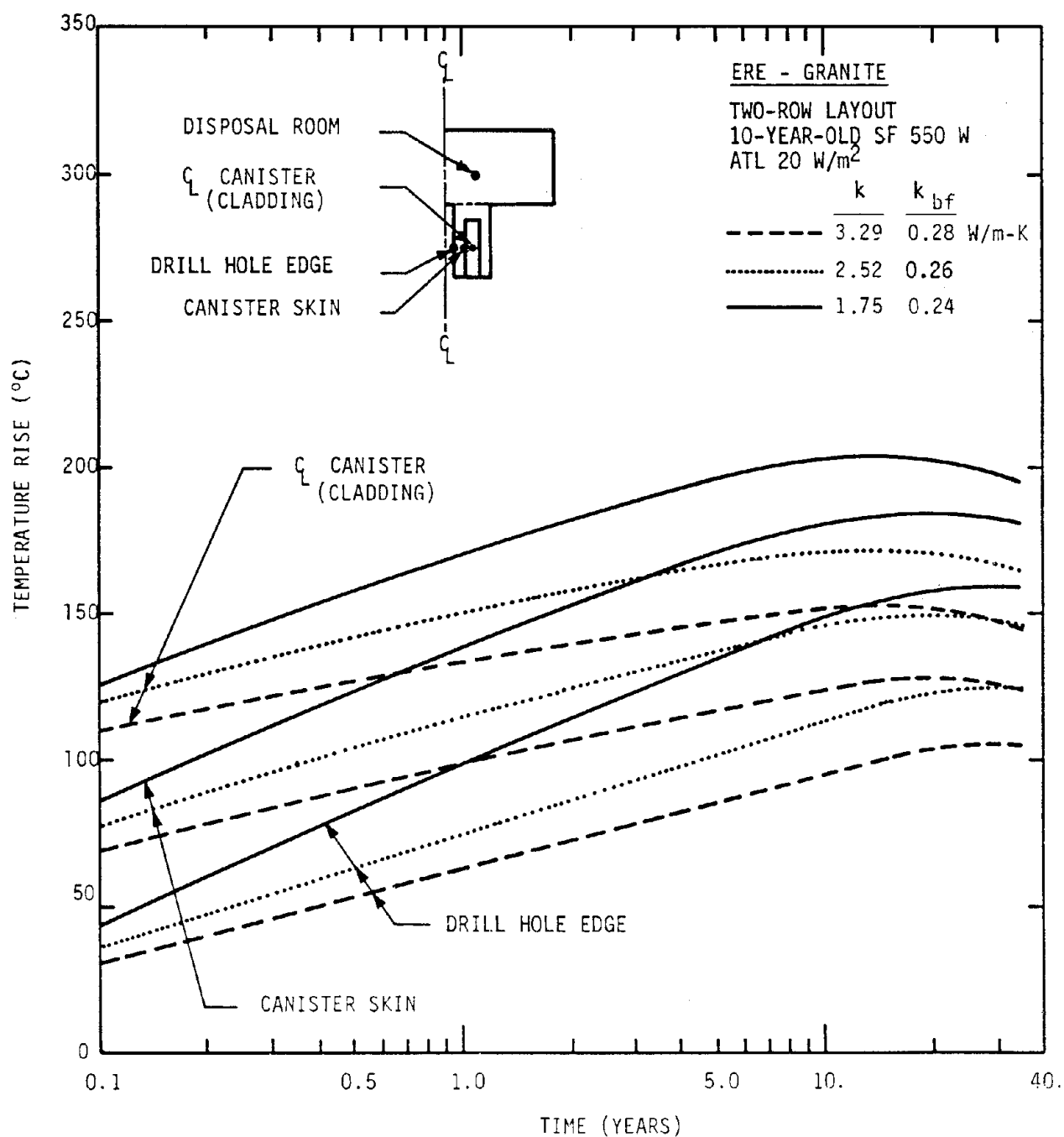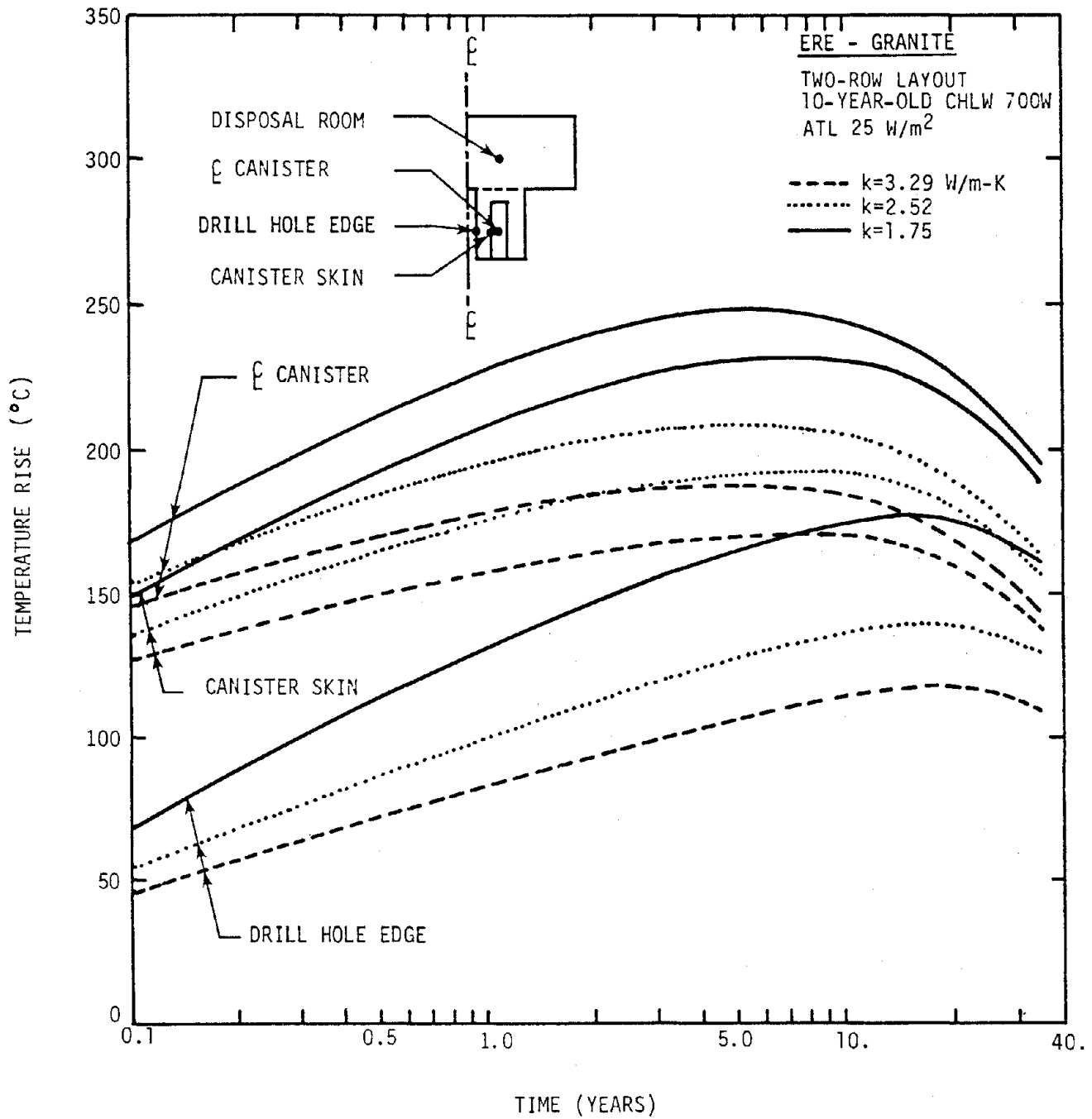
Figure 4-13.   VNF Thermal Response as a Function of Time for a CHLW
                Repository. Two-Canister Layout.
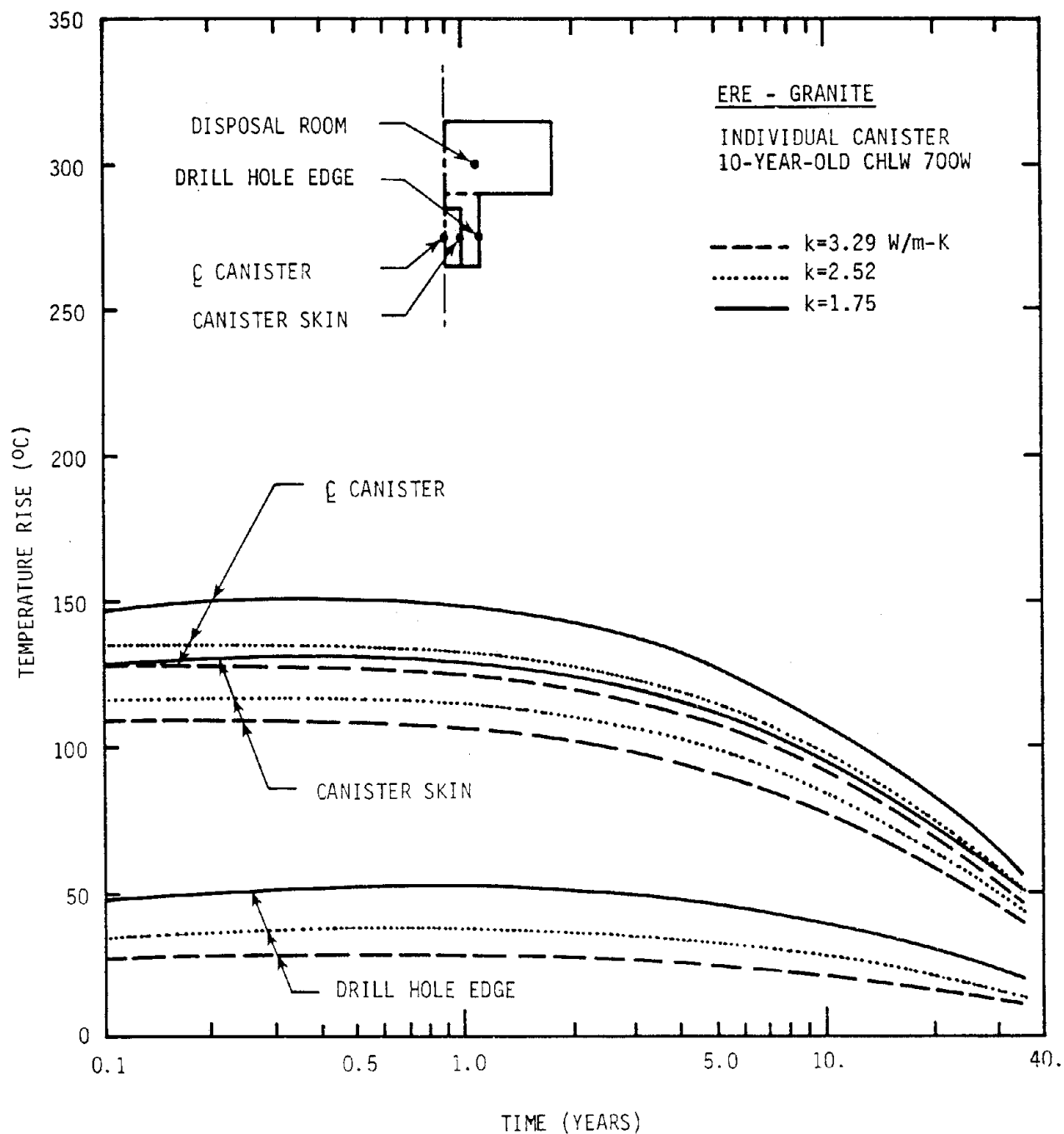
Figure 4-14.   VNF Thermal Response as a Function of Time for an Individual
               Canister in a Large Granitic Mass.
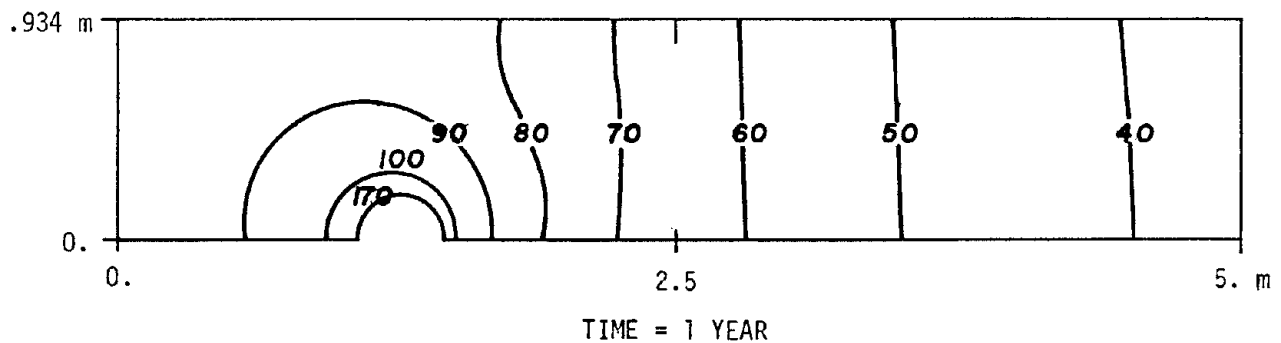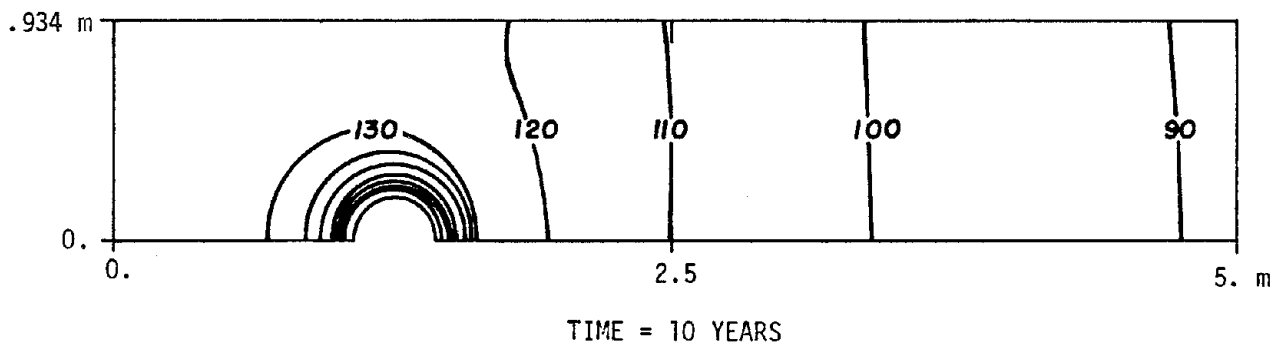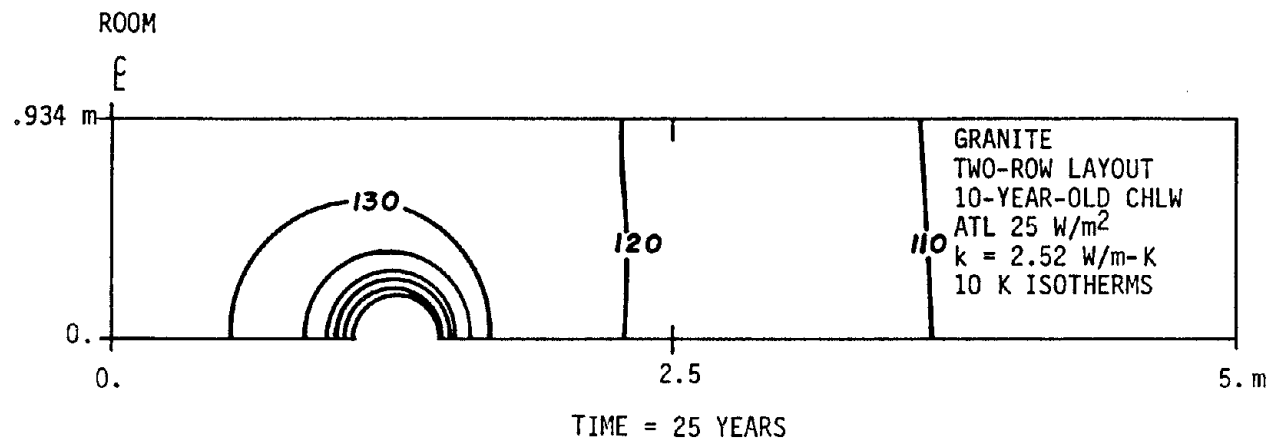
Figure 4-15. Temperature Rise Contours (°C) in VNF Region of a CHLW Repository.
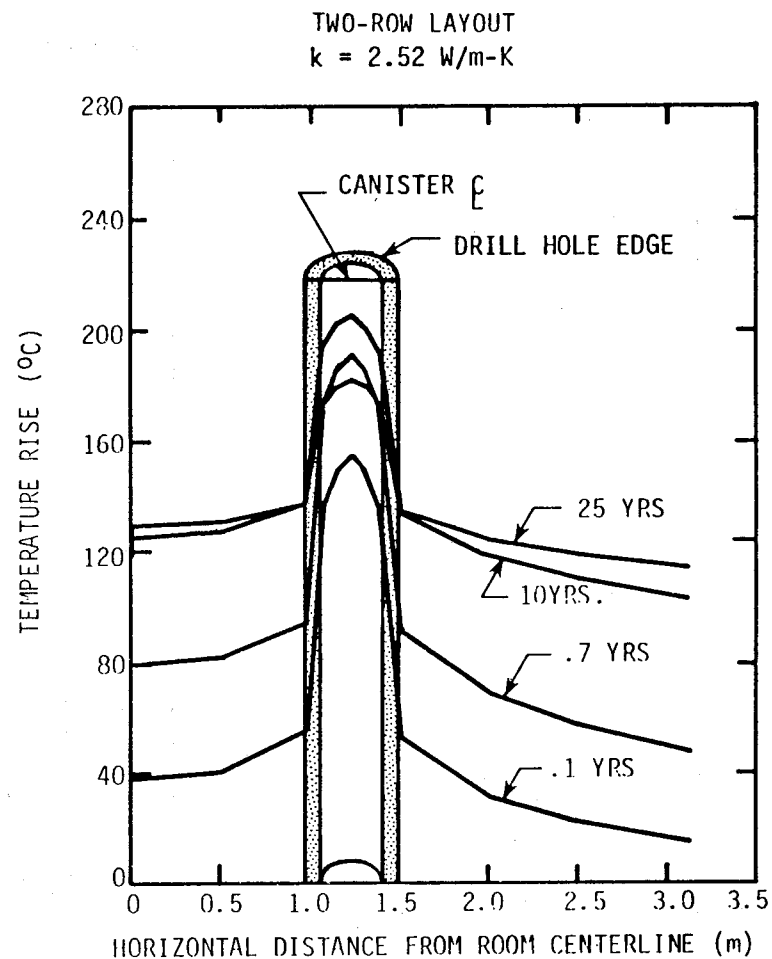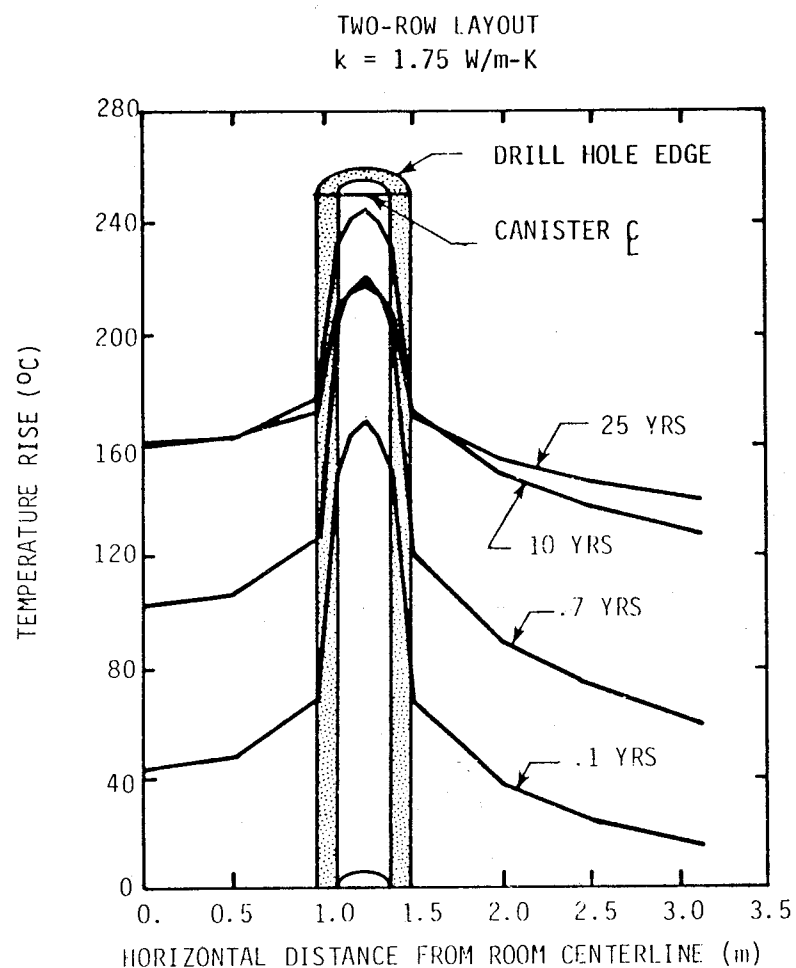
Figure 4-16. Temperature Rise for a 700 W CHLW Canister as a Function of Distance From the Disposal Room Centerline at the Canister Midplane.
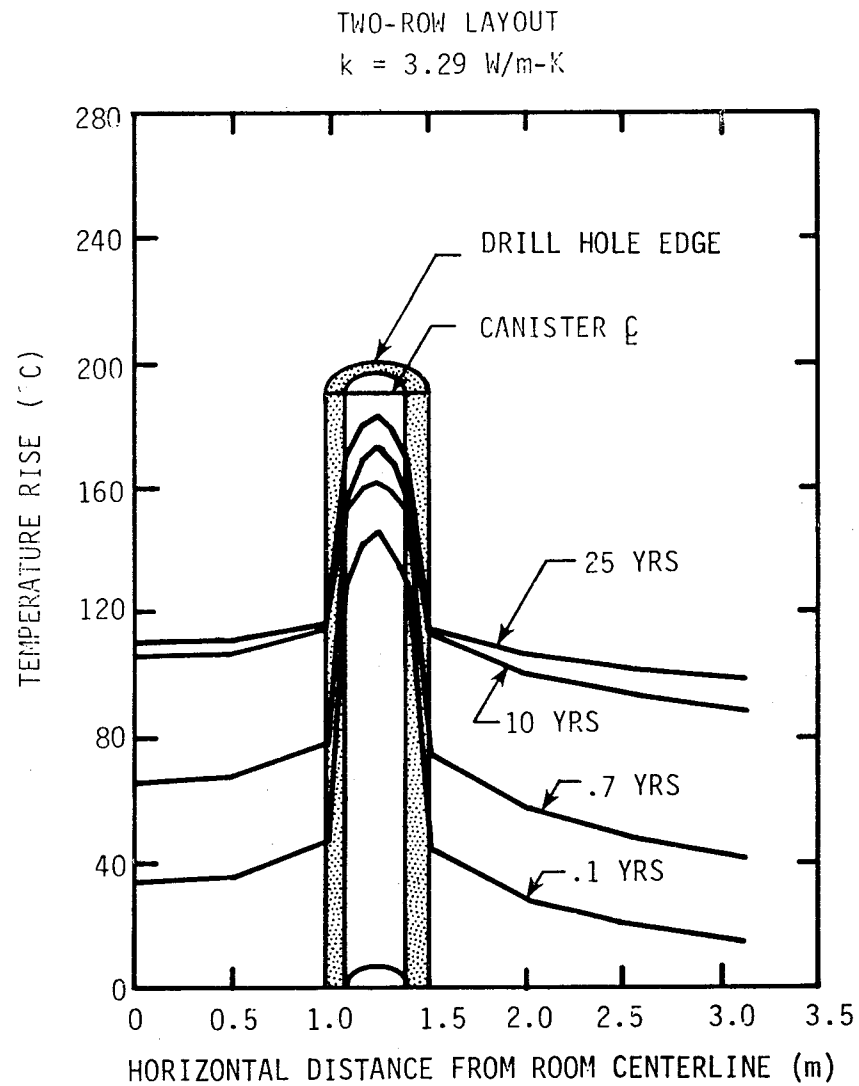
Figure 4-17. Temperature Rise for a 700 W CHLW Canister as a Function of Distance From the Disposal Room Centerline at the Canister Midplane.

66
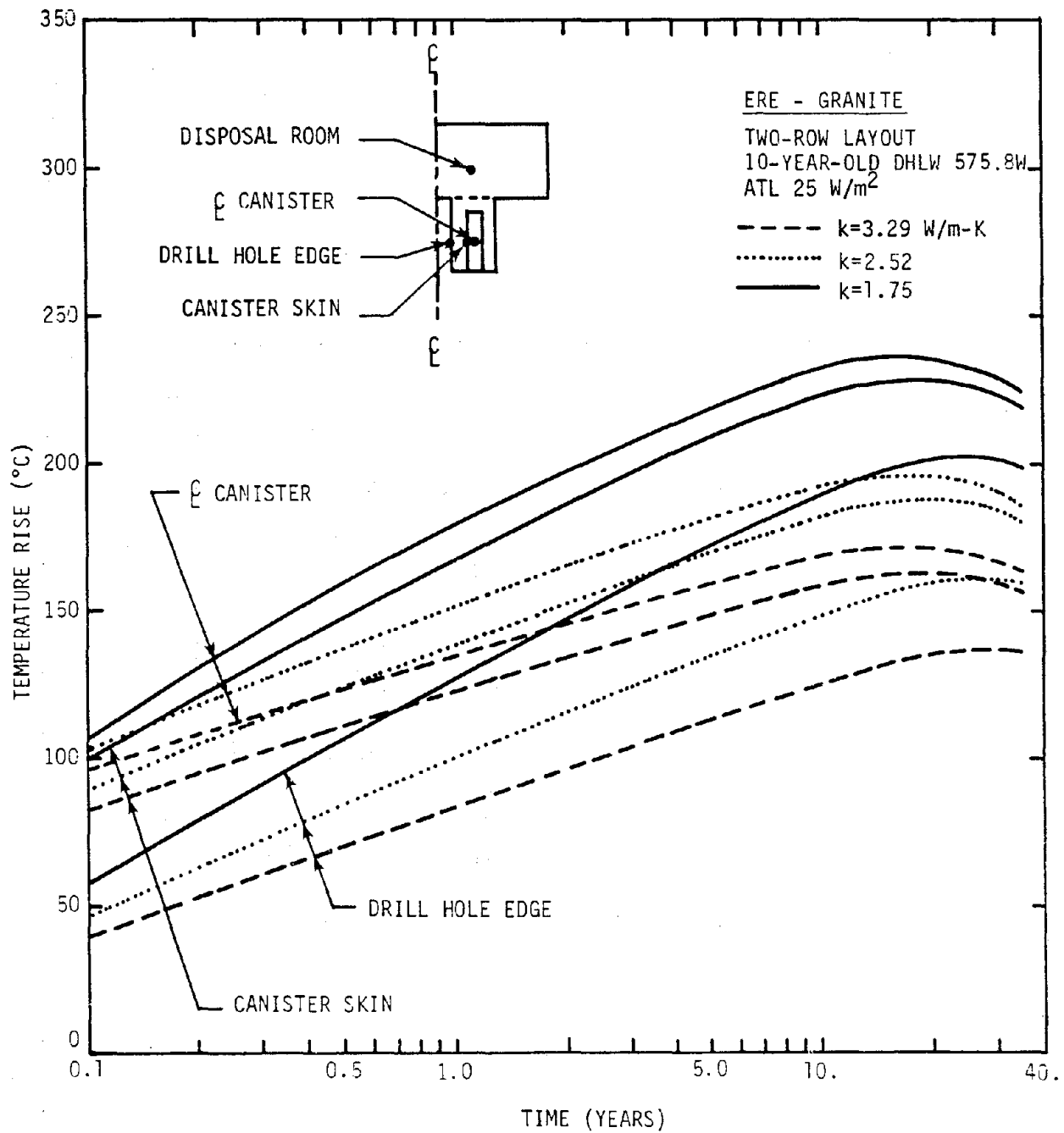
Figure 4-18.   VNF Thermal Response as a Function of Time for
             Repository. Two-Row Layout.

ROOM

.768 m

150   140   GRANITE
TWO-ROW LAYOUT
10-YEAR-OLD DHLW 130
ATL 25 W/m^2
k = 2.52 W/m-K
10 K ISOTHERMS

0.

0.   2.5   5. m

TIME = 25 YEARS

.768 m

140   130   120   110   100

0.

0.   2.5   5. m

TIME = 10 YEARS

.768 m

90   90   80   70   60   50   40

0.

0.   2.5   5. m

TIME = 1 YEAR
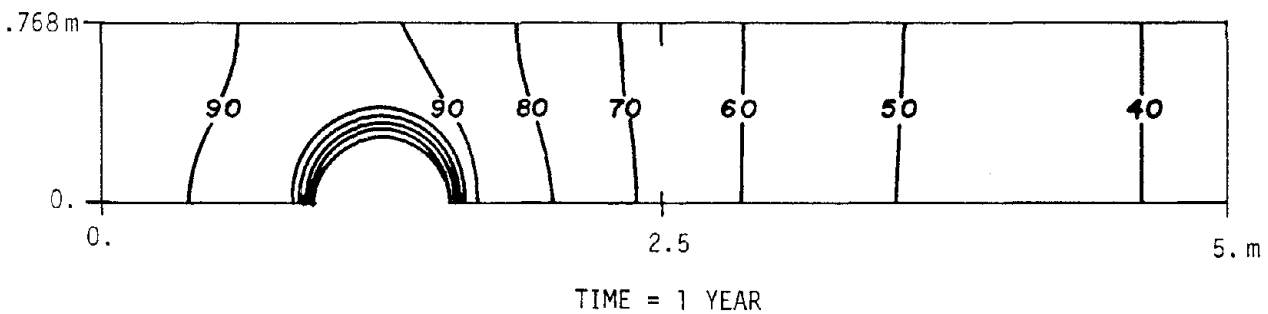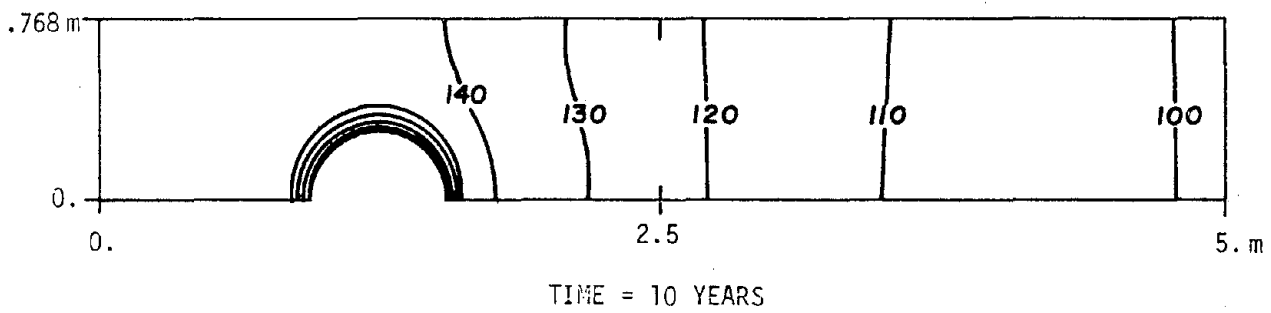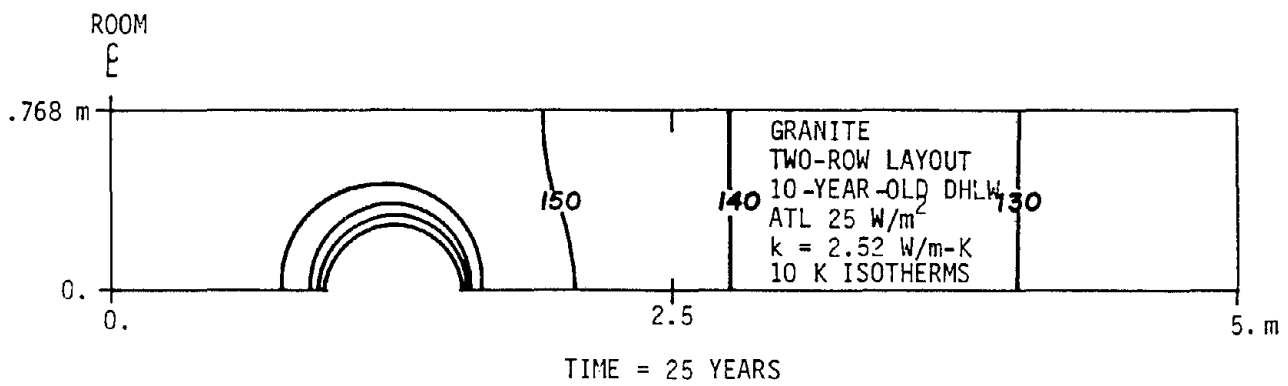
Figure 4-19.   Temperature Rise Isotherms (°C) in VNF Region of a DHLW
               Repository in Granite.

for SF (Figure 4-6) and CHLW (Figure 4-15) are similar to the DHLW contours at one year. During the first few years, the temperature rises in the area very close to the canister skin are influenced mainly by the initial canister thermal loading, while the temperature rises farther away from the canister skin are affected mainly by the initial ATL. As time progresses, the canister thermal loading and the ATL decrease as a function of the decay characteristics of the waste material. Comparing the three figures shows that at one year the temperatures immediately around the waste canister are much higher for CHLW compared to DHLW and SF. This is because of the initial canister loading of 700 W for CHLW, compared to 575.8 W for DHLW, and 550 W for SF. DHLW and CHLW both have an initial ATL of 25 W/m^2, while SF has an initial ATL of 20 W/m^2. The figures show that at one year the temperatures farther away from the canister for DHLW and CHLW are approximately the same because of the same initial ATL and the isotherms for SF are 10°C to 20°C lower because of the lower initial ATL.

The isotherms for DHLW at one year have progressed outward slightly more than those for CHLW as can be seen by comparing the 70°C isotherms. This is due to the waste decay characteristics shown in Figure 3-1, which shows that the CHLW decays faster than the DHLW.

The effect of waste decay becomes more apparent at 10 and 25 years. At 10 years, the CHLW canister skin is only 10°C higher than the DHLW canister skin, compared to a 40°C difference at one year. This is because the CHLW is losing power much faster than the DHLW. Even though the temperatures near the canister are still higher for CHLW, the temperatures farther away from the canister are higher for DHLW. This is because the ATL for CHLW at 10 years has decreased from 25.0 to 17.3 W/m^2, while the ATL for DHLW has only decreased from 25.0 to 20.0 W/m^2. At 25 years, the DHLW is hotter both near the canister skin and farther away from the canister skin compared to CHLW because of its slower decay characteristics.

The SF temperatures are not higher than any of the DHLW or CHLW temperatures during the first 25 years. However, at 25 years the SF isotherms are approximately 5°C lower than CHLW temperatures at approximately 3 m from the canister. The SF canister loading and ATL will eventually be higher than that of CHLW and even DHLW due to its slower decay in later years.

Figure 4-20 shows the temperature rises as a function of radial distance from the room centerline for conductivities of 1.75 and 2.52 W/m-K, while Figure 4-21 shows the temperature rises for a granite conductivity of 3.29 W/m-K. As
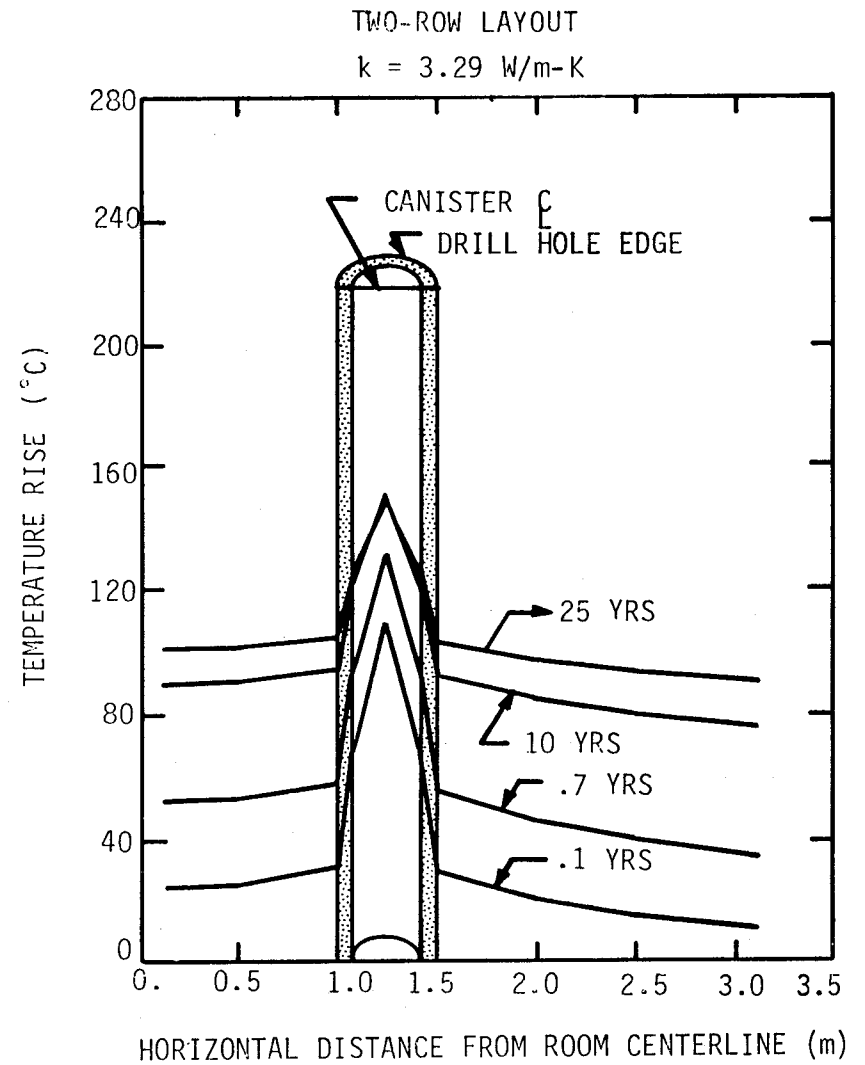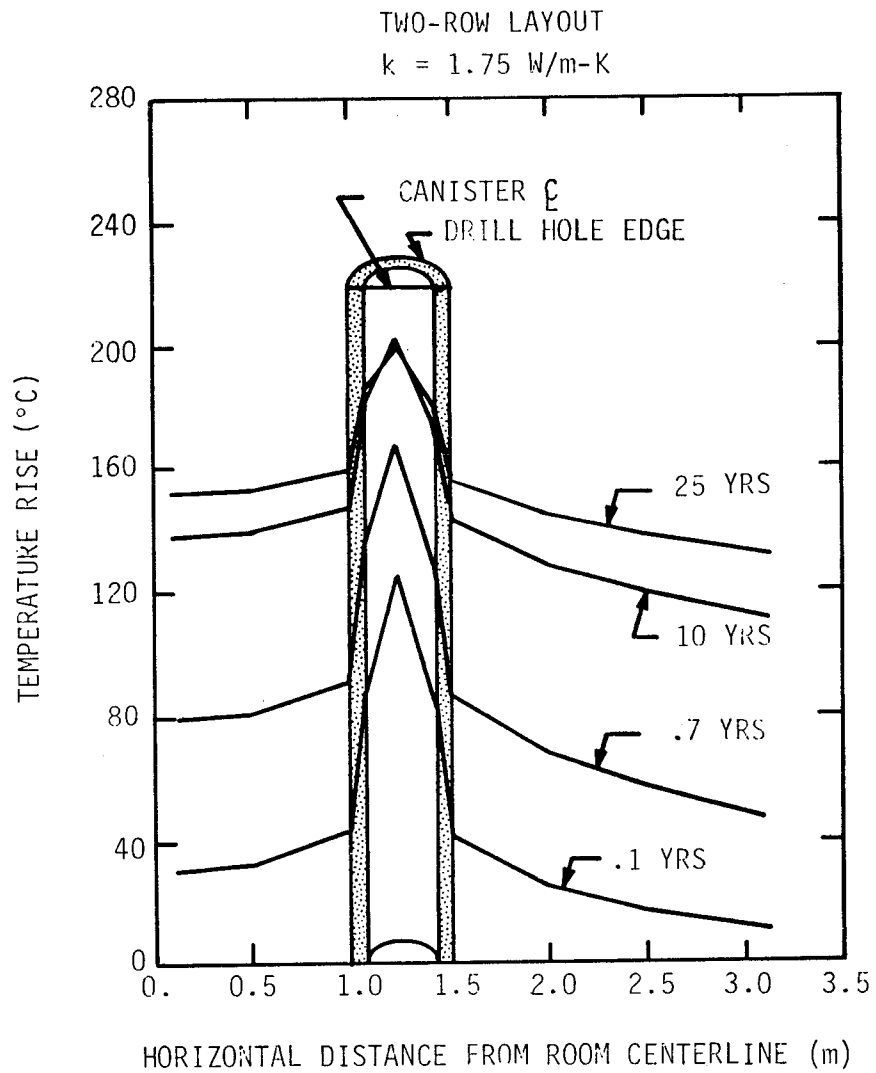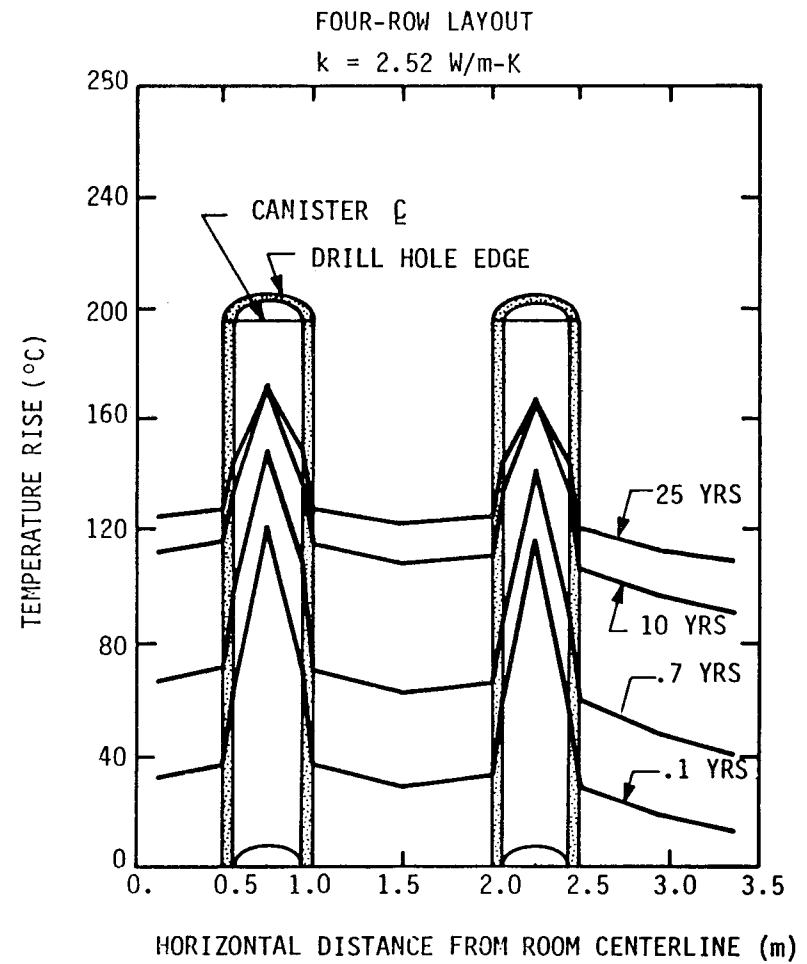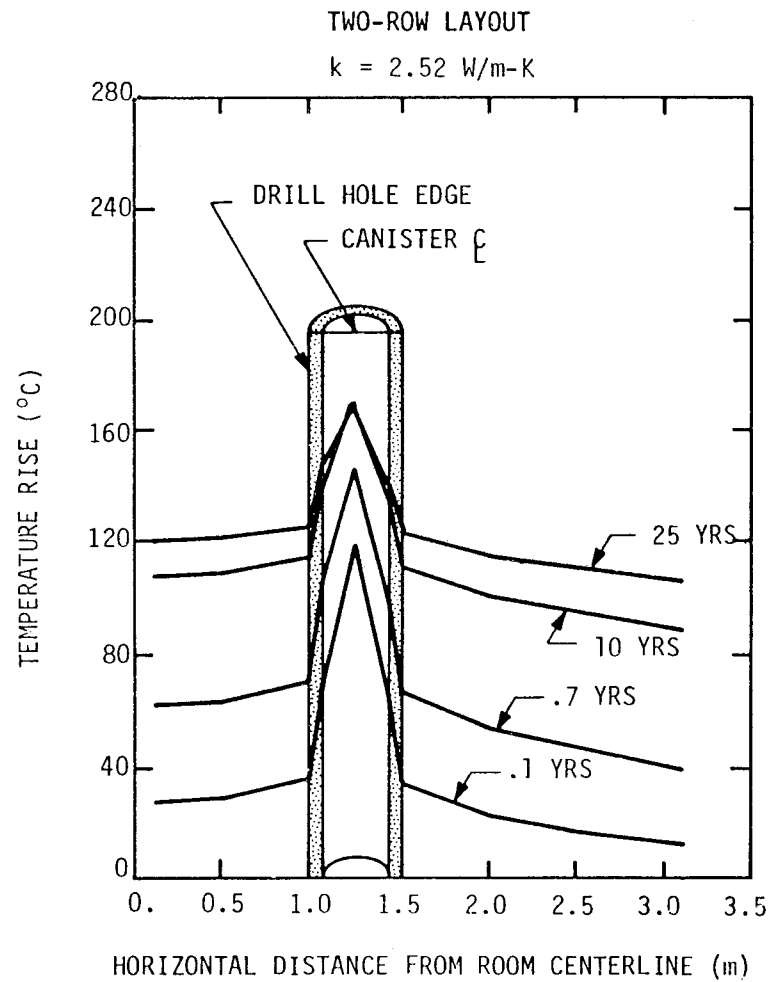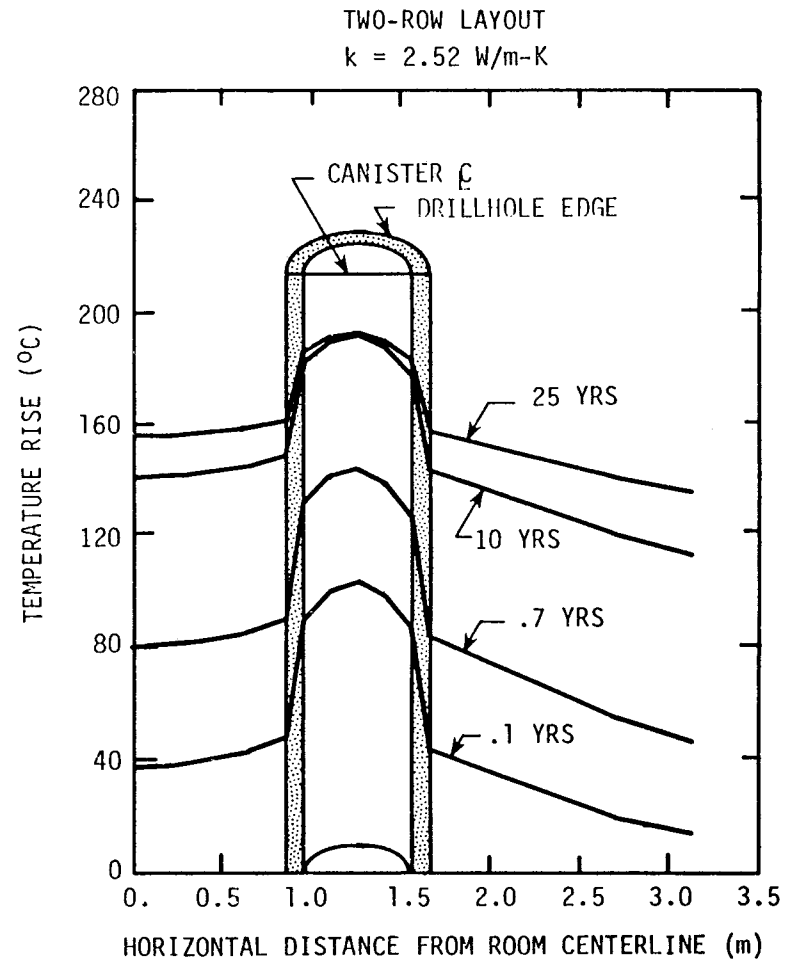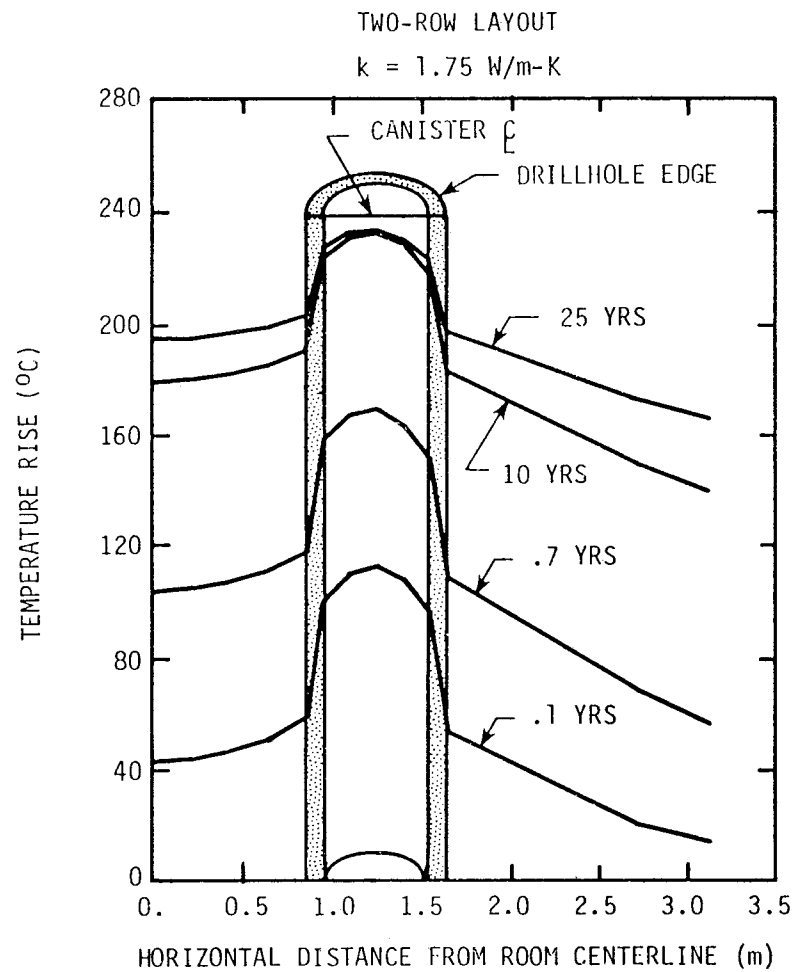
Figure 4-20. Temperature Rise for a 575.8 W DHLW Canister as a Function of Distance From the Disposal Room Centerline at the Canister Midplane.

TWO-ROW LAYOUT

k = 3.29 W/m-K
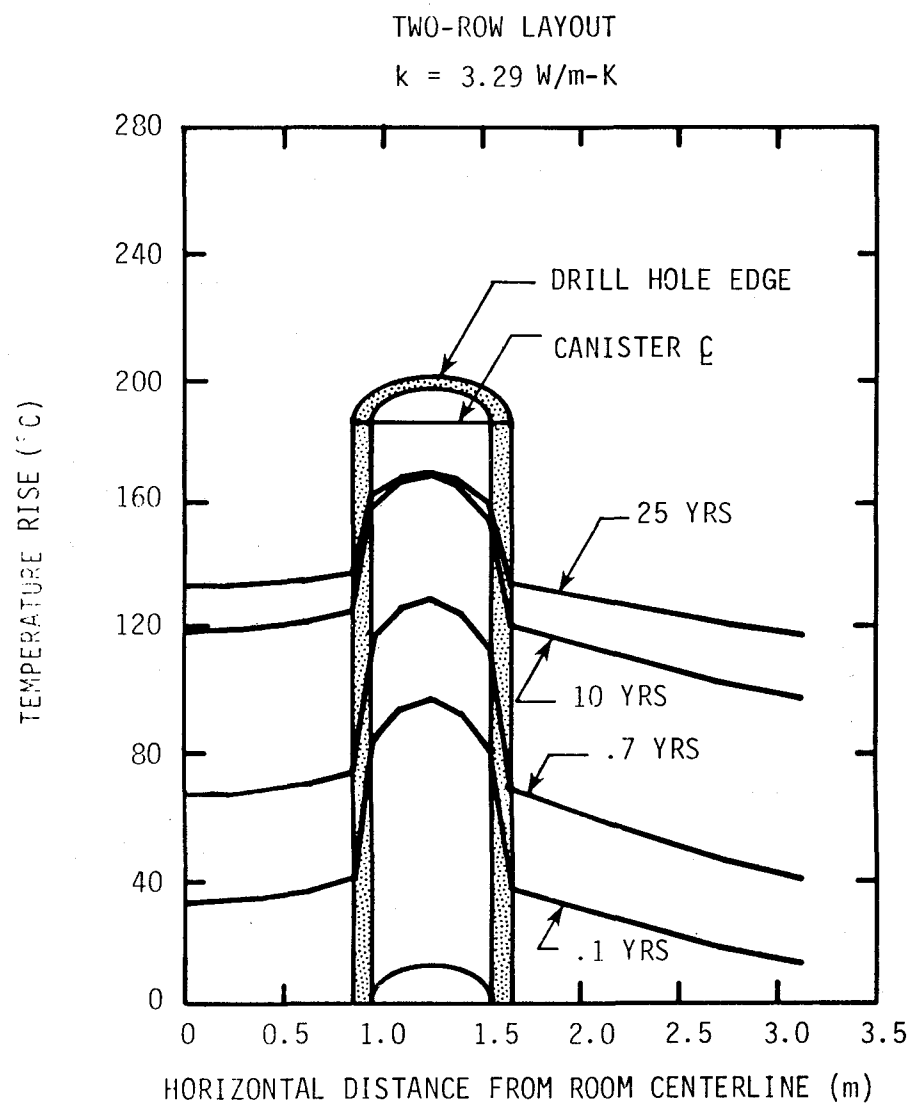
expected, the lower the thermal conductivity is, the higher the temperatures are in and near the canister.

4.2 NEAR-FIELD ANALYSES OF HEAT TRANSFER

4.2.1 Near-Field Modeling Methods

The near-field (NF) region is defined as the rock mass which contains the disposal room-and-pillar and extends one or two pillar widths above and below the disposal room. This particular NF analysis considers three parameters: waste type, thermal conductivity, and canister arrangement (Table 4-5). Both the CHLW and DHLW analyses assumed an initial areal thermal loading of 25 W/m^2; whereas, the SF calculations assumed an areal thermal loading of 20 W/m^2. The 20 percent reduction in thermal loading for the spent fuel provides closer agreement in total thermal energy produced over time since the decay of spent fuel is more gradual than for either of the two high-level waste types.

The physical description of the two-dimensional model used in the numerical (finite element) NF thermal analyses is shown in Figure 4-22. Only half of the room and pillar are included in the model because the room centerline and the pillar centerline are symmetry planes. The vertical boundaries are adiabatic, and a time-dependent heat flux is specified along the upper and lower boundaries. These upper and lower boundary conditions provide approximately the same heat removal rate as an infinitely long model. A discussion of this approximation for the upper and lower boundaries and its validity has been published previously [Wagner, 1980]. The ambient room temperature of this model was assumed to be 20°C based on a repository depth of 1,000 meters, which corresponds to a geothermal gradient of 20°C/km.

The NF model (Figure 4-22) consists largely of granite with other materials designated for the disposal room and waste canister. The thermal properties of the host rock (granite), backfill (crushed granite), disposal room air, and waste canister used in the NF analysis are presented in Section 2, with the exception of the thermal conductivity of the disposal room air. Discussion concerning the thermal conductivity of the disposal room air is required since a modified value was chosen. This modified value of thermal conductivity more realistically simulates the dominant heat transfer processes (both radiation and

Table 4-5. Parameter Matrix - NF Thermal Analysis

Waste Type	Thermal Conductivity of the Host Rock (Granite) W/m-K	Number of Canister Rows
CHLW	2.52	1
SF	3.29	2
DHLW	1.75	
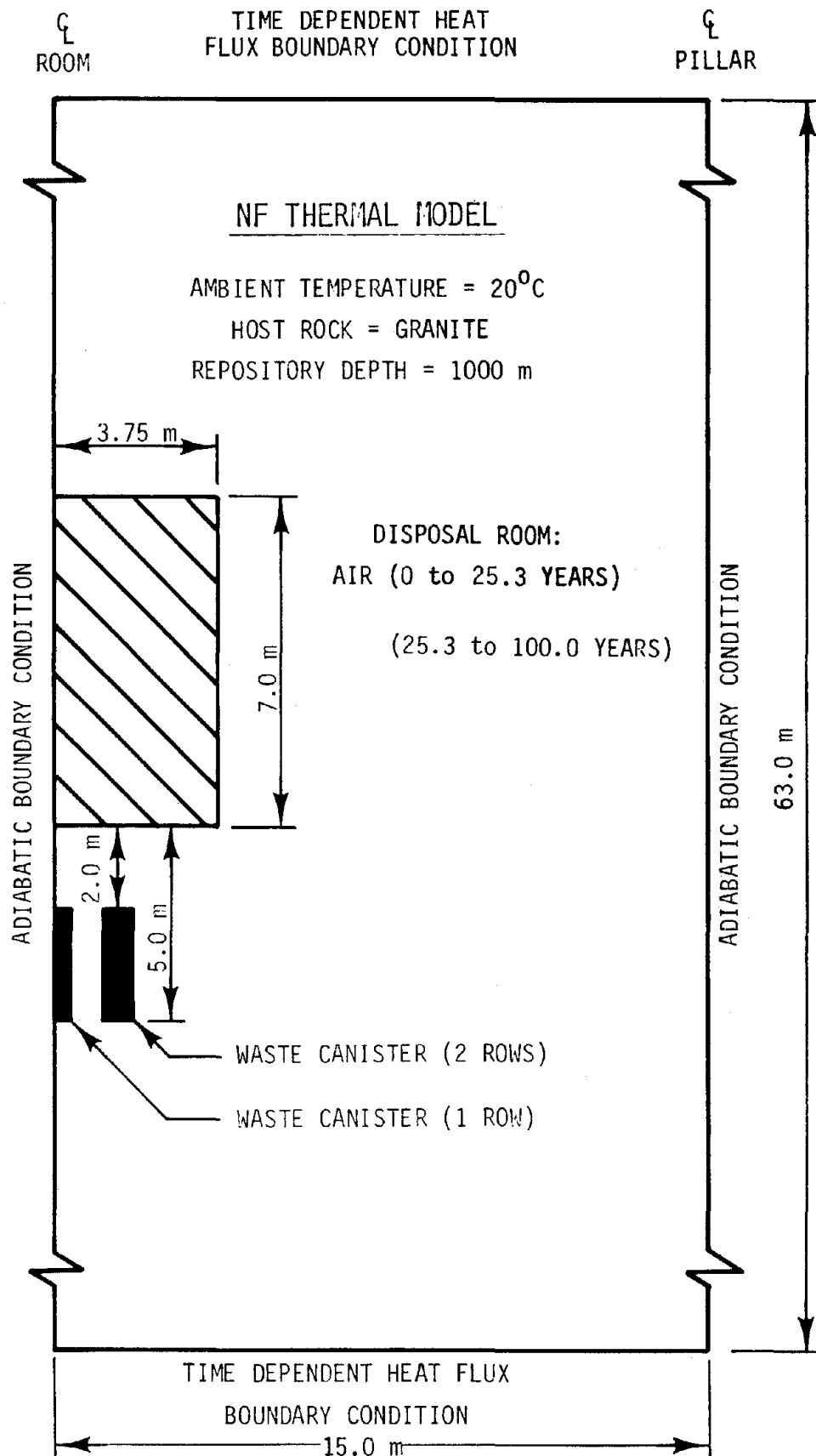
Figure 4-22. Two-Dimensional Model Used in the NF Thermal Analyses.

conduction) existing in the sealed and unventilated disposal room the first 25 years after waste emplacement. Briefly, the heat transfer through the sealed and unventilated disposal room during the initial 25 years was investigated by considering various values of thermal conductivity in the disposal room and radiative transfer from floor to roof. The investigation showed that after a specific increase in thermal conductivity of the disposal room air, the magnitude could be greatly increased without significantly affecting the room temperature. The chosen "effective" thermal conductivity of the disposal room is approximately 2,700 times greater than thermal conductivity of air. This somewhat arbitrary and seemingly large value of thermal conductivity provides close agreement in the roof and floor temperatures predicted from the modeling of one-dimensional radiative heat transfer. Further discussion of the selection of the effective thermal conductivity in the disposal room is presented in Appendix B.

The NF thermal analysis predicts the temperature distributions for 100 years after waste canister emplacement. During the initial 25 years after emplacement, the disposal room was assumed to be sealed, unventilated, and unbackfilled. Subsequently, the disposal room requires ventilation to reduce the room temperature such that backfilling operations can commence. One hundred days of blast cooling has been assumed as a reasonable amount of time for the disposal room temperatures to decrease to an acceptable level. The ventilation of the disposal room was simulated with a convective film coefficient, h, of 11.35 W/m^2-K. This value represents twice the measured value in a typical underground mine [Van Sambeek, 1979]. The increase in ventilation simulates the blast cooling effect in the disposal room. The modeling of ventilation assumes the rate of heat removal is constant throughout the length of the disposal room (i.e., the removal of heat does not increase the temperature of the room air which would retard the rate of heat removal). Therefore, the ventilation period may be longer than the 100 days investigated in this study. Upon completion of the backfilling operation with crushed granite, the disposal room was assumed once again to be sealed, unventilated and undisturbed for the balance of the 100 years. Also, the backfill material was assumed to occupy 100 percent of the disposal room.

4.2.2 Near-Field Thermal Environments in a SF Repository

Figure 4-23 shows the time history of temperature rise along the room periphery at three locations for the three values of the granite thermal conductivity. The three locations along the room periphery (floor centerline, roof centerline, and rib midheight) provide an indication of thermal behavior within the disposal room. The temperature rises very rapidly along the room periphery in the initial 25 years after waste emplacement. During this period, the temperature rise along the room, rib, and floor is nearly the same ($\pm$ 2°C) difference. After 25 years, the disposal room is ventilated for approximately 100 days. This ventilation reduces the room periphery temperature rises by at least 70°C, so that the room periphery temperature is 5°C above ambient temperature. This should provide favorable working conditions required for the backfilling of the disposal room. Following the reduction in the room temperature, the crushed granite is assumed to be placed in the disposal room. Thereafter, the thermal response (Figure 4-23) indicates a greater variation in room periphery temperatures than was observed in the initial 25 years after waste emplacement. The addition of crushed-granite backfill retards the heat transfer through the room. This response is because of the reduction of the thermal conductivity and the elimination of radiative heat transfer within the disposal room.

The maximum temperature rise and time of occurrence for the three conductivity values at each of the three designated room periphery locations (Figure 4-23) is presented in Table 4-6. The maximum temperature rise in the floor is reached at approximately 50 years; whereas, the maximum temperature rise in the rib and roof occur at approximately 95 years. The close agreement in the maximum temperature rise and its time of occurrence between the rib and roof locations indicates the transfer of heat through the pillar is considerable and greatly influences the temperature along the rib and roof. This behavior along the rib and roof contrasts the thermal response along the floor where the heat transfer medium in the disposal room (crushed granite) largely influences the predicted temperatures in the floor. Table 4-6 indicates the sensitivity of changes in the thermal conductivity of the host rock. Again, the change in conductivity influences the temperature rise along the floor (approximately 40 percent) more than for either rib or roof (approximately 20 percent).
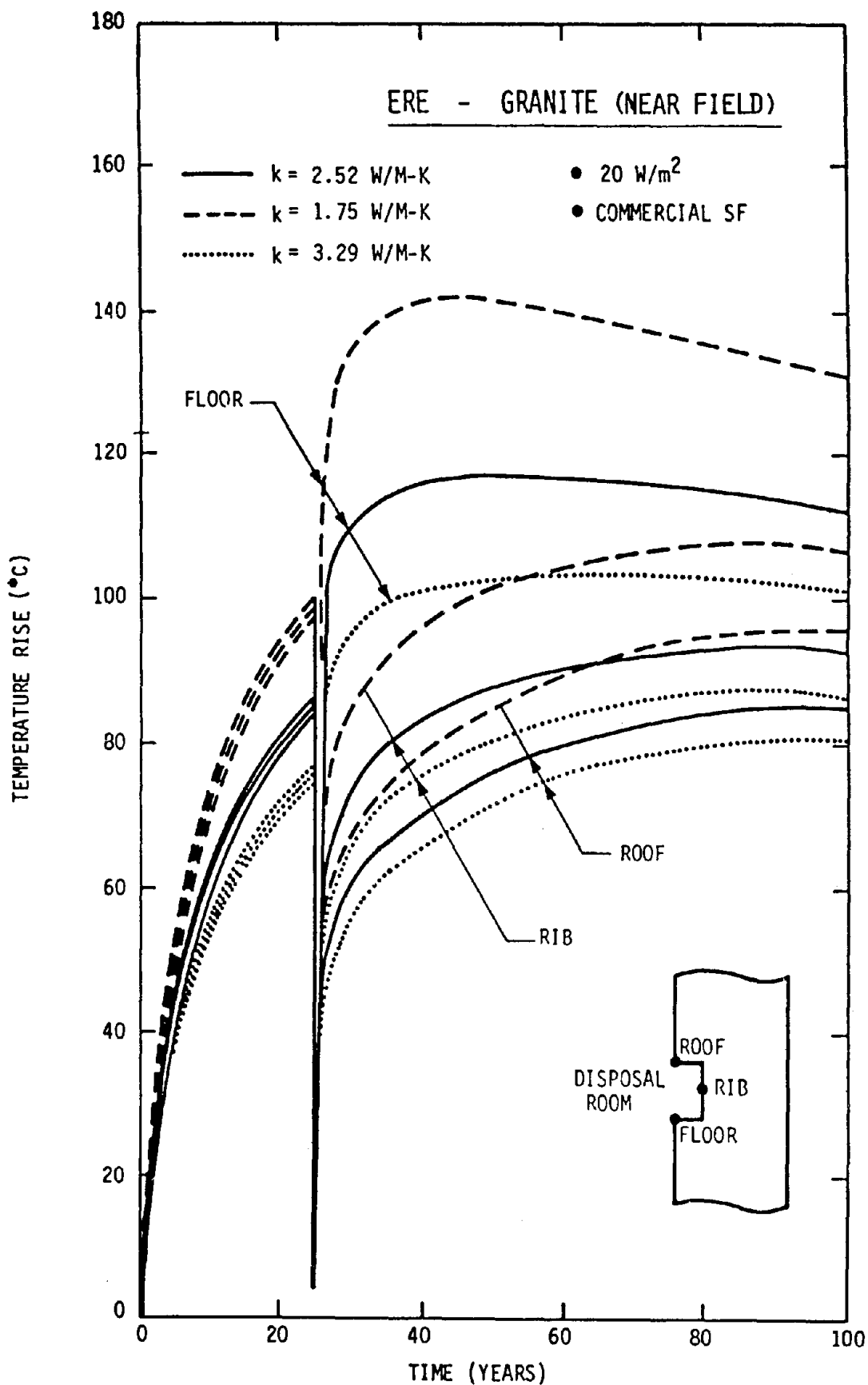
Figure 4-23. Time History of Temperature Rise From a Near-Field Analysis
Involving Three Values of Thermal Conductivity and Spent Fuel.

Table 4-6. Maximum Temperature Rise Along Room Periphery (SF)

Location[a]/Conductivity (W/m-K)	Maximum Temperature Rise (°C)	Time (Years)
Floor:		
1.75	142	45
2.52	118	50
3.29	104	65
Rib:		
1.75	108	85
2.52	93	100
3.29	88	90
Roof:		
1.75	97	95
2.52	86	95
3.29	81	95

(a) Location.
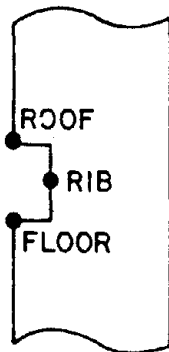
Figure 4-24 illustrates temperature rise contours near the disposal room 25.0, 25.3, 30.0, and 100.0 years after waste emplacement for a conductivity of 2.52 W/m-K. The contours shown at 25.0 and 25.3 years represent the thermal behavior immediately before and after the 100-day ventilation of the disposal room. The ventilation greatly reduces the temperature fields within 10 meters of the room periphery. Beyond this 20-meter region, the influence of the 100 days of ventilation diminishes considerably. The other two contour plots (30.0 and 100.0 years) show the dispersion of high temperature contours away from the waste canister region. During this 70-year period, the temperatures do not change more than 30°C anywhere in the region shown in Figure 4-24. This agrees with the thermal response along the room periphery, where the greatest increase in temperature is observed in the initial 25 years after waste emplacement.

4.2.3 Near-Field Thermal Environments in a CHLW Repository

The NF thermal results for CHLW at an areal thermal loading of 25 W/m^2 are presented in this section. Single and double rows of canisters are compared to determine the effect of canister arrangement on the NF temperatures. Also, three granite thermal conductivities are investigated to determine the sensitivity of the thermal response to this parameter.

A model with a single row of canisters was used to generate the time history of temperature rise at three distinct locations (Figure 4-25). The greatest increase in temperature rise along the room periphery occurs in the initial 25 years after waste emplacement. The temperature rise along the roof, rib, and floor during the initial 25 years is nearly the same. Ventilation for 100 days reduces the room periphery temperature rises by at least 80°C. Room periphery temperatures after backfilling are much more varied than those in the initial 25 years after waste emplacement.

The maximum temperature rise in the floor is reached at approximately 35 years (Table 4-7); whereas, the maximum temperature rise in the rib and roof occur at approximately 50 and 60 years, respectively. Increasing the thermal conductivity of granite 88 percent reduces the temperature rise along the floor (approximately 40 percent) more than for either the rib (approximately 30 percent) or roof (approximately 20 percent).

One of the parameters considered in the NF thermal analysis is the number of canister rows in the disposal room. The influence of canister arrangements is
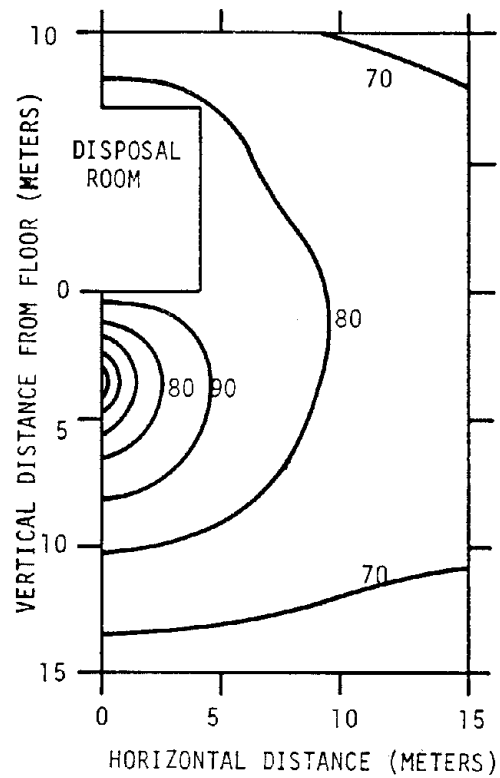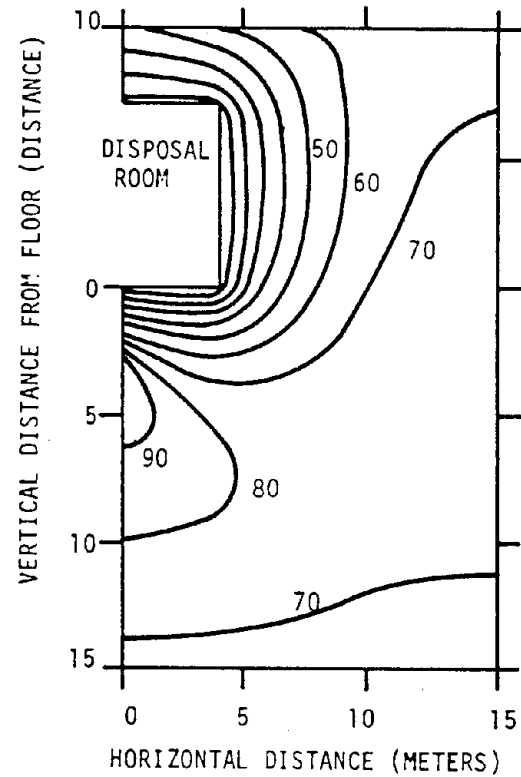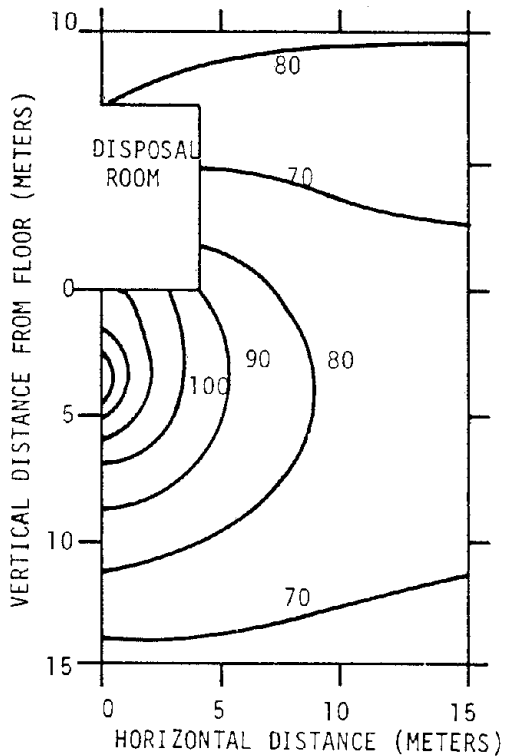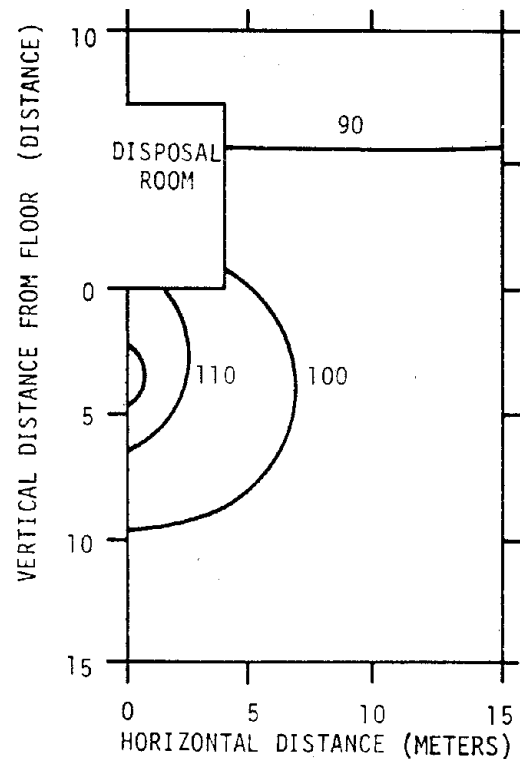
Figure 4-24.   Temperature Rise Contours (°C) From Near-Field Analyses of
10-Year-Old Spent Fuel for ERE-Granite (k = 2.52 W/m-K).
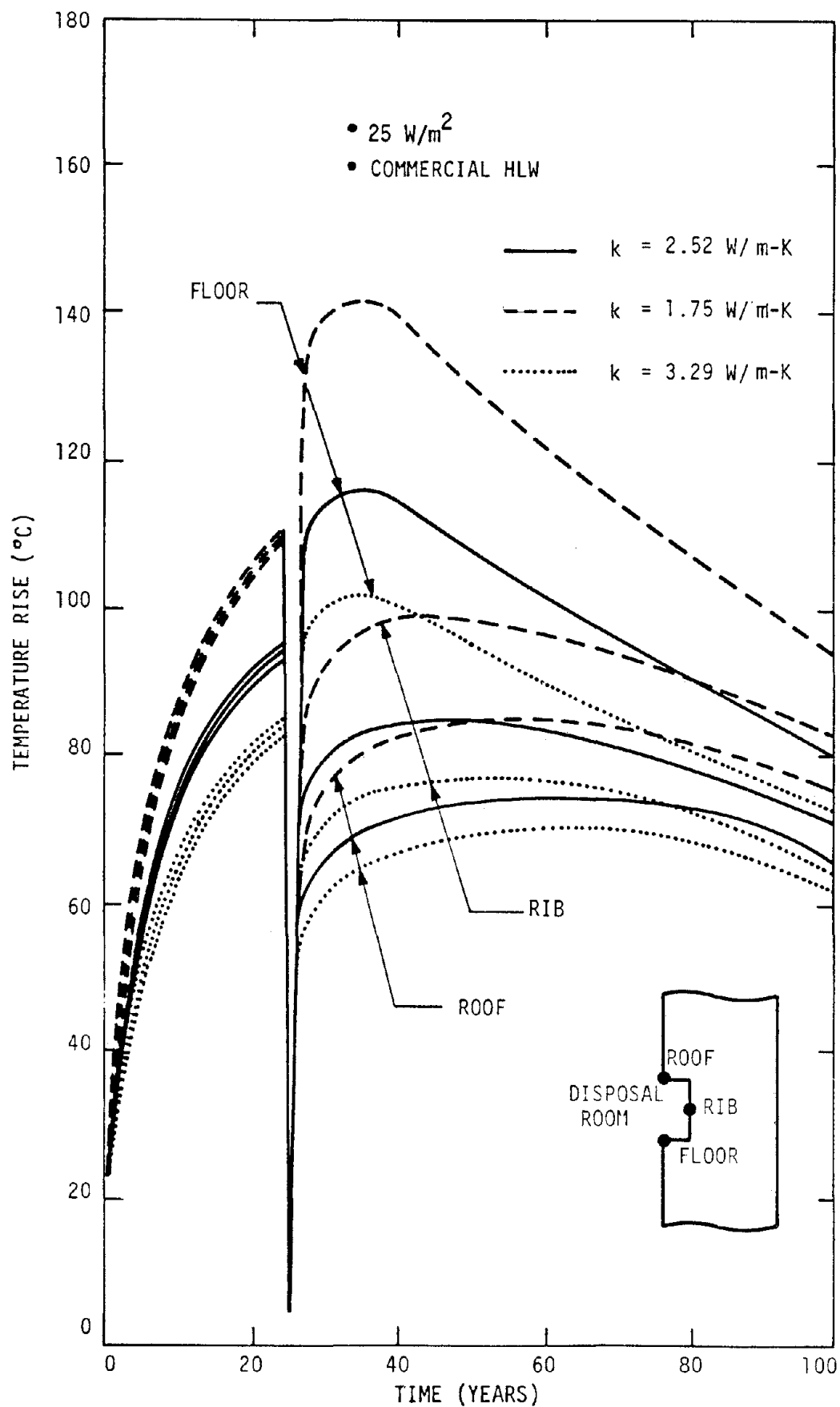
Figure 4-25. Time History of Temperature Rise From a Near-Field Analysis
              Involving Three Values of Thermal Conductivity and Commercial
              High-Level Waste.

Table 4-7. Maximum Temperature Rise Along Room Periphery (CHLW)

Location[a]/Conductivity (W/m-K)	Maximum Temperature Rise (°C)	Time (Years)
Floor:		
1.75	142	35
2.52	117	35
3.29	103	35
Rib:		
1.75	100	45
2.52	85	50
3.29	77	55
Roof:		
1.75	85	55
2.52	76	60
3.29	71	65

(a) Location.

ROOF

RIB

FLOOR
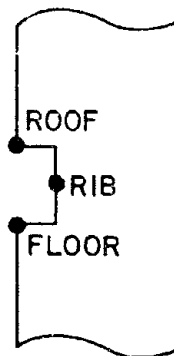
determined by comparing temperatures around the room periphery for CHLW with a thermal conductivity of 2.52 W/m-K (Table 4-8). Similar to the VNF thermal analyses which demonstrated that canister arrangement had a minor effect on the temperatures near a canister, the close agreement in the room temperatures indicates the minor influence of the canister arrangement on the near-field temperatures. Therefore, subsequent calculations of NF temperatures were conducted with a single-canister arrangement.
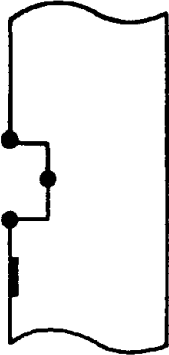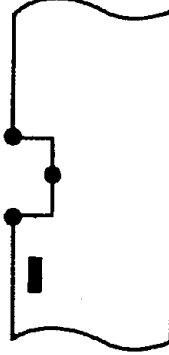
Figure 4-26 illustrates temperature rise contours near the disposal room 25.0, 25.3, 30.0, and 100.0 years after CHLW waste emplacement using a thermal conductivity of 2.52 W/m-K for the granite. The other two contours (30 and 100 years) show the dispersion of high temperature contours away from the waste canister region. During this 70-year period, the decrease in temperature in the floor and canister region is between 25°C and 60°C. The remaining portion of the NF region experiences a temperature decrease of less than 20°C.

Figures 4-27 and 4-28 show temperature rise contours for a conductivity of 1.75 W/m-K and 3.29 W/m-K, respectively. The times of these two sets of contours agree with those used in Figure 4-26. A comparison of temperature rise contours in Figures 4-27 and 4-28 gives an indication of the effect of conductivity on temperatures. The lower value of conductivity produces higher temperature rises at the four designated times. This response is reasonable since the thermal resistance of the rock mass is inversely related to its thermal conductivity. As expected, the difference in temperature rise contours between the two extreme conductivity values is the greatest near the canister, but a temperature difference of at least 15°C is noticed throughout the designated NF region.

4.2.4 Near-Field Thermal Environments in a DHLW Repository

The NF thermal results for a DHLW repository with an areal thermal loading of 25 W/m^2 are presented in this section. The two-dimensional model shown in Figure 4-22 (but assuming a single row of waste canisters) was used exclusively in the numerical NF thermal analysis of DHLW. A single or double row of waste canisters provides nearly identical NF temperature distributions. The three conductivity values are investigated to determine the importance of this parameter on the thermal response of DHLW in the NF region.

Table 4-8. Temperature Rise (°C) Comparison of Single and
Double Canister Rows (CHLW, 2.52 W/m-K)

Time (Years)	One-Row Layout			Two-Row Layout		
	Floor	Rib	Roof	Floor	Rib	Roof
1.0	25.9	23.9	23.3	25.3	23.6	23.0
5.0	56.1	54.3	53.6	55.6	54.0	53.3
15.0	84.5	83.1	82.5	84.1	82.9	82.3
25.0	94.9	93.8	93.3	94.6	93.6	93.1
30.0	116.3	80.1	66.2	113.7	80.3	66.2
40.0	114.4	85.0	72.2	112.4	85.1	72.3
50.0	108.4	84.6	73.7	106.7	84.7	73.8
70.0	97.4	82.0	74.8	96.3	82.0	74.8
100.0	80.0	71.2	66.6	79.4	71.2	66.6

a.) Time = 25.0 Years

b.) Time = 25.3 Years

c.) Time = 30.0 Years
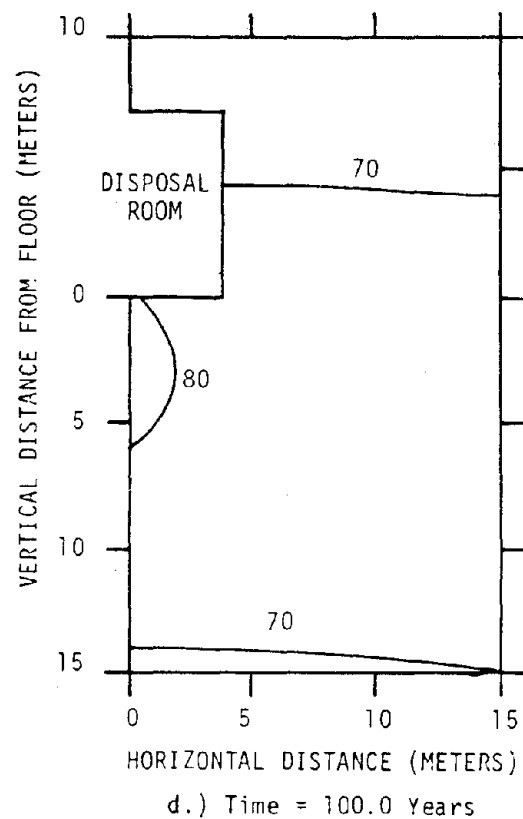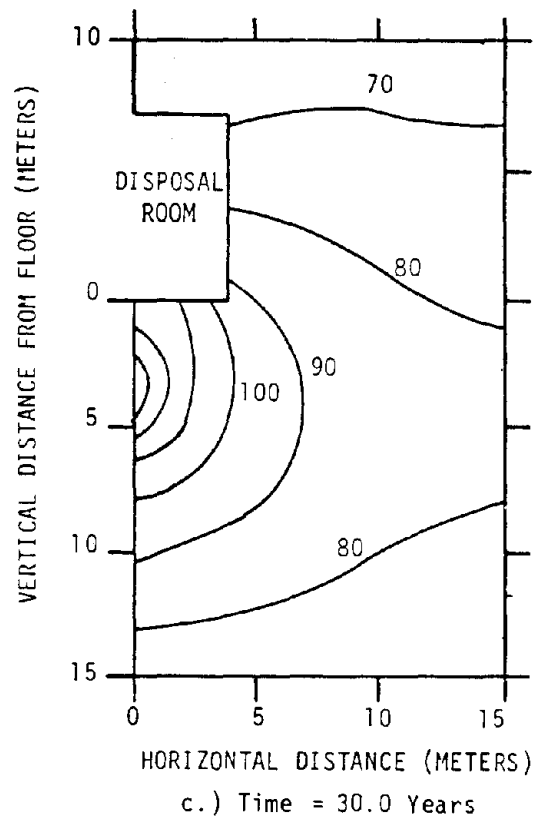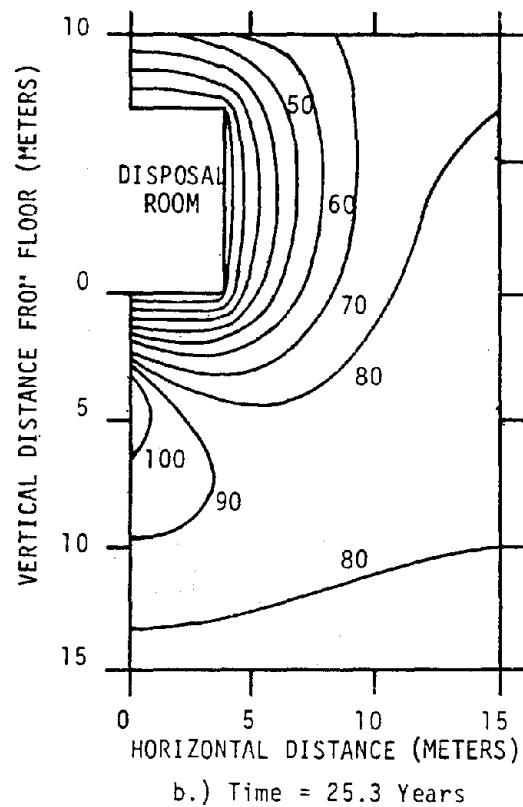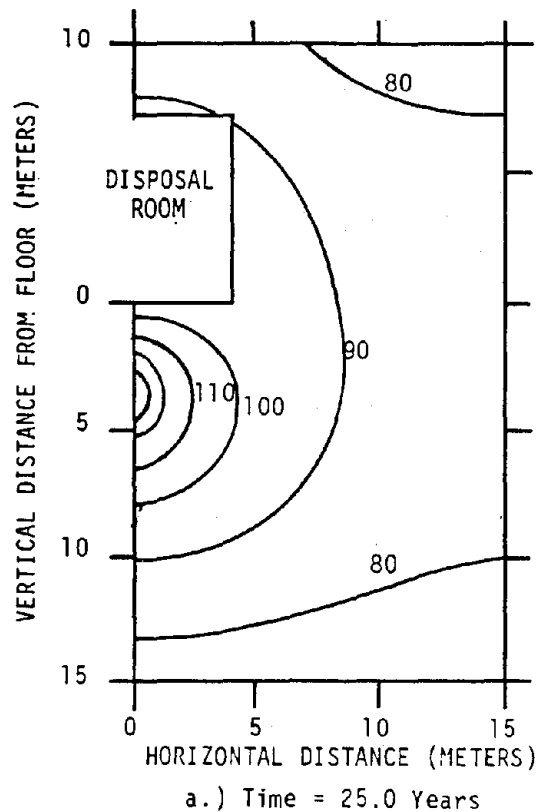
d.) Time = 100.0 Years

Figure 4-26.   Temperature Rise Contours (°C) From Near-Field Analyses of 10-Year-Old Commercial HLW (25 W/m²) for k = 2.52 W/m-K.
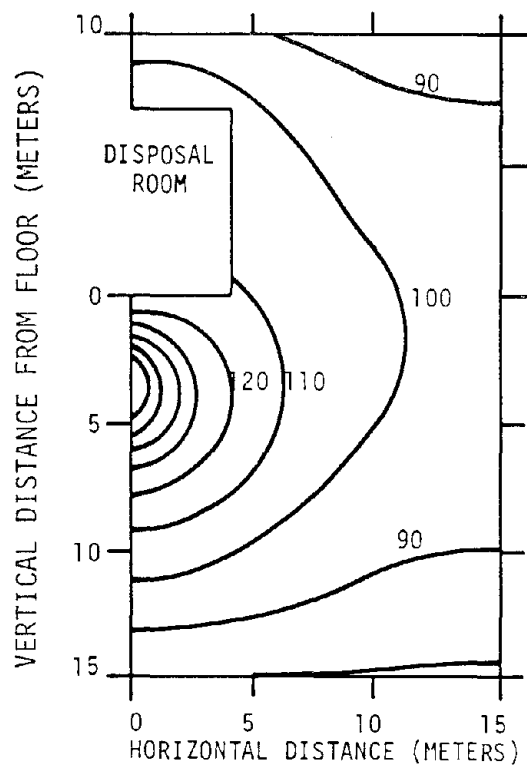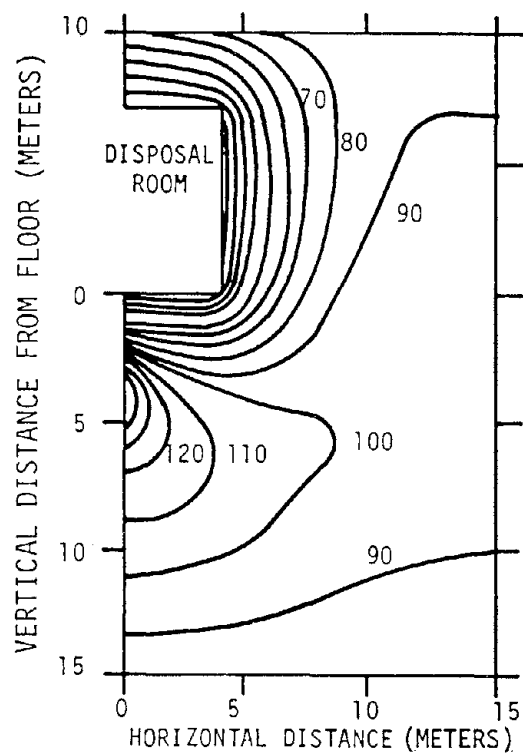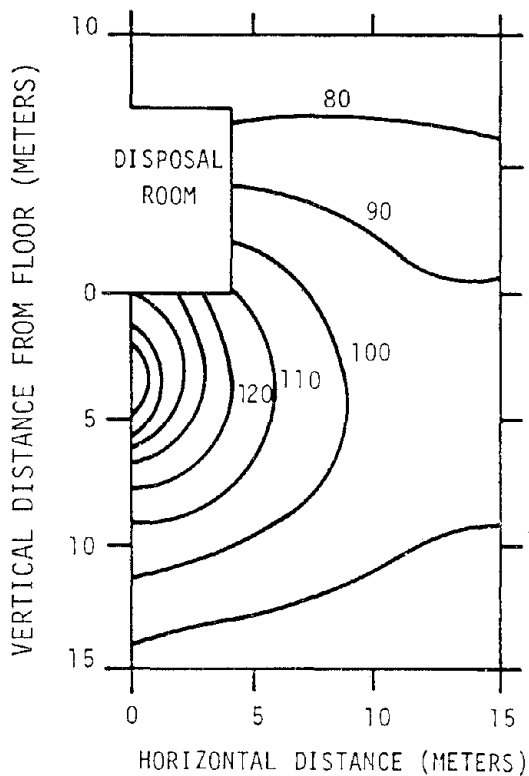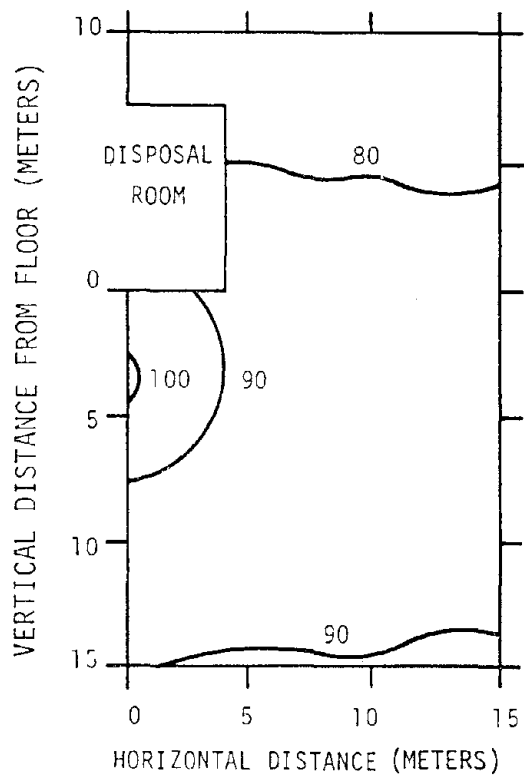
Figure 4-27. Temperature Rise Contours (°C) From Near-Field Analyses of
10-Year-Old Commercial HLW (25 W/m^2) for k = 1.75 W/m-K.
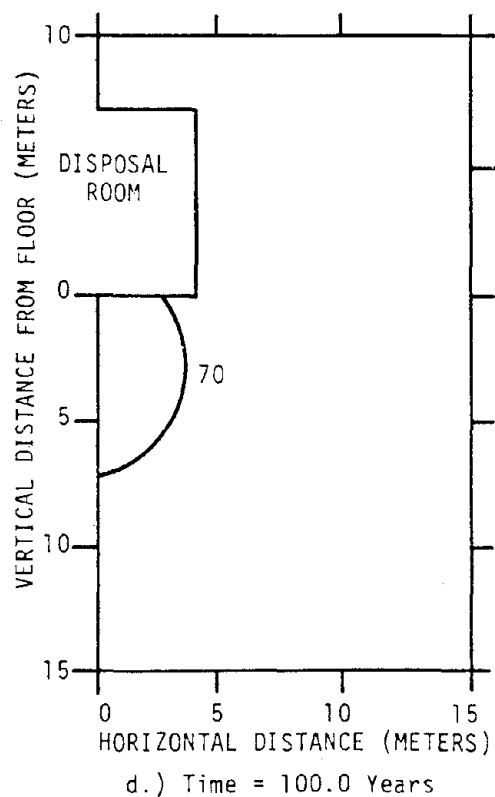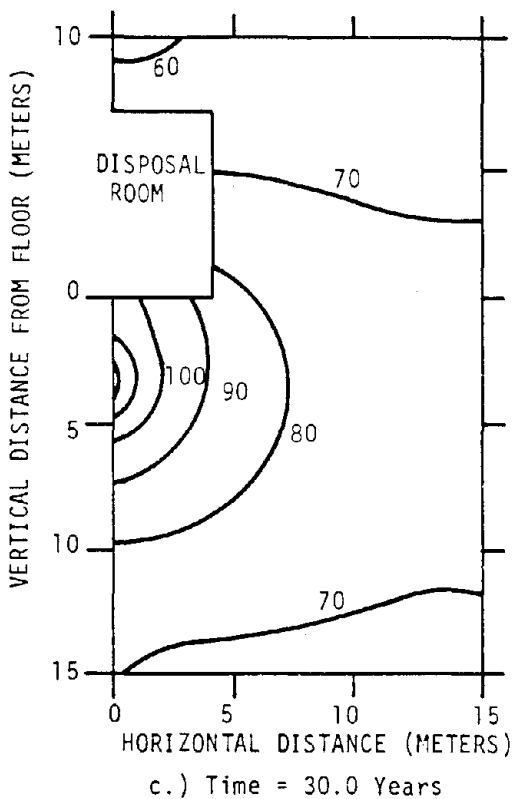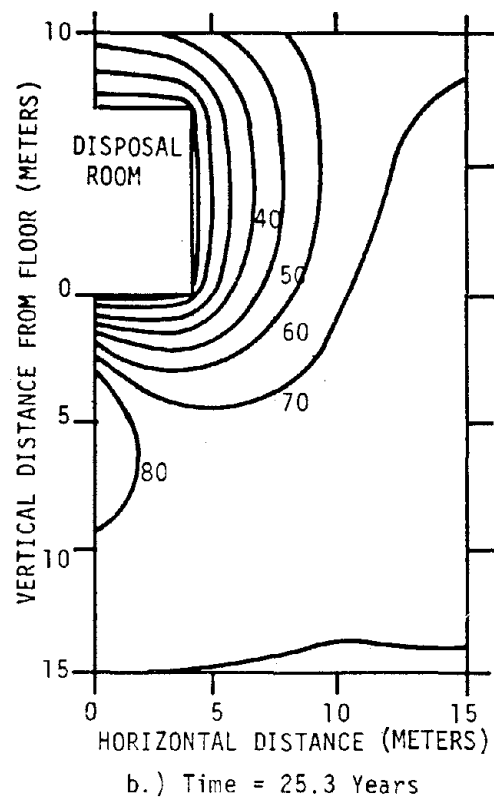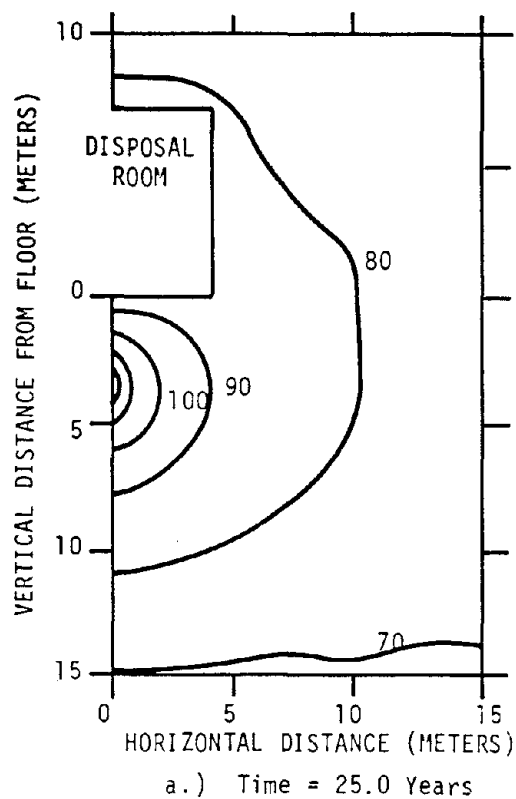
Figure 4-28.   Temperature Rise Contours (°C) From Near-Field Analyses of
10-Year-Old Commercial HLW (25 W/m^2) for k = 3.29 W/m-K.

Figure 4-29 shows the time history of temperature rise along the room periphery at three locations for the three conductivity values. The temperature distribution along the room periphery closely approximates the thermal behavior of SF and CHLW. Ventilation before backfilling reduces the room periphery temperature rises by at least 90°C which results in a temperature of 5°C above ambient temperature.

The maximum temperature rise and time it occurs for the three thermal conductivities of the host rock at each of the three designated room periphery locations is presented in Table 4-9. The maximum temperature rise in the floor is reached at approximately 35 years; whereas, the maximum temperature rise in the rib and roof occur at approximately 70 and 80 years, respectively. The change in the thermal conductivity influences the temperature rise along the floor (approximately 40 percent) more than at either the rib (approximately 25 percent) or the roof (approximately 20 percent).

Figure 4-30 illustrates temperature rise contours near the disposal room 25.0, 25.3, 30.0, and 100.0 years after waste emplacement for a conductivity of 2.52 W/m-K. These contours show similar trends to those discussed for spent fuel. The temperatures are greater for DHLW than for either SF and CHLW. The other two contours (30.0 and 100.0 years) show the dispersion of high temperature contours away from the waste canister region. During this 70-year period, the decrease in temperature in the floor and canister region is between 20°C and 45°C. The remaining portion of the NF region experiences a temperature change of less than 15°C.

4.3 FAR-FIELD ANALYSES OF HEAT TRANSFER AND GROUND-WATER FLOW

A study of long-term radioactive waste containment necessarily requires investigations involving the global or far-field response of the repository site geology. Long-term heating provided by the isolated radiogenic material may create irreversible processes resulting in structural damage or perturbation of the ground-water flow system. This section examines the effects of heat transfer and ground-water flow surrounding a spent fuel and a commercial high-level waste repository in granite. The perturbation of regional flow fields due to thermally induced flow is of particular interest in this study. Also, the temperature rise in the granite surrounding the repository and the effects of
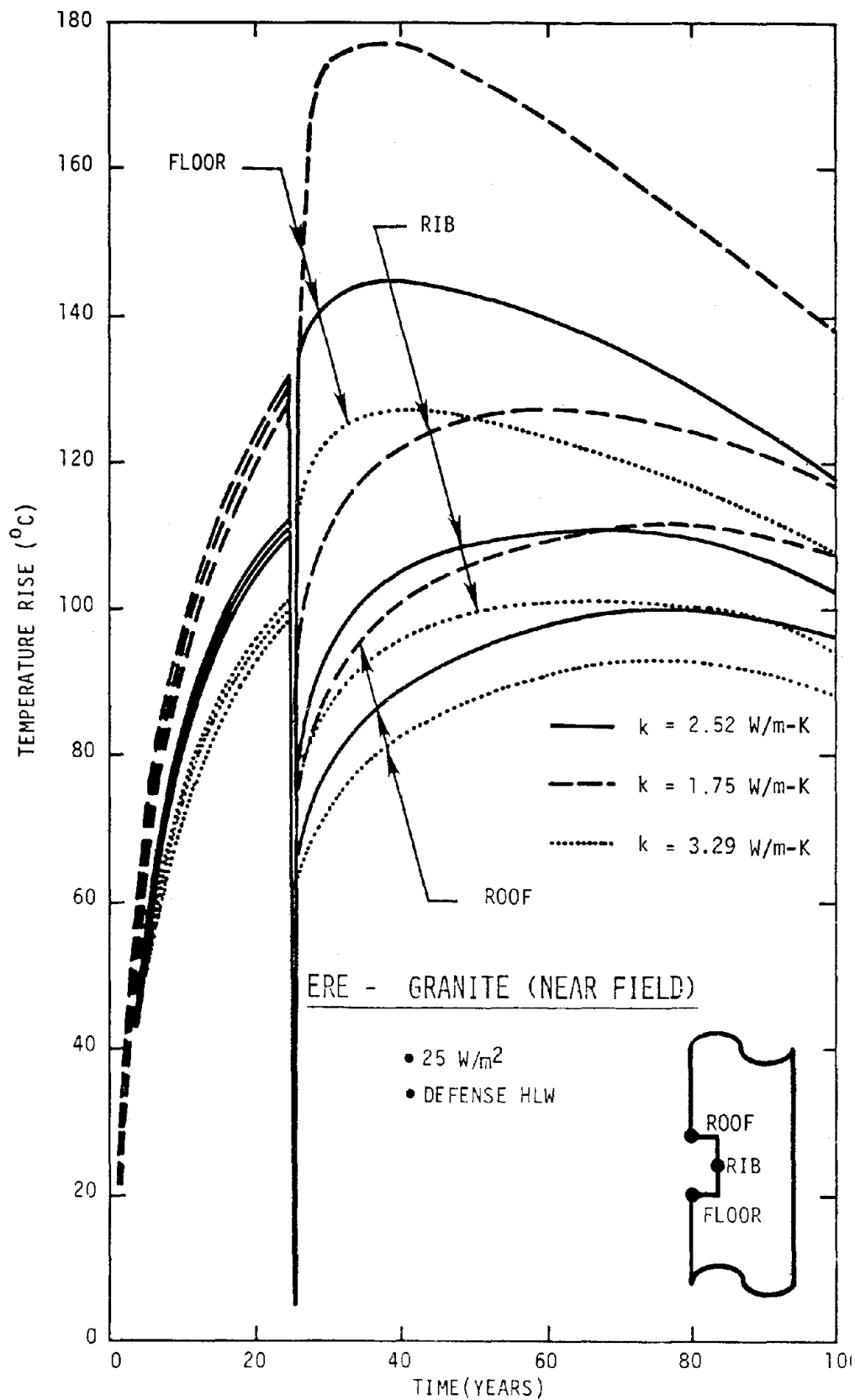
Figure 4-29. Time History of Temperature Rise From a Near-Fie Analysis Involving Three Values of Thermal Conductivity and Defense High-Level Waste (ERE-Granite).

Table 4-9. Maximum Temperature Rise Along Room Periphery (DHLW)

Location[a]/Conductivity (W/m-K)	Maximum Temperature Rise (°C)	Time (Years)
Floor:		
1.75	177	35
2.52	145	35
3.29	127	40
Rib:		
1.75	127	60
2.52	112	70
3.29	101	70
Roof:		
1.75	113	80
2.52	100	80
3.29	93	75

(a) Location.
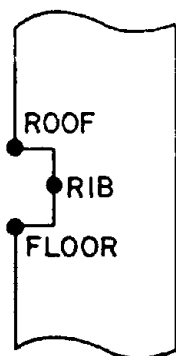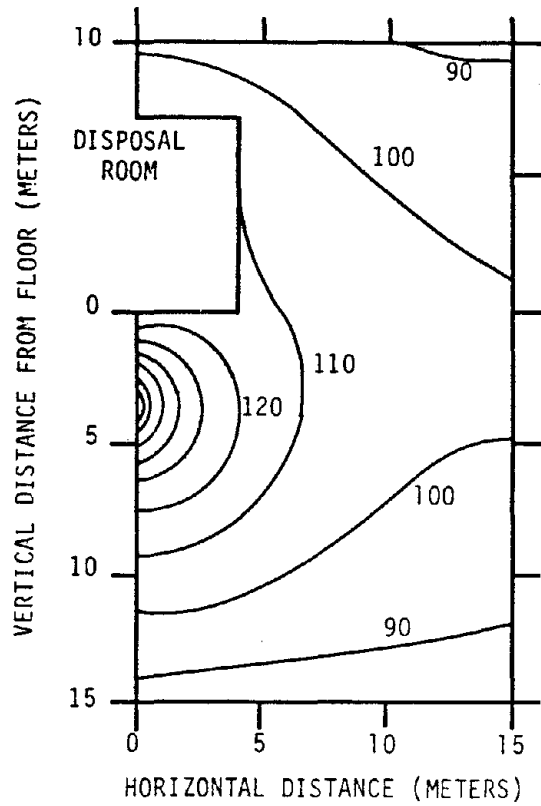
a.) Time = 25.0 Years
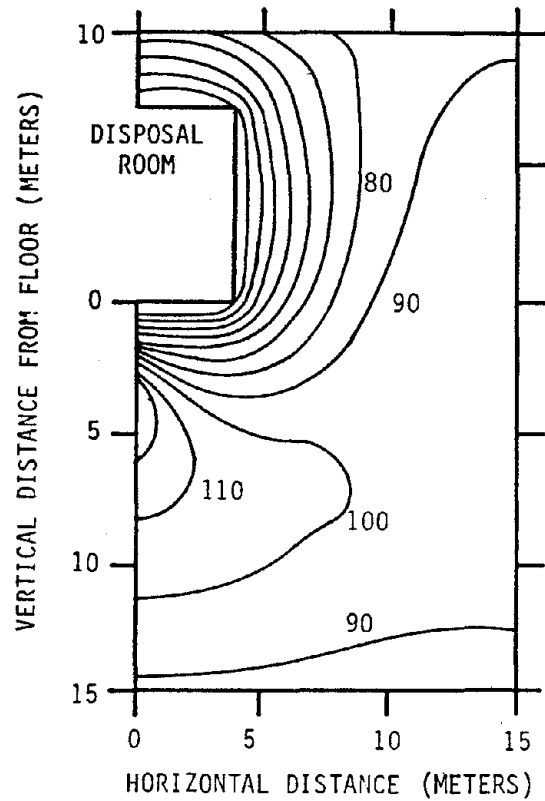
b.) Time = 25.3 Years
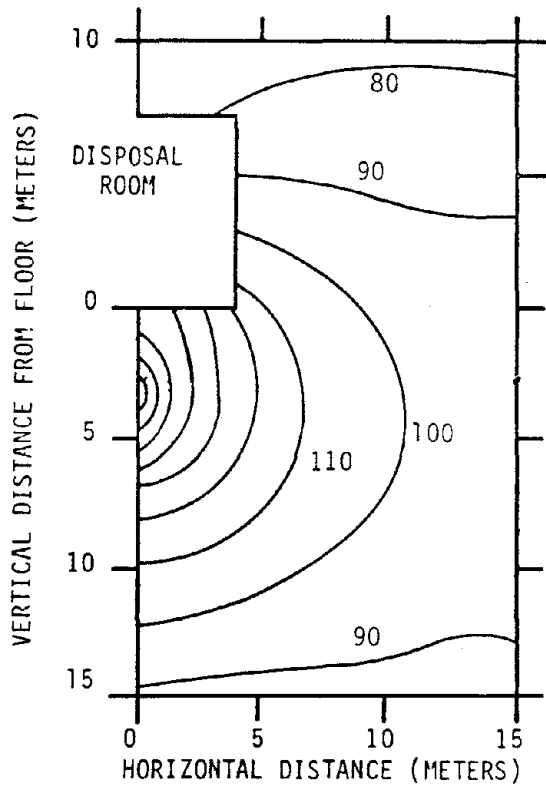
c.) Time = 30.0 Years
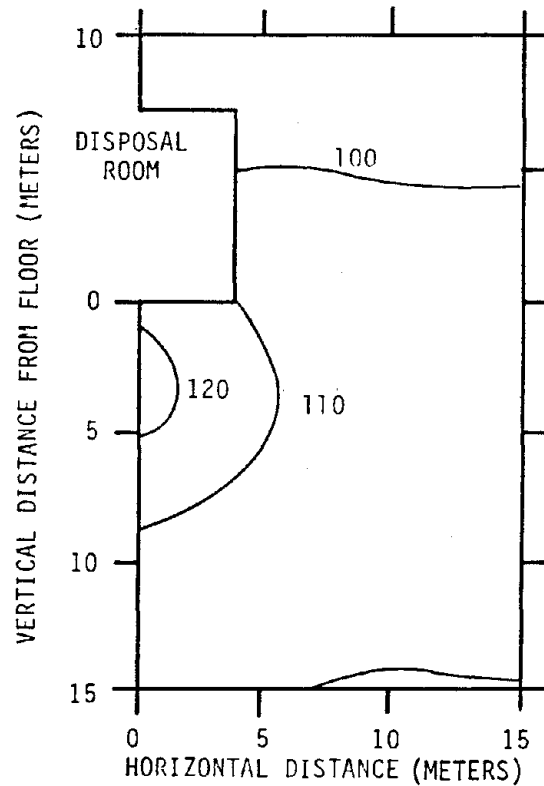
d.) Time = 100.0 Years

Figure 4-30.   Temperature Rise Contours (°C) From Near-Field Analyses of 10-Year-Old Defense HLW (25 W/m^2) for k = 2.52 W/m-K.

convective heat transfer on the far-field temperatures are important considerations. The response of the far-field region surrounding a DHLW repository was not considered in this study because of insufficient information regarding long-term decay characteristics and waste inventory to develop a model.

4.3.1 Modeling Methods

A generalized plan view of the underground waste repository and the surrounding granite which was used in this study is shown in Figure 4-31. The shaft pillar is located in an inactive area at the center of the repository. This inactive area also contains maintenance shops and other facilities and is assumed to be 700 m square based on the conceptual design for NWTS repository number one [Woodward-Clyde Consultants, 1978]. The nuclear waste repository is located 1,000 m below the surface. A vertical cross section (Section A-A) is modeled as a two-dimensional problem with infinite extent in the direction perpendicular to the paper. No room-and-pillar detail is included in the far-field model of the repository. Instead, the entire plan area of the repository is assumed to be generating heat. The preexisting ground-water flow is assumed to be horizontal and parallel to the plane of Section A-A.

Sequential loading of the repository was implemented to more accurately simulate the time-dependent burial of waste for both CHLW and SF. The emplacement of the waste was modeled to best approximate the arrival rates for both waste types over a 20-year emplacement period [Office of Waste Isolation, 1978a]. Sequential loading causes horizontal temperature gradients across the repository which do not occur with instantaneously loaded models. This is important since the temperature gradient is a driving mechanism in the thermally induced flow.

To simulate sequential loading, the waste canisters were grouped to form heat-generating elements. These elements started generating heat at times which best approximated the arrival dates of the waste. The periphery elements started generating heat first and loading proceeded toward the center of the repository. In 20 years, the entire repository, except for the central shaft pillar, was loaded with heat-generating elements.

Using the models developed from Section A-A, the size of each repository was calculated based on the areal thermal loading, canister loading, and number of

Shaft Pillar

Repository

A

A

700 m

1,870 m

Granite

Plan View

1,000 m

Repository
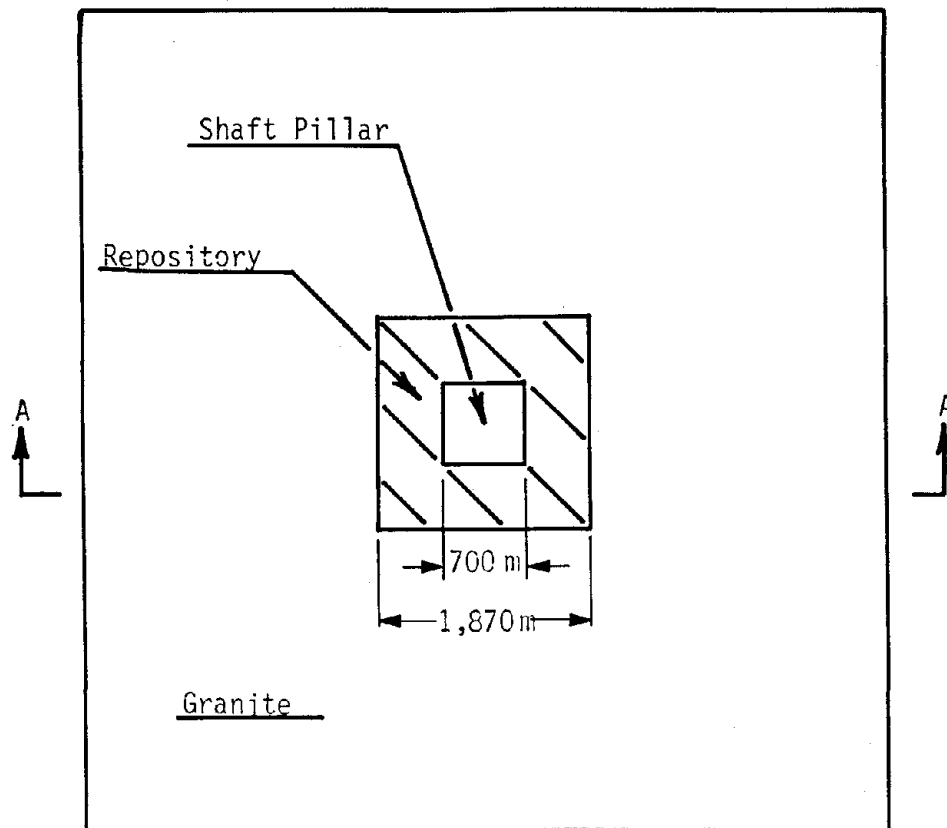
Ground-water Flow
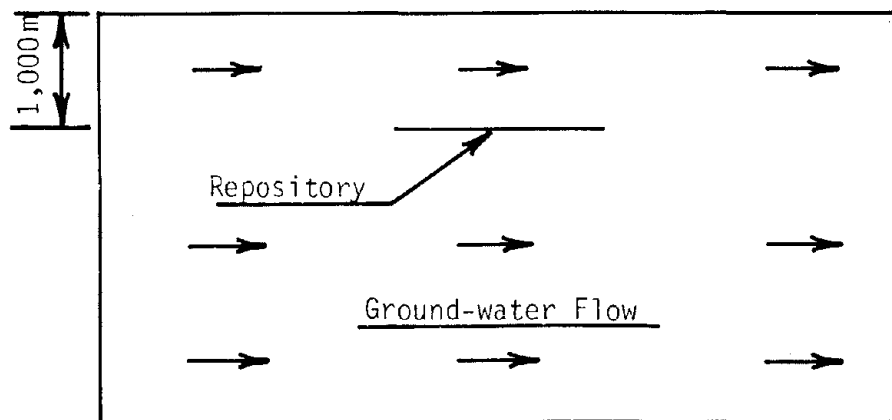
Section A-A

Figure 4-31. Generalized Plan View and Section of an Underground Waste
             Repository.

canisters per repository as shown in Table 4-10. Assuming a 700-m-square inactive area in the center of each repository, the total areas are 3.50×10^6 m^2 and 3.27×10^6 m^2, respectively, for CHLW and SF. Since these areas are approximately the same, an 1,870-m-square repository was assumed for both waste types.

The repository elements were 15 m high because the combined height of the repository room and borehole is 13.7 m.

To clarify the relationship between thermally induced flow and the preexisting regional flow, two preexisting flow fields were modeled. In one flow field, the ground water was initially at rest and all flow was thermally induced. In the other flow field, a horizontal hydraulic gradient in the granite was assumed to be approximately 0.1 percent. This gradient is equivalent to a horizontal pressure gradient of 9.8×10^{-6} MPa/m. From this case, the perturbation of a typical preexisting flow field by thermally induced flow can be assessed. By comparing the transient flow fields predicted for the two cases, the reduction or inhibition of convection cell formation by preexisting regional flow can also be studied. The "sweeping away" of thermally induced convection cells by regional flow has been reported by Ratigan [1977].

Previous far-field thermal analyses of rock masses containing nuclear waste repositories [Callahan and Ratigan, 1978; Osnes et al, 1978; Callahan, 1981] have considered only heat transfer by conduction. In this study, heat transfer by forced and free convection of ground water is included. If the far-field temperature distributions based on combined conductive-convective heat transfer differ significantly from those predicted when convection is neglected, the value of the previous far-field thermal analyses and subsequent thermomechanical analyses are diminished.

To evaluate the consequence of neglecting convective heat transfer, a baseline conduction analysis of the granitic stratigraphy must first be performed. No preexisting regional flow must occur in this model, and thermally induced flow must be eliminated. The "no regional flow" condition has been described previously in this section, and it is specified by assuming the horizontal hydraulic gradient is zero. Since thermally induced flow is due to the change of fluid density with respect to temperature, thermally induced flow may be eliminated by assuming density to be independent of temperature.

To analyze independently the convective heat transfer due to regional flow and the convective heat transfer due to thermally induced flow, two additional

Table 4-10. Repository Size

Type of Waste	CHLW	SF
Areal Thermal Loading	25 W/m^2	20 W/m^2
Canister Loading	2100 W/can	550 W/can
Canisters/Repository[a]	35,820	101,117
Active Area of Repository	3.01 x 10^6 m^2	2.78 x 10^6 m^2
Total Area of Repository	3.50 x 10^6 m^2	3.27 x 10^6 m^2

(a) Inventories based on Office of Waste Isolation [1978a].

models are required. In one case, regional flow is included by specifying a horizontal hydraulic of 0.1 percent and thermally induced flow is neglected by assuming the ground-water density to be independent of temperature. Therefore, the convective heat transfer is due solely to the forced convection of the regional flow which remains constant throughout time and is unperturbed by thermally induced flow. In the other case, the regional flow is eliminated by specifying a horizontal hydraulic gradient of zero, but the ground-water density is assumed to be a function of temperature. In this case, the convective heat transfer is due solely to thermally induced flow.

Finally, a thermal analysis, which includes conductive heat transfer and convective heat transfer due to both the preexisting regional flow and any thermally induced flow, should be performed. This analysis, based on combined conductive-convective heat transfer, can be compared with the baseline conduction analysis to assess the validity of neglecting convective heat transfer in far-field thermal analyses.

Table 4-11 summarizes the four flow conditions (FC-1 through FC-4) that were analyzed for repositories containing two waste types (SF and CHLW).

The models used for the far-field heat transfer and ground-water flow analyses are shown in Figure 4-32 (a and b). These models are two-dimensional plane models representing Section A-A for FC-1 through FC-4. They are analyzed using finite element program SPECTROM-55 which uses eight-noded isoparametric elements exclusively. Far-field temperature and pressure distributions were computed throughout these models from 0 to 1,000 years after emplacement of both the CHLW and SF. From these temperature and pressure distributions, the flow fields were calculated based on Darcy's Law:

$$\overline{v} = \frac{\kappa}{\mu} \cdot (\overline{\nabla}P - \rho \, \overline{g}) \qquad (4-2)$$

where:

v = superficial velocity of ground water (m/yr)

κ = permeability of granite (m^2)

μ = viscosity of ground water (MPa $\cdot$ yr)

P = pressure (MPa)

ρ = ground-water density (kg/m^3)

g = gravitational vector (MPa $\cdot$ m^2/kg).

Table 4-11. Flow Conditions

	Regional Flow	Thermally Induced Flow
FC-1	No	No
FC-2	No	Yes
FC-3	Yes	No
FC-4	Yes	Yes
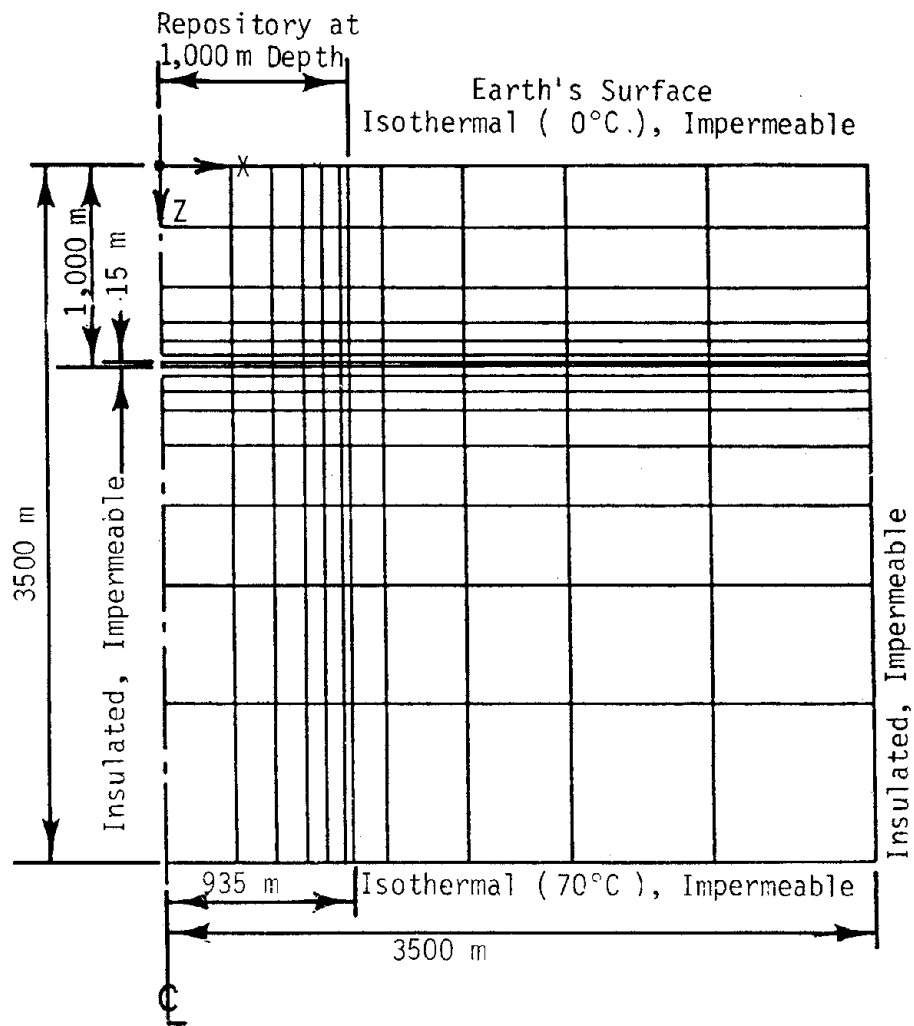
Figure 4-32a. Model Used to Simulate Conduction Baseline (FC-1)
and Thermally Induced Flow Only (FC-2) for Both
CHLW and SF.

Repository at 1000 m Depth

Earth's Surface

Isothermal (0°C), Impermeable

Z   X

1000 m

15 m

3500 m

Insulated, Isobaric

Insulated, Isobaric

Isothermal (70°C , Impermeable

1870 m

3500 m

7000 m
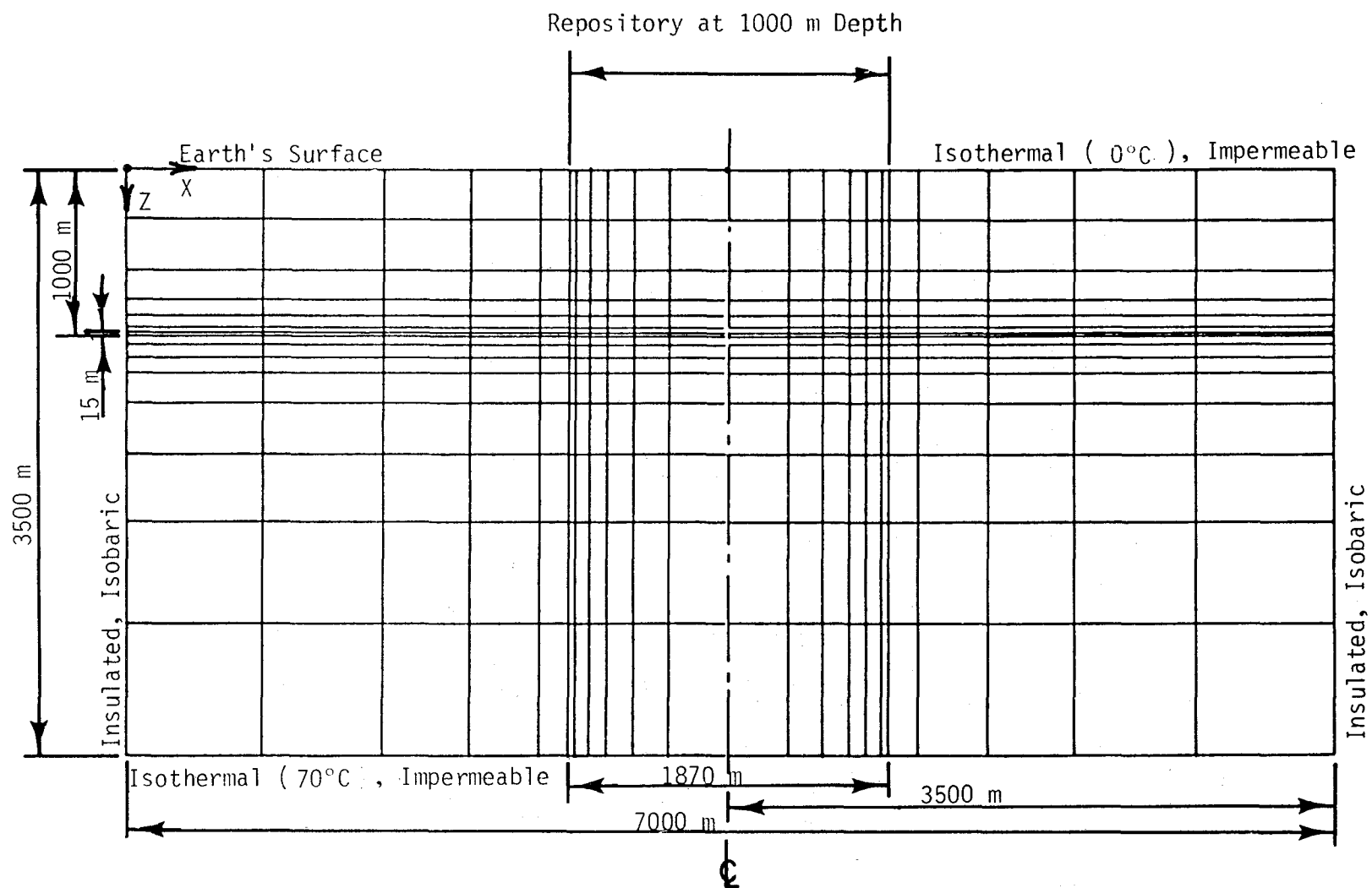
Figure 4-32b.   Model Used to Simulate Regional Flow Only (FC-3) and Regional Flow Perturbed by Thermally Induced Flow (FC-4) for Both CHLW and SF.

Details of the development and examples of the capabilities of SPECTROM-55 are given in Appendix C.

In the far-field models of FC-3 and FC-4, the left, right, and lower boundaries are sufficiently far removed from the repository that they are beyond the thermal influence of the repository during the modeling period. Hence, the left and right boundaries were assumed to be insulated and the lower boundary was assumed to be isothermal. The upper boundary of the models represents the earth's surface and was assumed to be isothermal at 0°C. This assumption is physically realistic because at depths greater than a few meters, the subsurface temperature remains nearly constant from day-to-day and season-to-season. The left boundary in the models of FC-1 and FC-2 is also assumed to be insulated since it represents a line of symmetry and the heat transfer across this boundary zero.

The initial temperature distribution was based on a geothermal gradient of 20°C/km (Section 2.1.1). At the level of the repository (1,000 m below the surface), the initial temperature was 20°C. The lower boundary of the models (3,500 m below the surface) was assumed to be isothermal at 70°C since it is beyond the thermal influence of the repository.

The lower boundary of the models is far enough removed from the flow region surrounding the repository that it can be assumed to be impermeable. This boundary is contrived for modeling purposes, and does not represent any physical interface or boundary. Consequently, flow in the vicinity of the lower boundary is assumed to have little effect on the overall regional flow system.

Since the upper boundary represents the earth's surface, it can be assumed to be impermeable if precipitation and evaporation are neglected. All the rock below the surface is assumed to be saturated. In a physical sense, this assumption presumes that the water table and the earth's surface coincide throughout the modeling period. Of course, the water table generally lies several meters or tens of meters below ground level and depth varies seasonally and yearly. However, the rock between the surface and the repository is probably part of the primary aquifer in the region. In this instance, the water table is probably within meters of the surface, and assuming no major pumping centers in the region, its depth probably remains fairly constant.

For all four flow conditions, the initial pressure distribution was determined by applying appropriate boundary conditions to the models and calculating the steady-state pressure distributions. These boundary conditions will be

explained for each flow condition later. The steady-state distribution would then define the preexisting regional flow prior to waste emplacement. This initial pressure distribution throughout the entire model is assumed to be a function of both depth and horizontal distance along the model and is described by the following equation:

$$P\ (x,z) = \int_0^z (\rho(\varsigma) \cdot g)\ d\varsigma + P_x \cdot x \qquad (4\text{-}3)$$

where:

P = pressure (MPa)

ρ = density of ground water (kg/m^3)

x = horizontal distance along model (m)

z = depth (m)

g = gravity (9.8 m/s^2 = 9.8 x 10^{-6} MPa $\cdot$ m^2/kg)

P_x = horizontal pressure gradient (MPa/m) = constant.

Based on this equation, the initial vertical and horizontal pressure gradients are, respectively, $\rho \cdot g$ and P_x.

In the conduction baseline analysis (FC-1), there is no flow and the ground-water density is assumed to be constant ($\rho = \rho_0$ = reference density of ground water at 20°C). It then follows that the vertical pressure gradient is constant all the time ($\partial P/\partial z = \rho_0 \cdot g$). Substituting this into Darcy's Law (Equation 4-2), it is apparent that the vertical velocity is zero.

In the free convection analysis (FC-2), ground-water density is assumed to be a linear function of temperature (Section 4.3.2) and $P_x = 0$. Equation (4-3) becomes:

$$P\ (x,z) = P\ (z) = \int_0^z (\rho(\varsigma) \cdot g)\ d\varsigma$$

where the ground-water density varies with depth because of the geothermal gradient. Consequently, the pressure can be expressed as a quadratic function of depth:

$$P(z) = \rho_0 \, g \, (1 - \beta_T \cdot T_0) \, z + \frac{1}{2} \, \rho_0 \, \beta_T \, g'' \, z^2 + P_0 \qquad (4\text{-}4)$$

where:

ρ_0 = density of ground water at 20°C (1000 kg/m^3)

β_T = coefficient of thermal expansion for ground water (K^{-1})

T_0 = reference temperature (20°C)

g'' = geothermal gradient (20°C/m)

P_0 = atmospheric pressure at z = 0 (0.1014 MPa).

This is the steady-state pressure distribution applied to the model prior to waste emplacement. This results in an initial pressure of 34.27 MPa at the base of the model and 9.91 MPa at the level of the repository. After waste emplacement, the pressure distribution necessarily changes because the temperature varies.

In the case of regional flow only (FC-3), ground-water density is assumed to be constant ($\rho = \rho_0$) and the horizontal hydraulic gradient (P_x) is nonzero. Consequently, pressure varies linearly with depth and horizontal distance:

$$P(x,z) = \rho_0 \cdot g \cdot z + P_x \cdot x + P_0 \qquad (4\text{-}5)$$

This is the initial steady-state pressure distribution applied to the model after waste emplacement. At ground level along the left boundary, the pressure was assumed to be atmospheric pressure (0.1014 MPa). Because regional flow was simulated left-to-right, the horizontal hydraulic gradient was negative; i.e., -9.80665 (10^{-6}) MPa/m. This resulted in a pressure difference of 0.0686 MPa from the left boundary to the right boundary. For example, the pressure along the right boundary at the surface was 0.0328 MPa. At the left boundary, the initial pressure at the base of the model was 33.36 MPa and was 9.89 MPa at the level of the repository. This was only slightly different than the temperature-dependent density case (Equation 4-4). In this case, since the regional flow was nonzero, the left and right boundaries were assumed to be isobaric to maintain the pressure difference. Since $\partial P / \partial z = \rho_0 \cdot g$, it is apparent that the

vertical component of velocity is zero everywhere (Equation 4-2) and all flow is strictly horizontal throughout time.

Finally, when considering both thermally-induced and regional flow (FC-4), ground-water density is assumed to depend on temperature and the horizontal hydraulic gradient is 0.1 percent. Equation (4-3) becomes:

$$P(x,z) = P(z) + P_x \cdot x \tag{4-6}$$

where $P(z)$ is given by Equation (4-4).

Left and right boundaries are assumed isobaric in order to maintain the regional flow. Initially the velocities are everywhere horizontal and remain horizontal at the left and right boundaries under the assumption that these boundaries are far enough removed from the repository that they do not experience any temperature change.

4.3.2 Material Properties and Characterization

The intact rock in each of the models is assumed to be a continuous mass of isotropic, homogeneous, and incompressible granite that is saturated with water. All of the thermal properties of the rock are assumed to be temperature independent. The thermal and hydrogeological properties assumed for the granite (Table 4-12) are based on values for dry rock. In FC-2 and FC-4, the ground-water density and viscosity are assumed to vary with temperature. All other properties of ground water are the properties of pore water at 20°C (Table 4-13).

These simplifying assumptions may seem quite restrictive and perhaps unrealistic in certain instances, but they are necessary in an analysis which encompasses such a large volume. The primary purpose of this study is to establish a baseline and identify potential problems or areas for further analysis related to the hydrogeological environment of the far-field rock mass surrounding a nuclear waste repository in granite.

Where thermally induced flow was modeled, the density of the ground water was assumed to be temperature dependent and was calculated from the following equation:

$$\rho = \rho_0 (1 + \beta_T (T - T_0)) \tag{4-7}$$

Table 4-12. Properties of Intact Granite

Property	Units	Value
Thermal Conductivity	W/m-K	2.52
Specific Heat	J/kg-K	809.24
Density	kg/m^3	2650.
Permeability	m^2	1.02×10^{-15}
Porosity	%	0.01

Table 4-13. Properties of Ground Water

Property	Units	Value
Thermal Conductivity	W/m-K	0.6058
Specific Heat	J/kg-K	4187.0
Density	kg/m^3	Equation (4-7)
Viscosity	MPa-yr	Equation (4-8)

where:

ρ_0 = reference density at 20°C (1000 kg/m^3)

β_T = thermal expansion coefficient (-1.8 (10^{-4})/°C)

T_0 = reference temperature (20°C).

When thermally induced flow is neglected, the density is assumed to be independent of temperature and the coefficient of thermal expansion, β_T, is zero.

Although the compressibility of water is very small, the density variation caused by the change of pressures encountered from the top to the bottom of the far-field models (0.1 to 34.3 MPa) is approximately equal to the density change caused by a temperature rise of 40°C. However, since this study is concerned with the transient nature of thermally induced flow, the compressibility of the ground water due to hydrostatic pressure is of little consequence. The change in the far-field pressure distribution caused by the thermal effects of a repository is very minor. Consequently, the transient change in water density at a given location due to compressibility is neglected.

The viscosity of water, unlike the density, is highly dependent on temperature (water at 15°C is nearly twice as viscous as water at 50°C), and according to Darcy's Law (Equation 4-2), velocity is inversely proportional to viscosity. The temperature dependent viscosity used in this analysis is expressed as [Mercer and Pinder, 1974]:

$$\frac{1}{\mu} = \frac{1}{5.6878 \times 10^{-17}} + 6.4491 \times 10^{14} T + 3.6897 \times 10^{12} T^2 - 8.1994 \times 10^9 T^3 \quad (4-8)$$

where:
μ = viscosity (MPa · yr)

T = temperature (°C).

Temperature-dependent viscosity and density were used in this analysis to couple the driving mechanisms of the fluid motion (pressure and density) with the magnitude of fluid movement (velocity).

4.3.3 Thermal and Hydrogeological Properties of the Repository

In each of the CHLW and SF analyses, the repository was assumed to have the same thermal and hydrogeological properties as the host granite (Table 4-12). These properties have been discussed previously. However, the entire repository was assumed to generate heat at a volumetric rate equal to the areal thermal loading (ATL) divided by the height of the repository elements.

4.3.4 Far-Field Thermal Environments in a SF Repository

Temperatures along the horizontal midplane of the repository are used primarily in presenting the results of the thermal analysis. It must be emphasized that these temperatures are not realistic in the sense that they could be measured at a specific point within the repository, such as the floor or rib of the room. The far-field models do not include any room, pillar, or drift detail upon which to base such predictions so the midplane represents a convenient reference plane. Midplane temperatures represent a collective average temperature within the repository in the same sense that the nuclear waste was assumed to be uniformly distributed throughout the entire repository. Finally, the midplane temperatures indicate trends in the thermal history of the repository as a whole without regard to local events such as excavation, ventilation, or backfill.

4.3.4.1 Baseline Conduction Analyses of SF Far-Field

Figure 4-33 shows temperature distributions along the midplane of the SF repository at various times. In addition to the peak temperature of 115°C (95°C rise from the initial geothermal temperature of 20°C) at 100 years after emplacement, it displays the steep horizontal temperature gradients occurring within the repository along the midplane during the 20-year emplacement period. It also shows the extent of the horizontal thermal influence along the midplane of the repository into the surrounding granite during the first 1,000 years after emplacement. During the initial 100 years, the horizontal thermal gradients are very steep adjacent to the repository. However, after 100 years,
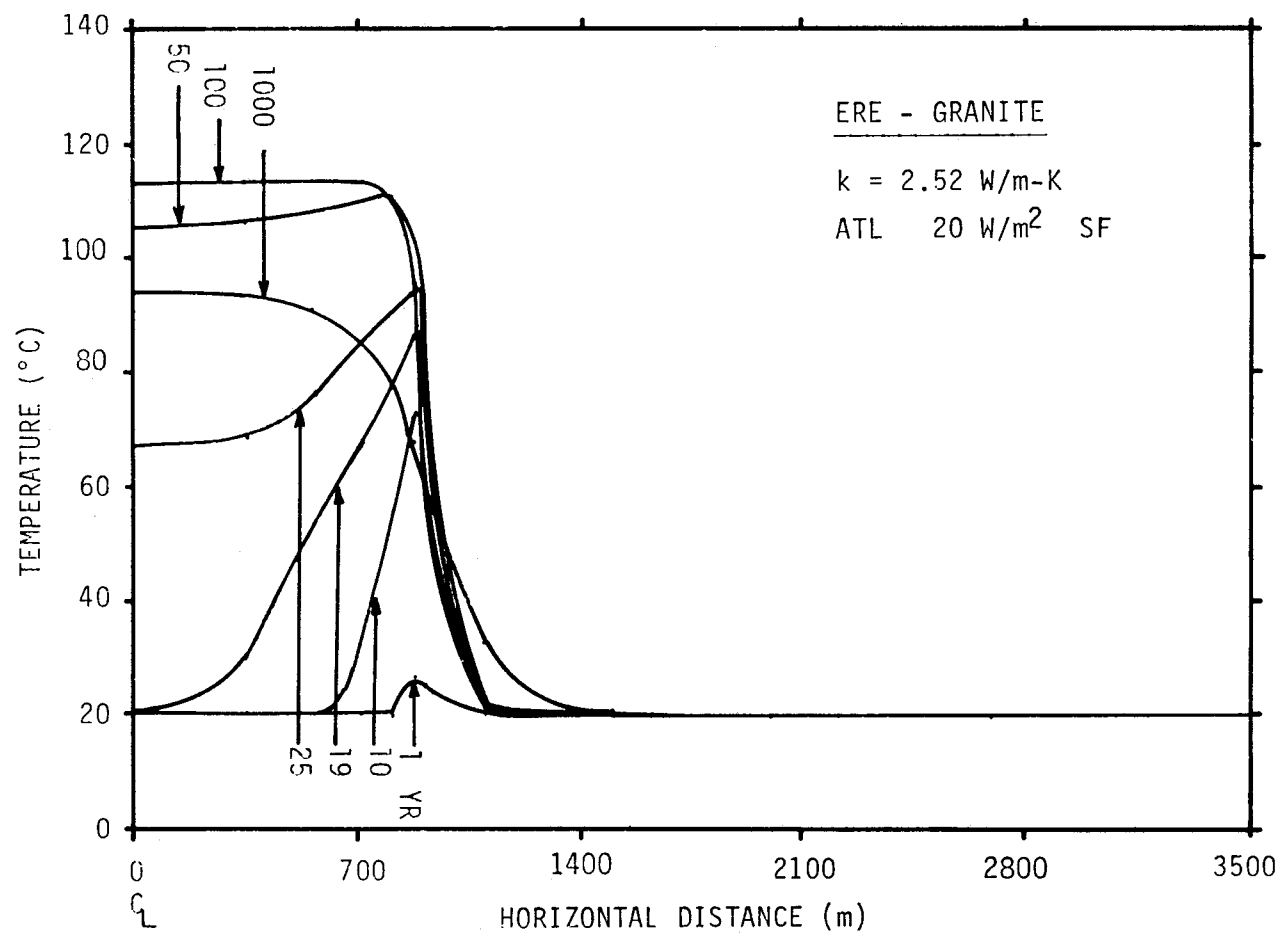
Figure 4-33. Temperature Distribution Along Midplane of an SF Repository (1000 m Deep) at Various Times After Emplacement. Sequential Loading. Conduction Heat Transfer Only.

the repository cools, the temperatures in the surrounding granite increase, and the temperature gradients become less severe.

The peak temperature rise found in this SF thermal analysis is in good agreement with that reported previously [Osnes et al, 1978] for a far-field thermal analysis of a SF repository in granite at a depth of 3,000 feet (914.4 m). Using the thermal property scaling technique discussed in that analysis and an equivalent ATL, the peak temperature rise would be approximately 100°C and would occur at about 80 years after emplacement. Accounting for the variance in decay characteristics of the SF in these two studies, the peak temperature rise of 95°C occurring at about 100 years reported here seems very acceptable.

This peak temperature rise and corresponding time is also in good agreement with an average of the maximum temperature rises and corresponding times at the floor, rib, and roof of the room predicted in the NF analyses (Table 4-6).

The vertical thermal influence is very similar to the horizontal thermal influence as shown in Figure 4-34. At 1,000 years after emplacement the temperature at the centerline of the SF repository is about 94°C. Temperature rise contours show clearly the extent of the thermal influence of the repository. Figure 4-35 through 4-38 show the temperature rise at 50, 100, 1,000, and 10,000 years after emplacement. For times before 1,000 years, the isotherms remain symmetric about the repository as the heat is flowing uniformly away from the repository and there is no boundary interference of the model. At 1,000 years after emplacement, the 1°C rise isotherm is about 450 m to the right of the repository edge and about 750 m above and below the repository midplane. At 10,000 years after emplacement, the isothermal surface causes the temperature rises above the repository to be lower than those at similar locations below the repository.

The transient thermal response at various points in the far-field region is shown in Figure 4-39. At the repository midpoint (point A), there is a rapid increase in temperature after waste emplacement at this location (19 years) and a relatively slow decrease in temperature after 100 years. The temperature at points 400 m above and below the repository is not perturbed until approximately 200 years after emplacement and these points reach a peak temperature at about 9,000 years.
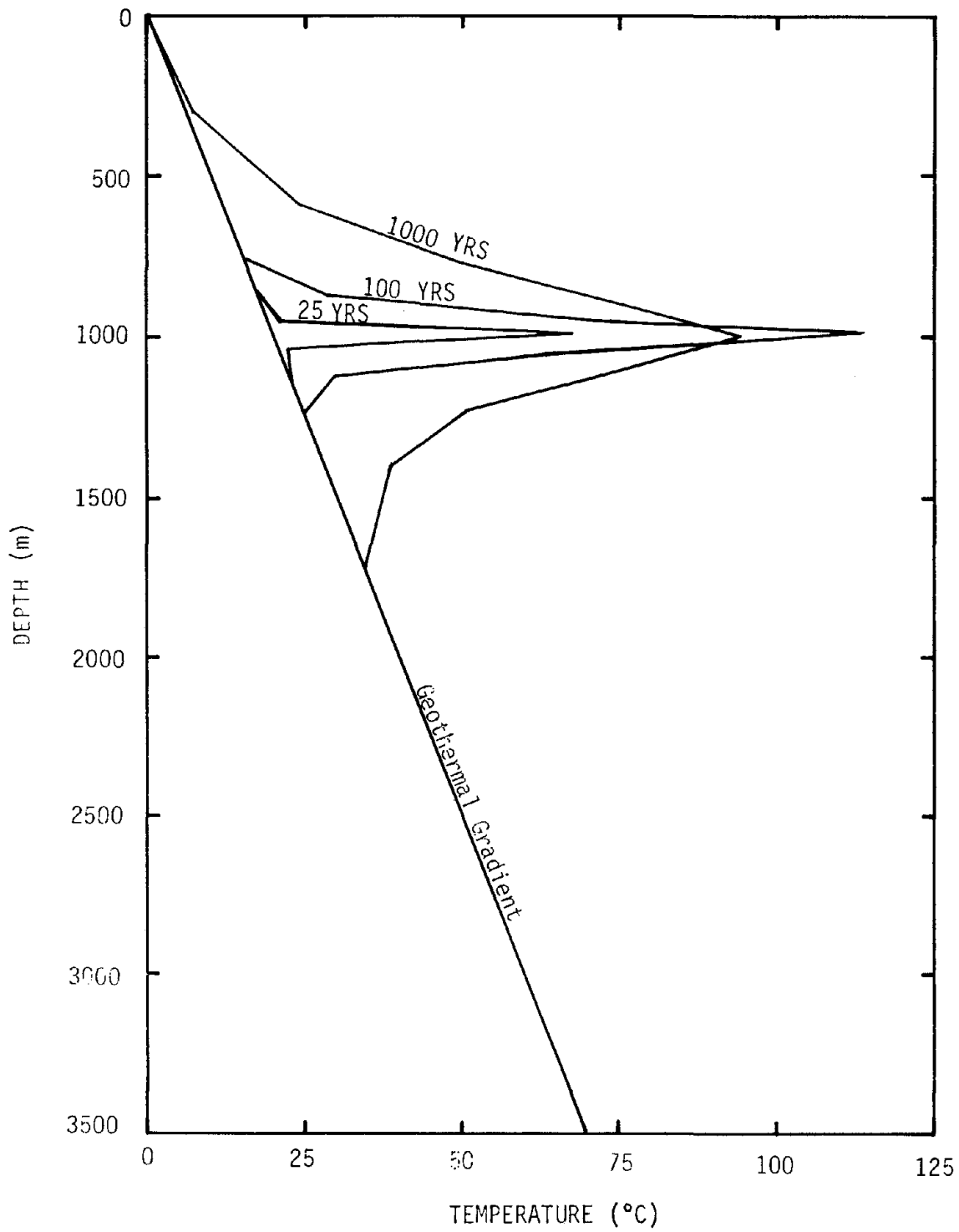
Figure 4-34. Temperatures Along Vertical Centerline of a SF
Repository at Various Times. ATL = 20 W/m².
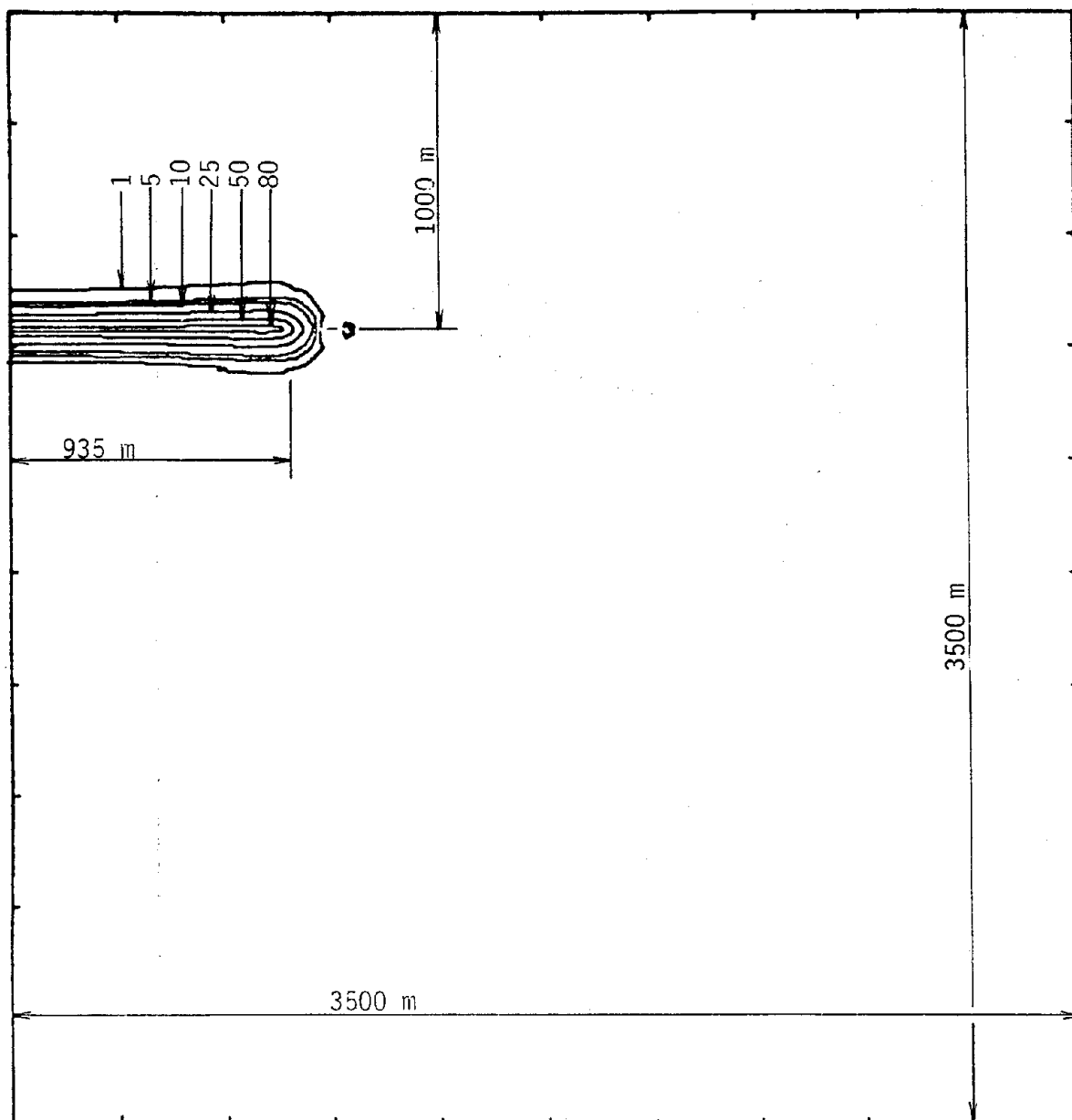
Figure 4-35. Temperature Rise Isotherms (°C) Surrounding a SF Repository in Granite at 50 Years.
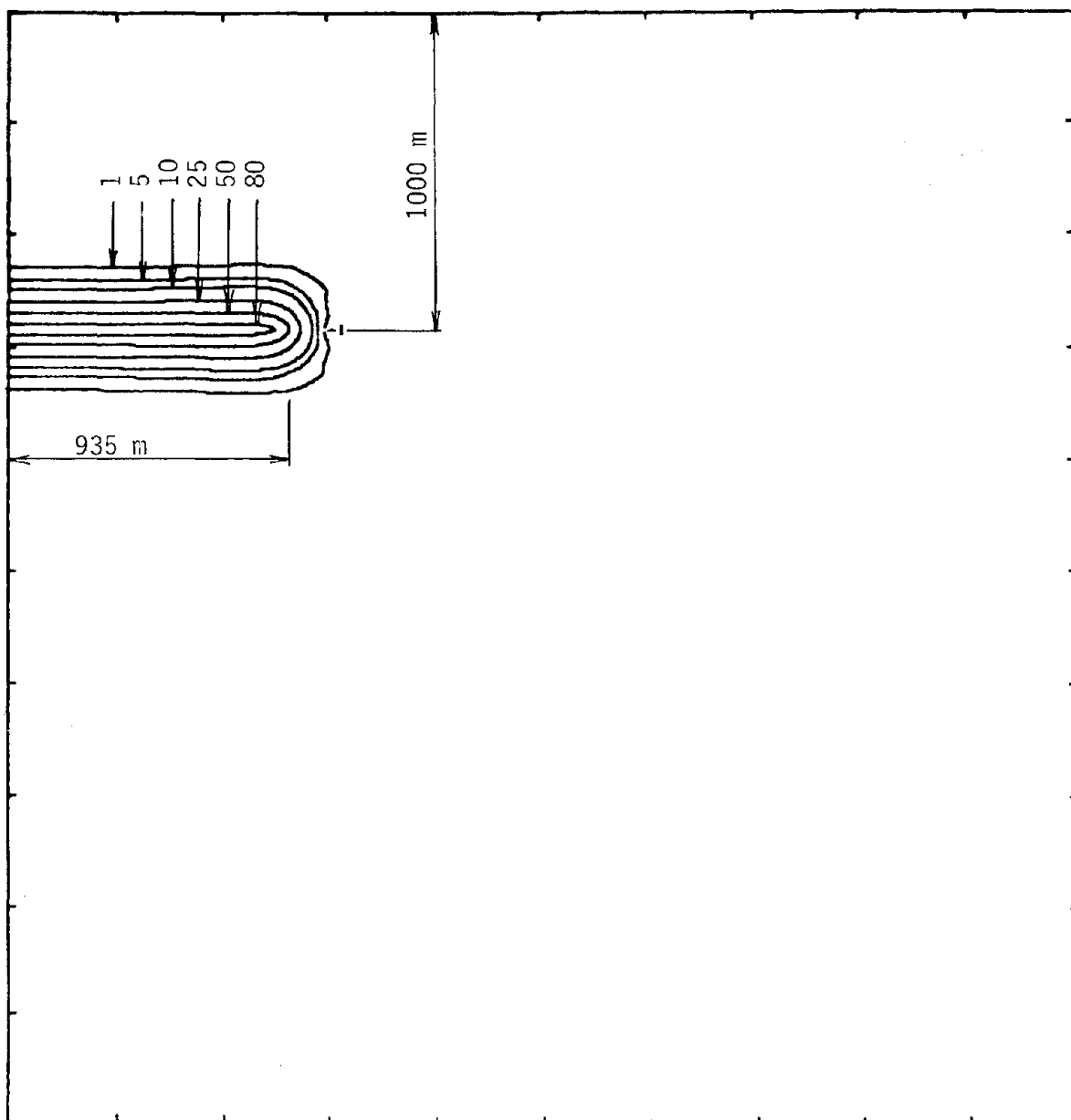
Figure 4-36.   Temperature Rise Isotherms (°C) Surrounding a SF Repository
               in Granite at 100 Years.
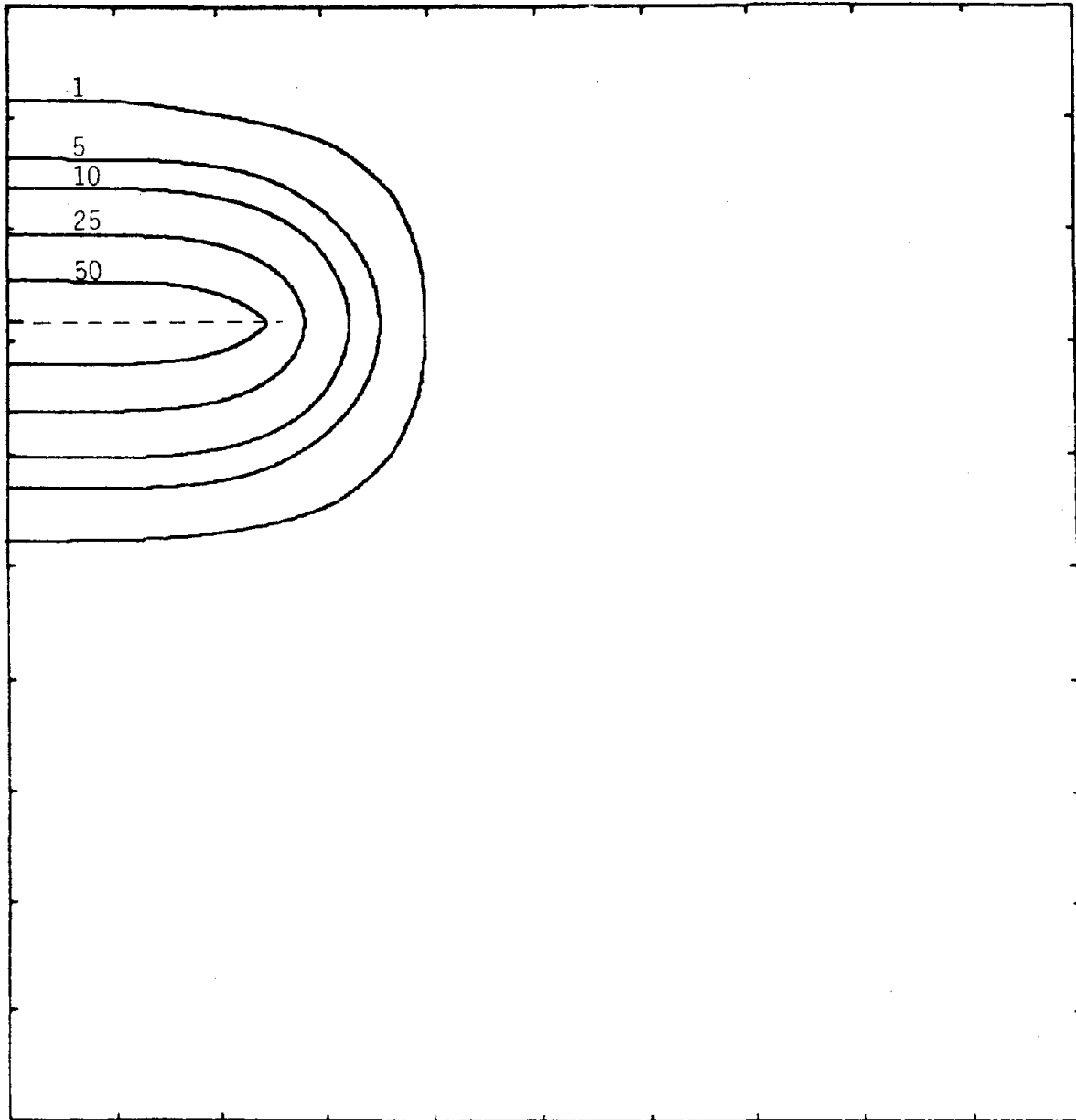
Figure 4-37. Temperature Rise Isotherms (°C) Surrounding a SF Repository in Granite at 1,000 Years.
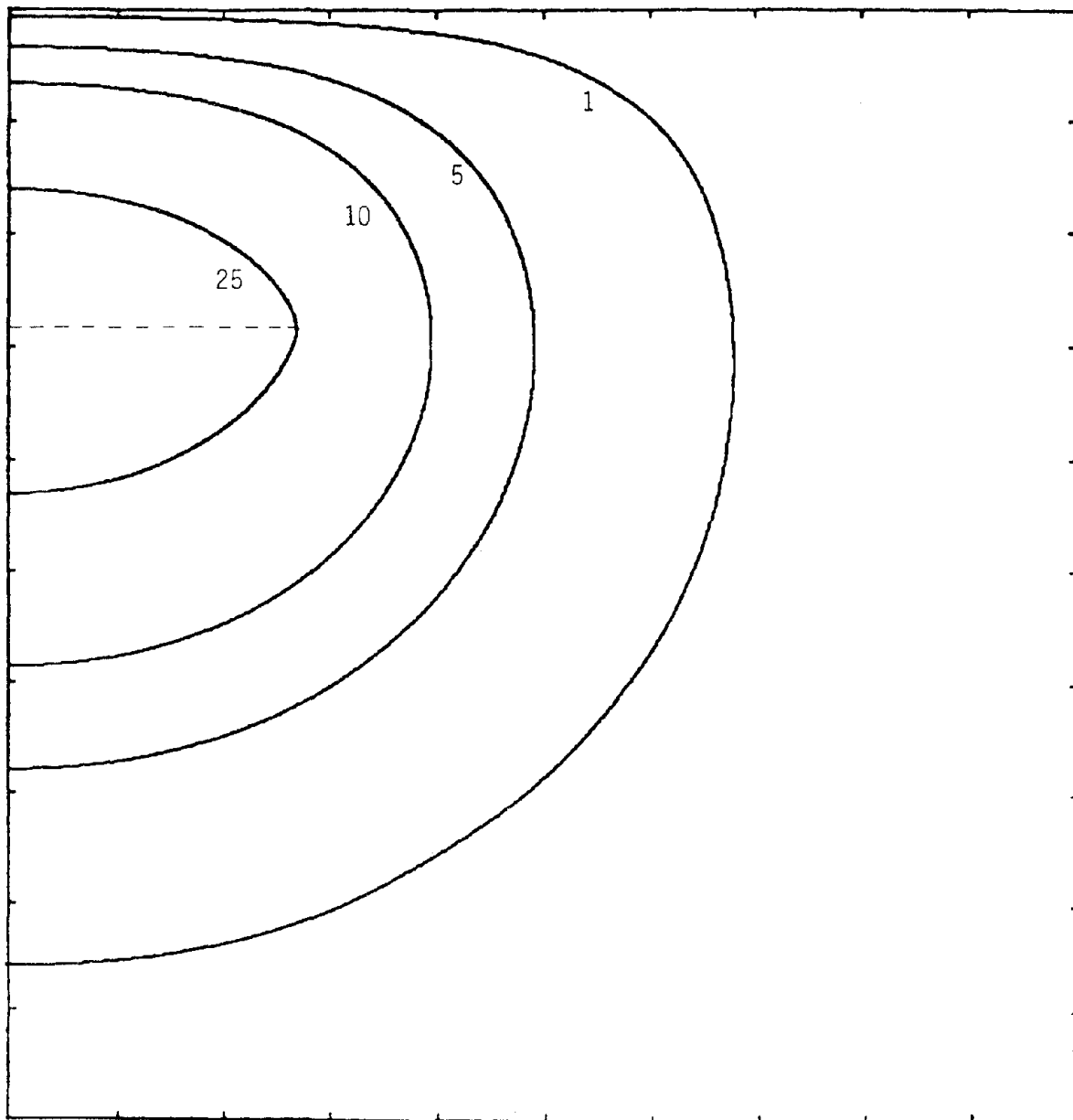
Figure 4-38. Temperature Rise Isotherms (°C) Surrounding a SF Repository in Granite at 10,000 Years.
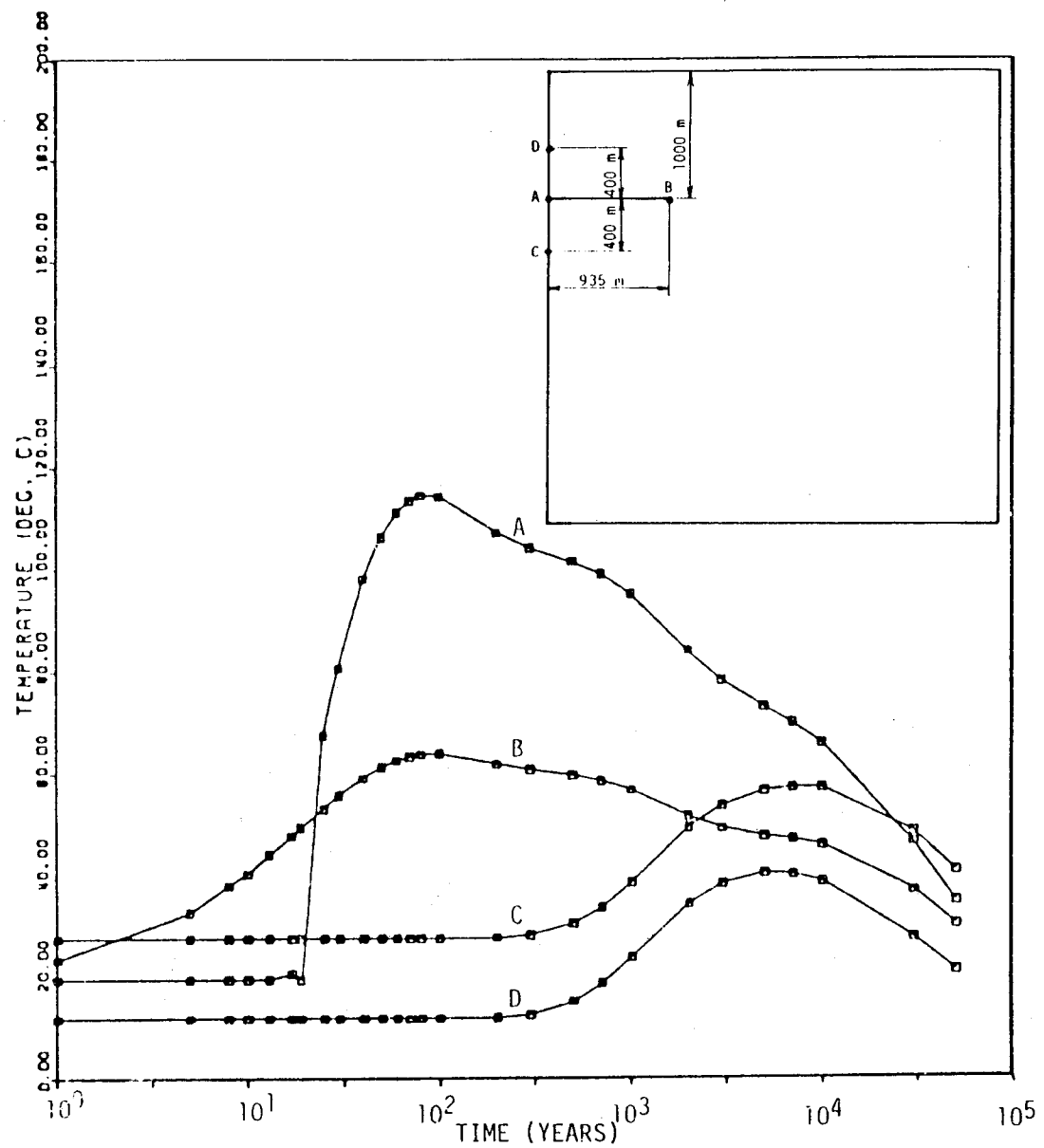
Figure 4-39.   Thermal Response at Various Points Surrounding a SF
Repository in Granite.

4.3.4.2 Combined Conduction-Convection Analyses of SF Far-Field

The effect of convective heat transfer on the thermal response of the far-field region surrounding a SF repository was minimal. Table 4-14 shows a comparison of temperatures at several points in the far-field for both the baseline conduction model and a combined conduction-convection model considering both regional and thermally induced flow. All temperatures based on the latter model are within 1°C of the conduction temperatures during the first 1,000 years after emplacement. Also, the left-to-right regional flow introduces very little asymmetry in the far-field temperatures, as indicated by points B and C. These comparisons show that convective heat transfer is negligible as far as temperature predictions in the far-field are concerned.

4.3.5 Far-Field Thermal Environments in a CHLW Repository

As in the case of SF, midplane temperatures are primarily used in presenting the CHLW thermal results. Also, a direct comparison can be made between the SF and CHLW results since both analyses used the same repository size and the same finite element mesh.

4.3.5.1 Baseline Conduction Model of CHLW Far-Field

Because of the relatively rapid decay of the CHLW, the peak temperatures occur at an early time and the bulk of the granite is not perturbed thermally by the heat-generating repository. Sequential loading created both severe horizontal thermal gradients and high rates of temperature change in early time, providing the potential for thermally induced flow.

The peak temperature rise occurred at the midplane of the repository almost uniformly along its length. This temperature rise was found to be approximately 93°C and occurred at about 50 years after emplacement. This is in good agreement with an average of the floor, rib, and roof maximum temperature rises and corresponding times predicted in the NF analyses (Table 4-7). Figure 4-40 shows the transient thermal response at the midpoint of a CHLW repository and at the repository's periphery (the thermal response of the same points in a SF

Table 4-14. Comparison of Temperatures Predicted by Four Flow Conditions at Various Times and Locations -- SF
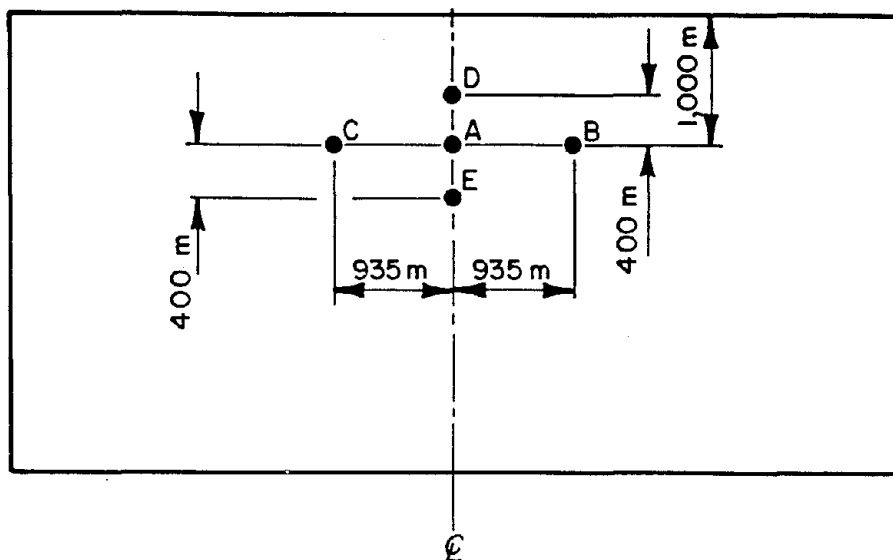
Location	Time (Years)	Temperature (°C)			
		FC-1	FC-2[a]	FC-3[a]	FC-4
A	19 100 1,000	19.73 113.52 94.26			19.73 113.96 94.76
B	19 100 1,000	49.55 63.66 56.53			49.56 63.83 56.86
C	19 100 1,000	49.55 63.66 56.53			49.55 63.77 56.70
D	19 100 1,000	12.00 12.02 24.07			12.00 12.02 24.18
E	19 100 1,000	28.00 28.02 38.82			28.00 28.02 38.91

(a) Analysis not performed.
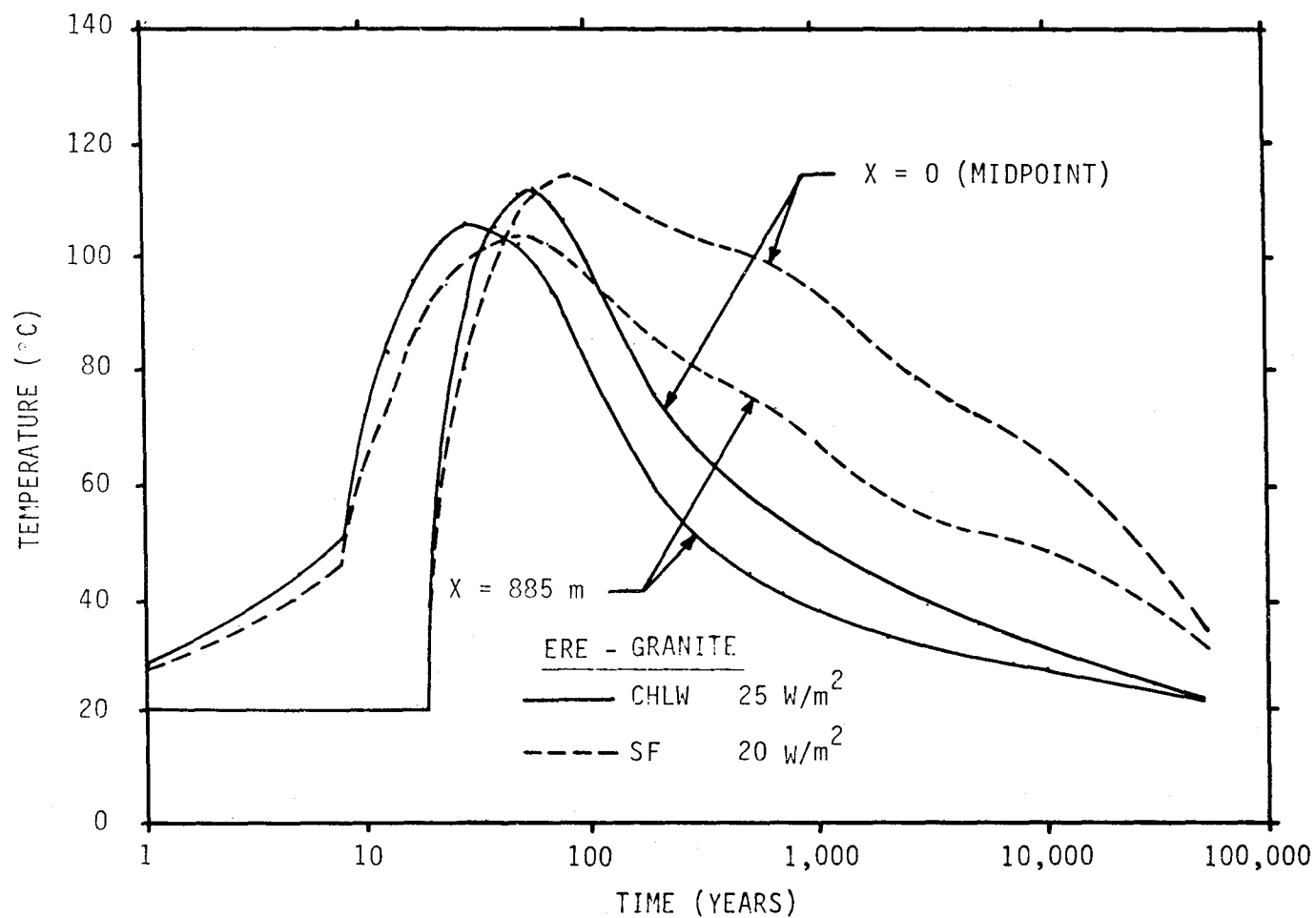
Figure 4-40. Transient Thermal Response Predicted by Far-Field Model at Two Locations on Midplane of a Nuclear Waste Repository (1,000 m Deep) in Granite. Conduction Heat Transfer Only.

repository is also shown in this figure). Figure 4-41 shows temperatures along the midplane of a CHLW repository at various times. As can be seen in these figures, the peak temperature is about 113°C (93°C rise from the initial geothermal temperature of 20°C) and occurs at 50 years along almost the entire length of the repository. Figure 4-41 also shows the sequential-loading effect on the horizontal temperature gradients within the repository during the emplacement period (0-19 years). During this time, these gradients are very severe, creating the potential for thermally induced perturbations to the regional ground water. At later times, the horizontal temperature gradients within the repository decrease until the entire length of the repository is heated nearly uniformly after 100 years. Consequently, the effects of sequential loading are most pronounced during the first 100 years after emplacement. This conclusion was also reached in a previous far-field thermal analysis [Osnes et al, 1978] which showed that the far-field thermal response is nearly the same for both instantaneously and sequentially loaded models after the first 100 years.

The vertical temperature gradients are also very high surrounding the repository in early time. Figure 4-42 shows the temperatures along the vertical centerline of the far-field model of a CHLW repository. At 50 years (when peak temperatures occur within the repository), very little of the granite above and below the repository is affected thermally. The steep gradients again provide the mechanism for perturbed ground-water flow. Even at 1,000 years most of the rock mass remains at its initial geothermal temperature. However, at this time, the vertical gradients are much less severe since the repository temperatures are decreasing while the surrounding granite is still slowly heating up.

Temperature rise isotherms for the conduction baseline model are contained in Figures 4-43 through 4-46. The steep temperature gradients surrounding the repository are observed during the early time. The isotherms are distributed essentially symmetrically around the repository, as the heat is being transferred uniformly through the granite. As can be seen, there is no boundary interference through the first 1,000 years. During this time all of the isotherms are sufficiently contained within the model, indicating that the boundaries are far enough removed from the repository during the first 1,000 years after emplacement. At 1,000 years, the edge of the repository is cooler than the center since the peripheral waste is 20 years older than the central waste and, consequently, generating less heat. At 10,000 years, the earth's
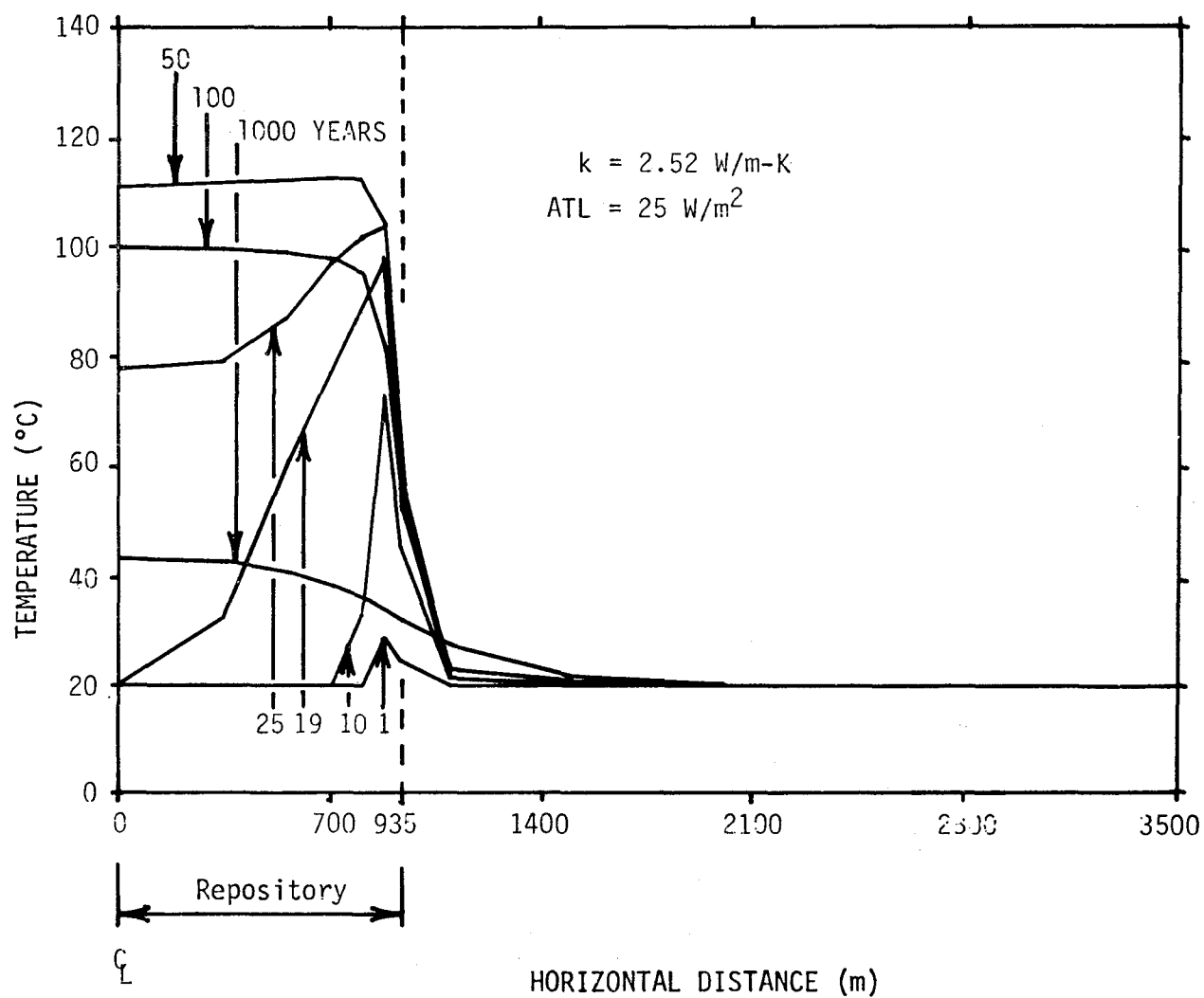
Figure 4-41. Temperature Distribution Along Midplane of a CHLW Repository (1,000 m Deep) at Various Times After Emplacement. Sequential Loading. Conduction Baseline (FC-1).
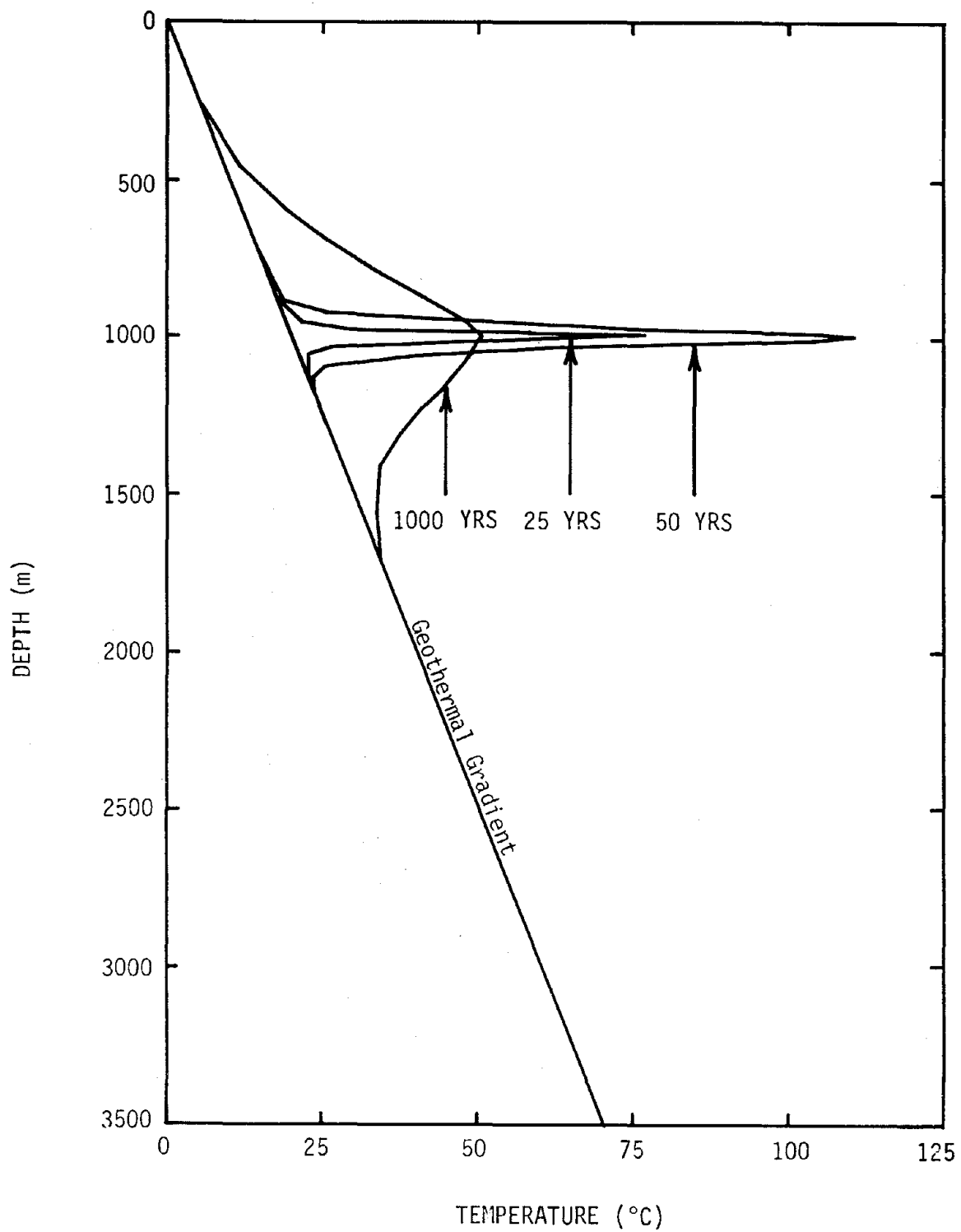
Figure 4-42. Temperatures Along Vertical Centerline of a CHLW
              Repository at Various Times. ATL = 25 W/m².
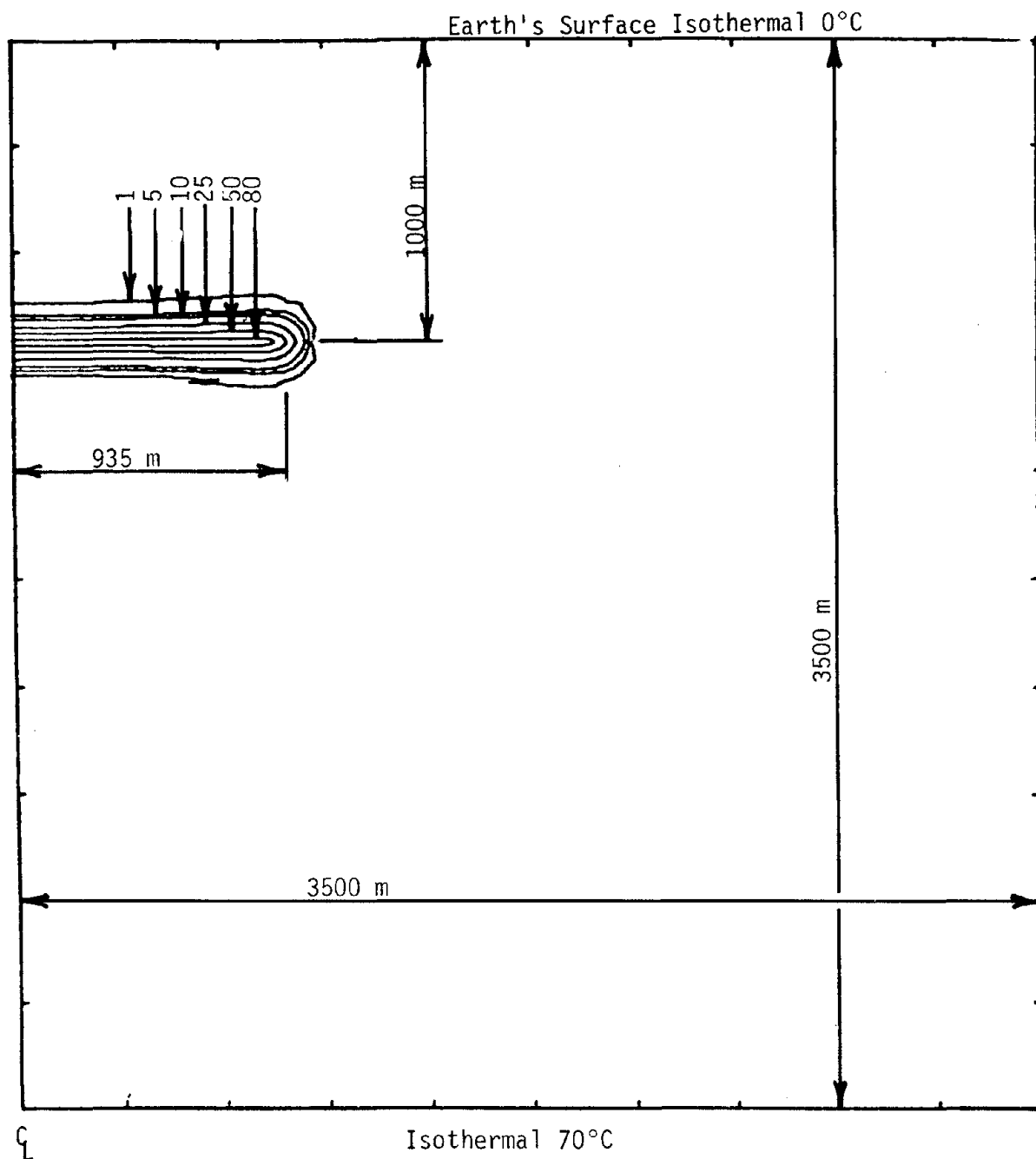
Figure 4-43.   Temperature Rise Isotherms (°C) Surrounding a CHLW Repository
in Granite at 50 Years.
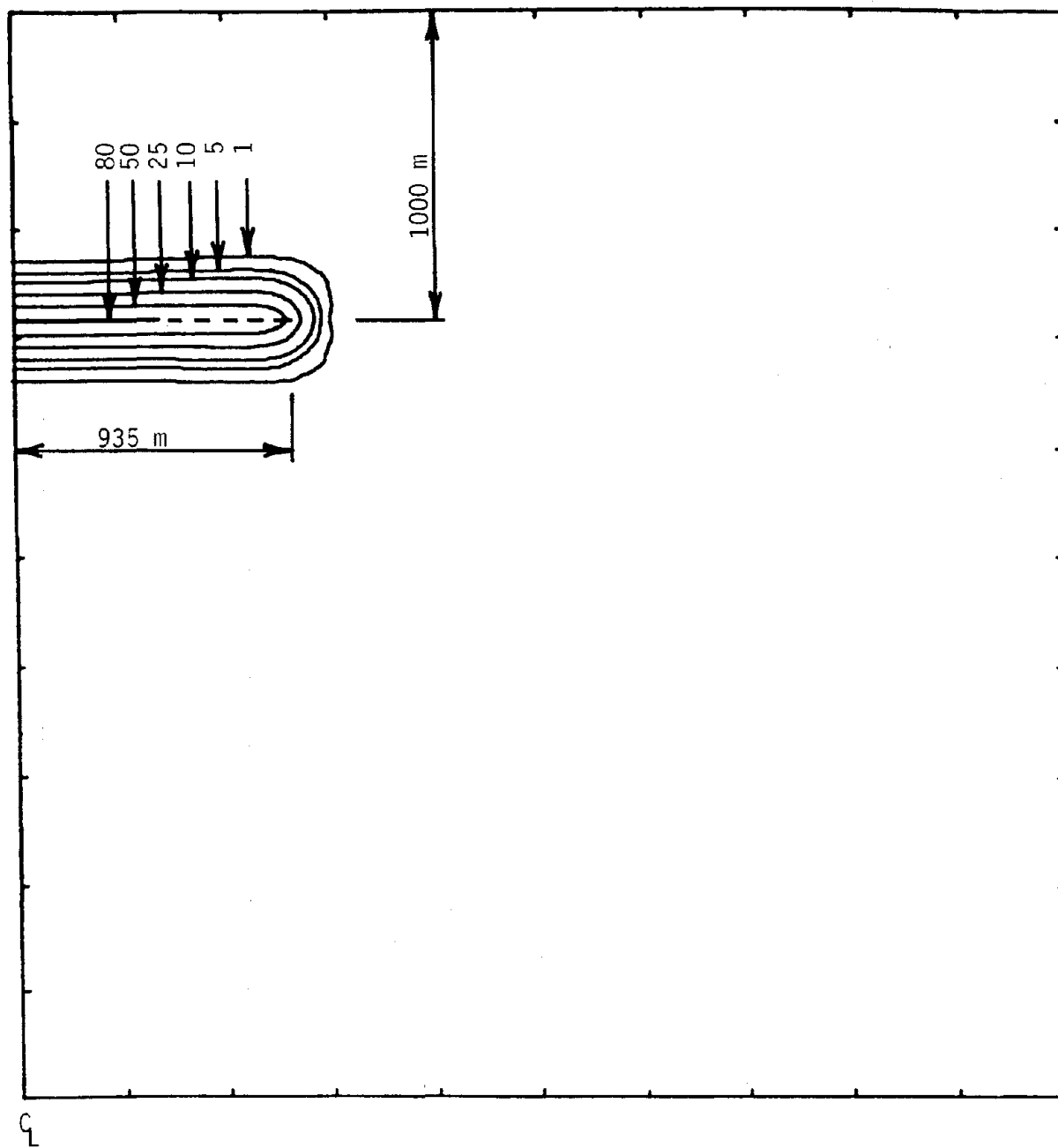
Figure 4-44.   Temperature Rise Isotherms (°C) Surrounding a CHLW Repository
               in Granite at 100 Years.
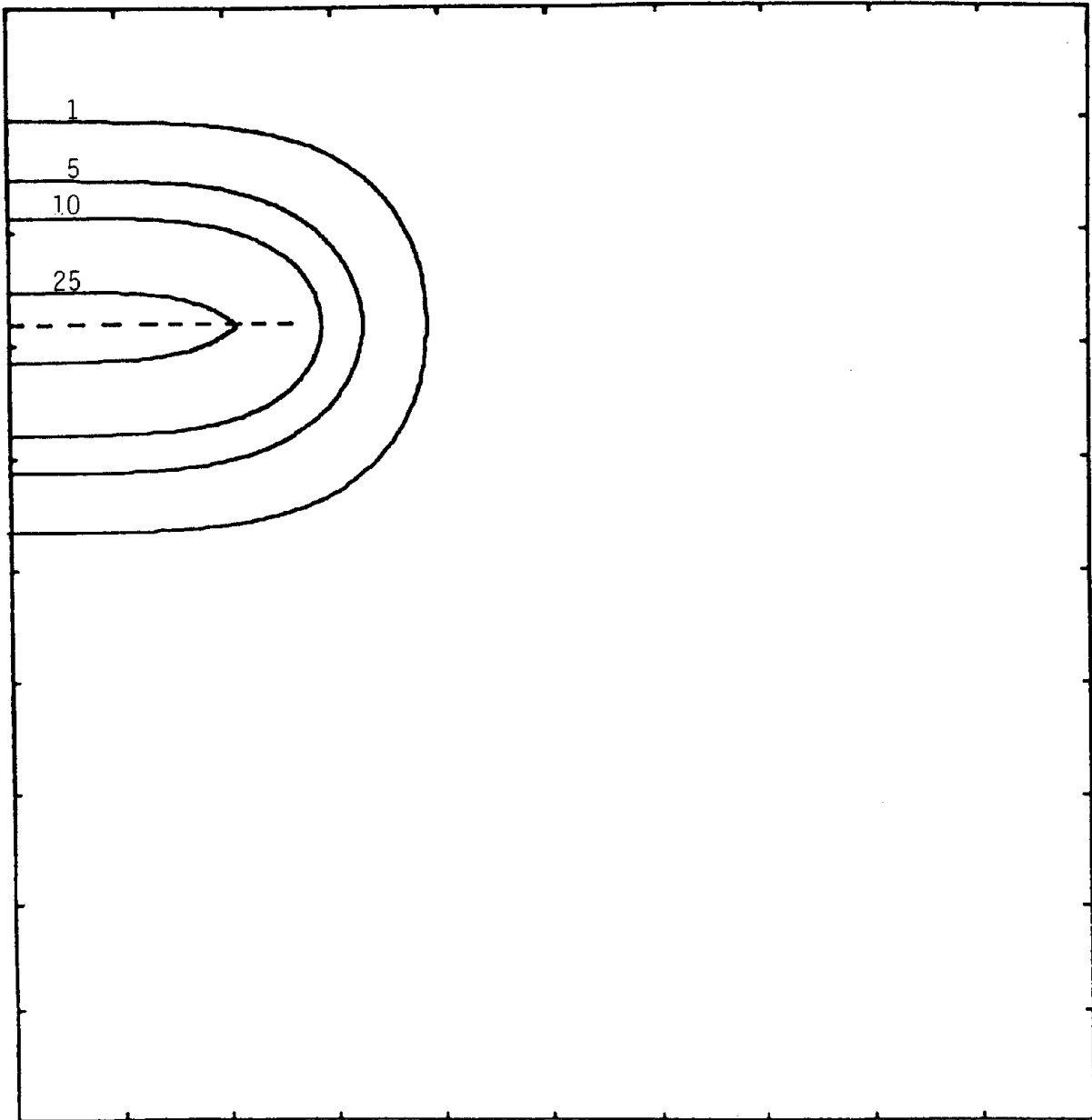
Figure 4-45. Temperature Rise Isotherms (°C) Surrounding a CHLW Repository in Granite at 1,000 Years.
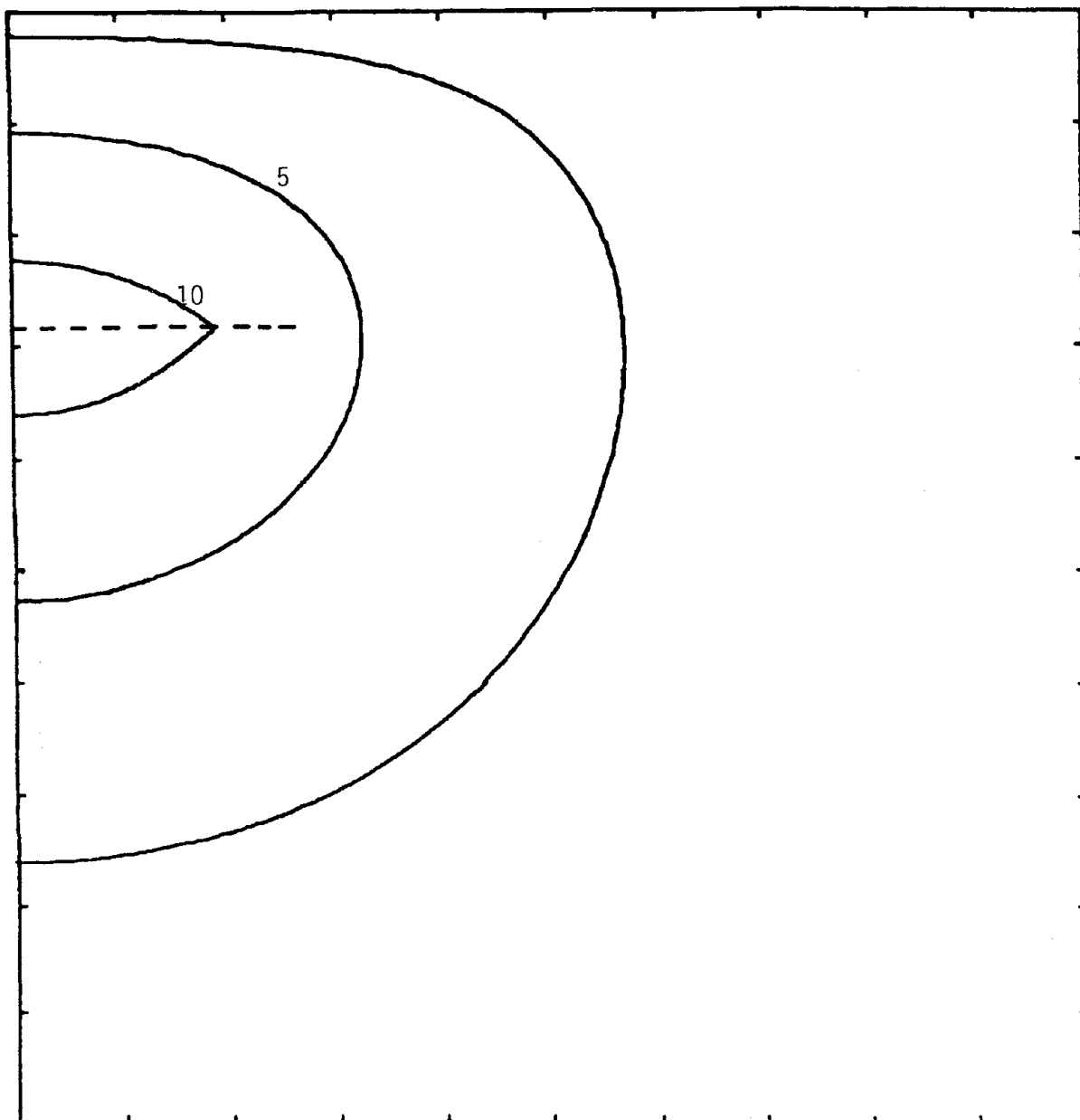
Figure 4-46. Temperature Rise Isotherms (°C) Surrounding a CHLW Repository in Granite at 10,000 Years.

surface influences the heat transfer near the top of the model. However, the 1°C rise isotherm does not intersect the right and lower boundaries and most of the granite is unaffected thermally, even after 10,000 years.

The transient thermal response at various points in the far-field region is shown in Figure 4-47. The repository midpoint (point A) undergoes a 93°C temperature rise during the first 30 years. Then the rapid decay of the CHLW causes the temperature to decrease at a relatively rapid rate until the midpoint is within 3°C of the initial repository horizon temperature (20°C) at 50,000 years. The temperature at points 400 m above and below the repository is not perturbed until approximately 200 years after emplacement and these points reach a peak temperature at about 3,000 years.

A comparison of the results of the baseline conduction models of a SF and a CHLW repository shows that the temperatures throughout the far-field region peak at later times and decrease at a slower rate in the SF model. This difference is particularly visible in the temperature rise isotherms shown in Figures 4-35 through 4-38 for SF and Figures 4-43 through 4-46 for CHLW. The temperatures in a larger volume of the surrounding host granite are perturbed by 1°C or more in the SF far-field model. Not only is the extent of the temperature rise isotherms significantly larger for SF, but the magnitude of the isotherms is also greater. The higher concentration of long-lived isotopes in SF, which results in a slower decay rate, is responsible for these differences.

Figure 4-40 shows that the transient thermal response near the repository is similar for both SF and CHLW during the first 100 years. The maximum temperature rise in both repositories is approximately 95°C. However, the ATL of the SF repository is only 80 percent of the ATL of the CHLW repository (20 W/m^2 for SF, 25 W/m^2 for CHLW). A similar result was reported in a previous far-field thermal study [Osnes et al, 1978]. In that study, it was found that the peak temperatures near a CHLW repository were approximately 75 percent of the temperatures near a SF repository for any of the ATLs, repository depths, and rock types (including granite) considered in the study. Since the thermal properties used in the far-field models in that study were temperature independent, the models were linear and the temperatures predicted were proportional to ATL. Consequently, that study indicates that an ATL for a SF repository of 75 percent of the ATL for a CHLW repository would result in approximately the same peak temperatures near both repositories.
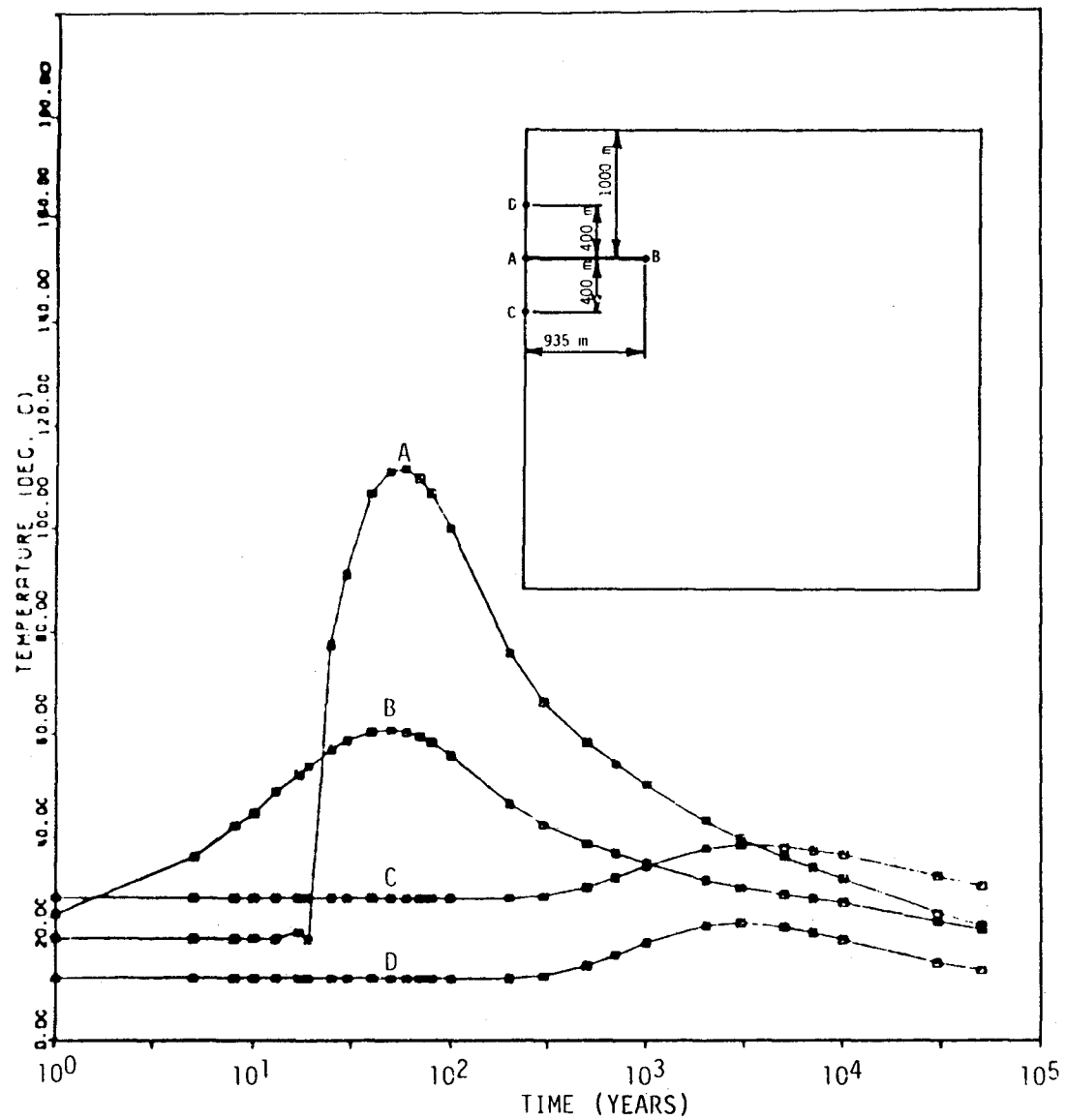
Figure 4-47. Thermal Response at Various Points Surrounding a CHLW
Repository in Granite.

4.3.5.2 Combined Conduction-Convection Analyses of CHLW Far-Field

Comparison of the temperatures predicted by the four flow conditions is given in Table 4-15 at five locations in the model. All analyses which included convective heat transfer (FC-2 through FC-4) showed no significant deviation from the conduction temperatures discussed previously. All temperatures, which were based on models that included convection, were within 0.8°C of the conduction-based temperatures at all times; thus, demonstrating that convective heat transfer is negligible as far as temperature predictions in the far-field region are concerned.

Table 4-15. Comparison of Temperatures Predicted by Four Flow Conditions at Various Times and Locations -- CHLW
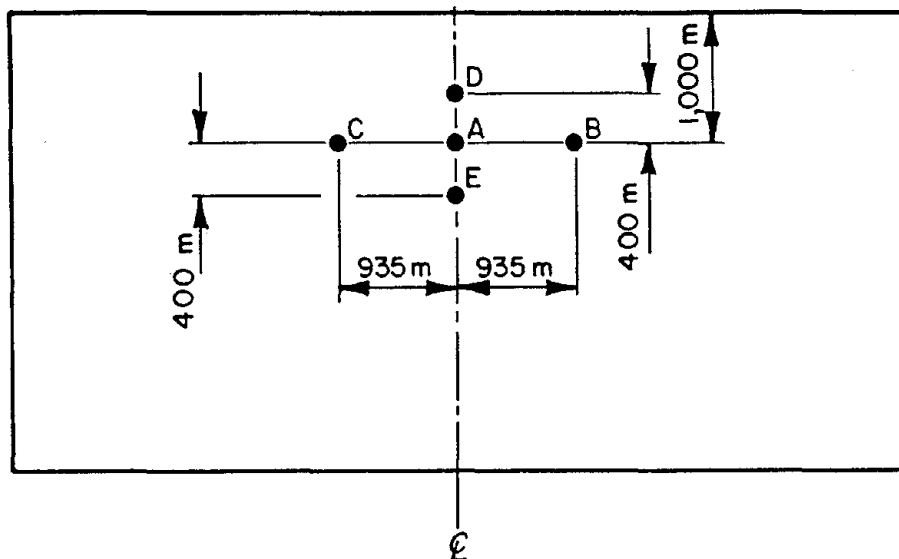
Location	Time (Years)	Temperature (°C)			
		FC-1	FC-2	FC-3	FC-4
A	19	19.67	19.67	19.67	19.67
	100	100.19	100.79	100.40	100.79
	1,000	50.02	50.76	50.50	50.76
B	19	53.93	53.93	53.94	53.94
	100	56.15	56.31	56.22	56.34
	1,000	35.08	35.18	35.10	35.21
C	19	53.93	53.93	53.92	53.92
	100	56.15	56.31	56.17	56.28
	1,000	35.08	35.18	35.03	35.15
D	19	12.01	12.01	12.01	12.01
	100	12.02	12.02	12.02	12.02
	1,000	19.21	19.27	19.15	19.27
E	19	28.01	28.01	28.01	28.01
	100	28.02	28.02	28.02	28.02
	1,000	34.56	34.59	34.51	34.59

5 CHEMICAL AND RADIATION ENVIRONMENTS

5.1 CHEMICAL COMPOSITION OF GRANITE

The average chemical composition of granitic rock was obtained from the literature [Office of Waste Isolation, 1978b; Travis, 1955] and general geologic knowledge. Table 5-1 lists the average chemical composition for a typical granite. This is a site-specific property, and Table 5-1 should be used only as a reference guide.

5.2 GROUND-WATER COMPOSITION

Water contained in bedrock pores at great depth is "very old water" [Office of Waste Isolation, 1978d], which has been in contact with the minerals in the bedrock for a geologically long time period. The ground water will be in chemical equilibrium with the existing minerals, comprising a relatively stable and constant ground-water composition. Therefore, the chemical composition of ground water in the repository rock depends on the composition of the specific granite.

The chemical composition of the ground water within the granite repository is important in determining the stability of the canister and the leach rates of waste products if the canister is breached. Determining the composition of ground water from great depths in a crystalline rock such as granite is difficult since it is not easy to obtain uncontaminated specimens for analysis. The literature contains few chemical analyses of ground water at the depth of 1,000 m. Estimates of ground-water composition in this study are based on the generic granite composition in Table 5-1 [Office of Waste Isolation, 1978b; Travis, 1955] and Swedish reports [Korrosionsinstituet, 1977; Kärnbränslesäkerhet, 1978a; 1978b] which deal with the composition of ground water at depths up to 450 m. Table 5-2 lists major and minor constituents expected to be found in the ground water of an unweathered, intact granite 1,000 m below the earth's surface. Natural environments contain many chemical constituents which may vary over wide ranges. Certain constituents in a rock mass may exist in either a reduced or oxidized state. The oxidation-reduction

Table 5-1. Average Chemical Composition of a Generic Granite

Component	Weight Percent
SiO_2	71.5
Al_2O_3	14.0
Fe_2O_3	1.5
FeO	1.4
MgO	0.6
CaO	1.6
Na_2O	3.4
K_2O	4.3
H_2O	0.8
TiO_2	0.4
P_2O_5	0.2
MnO	0.1

Table 5-2. Ground-Water Composition of a Generic Granite

Component	Range (mg/l)
Ca^{2+}	20 - 50
Na^+	10 - 100
Mg^{2+}	5 - 30
Fe^{2+}	0.5 - 15
Fe_{tot}	1 - 20
K^+	1 - 5
Mn^{2+}	0.1 - 0.5
HCO_3^-	60 - 400
Cl^-	5 - 100
SO_4^{2-}	1 - 40
NO_3^-	0.1 - 2
PO_4^{3-}	0.01 - 0.6
F^-	0.5 - 3
HS^-	<0.1 - 5
CO_2	0 - 25
SiO_2	5 - 40
NH_4	0.1 - 0.4
NO_2	<0.01 - 0.1
O_2	<0.01 - 0.07

or redox potential (Eh) has a marked effect upon the chemical reactivity, composition, and organic content of a natural environment.

In situ values of Eh and pH for deep ground water in granite are almost nonexistent in the literature. Estimates must be based on values for ground water in soils and known chemical reactions. Baas Becking et al [1960] use the Eh-pH diagram to illustrate mineral stability in natural environments. Research by Baas Becking et al [1960], which includes published data by Zyka [1958], shows the pH of connate waters ranges from approximately 5 to 8 and the Eh ranges from -0.30 V to +0.10 V. Garrels and Christ [1965] report pH and Eh values of 6.7 to 8.5 and -0.23 V to +0.12 V, respectively, for naturally occurring ground water. Analyses of the deepest ground water are provided by Korrosionsinstituet [1977] and Kärnbränslesäkerhet [1978a; 1978b]. Ground water from 500 m deep in Stripa granite have Eh values ranging between -0.21 V and -0.14 V. The observation that the pH and Eh values of deep ground waters are bracketed by connate and near-surface ground water suggests that the pH and Eh of deeper ground waters are likely to be within the range of granite far below the surface level. However, to assess accurately the chemistry of deep ground water, laboratory analyses must be conducted on water from the specific repository site.

5.3 CORROSION

The canister material that will come into contact with the granite backfill is 304 stainless steel. The presence of water within the repository may lead to the eventual corrosion of the canister wall. Chloride content is one of the main factors determining whether or not water will corrode stainless steel [Shrier, 1976]. Other significant factors include the oxygen content of the water, the hydrogen-ion concentration (pH), and the redox potential (Eh). The water hardness, temperature, velocity, and presence of other cations and anions can also be important.

The amount of water reaching the canister surface will depend on the permeability of the granite surrounding the canister. High permeability, allowing more water to reach the canister, causes an increase in the rate of corrosion.

Redox reactions involve the exchange of electrons or the migration of electronic charge which can be measured in volts. The negative electrode

potential measured in granite at depth indicates a reducing system [Zobelle, 1946]. The redox potential is dependent on the pH or hydrogen-ion concentration of the chemical reaction. As pH values increase, oxidation-reduction systems generally become more reducing.

According to Garrels and Christ [1965], confined waters entrapped in rock pores rapidly lose their oxygen content. Organic-free water entrapped in granite pore spaces reacts with silicates such as biotite and chlorite, containing ferrous iron or with sulfides such as pyrite and phyrrotite. The most important reducing agents in granite are the iron compounds within the silicate structure [Kärnbränslesäkerhet, 1978b]. The general redox reaction for this mechanism is:

$$2 \; FeO + H_2O \rightleftharpoons Fe_2O_3 + 2H^+ + 2e^- \tag{5-1}$$
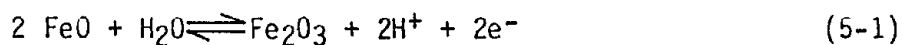
At depth, this environment is reducing and alkaline, because hydrolysis of the silicates causes an increase in the pH [Garrels and Christ, 1965].

The stainless steel canister chosen for this study, a chromium-nickel alloy, has a high resistance to many corrosive environments. Chromium (18-20 percent) is chemically inert in an oxygenated environment. However, to minimize corrosion effects, the granitic bedrock ultimately chosen for a repository should have low permeability and chloride concentration, a negative Eh value, and a pH range of 6.7 to 8.5.

Temperatures no greater than 250°C are expected at the canister skin. This temperature is not high enough to accelerate intergranular corrosion and stress-corrosion cracking significantly [Butler and Ison, 1966].

Living organic matter can produce changes in the composition of water. Actions including carbon dioxide/oxygen exchange, consumption of oxygen, production of sulphides, or production of corrosive amino acids may occur, if living organisms are present, in water. The possibility of organic matter existing at the depth considered is negligible. If organisms are introduced during the construction or filling stages of the repository, the environment would not permit them to persist. Therefore, organic chemical corrosion does not seem to be a significant problem.

5.4 RADIATION ENVIRONMENTS

Figures 5-1, 5-2, and 5-3 show the absorbed gamma dose rate as a function of distance from the centerline of the canister for CHLW, SF, and DHLW, respectively. The data for these figures was calculated by Science Applications, Inc., and copies of the letters containing this data are in Appendix D. Total absorbed doses for CHLW and SF were found by integrating the dose rates at a reference distance of 20.74 cm and at the emplacement hole wall. Because the gamma ray spectrum changes with time, approximate reduction factors were used to convert the dose rates in Figures 5-2 and 5-3 to longer decay times. This extrapolation beyond 100 years is a conservative estimate, and the actual absorbed dose would be less than calculated.

Figure 5-4 shows the total absorbed dose as a function of time found by integrating the dose rates through 10,000 years after emplacement. The total dose absorbed at the reference distance of 20.74 cm through 10,000 years is 7.2 and 0.91 gigarads for the CHLW and the SF canisters, respectively. At the emplacement hole wall, the granite absorbs 3.7 and 0.35 gigarads of gamma radiation through 10,000 years for the CHLW and the SF canisters, respectively.

Although the total absorbed dose is not shown for the DHLW canister, it would be much lower than either the CHLW or the SF canisters because of the more rapid decay and the lower radionuclide concentration of the DHLW.

Note that the radiation environments for CHLW and DHLW are based on 1 kW and 310 W canister thermal loadings, respectively. For reprocessed wastes like CHLW and DHLW, different canister thermal loadings can be obtained simply by diluting the waste with additional bulking material (glass). Since the canister geometry does not change in this process, the self-shielding provided by the canister and its contents does not change significantly. Consequently, the dose rates are nearly proportional to the canister thermal loadings for CHLW and DHLW as long as the isotopic composition of the waste does not change.
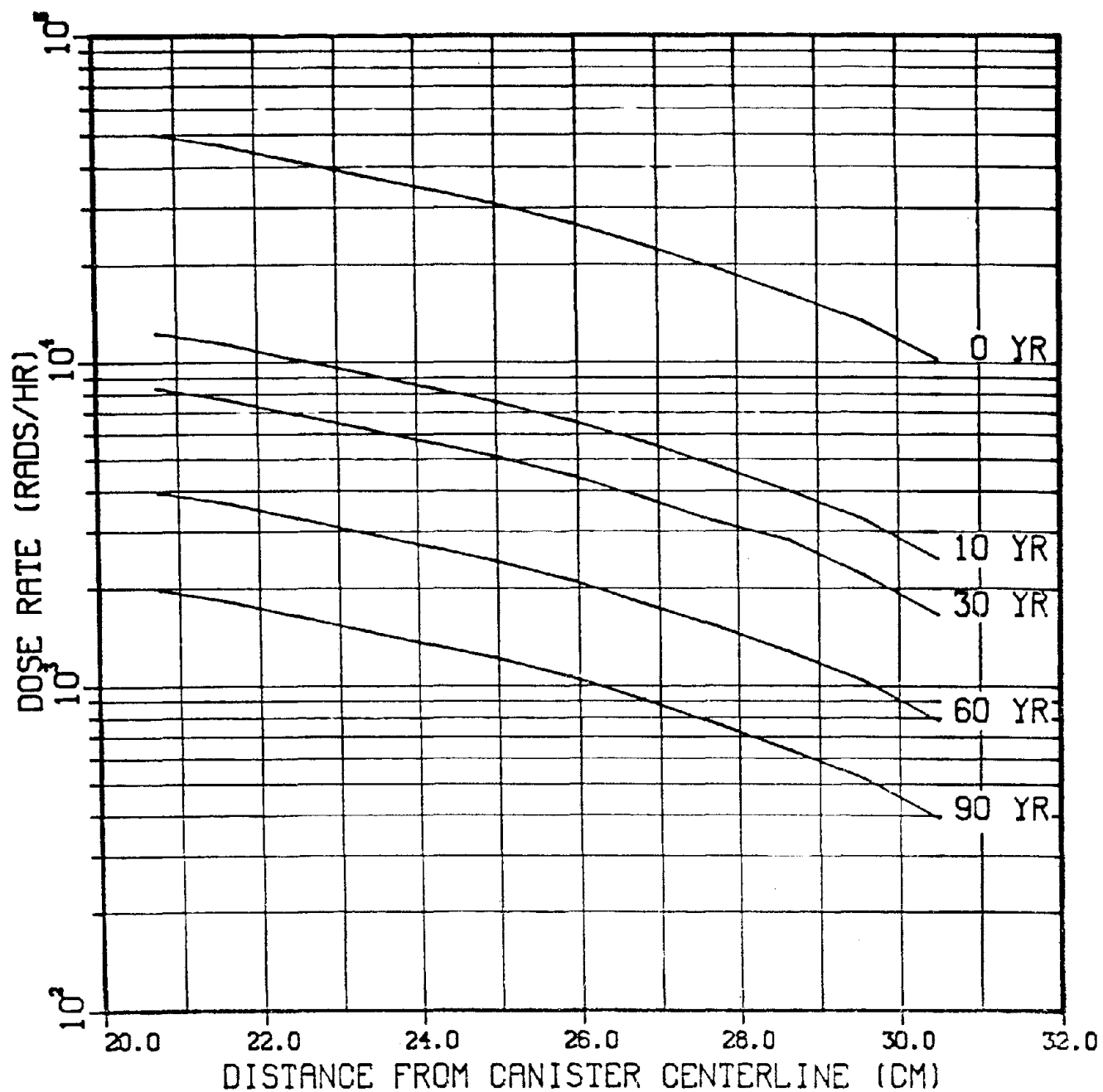
Figure 5-1.　Rate of Gamma Radiation Absorption at Several Times After
Emplacement of a 1 kW CHLW Canister in Granite.
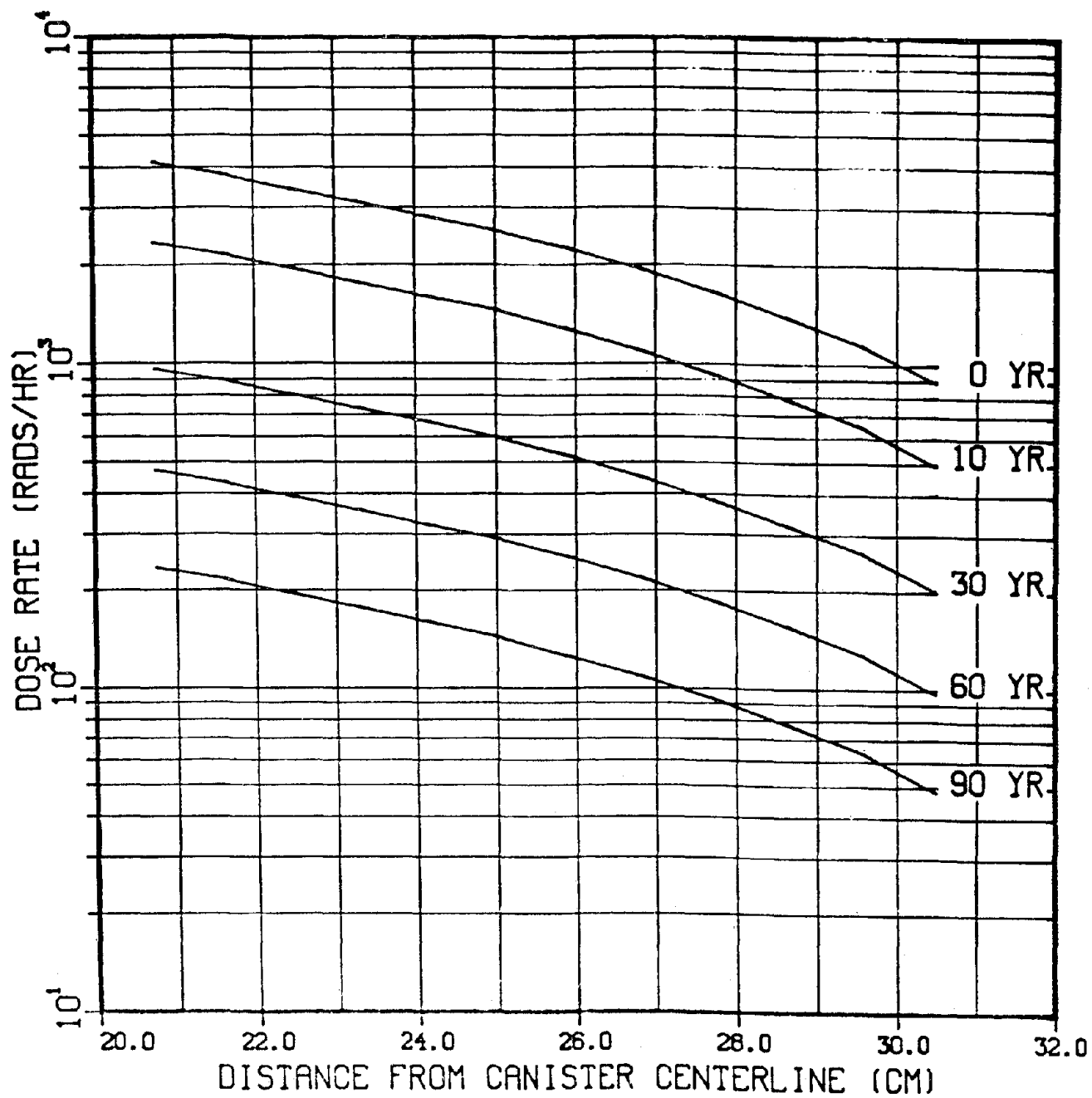
Figure 5-2. Rate of Gamma Radiation Absorption at Several Times After
Emplacement of 550 W SF Canister in Granite.
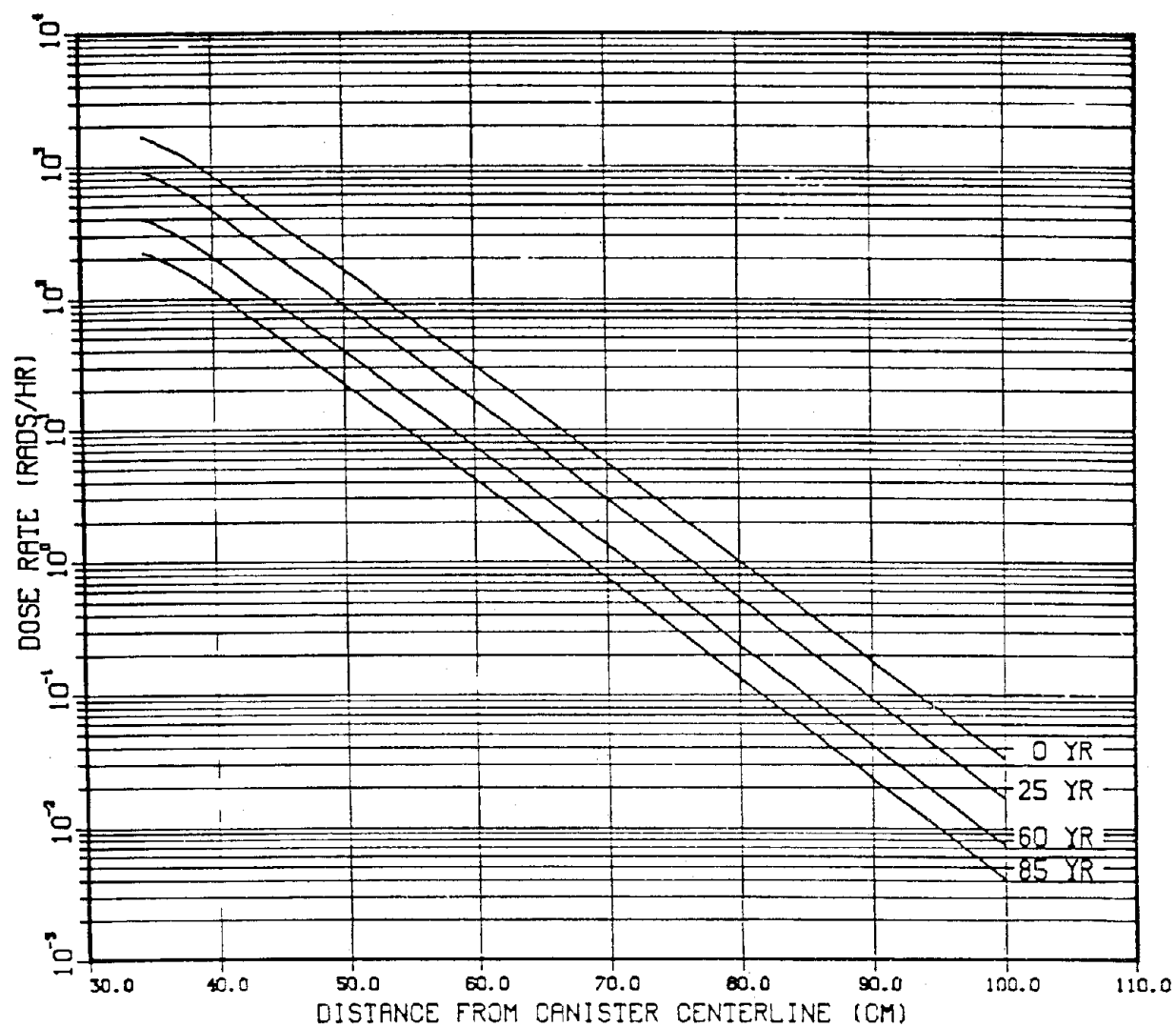
Figure 5-3. Rate of Gamma Radiation Absorption at Several Times After
Emplacement of 310 W DHLW Canister in Granite.
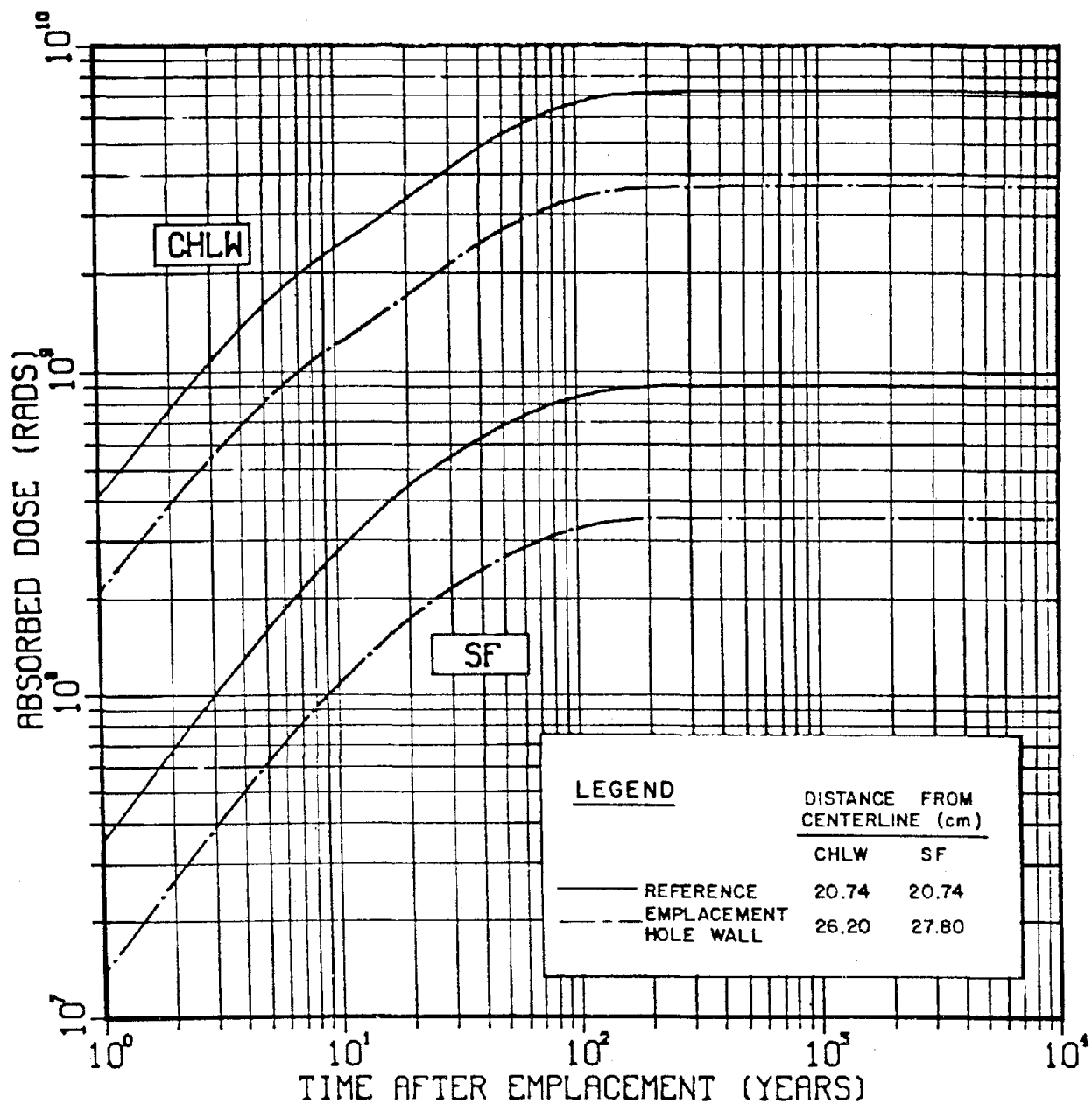
Figure 5-4. Total Absorbed Gamma Radiation in Granitic Rock Surrounding a 1 kW CHLW Canister and a 550 W SF Canister.

6 SUMMARY

This report describes the thermal, hydrogeological, geochemical, and radiation environments expected in and around a repository in granitic rock. It will be used by the Reference Repository Conditions - Interface Working Group to develop standardized repository conditions for the CWRM Program*.

Thermal, mechanical, and hydrogeological properties are defined for a granitic rock, both for intact rock and for discontinuities such as joints and fractures. In addition, expected temperature gradients and in situ stress conditions are described.

The baseline repository consists of a series of tunnels on one horizontal level at a depth of 1,000 m with cylindrical waste containers emplaced into vertical drill holes in the tunnel floors. In plan view, the repository is square with a square shaft pillar located in the center. Three types of nuclear waste are considered: unreprocessed spent fuel (SF), commercial high-level waste (CHLW), and defense high-level waste (DHLW) with areal thermal loadings of 20, 25, and 25 W/m^2, respectively. The operational sequence consists of a 20-year waste emplacement period, a 5-year monitoring period, and 100 days of blast-cooling followed by backfilling and decommissioning of the repository.

Numerical analyses were performed on three scales (the very-near field, near field, and far field) to determine thermal environments. Two parameters, thermal conductivity of granite and number of rows of waste cans across a room, were varied and calculations were performed for each of the three waste types. In the very-near field, the DHLW and SF produced similar results with the number of rows of cans having a minimal effect. For example, the maximum temperature rises predicted for the canister skin occurs at about 20 years after emplacement and is about 180°C for a granite thermal conductivity of 2.52 W/m-K. CHLW, with an initial canister heat load of 2,100 W, yielded maximum temperature rises of about 400°C which was considered to be unacceptable. An initial CHLW heat load of 700 W was then examined and found to yield similar thermal results to the SF and DHLW.

The near-field calculations also resulted in comparable results for the three waste types with maximum floor centerline temperature increases ranging from 117°C to 145°C for a granite thermal conductivity of 2.52 W/m-K. The peak floor temperatures occurred at 35, 35, and 50 years for CHLW, DHLW, and SF, respectively.

*Formerly the National Waste Terminal Storage (NWTS) program.

The far-field analyses incorporate sequential loading of the repository and have been performed only for SF and CHLW. The CHLW yielded a maximum repository temperature rise of about 93°C at 50 years. The spent fuel yielded a similar temperature rise, but the peak temperature occurred somewhat later at 100 years. A significant difference between the two waste types is that the temperatures in a SF repository stay relatively high for a considerable period of time (thousands of years); whereas, the CHLW repository temperatures decay fairly rapidly (hundreds of years). Thus, the rock mass, including any ground water above the SF repository, is heated significantly for an appreciable time.

Analyses of regional and thermally-induced ground-water flow indicated that the perturbations to the temperatures calculated, assuming conductive heat transfer alone, would be insignificant.

The chemistry of typical granite and ground water are presented, as are calculations of the expected radiation fields near the waste containers.

Future studies of the expected repository environments in granite will deal with mechanical effects, including analyses of the stress perturbations caused by the construction of the repository and by the heat emitted by the nuclear wastes. Displacements will be calculated, and zones where potential for failure exist will be identified.

7 REFERENCES

Acres Consulting Services Limited, RE/SPEC Inc., Dilworth, Secord, Meagher and Associates, and Hagconsult AB, 1978. Radioactive Waste Repository Study: Part II, AECL-6188-2, prepared for Atomic Energy of Canada Limited, Pinawa, Manitoba.

Acres Consulting Services Limited, RE/SPEC Inc., Dilworth, Secord, Meagher and Associates, Atomic Energy of Canada, Ltd., and W. L. Wardrop and Associates Ltd., 1980a. A Disposal Centre for Immobilized Nuclear Waste: Conceptual Design, AECL-6416, prepared for Atomic Energy of Canada Limited, Pinawa, Manitoba.

Acres Consulting Services Limited, RE/SPEC Inc., Dilworth, Secord, Meagher and Associates, Atomic Energy of Canada, Ltd., and W. L. Wardrop and Associates Ltd., 1980b. A Disposal Centre for Irradiated Nuclear Fuel: Conceptual Design Study, AECL-6415, prepared for Atomic Energy of Canada Limited, Pinawa, Manitoba.

Baas Becking, L. G. M., I. R. Kaplan, and D. Moore, 1960. "Limits of the Natural Environment in Terms of pH and Oxidation-Reduction Potentials," Journal of Geology, Vol. 68, No. 3, pp. 243-284.

Barton, N., 1973. "Review of a New Shear-Strength Criterion for Rock Joints," Engineering Geology, Vol. 7.

Beck, J. M. and A. E. Beck, 1965. "Computing Thermal Conductivities of Rocks From Chips and Conventional Specimens," Journal of Geophysical Research, Vol. 70, pp. 5227-5239.

Birch, F., J. F. Schairer, and H. C. Spicer, (Ed.), 1942. Handbook of Physical Constants, Geological Society of America, Special Papers No. 36.

Brace, W. F. and A. S. Orange, 1968. "Electrical Resistivity Changes in Saturated Rocks During Fracture and Frictional Sliding," Journal of Geophysical Research, Vol. 73, pp. 1433-1445.

REFERENCES

(Continued)

Brown, E. T. and E. Hoek, 1978. "Trends in Relationships Between Measured In-Situ Stresses and Depth," International Journal of Rock Mechanics and Mining Sciences, Vol. 15, pp. 211-215.

Brown, R. H., A. A. Konoplyantsev, J. Ineson, and V. S. Kovalevsky, (Ed.), 1975. Groundwater Studies, Unesco Press, New York, NY.

Butler, G. and H. C. K. Ison, 1966. Corrosion and its Prevention in Waters, Van Reinhold, New York, NY.

Callahan, G. D., 1981. Inelastic Thermomechanical Analysis of a Generic Bedded Salt Repository, ONWI-125, prepared by RE/SPEC Inc. for Office of Nuclear Waste Isolation, Battelle Memorial Institute, Columbus, OH.

Callahan, G. D. and J. L. Ratigan, 1978. Thermoelastic Analyses of Spent Fuel Repositories in Bedded and Dome Salt, Y/OWI/SUB-77/22303/4, prepared by RE/SPEC Inc. for Office of Waste Isolation, Union Carbide Corporation, Nuclear Division, Oak Ridge, TN.

Carlsson, A. and T. Olsson, 1977. "Variations in Hydraulic Conductivity in Some Swedish Rocks," Rockstore 77, Vol. 2, pp. 301-307.

Cermak, V. and A. M. Jessop, 1971. "Heat Flow, Heat Generation and Crystal Temperature in the Kapuskasing Area of the Canadian Shield," Tectonophysics, Vol. 11, pp. 287-303.

Coates, D. F. and Y. S. Yu, 1969. "Analysis of Grading Effects on Hydraulic and Consolidated Fill," C.I.M. Transcriptions, Vol. 72, pp. 279-284.

Crane, R. A., M. S. Khader, and R. I. Vachon, 1977. "Thermal Conductivity of Granular Materials - A Review," Proceedings of the Seventh Symposium on Thermophysical Properties, ASME.

Davis, S. N. and R. J. M. DeWiest, 1966. Hydrology, John Wiley & Sons, New York, NY.

REFERENCES

(Continued)

Dmitriyev, A. P., L. S. Kuzyayev, and Y. I. Protasov, 1969. Physical Properties of Rocks at High Temperatures, NASA Technical Translation No. TT F-684.

Finne, A. and A. Engelbrektson, 1977. Utformning av bergrumsanlaggningar (Description of the Construction of Temporary Storage and Final Repository for Vitrified Radioactive Waste), KBS TR 38, Karnbranslesakerhet, Stockholm, Sweden.

Garrels, R. M. and C. L. Christ, 1965. Solutions, Minerals, and Equilibria, Harper & Row Publishers, Inc, New York, NY.

Geller, L. B., 1970. "A New Look at Thermal Rock Fracturing," extract from Transactions/Sec. American Institute of Mining and Metallurgical, Vol. 79, pp. A133-A170.

Griffin, J. R., H. Beale, W. R. Burton, and J. W. Davies, 1979. "Geological Disposal of High Level Radioactive Waste, Conceptual Repository Design in Hard Rock," Proceedings of the International Symposium on the Underground Disposal of Radioactive Wastes, Otaniemi, IAEA-SM-243/93, July.

Hast, N., 1965. "Spanningstillstand i den fasta jordskorpans ovre del," IVA, nr 142, Stockholm, Sweden.

Hengst, G., 1934. "The Thermal Conductivity of Powdered Thermal Insulators at High Pressure", Ph.D. Dissertation, Technische Hochschule Munchen.

Herget, G., 1973. "Variations of Rock Stresses with Depth at a Canadian Iron Mine," International Journal of Rock Mechanics and Mining Sciences, Vol. 10, No. 1, pp. 37-51.

Hooker, V. E., D. L. Bickel, and J. R. Aggson, 1972. "In Situ Determination of Stresses in Mountainous Topography," U.S. Bureau of Mines Report of Investigation No. 7654, Denver, CO.

INFCE, 1979. Release Consequence Analysis for a Hypothetical Geologic Radioactive Waste Repository Intact Rock, prepared for Working Group 7 of the International Nuclear Fuel Cycle Evaluation, INFCE/DEP/WG.7/21.

REFERENCES
(Continued)

Jaeger, J. C. and N. G. W. Cook, 1969. Fundamentals of Rock Mechanics, Methuen & Co., Ltd, New York, NY.

Kaganer, M. G., 1966. "Thermal Insulation in Low Temperature Engineering," Izd. Mashinostronenie.

Kärnbränslesäkerhet, 1978a. Handling of Spent Nuclear Fuel and Final Storage of Vitrified High Level Reprocessing Waste: II Geology, Stockholm, Sweden.

Kärnbränslesäkerhet, 1978b. Handling and Final Storage of Unreprocessed Spent Nuclear Fuel: II Technical, Stockholm, Sweden.

Korrosionsinstituet ock dess referensgrupp (Swedish Corrosion Institute and its Reference Group), 1977. Bedomning av korrosionsbestandigheten hos material avsedda for kapsling av karnbransleavfall. Lagesrapport 1977-09-27 samt kompletterande yttranden (Evaluation of the Corrosion Resistance of Material Intended for the Encapsulation of Nuclear Fuel Waste), KBS TR 31, Kärnbränslesäkerhet, Stockholm, Sweden.

Kulhawy, F. H., 1975. "Stress Deformation Properties of Rock and Rock Discontinuities," Engineering Geology, Vol. 9, pp. 327-350.

Kunii, D. and J. M. Smith, 1960. "Heat Transfer Characteristics of Porous Rocks," American Institute of Chemical Engineers Journal, Vol. 6, No. 1, pp. 71-78.

Lindroth, D. P. and W. G. Krawza, 1971. "Heat Content and Specific Heat of Six Rock Types at Temperature to 1000°C," U.S. Bureau of Mines Report of Investigation No. 7503, Denver, CO.

Marcuson III, W. F. and W. A. Bieganousky, 1977. "SPT and Relative Density in Coarse Sands," Journal of Geotechnical Engineering Division, GT11, pp. 1295-1309.

REFERENCES
(Continued)

McCann, R. A., 1980. HYDRA-1: A Three-Dimensional Finite Difference Code for Calculating the Thermohydraulic Performance of a Fuel Assembly Contained Within a Canister, PNL-3367, prepared by Pacific Northwest Laboratory, Richland, WA, for Office of Nuclear Waste Isolation, Battelle Memorial Institute, Columbus, OH.

Mercer, J. W. and G. F. Pinder, 1974. Finite Element Analysis of Hydrothermal Systems, University of Alabama in Huntsville Press.

Neff, J. O., 1980. "1980: The Year of the Plan," Proceedings of the 1980 National Waste Terminal Storage Program Information Meeting, ONWI-212, Office of Nuclear Waste Isolation, Battelle Memorial Institute, Columbus, OH, December.

Office of Waste Isolation, 1978a. Nuclear Waste Projections and Source-Term Data for FY 1977, Y/OWI/TM-34, Oak Ridge, TN.

Office of Waste Isolation, 1978b. Technical Support for GEIS: Radioactive Waste Isolation in Geologic Formations - Stratigraphies of Salt, Granite, Shale, and Basalt, Y/OWI/TM-36/3, Vol. 3, Oak Ridge, TN.

Office of Waste Isolation, 1978c. Technical Support for GEIS: Radioactive Waste Isolation in Geologic Formations - Baseline Rock Properties - Granite, Y/OWI/TM-36/5, Vol. 5, Oak Ridge, TN.

Office of Waste Isolation, 1978d. Technical Support for GEIS: Radioactive Waste Isolation in Geologic Formations - Ground Water Movement and Nuclide Transport, Y/OWI/TM-36/21, Vol. 21, Oak Ridge, TN.

Osnes, J. D. and T. Brandshaug, 1980. Irradiated Fuel Vault: Far-Field Thermal-Rock Mechanics Analyses, TR-51, prepared by Acres Consulting Services Limited, Niagara Falls, Ontario, for Atomic Energy of Canada Limited, Pinawa, Manitoba.

REFERENCES

(Continued)

Osnes, J. D., R. A. Wagner, and H. Waldman, 1978. Parametric Thermoelastic Analyses of High-Level Waste and Spent Fuel Repositories in Granite and Other Non-Salt Rock Types, Y/OWI/SUB-78/22303/12, prepared by RE/SPEC Inc. for Office of Waste Isolation, Union Carbide Corporation, Nuclear Division, Oak Ridge, TN.

Perloff, W. H. and W. Baron, 1976. Soil Mechanics: Principals and Applications, John Wiley & Sons, New York, NY.

Port-Keller, D. S. and P. F. Gnirk, 1981. CAES and UPHS in Hard Rock Caverns: I. Geological and Geotechnical Aspects, prepared by RE/SPEC Inc. for Pacific Northwest Laboratory, Richland, WA.

Portland Cement Association, 1968. "Design and Control of Concrete Mixtures," Engineering Bulletin: 3. General Information, Los Angelos, CA.

Ranalli, G. and T. E. Chandler, 1975. "The Stress Field in the Upper Crust as Determined From In Situ Measurements," Geologische Rundschau, Vol. 64, pp. 653-676.

Ratigan, J. L., 1977. Groundwater Movements Around a Repository: Thermal Analyses - Part 1: Conduction Heat Transfer, KBS TR 54:02, Kärnbränslesäkerhet, Stockholm, Sweden.

Ratigan, J. L., 1980. Immobilized Waste Vault: Container Near-Field Thermal-Rock Mechanics Analyses, TR-53, prepared by Acres Consulting Services Limited, Niagara Falls, Ontario, for Atomic Energy of Canada Limited, Pinawa, Manitoba.

Ratigan, J. L. and R. A. Wagner, 1978. Thermomechanical Analysis of Crushed-Salt Backfilled Disposal Rooms in a Conceptual Radioactive Waste Repository in Dome Salt, prepared by RE/SPEC Inc. for Stearns-Roger Engineering Company, Denver, CO.

REFERENCES

(Continued)

Roy, R. F., D. D. Blackwell, and F. Birch, 1968. "Heat Generation of Plutonic Rocks and Continental Heat Flow Provinces," Earth and Planetary Science Letters, Vol. 5, pp. 1-12.

Saint Goubain Techniques Nouvelles, 1977. Project for the Handling and Storage of Vitrified High-Level Waste, KBS TR 35, Kärnbränslesäkerhet, Stockholm, Sweden.

Sass, J. H. and A. H. Lachenbruch, 1971. "Uniform Heat Flow in a Deep Hole in the Canadian Shield and its Paleoclimatic Implications," Journal of Geophysical Research, Vol. 76, pp. 3586-8596.

Shrier, L. L., 1976. Corrosion: Volume 1, Newnes-Butterworths.

Snow, D. T., 1968. "Hydraulic Character of Fractured Metamorphic Rocks of the Front-Range and its Implications to the Rocky Mountains Arsenal Wells," Colorado School of Mines Quarterly, Vol. 63, pp. 167-199.

Swan, G., 1977. The Mechanical Properties of the Rocks in Stripa, Krakemala, Finnsjohn, and Blekinge, KBS TR 48, Kärnbränslesäkerhet, Stockholm, Sweden.

Travis, R. B., 1955. "Classification of Rocks," Colorado School of Mines Quarterly, Vol. 50, No. 1.

Van Sambeek, L. L., 1979. Long-Term Monitoring and Analysis of the Avery Island Heater Experiments, ONWI/SUB-79/E512-02200/6, prepared by RE/SPEC Inc. for Office of Nuclear Waste Isolation, Battelle Memorial Institute, Columbus, OH.

Wagner, R. A., 1980. Parametric Study Involving Thermo/Viscoelastic Analyses of a Room and Pillar Configuration, ONWI-115, prepared by RE/SPEC Inc. for Office of Nuclear Waste Isolation, Battelle Memorial Institute, Columbus, OH.

REFERENCES
(Concluded)

Waldman, H., 1980. Assessment of Numerical Technique for Thermal Analyses About a Waste Canister Array, ONWI-215, prepared by RE/SPEC Inc. for Office of Nuclear Waste Isolation, Battelle Memorial Institute, Columbus, OH.

Wingquist, C. F., 1969. "Elastic Moduli of Rock at Elevated Temperatures", U.S. Bureau of Mines Report of Investigation No. 7269, Denver, CO.

Woodside, W. and J. H. Messmer, 1961. "Thermal Conductivity of Porous Media. I. Unconsolidated Sands, II. Consolidated Rocks," Journal of Applied Physics, Vol. 32, pp. 1688-1706.

Woodward-Clyde Consultants, 1978. National Waste Terminal Storage Repository No. 1 Supporting Studies for Conceptual Design of Underground Facilities, prepared for Stearns-Roger Engineering Company, Denver, CO.

Yagi, S. and D. Kunii, 1957. "Studies on Effective Thermal Conductivities on Packed Beds," American Institute of Chemical Engineers Journal, Vol. 3, No. 3, pp. 373-381.

Zobelle, C. E., 1946. "Studies on Redox Potential of Marine Sediments," Bulletin of the American Association of Petroleum Geologists, Vol. 30, No. 4, pp. 477-513.

Zyka, V., 1958. "Hydrogeochemie a genese sirovodikovich pramenu na Gottwaldovsku", Geologicky Sbornik, Vol. 9, pp. 129-157.

APPENDIX A

A COMPILATION OF THERMAL/HYDROGEOLOGICAL

AND MECHANICAL PROPERTIES FOR GRANITE

APPENDIX A
TABLE OF CONTENTS

152

APPENDIX A
LIST OF TABLES

APPENDIX A

A.1 INTRODUCTION

The values that appear in Appendix A are the result of an extensive literature survey to establish the thermal/hydrogeological, mechanical, and in situ properties of a generic granite rock. Included in the tables are rocks not strictly classified as granite by R. B. Travis ("Classification of Rocks," Quarterly Colorado School of Mines, Vol. 50, No. 1, 1955), but which display properties similar to those of granite and should be included with the granitic data.

Where possible, the name, location, and description of the specimen is included. Most of the data represents intact rock tested in a laboratory. In situ testing is designated in the description column. Blank spaces appear where properties were not available.

Except where conversions were made for unit conformity, the data is reported as found in the original reference. Table A-1 lists the nomenclature and units used in Appendix A.

Table A-1. Nomenclature

Property	Symbol	Units
Thermal Conductivity	k	W/m-K
Specific Heat	C_p	J/kg-K
Thermal Expansion	α_T	10^{-6}/K
Hydraulic Conductivity	k_h	m/s
Permeability	κ	cm^2
Porosity	θ	%
Thermal Diffusivity	α	cm^2/s
Temperature	T	K
Density	ρ	g/cm^3
Young's Modulus of Elasticity	E	GPa
Poisson's Ratio	ν	-
Unconfined Compressive Strength	C_0	MPa
Tensile Strength	T_0	MPa

A.2 THERMAL/HYDROGEOLOGICAL PROPERTIES

ROCK TYPE: GRANITE	THERMAL/HYDROGEOLOGICAL PROPERTIES							TEST CONDITIONS						
NAME; DESCRIPTION: LOCATION	k (W/m-K)	C_p (J/kg-K)	α_T (10^{-6}/K)	k_h (m/s)	κ (cm^2)	θ (%)	α (cm^2/s)	T (K)	No. TESTS / SHAPE	MOISTURE CONTENT (%)	SAMPLE L:D LENGTH (cm)	SATURATION (%) / MEDIUM	NOTES	REF.
Albite Granite Medium grained Canada		1009.04						298						7
			5.0					373					P	7
			9.3					473					P	7
			11.5					573					P	7
Alpine Granites Central Alps, Europe	2.2	753.64				1.06	.0111	293	8					27
Barre Granite Barre, VT						1.4		293	CYL	0.24	2.0 / 11.43	46.2 / Water	C	1
						0.24		293	6 / CYL	0.0	2.0 / 10.795		W	5
						0.24		293	1 / CYL		2.0 / 10.795		X	5
						0.24		293	960 / CYL	0.0	2.0 / 10.795		bb	5
	2.72	904.40	7.20					298					P	15

ROCK TYPE: GRANITE	THERMAL/HYDROGEOLOGICAL PROPERTIES							TEST CONDITIONS						
NAME; DESCRIPTION; LOCATION	k (W/m-K)	C_p (J/kg-K)	α_T (10^{-6}/K)	k_h (m/s)	κ (cm^2)	θ (%)	α (cm^2/s)	T (K)	No. TESTS / SHAPE	MOISTURE CONTENT (%)	SAMPLE L:D / LENGTH (cm)	SATURATION (%) / MEDIUM	NOTES	REF.
Granite Medium grained Canada		992.29						298						7
	2.18	996.48	7.00				.0084	373					P	7
	2.04		10.30				.0079	473					P	7
	1.95		13.50				.0075	573					P	7
	2.50		7.50				.0096	373					P	7
	2.26		10.30				.0086	473					P	7
	2.06							573					P	7
			12.70				.0079	473					P	7
Casco Granite	3.06							298		0.0			conf. press. 5.0 MPa	23
	3.11							298		0.0			conf. press. 10.0 MPa	23

157

ROCK TYPE: GRANITE	THERMAL/HYDROGEOLOGICAL PROPERTIES							TEST CONDITIONS							
NAME; DESCRIPTION; LOCATION	k $(W/m\text{-}K)$	c_p $(J/kg\text{-}K)$	α_T $(10^{-6}/K)$	k_h (m/s)	κ (cm^2)	θ $(\%)$	α (cm^2/s)	T (K)	No. TESTS / SHAPE	MOISTURE CONTENT $(\%)$	SAMPLE L:D / LENGTH (cm)	SATURATION $(\%)$ / MEDIUM	NOTES	REF.
Westerly Granite					.16 (10^{-14})			298	/ CYL		1.28 / 1.61	/ Argon	Conf./ Pore Pres 40/15 MPa	25
					.51 (10^{-15})			301	/ CYL		1.28 / 1.61	/ Argon	Conf./ Pore Pres 60/10 MPa	25
					.69 (10^{-15})			295	/ CYL		1.28 / 1.61	/ Argon	Effective Pres 50 MPa	25
					.28 (10^{-15})			295	/ CYL		1.28 / 1.61	/ Argon	Conf./ Pore Pres 100/11 MPa	25
					.43 (10^{-15})			298	/ CYL		1.28 / 1.61	/ Argon	Conf./ Pore Pres 115/15 MPa	25
					.30 (10^{-15})			295	/ CYL		1.28 / 1.61	/ Argon	Conf./ Pore Pres 115/15 MPa	25
					.16 (10^{-14})			298	/ CYL		1.28 / 1.61	/ Water	Conf./ Pore Pres 50/41 MPa	25
					.23 (10^{-14})			282	/ CYL		1.28 / 1.61	/ Water	Conf./ Pore Pres 52/40 MPa	25
					.13 (10^{-14})			282	/ CYL		1.28 / 1.61	/ Water	Conf./ Pore Pres 40/17.5 MPa	25
					.72 (10^{-15})			298	/ CYL		1.28 / 1.61	/ Water	Conf./ Pore Pres 89.5/36.5 MPa	25

ROCK TYPE: GRANITE	THERMAL/HYDROGEOLOGICAL PROPERTIES							TEST CONDITIONS						
NAME; DESCRIPTION; LOCATION	k (W/m-K)	c_p (J/kg-K)	α_T (10^{-6}/K)	k_h (m/s)	κ (cm^2)	θ (%)	α (cm^2/s)	T (K)	No. TESTS / SHAPE	MOISTURE CONTENT (%)	SAMPLE L:D / LENGTH (cm)	SATURATION (%) / MEDIUM	NOTES	REF.
Stripa Granite							.0775	588					P	7
Unaweep Granite Coarse grain Grand Junction, CO						.50		298	CYL	0.0	1.0 / 5.3975		F	16
						.60		298	CYL	0.0	1.0 / 5.3975		F	16
Unaweep Granite Coarse grain, || to bedding Colorado						.60		298						16
Wausau Granite			6.60					298					P	26
			25.80					673					P	26
Westerly Granite						.106		293		0.0				21
						.11		293						21
					.26 (10^{-14})			298	CYL		1.28 / 1.61	Argon	Conf./Pore Pres 25/15 MPa	25
					.15 (10^{-14})			301	CYL		1.28 / 1.61	Argon	Conf./Pore Pres 25/5 MPa	25

ROCK TYPE: GRANITE	THERMAL/HYDROGEOLOGICAL PROPERTIES							TEST CONDITIONS					
NAME; DESCRIPTION; LOCATION	k (W/m-K)	c_p (J/kg-K)	α_T (10^{-6}/K)	k_h (m/s)	κ (cm^2)	θ (%)	α (cm^2/s)	T (K)	No. TESTS / SHAPE	MOISTURE CONTENT (%)	SAMPLE L:D / LENGTH (cm)	SATURATION (%) / MEDIUM	NOTES	REF.
Shartashskoye Granite Medium grained USSR	0.95	868.41	9.00			0.56	.0041	423					P	19
	0.91	938.69	9.50			0.56	.0036	473					P	19
	0.89	965.24	10.00			0.56	.0034	523					P	19
	0.88	982.43	13.00			0.56	,0033	573					P	19
	0.87	1002.73	15.00			0.56	.0033	623					P	19
	0.87	1054.27	17.50			0.56	.0031	673					P	19
	0.87	1080.82	18.90			0.56	،0033	723					P	19
Smaland Granite Ylen Region, Sweden			.50 (10^{-6})					298				Water	P,aa	30
Smaland Granite Stenjon Region, Sweden			.60 (10^{-6})					298					P,aa	30
Stripa Granite			22.50					298					P	3

ROCK TYPE: GRANITE	THERMAL/HYDROGEOLOGICAL PROPERTIES								TEST CONDITIONS					
NAME; DESCRIPTION; LOCATION	k (W/m-K)	C_p (J/kg-K)	α_T (10^{-6}/K)	k_h (m/s)	κ (cm^2)	θ (%)	α (cm^2/s)	T (K)	No. TESTS / SHAPE	MOISTURE CONTENT (%)	SAMPLE L:D / LENGTH (cm)	SATURATION (%) / MEDIUM	NOTES	REF.
Shartashskoye Granite Fine Grained USSR	0.86	869.97	9.90			0.0	.0037	423					P	19
	0.81	940.25	10.50			0.0	.0032	473					P	19
	0.79	1280.75	11.50			0.0	.0031	523					P	19
	0.78	980.86	13.50			0.0	.0030	573					P	19
	0.77	1015.22	14.00			0.0	.0028	623					P	19
	0.76	1054.27	15.00			0.0	.0027	673					P	19
	0.76	1077.70	18.00			0.0	.0026	723					P	19
Shartashskoye Granite Medium grained USSR	1.19	655.99				0.56	.0068	291					P	19
	1.14	718.47				0.56	.0059	323					P	19
	1.05	780.94				0.56	.0050	373					P	19

ROCK TYPE: GRANITE	THERMAL/HYDROGEOLOGICAL PROPERTIES							TEST CONDITIONS						
NAME; DESCRIPTION; LOCATION	k (W/m-K)	C_p (J/kg-K)	α_T (10^{-6}/K)	k_h (m/s)	κ (cm^2)	θ (%)	α (cm^2/s)	T (K)	No. TESTS / SHAPE	MOISTURE CONTENT (%)	SAMPLE L:D / LENGTH (cm)	SATURATION (%) / MEDIUM	NOTES	REF.
Rovnenskoye Granite Medium to fine grained USSR	1.96	952.75	13.50			0.6	.0077	473					P	19
	1.92		15.00			0.6	.0074	523					P	19
	1.88		16.00			0.6	.0072	573					P	19
	1.86	1008.98	17.50			0.6	.0069	623					P	19
	1.82	1052.71	21.00			0.6	.0066	673					P	19
	1.80	1093.32	26.00			0.6	.0081	723					P	19
Scotstown Granite USA							.0058	588					P	7
Shartashskoye Granite Fine grained USSR	0.91	648.18				0.0	.0053	291					P	19
	0.88	721.59				0.0	.0046	323					P	19
	0.87	785.63				0.0	.0041	373					P	19

162

ROCK TYPE: GRANITE	THERMAL/HYDROGEOLOGICAL PROPERTIES								TEST CONDITIONS					
NAME; DESCRIPTION; LOCATION	k (W/m-K)	$\overset{\cdot}{c}_p$ (J/kg-K)	α_T (10^{-6}/K)	k_h (m/s)	κ (cm^2)	θ (%)	α (cm^2/s)	T (K)	No. TESTS / SHAPE	MOISTURE CONTENT (%)	SAMPLE L:D / LENGTH (cm)	SATURATION (%) / MEDIUM	NOTES	REF.
Rovnenskoye Granite Coarse grained USSR	1.77	960.56	9.00			0.4	.0069	473					P	19
	1.73	966.81	12.00			0.4	.0067	523					P	19
	1.72	999.61	14.00			0.4	.0064	573					P	19
	1.71	1015.22	16.00			0.4	.0063	623					P	19
	1.70	1054.27	19.20			0.4	.0061	673					P	19
	1.68	1102.69	22.60			0.4	.0057	723					P	19
Rovnenskoye Granite Medium to fine grained USSR	2.50	626.32				0.6	.0149	291					P	19
	2.38	724.71				0.6	.0123	323					P	19
	2.17	937.13				0.6	.0104	373					P	19
	2.03	865.28	10.50			0.6	.0088	423					P	19

163

ROCK TYPE: GRANITE	THERMAL/HYDROGEOLOGICAL PROPERTIES								TEST CONDITIONS					
NAME; DESCRIPTION; LOCATION	k (W/m-K)	C_p (J/kg-K)	α_T (10^{-6}/K)	k_h (m/s)	κ (cm²)	θ (%)	α (cm²/s)	T (K)	No. TESTS / SHAPE	MOISTURE CONTENT (%)	SAMPLE L:D / LENGTH (cm)	SATURATION (%) / MEDIUM	NOTES	REF.
Rovnenskoye Gray Granite USSR	2.03	943.38					.0081	473					P	19
	1.98	949.63					.0078	523					P	19
	1.94	976.18					.0074	573					P	19
	1.93	998.04					.0073	623					P	19
	1.93	1033.97					.0070	673					P	19
	1.86	1062.08					.0065	723					P	19
Rovnenskoye Granite Coarse grained USSR	2.24	640.37				0.4	.0131	291					P	19
	2.11	734.09				0.4	.0106	323					P	19
	1.88	780.94				0.4	.0090	373					P	19
	1.85	827.80	7.00			0.4	.0083	423					P	19

ROCK TYPE: GRANITE	THERMAL/HYDROGEOLOGICAL PROPERTIES							TEST CONDITIONS						
NAME; DESCRIPTION; LOCATION	k	C_p	α_T	k_h	κ	θ	α	T	No. TESTS	MOISTURE CONTENT	SAMPLE L:D	SATURATION (%)	NOTES	REF.
	(W/m-K)	(J/kg-K)	(10^{-6}/K)	(m/s)	(cm^2)	(%)	(cm^2/s)	(K)	SHAPE	(%)	LENGTH (cm)	MEDIUM		
Granite Quincy, MA					.46 (10^{-13})			298					P	29
Raymond Granite						3.3		293	CYL	0.30	2.0 11.43	24.2 Water	C	1
Revsund Granite Juktan Region, Sweden			.18 (10^{-5})				.0180	298				Water	P,aa	30
Ries Granite Uncracked Temp. range 298 to 473 K			7.83					298	CYL		4.5			22
Ries Granite Highly Cracked Temp. range 298 to 473 K			6.47					298	CYL		4.5			22
Rose Granite						2.5		293	CYL	0.27	2.0 11.43	28.1 Water	C	1
Rovnenskoye Gray Granite USSR	2.85	609.13					.0174	291					P	19
	2.61	702.85					.0139	323					P	19
	2.15	791.88					.0101	373					P	19
	2.03	834.05					.0091	423					P	19

ROCK TYPE: GRANITE	THERMAL /HYDROGEOLOGICAL PROPERTIES							TEST CONDITIONS							
NAME; DESCRIPTION; LOCATION	k $(W/m\text{-}K)$	$\bar{c}_p$ $(J/kg\text{-}K)$	α_T $(10^{-6}/K)$	k_h (m/s)	κ (cm^2)	θ $(\%)$	α (cm^2/s)	T (K)	No. TESTS / SHAPE	MOISTURE CONTENT $(\%)$	SAMPLE L:D / LENGTH (cm)	SATURATION $(\%)$ / MEDIUM	NOTES	REF.
Graniteville Granite			25.60					673					P	26
Granite Manitouwadge, Canada	3.29					.32		293	6					28
Granite Unknown						1.70		293	CYL		2.0 / 11.43		C	1
Opalescent Granite USA							.0061	588					P	7
Ortonville Granite							.0125	373						7
							.0115	473						7
							.0082	573					P	7
Pikes Peak Granite Colorado Springs, CO						0.10		293	12 / CYL	0.0				5
						0.05		293	6 / CYL	0.0				5
						0.05		293	1 / CYL				X	5

ROCK TYPE: GRANITE	THERMAL/HYDROGEOLOGICAL PROPERTIES							TEST CONDITIONS						
NAME; DESCRIPTION; LOCATION	k (W/m-K)	C_p (J/kg-K)	α_T (10^{-6}/K)	k_h (m/s)	κ (cm^2)	θ (%)	α (cm^2/s)	T (K)	No. TESTS / SHAPE	MOISTURE CONTENT (%)	SAMPLE L:D / LENGTH (cm)	SATURATION (%) / MEDIUM	NOTES	REF.
Chelmsford Granite			7.20					298					P	26
			24.40					673					P	26
Chelmsford Grey Granite USA							.0150	373					P	7
							.0139	473					P	7
							.0123	588					P	7
Chelmsford White Granite USA							.0085	588					P	7
Granite; Medium grain, ‖ to slight foliate Mt. Airy, NC						0.70		298						10
Granite ⊥ to slight foliate Mt. Airy, NC						0.70		298						10
Gneiss Granite Forsmark Region Sweden			.16 (10^{-5})					98				Water	P,aa	30
Graniteville Granite			8.40					298					P	26

167

ROCK TYPE: GRANITE	THERMAL/HYDROGEOLOGICAL PROPERTIES							TEST CONDITIONS						
NAME; DESCRIPTION; LOCATION	k (W/m-K)	C_p (J/kg-K)	α_T (10^{-6}/K)	k_h (m/s)	κ (cm^2)	θ (%)	α (cm^2/s)	T (K)	No. TESTS / SHAPE	MOISTURE CONTENT (%)	SAMPLE L:D / LENGTH (cm)	SATURATION (%) / MEDIUM	NOTES	REF.
Casco Granite	3.19							298		0.0			conf. press. 25.0 MPa	23
	3.23							298		0.0			conf. press. 50.0 MPa	23
	3.27							298		0.0			conf. press. 100.0 MPa	23
	2.97							298		0.0			conf. press. 5.0 MPa	23
	3.22							298					conf. press. 10.0 MPa	23
	3.24							298					conf. press. 25.0 MPa	23
	3.26							298					conf. press. 50.0 MPa	23
	3.27							298					conf. press. 100.0 MPa	23
	3.28							298						23
	3.30							298						23

ROCK TYPE: GRANITE	THERMAL/HYDROGEOLOGICAL PROPERTIES							TEST CONDITIONS						
NAME; DESCRIPTION; LOCATION	k (W/m-K)	C_p (J/kg-K)	α_T (10^{-6}/K)	k_h (m/s)	κ (cm^2)	θ (%)	α (cm^2/s)	T (K)	No. TESTS / SHAPE	MOISTURE CONTENT (%)	SAMPLE L:D / LENGTH (cm)	SATURATION (%) / MEDIUM	NOTES	REF.
Barre Granite Barre, VT						0.079	.0137	293	Disk	0.0			Y	21
						0.079	.0088	293	Disk	0.0		0.0	Y,Z	21
						0.079	.0158	293	Disk			Water	Y	21
Barre Granite Temp. Range 298 to 473 K			7.73					298	CYL		4.5			22
Granite Medium to coarse grain Barre, VT						0.9		298		0.0				10
Granite; medium to coarse grain, ‖ to bedding; Barre, VT						0.9		298		0.0				10
Barre Granite Medium to fine grain, uniform Barre, VT						0.51		298	20 / CYL	0.0	2.0 / 5.08		J	9
						0.51		298	20 / CYL		1.0 / 2.54		A,M	9
Granite Barriefield, Ont., Canada					.50 (10^{-15})			298	UNK				P	29
Biotite Granite Medium to fine grain Lincoln Co., NV						0.9		298		0.0				10

ROCK TYPE: GRANITE	THERMAL/HYDROGEOLOGICAL PROPERTIES							TEST CONDITIONS						
NAME; DESCRIPTION; LOCATION	k $(W/m\text{-}K)$	C_p $(J/kg\text{-}K)$	α_T $(10^{-6}/K)$	k_h (m/s)	κ (cm^2)	θ $(\%)$	α (cm^2/s)	T (K)	No. TESTS / SHAPE	MOISTURE CONTENT (%)	SAMPLE L:D / LENGTH (cm)	SATURATION (%) / MEDIUM	NOTES	REF.
Westerly Granite					$.27$ (10^{-15})			298	/ CYL		1.28 / 1.61	/ Water	Conf./ Pore Pres 150/41.5 MPa	25
					$.31$ (10^{-15})			298	/ CYL		1.28 / 1.61	/ Water	Conf./ Pore Pres 150/39 MPa	25
					$.28$ (10^{-15})			282	/ CYL		1.28 / 1.61	/ Water	Conf./ Pore Pres 203/41 MPa	25
					$.20$ (10^{-15})			282	/ CYL		1.28 / 1.61	/ Water	Conf./ Pore Pres 203/41 MPa	25
					$.15$ (10^{-15})			298	/ CYL		1.28 / 1.61	/ Water	Conf./ Pore Pres 250/39.5 MPa	25
					$.42$ (10^{-16})			298	/ CYL		1.28 / 1.61	/ Water	Conf./ Pore Pres 444/39 MPa	25
					$.35$ (10^{-14})			298					P	23
					$.23$ (10^{-14})			298					P	23
					$.12$ (10^{-14})			298					P	23
					$.63$ (10^{-15})			298					P	23

ROCK TYPE: GRANITE	THERMAL/HYDROGEOLOGICAL PROPERTIES							TEST CONDITIONS						
NAME; DESCRIPTION; LOCATION	k (W/m-K)	C_p (J/kg-K)	α_T (10^{-6}/K)	k_h (m/s)	κ (cm²)	θ (%)	α (cm²/s)	T (K)	No. TESTS / SHAPE	MOISTURE CONTENT (%)	SAMPLE L:D / LENGTH (cm)	SATURATION (%) / MEDIUM	NOTES	REF.
Westerly Granite					.35 (10^{-15})			298					P Conf. Pres 5 MPa	23
					.15 (10^{-15})			298					P	23
					.42 (10^{-16})			298					P	23
					.23 (10^{-16})			298					P Conf. Pres 25 MPa	23
Westerly Granite Westerly, RI						.106	.0140	293	Disk	0.0		0.0	Y	21
						.106	.0101	293	Disk	0.0		0.0	Y,Z	21
						.106	.0155	293	Disk			Water	Y	21
			8.30					298						26
			22.30					673						26
Westerly Granite Temp. range 298 to 473 K			11.20					298	CYL		.45			22

171

ROCK TYPE: GRANITE	THERMAL/HYDROGEOLOGICAL PROPERTIES							TEST CONDITIONS						
NAME; LOCATION; DESCRIPTION	k (W/m-K)	C_p (J/kg-K)	α_T (10^{-6}/K)	k_h (m/s)	κ (cm^2)	θ (%)	α (cm^2/s)	T (K)	No. TESTS / SHAPE	MOISTURE CONTENT (%)	SAMPLE L:D / LENGTH (cm)	SATURATION (%) / MEDIUM	NOTES	REF.
Westerly Granite Fine grain, equigranular Westerly, RI						.08		298	30 / CYL	0.0	2.0 / 5.08			9
						.35		298	30 / CYL	0.0	1.0 / 2.54		A	9
Westerly Granite Homogeneous Westerly, RI						1.3		298						8
Granite, Woodstock Granite Quarry Woodstock, MD						.80		298		0.0				10

172

ROCK TYPE: GRANODIORITE	THERMAL/HYDROGEOLOGICAL PROPERTIES							TEST CONDITIONS						
NAME; DESCRIPTION; LOCATION	k (W/m-K)	C_p (J/kg-K)	α_T $(10^{-6}/K)$	k_h (m/s)	κ (cm^2)	θ (%)	α (cm^2/s)	T (K)	No. TESTS / SHAPE	MOISTURE CONTENT (%)	SAMPLE L:D / LENGTH (cm) / MEDIUM	SATURATION (%) / MEDIUM	NOTES	REF.
Granodiorite							.0110	298	51 / DISK	0.0	1.0 / 2.54		γ Conf./ Pore Pres .101 MPa	31
Granodiorite Medium grained Canada		992.29						298						7
	4.0		5.90				.0077	373					P	7
	1.77		11.70				.0065	573					P	7
			9.80				.0071	473					P	7
Granodiorite Jackfish, Canada	2.95					.30		293	62					28
Granodiorite Manitouwadge, Canada	3.42					.20		293	12					28
Smolinskoye Granodiorite Coarse grained USSR	1.74	749.70				.70	.0087	291					P	19
	1.70	827.80				.70	.0077	323					P	19
	1.57	890.27				.70	.0066	373					P	19

ROCK TYPE: GRANODIORITE	THERMAL/HYDROGEOLOGICAL PROPERTIES							TEST CONDITIONS					
NAME; DESCRIPTION; LOCATION	k (W/m-K)	C_p (J/kg-K)	α_T (10^{-6}/K)	k_h (m/s)	κ (cm²)	θ (%)	α (cm²/s)	T (K)	No. TESTS / SHAPE	MOISTURE CONTENT (%)	SAMPLE L:D / LENGTH (cm)	SATURATION (%) / MEDIUM	NOTES	REF.
Smolinskoye Granodiorite Coarse grained USSR	1.41	952.75				.70	.0055	423					P	19
	1.36	1015.22	13.50			.70	.0050	473					P	19
	1.36	1049.59	14.50			.70	.0048	523					P	19
	1.39	1068.33	15.40			.70	.0049	573					P	19
	1.39	1102.69	17.20			.70	.0047	623					P	19
	1.39	1132.37	18.50			.70	.0046	673					P	19
	1.38	1155.80	21.00			.70	.0045	723					P	19
St. Cloud Grey Granodiorite Medium grain St. Cloud, MN						.08		298	30 / CYL	0.0	1.0 / 2.54			9
St. Cloud Granodiorite St. Cloud, MN						.076		293		0.0			A	21
						.076	.0125	293		0.0		0.0 / 0.0	Y	21

ROCK TYPE: GRANODIORITE	THERMAL/HYDROGEOLOGICAL PROPERTIES								TEST CONDITIONS					
NAME; DESCRIPTION; LOCATION	k (W/m-K)	C_p (J/kg-K)	α_T (10^{-6}/K)	k_h (m/s)	κ (cm^2)	θ (%)	α (cm^2/s)	T (K)	No. TESTS / SHAPE	MOISTURE CONTENT (%)	SAMPLE L:D / LENGTH (cm)	SATURATION (%) / MEDIUM	NOTES	REF.
St. Cloud Granodiorite St. Cloud, MN						.076	.0087	293		0.0			Y,Z	21
						.047	.0151	293		0.0		Water	Y	21
						.08		293						21
Granodiorite Winnipeg, Canada	2.88							293	22				P	28

175

ROCK TYPE: MISC. GRANITIC	THERMAL/HYDROGEOLOGICAL PROPERTIES								TEST CONDITIONS					
NAME; DESCRIPTION; LOCATION	k (W/m-K)	C_p (J/kg-K)	α_T (10^{-6}/K)	k_h (m/s)	κ (cm^2)	θ (%)	α (cm^2/s)	T (K)	No. TESTS / SHAPE	MOISTURE CONTENT (%)	SAMPLE L:D / LENGTH (cm)	SATURATION (%) / MEDIUM	NOTES	REF.
Alpine Pegmatites Central Alps, Europe	0.6	753.64				1.17	.0128	293	3					27
Pegmatite; granitic Very coarse grain Star Lake, NY						1.1		298		0.0				10
Quartz Monzonite Coarse grained Canada		1000.85						298						7
	2.26		7.50				.0085	373					P	7
	2.04		10.30				.0077	473					P	7
	1.86		12.90				.0070	573					P	7
Red River Quartz Monzonite			7.10					298					P	26
			25.00					673					P	26
Quartz Monzonite Winnipeg, Canada	2.89							293	12				P	28
Granite and Quartz Syenite; Fine to medium grain; Star Lake, NY						0.4		298		0.0				10

ROCK TYPE: MISC. GRANITIC	THERMAL/HYDROGEOLOGICAL PROPERTIES							TEST CONDITIONS						
NAME; DESCRIPTION; LOCATION	k (W/m-K)	C_p (J/kg-K)	α_T $(10^{-6}/K)$	k_h (m/s)	κ (cm^2)	θ (%)	α (cm^2/s)	T (K)	No. TESTS / SHAPE	MOISTURE CONTENT (%)	SAMPLE L:D / LENGTH (cm)	SATURATION (%) / MEDIUM	NOTES	REF.
Granite and Quartz Syenite Lyon Mountain, NY						0.8		298		0.0				10
Meta-Rhyolite > Quartz Porphyry; Chloritic MN						0.4		298		0.0				10
Meta-Rhyolite > Quartz Porphry Soudan, MN						0.2		298		0.0				10
Rhyolite							.0064	298	50 / Disk	0.0			Y Conf./ Pore Pres .101 MPa	31
Rhyolite Fine grained Canada	2.60	992.29	7.00				.0100	373					P	7
	2.35		9.20				.0090	473					P	7
	2.13		12.10					573					P	7

A.3 MECHANICAL PROPERTIES

ROCK TYPE: GRANITE	MECHANICAL PROPERTIES						TEST CONDITIONS								
NAME DESCRIPTION LOCATION	ρ (g/cm^3)	E (GPa)	ν	C_o (MPa)	T_o (MPa)	ADDITIONAL PROPERTIES (**)	T (K)	No. TESTS SHAPE	PRESS.: CONF./ PORE (MPa)	MOISTURE CONTENT (%)	SAMPLE L:D LENGTH (cm)	SATURATION (%) MEDIUM	LOAD RATE (MPa/s)	NOTES	REF.
Albite Granite Medium grained Canada	2.64	41.4	.32	149.07			298								7
	2.64	41.4	.32	141.22			373								7
	2.64	41.4	.32	137.30			473								7
	2.64	41.4	.32	133.38			573								7
Alpine Granites Central Alps, Europe	2.63					2.55[e] 3.94[f]	293	8							27
Barre Granite Barre, VT	2.64	34.5	.15	195.61			293	0.0 CYL 0.0	0.0	2.0 11.43			C	1
		37.2		167.48		85.0[e]	293	0.0 CYL	0.24	2.0 11.43	46.2 Water		C	1
				194.40	10.69		293	8 0.0 CYL	0.0	2.04 10.79		0.26		5
					10.69		293	2 0.0 CYL	0.0	2.04 10.795			H	5
		61.5					293	6 0.0 CYL	0.0	2.0 10.795			M	5

**ADDITIONAL PROPERTIES
a) MODULUS OF RIGIDITY (GPa)   c) SHEAR WAVE VELOCITY (km/s)   e) SHORE SCLEROSCOPE HARDNESS   g) MODULUS OF RUPTURE (MPa)
b) COMPRESSIBILITY (10^{-6}/MPa)   d) IMPACT TOUGHNESS (m/m^2)   f) LONGITUDINAL WAVE VELOCITY (km/s)

ROCK TYPE: GRANITE	MECHANICAL PROPERTIES						TEST CONDITIONS								
NAME DESCRIPTION LOCATION	ρ (g/cm³)	E (GPa)	ν	C_0 (MPa)	T_0 (MPa)	ADDITIONAL PROPERTIES (**)	T (K)	No. TESTS / SHAPE	PRESS.: CONF./ PORE (MPa)	MOISTURE CONTENT (%)	SAMPLE L:D / LENGTH (cm)	SATURATION (%) / MEDIUM	LOAD RATE (MPa/s)	NOTES	REF.
Barre Granite Barre, VT		47.0	.14			5.06[f]	293	6 / CYL	0.0	0.0	2.0 / 10.795			K	5
	2.64	67.6	.39				293	6 / CYL	0.0	0.0	2.0 / 10.795			L,W	5
						93.00[e]	293	960 / CYL		0.0	2.0 / 10.795			bb	5
	2.66		.31	234.00	8.00		298		0.0					p	15
				197.00			298	20 / CYL	0.0	0.0	2.0 / 5.08		.10 (10^{-4})		9
	2.63						293			0.0					9
Barre Granite Anisotropic within samples		60.0	.30	220.00			298	/ CYL	0.0	0.0	2.7 / 3.427		.10 (10^{-3})		14
Granite; medium to coarse grain Barre, VT	2.66	30.4		228.90		16.8[a], 192.9[d] 95.00[e], 3.40[f] 20.0[g]	298		0.0	0.0					10
Granite; medium to coarse grain, || to bed Barre, VT		27.1		226.20		15.2[a] 192.9[d] 25.5[g]	298		0.0	0.0					10
		44.2		244.10		16.3[a] 18.6[g]	298		0.0	0.0					10

**ADDITIONAL PROPERTIES
a) MODULUS OF RIGIDITY (GPa) c) SHEAR WAVE VELOCITY (km/s) e) SHORE SCLEROSCOPE HARDNESS g) MODULUS OF RUPTURE (MPa)
b) COMPRESSIBILITY (10^{-6}/MPa) d) IMPACT TOUGHNESS (m/m²) f) LONGITUDINAL WAVE VELOCITY (km/s)

ROCK TYPE: GRANITE	MECHANICAL PROPERTIES						TEST CONDITIONS								
NAME DESCRIPTION LOCATION	ρ (g/cm³)	E (GPa)	ν	C_o (MPa)	T_o (MPa)	ADDITIONAL PROPERTIES (**)	T (K)	No. TESTS / SHAPE	PRESS.: CONF./ PORE (MPa)	MOISTURE CONTENT (%)	SAMPLE L:D / LENGTH (cm)	SATURATION (%) / MEDIUM	LOAD RATE (MPa/s)	NOTES	REF.
Barre Granite Medium to fine grain, uniform; Barre, VT				7.67	3.51[f]		298	20 / CYL	0.0	0.0	2.0 / 5.08		.16 (10⁻⁵)		9
	2.64	45.6				88.80[e]	298		0.0	0.0	2.0 / 5.08		.10 (10⁻⁵)	J	9
		32.5	.23				298				1.0 / 2.54			A,M	9
Granite, Biotite Medium to fine grain Lincoln Co., NV	2.63	51.3		272.30		22.5[a], 394.0[d] 100.0[e], 4.40[f] 26.9[g]	298		0.0	0.0					10
Bohus Granite		53.3	.20	157.00	10.50		293		0.0						3
	2.64	53.3		180.00		4.49[f]	298		0.0						11
Granite Medium grained Canada	2.61						298								7
	2.64						298								7
Chelmsford Granite						2.90[f]	273		0.1	0.0					24
						3.24[f]	303		0.1	0.0					24

**ADDITIONAL PROPERTIES   a) MODULUS OF RIGIDITY (GPa)   c) SHEAR WAVE VELOCITY (km/s)   e) SHORE SCLEROSCOPE HARDNESS   g) MODULUS OF RUPTURE (MPa)
b) COMPRESSIBILITY (10⁻⁶/MPa)   d) IMPACT TOUGHNESS (m/m²)   f) LONGITUDINAL WAVE VELOCITY (km/s)

181

ROCK TYPE: GRANITE NAME DESCRIPTION LOCATION	MECHANICAL PROPERTIES						TEST CONDITIONS								
	ρ (g/cm³)	E (GPa)	ν	C_o (MPa)	T_o (MPa)	ADDITIONAL PROPERTIES (**)	T (K)	No. TESTS SHAPE	PRESS.: CONF./ PORE (MPa)	MOISTURE CONTENT (%)	SAMPLE L:D LENGTH (cm)	SATURATION (%) MEDIUM	LOAD RATE (MPa/s)	NOTES	REF.
Chelmsford Granite						3.72^f	333		0.1	0.0					24
						3.92^f	363		0.1	0.0					24
Granite In situ Competent Zones		7.4					298	CYL			2.0			S	13
		11.2					298	CYL			2.0			T	13
		18.6					298	CYL			2.0			U	13
Granite In situ, jointed and competent zones	2.54	54.2				2.94^c 4.87^f	298	24	0.0	0.0				P	13
Granite In situ, high angle joint zones		7.2					298	CYL			2.0			S	13
		10.8					298	CYL			2.0			T	13
		20.8					298	CYL			2.0			U	13
Granite In situ, low angle joint zones		4.8					298	CYL			2.0			S	13

**ADDITIONAL PROPERTIES
a) MODULUS OF RIGIDITY (GPa)
b) COMPRESSIBILITY (10^{-6}/MPa)
c) SHEAR WAVE VELOCITY (km/s)
d) IMPACT TOUGHNESS (m/m²)
e) SHORE SCLEROSCOPE HARDNESS
f) LONGITUDINAL WAVE VELOCITY (km/s)
g) MODULUS OF RUPTURE (MPa)

ROCK TYPE: GRANITE	MECHANICAL PROPERTIES						TEST CONDITIONS								
NAME DESCRIPTION LOCATION	ρ (g/cm³)	E (GPa)	ν	C_0 (MPa)	T_0 (MPa)	ADDITIONAL PROPERTIES (**)	T (K)	No. TESTS / SHAPE	PRESS.: CONF./ PORE (MPa)	MOISTURE CONTENT (%)	SAMPLE L:D / LENGTH (cm)	SATURATION (%) / MEDIUM	LOAD RATE (MPa/s)	NOTES	REF.
Granite In situ, low angle joint zones		6.2					298	CYL			2.0			T	13
		10.6					298	CYL			2.0			U	13
Granite NX size laboratory cores				145.00			298	20 / CYL	0.0	0.0	2.0				13
				128.00			298	5 / CYL	0.0		2.0			B	13
		52.5					298	19 / CYL	0.0	0.0	2.0			Q	13
		59.2					298	19 / CYL	0.0	0.0	2.0			R	13
	2.81	54.6	.26			2.84ᶜ 5.49ᶠ	298	25	0.0	0.0					13
Granite Unknown	2.66	40.7	.18	253.18			293	CYL	0.0 / 0.0	0.0	2.0 / 11.43			C	1
		39.3		148.24			293	CYL	0.0	0.17	2.0 / 11.43	27.0 / Water		C	1
Krakemala Granite		61.4	.20	188.20	8.92		293	6 / CYL	0.0 / 0.0	0.0	2.5 / 10.5			I	3

**ADDITIONAL PROPERTIES
a) MODULUS OF RIGIDITY (GPa) c) SHEAR WAVE VELOCITY (km/s) e) SHORE SCLEROSCOPE HARDNESS g) MODULUS OF RUPTURE (MPa)
b) COMPRESSIBILITY (10^{-6}/MPa) d) IMPACT TOUGHNESS (m/m²) f) LONGITUDINAL WAVE VELOCITY (km/s)

ROCK TYPE: GRANITE	MECHANICAL PROPERTIES						TEST CONDITIONS								
NAME DESCRIPTION LOCATION	ρ (g/cm³)	E (GPa)	ν	C_0 (MPa)	T_0 (MPa)	ADDITIONAL PROPERTIES (**)	T (K)	No. TESTS / SHAPE	PRESS.: CONF./PORE (MPa)	MOISTURE CONTENT (%)	SAMPLE L:D / LENGTH (cm)	SATURATION (%) / MEDIUM	LOAD RATE (MPa/s)	NOTES	REF.
Krakemala Granite		57.1		152.70	6.77		293	6 / CYL	0.0	0.0	2.5 / 10.5			I	3
			.21				293	5 / CYL	0.0	0.0	2.5 / 10.5				3
Granite; Medium grain ⊥ to slight foliate Mt. Airy, NC	2.60	15.7		209.60		12.4[a], 204.7[d] 90.0[e], 3.40[f] 11.1[g]	298		0.0	0.0					10
Granite, Medium grain ‖ to slight foliate Mt. Airy, NC	2.60	45.4				10.2[a] 2.40[f]	298		0.0	0.0					10
	2.60	26.5				12.3[a] 3.20[f]	298		0.0	0.0					10
Mt. Airy Granite				201.60			293	5 / CYL	0.0		2.0 / 10.909				4
Granite Dense, coarse grain NTS, Mercury, NV					12.00		298	CYL	0.0		2.0 / 10.795				17
Ortonville Granite				167.70			373								7
				155.93			473								7
				151.03			523								7

**ADDITIONAL PROPERTIES   a) MODULUS OF RIGIDITY (GPa)   c) SHEAR WAVE VELOCITY (km/s)   e) SHORE SCLEROSCOPE HARDNESS   f) MODULUS OF RUPTURE (MPa)
                                                                        b) COMPRESSIBILITY (10⁻⁶/MPa)   d) IMPACT TOUGHNESS (m/m²)   f) LONGITUDINAL WAVE VELOCITY (km/s)

184

ROCK TYPE: GRANITE	MECHANICAL PROPERTIES						TEST CONDITIONS								
NAME DESCRIPTION LOCATION	ρ (g/cm^3)	E (GPa)	ν	C$_0$ (MPa)	T$_0$ (MPa)	ADDITIONAL PROPERTIES (**)	T (K)	No. TESTS / SHAPE	PRESS.: CONF./ PORE (MPa)	MOISTURE CONTENT (%)	SAMPLE L:D / LENGTH (cm)	SATURATION (%) / MEDIUM	LOAD RATE (MPa/s)	NOTES	REF.
Ortonville Granite				145.14			573							P	7
Pikes Peak Granite Colorado Springs, CO				226.20			293	3 / CYL	0.0	0.0	2.02 / 10.795		0.42		5
				88.90			293	3 / CYL	0.0	0.0	2.02 / 10.795		0.16		5
					11.90		293	1 / CYL	0.0	0.0	2.02 / 10.795				5
					3.93		293	2 / CYL	0.0	0.0	2.02 / 10.795			H	5
		70.6	.31			5.79^f	293	3 / CYL	0.0	0.0	2.0 / 10.795			J	5
		63.3	.21				293	3 / CYL	0.0	0.0	2.0 / 10.795			K	5
		77.9					293	3 / CYL	0.0	0.0	2.0 / 10.795			L	5
		33.4	.37				293	3 / CYL	0.0	0.0	2.0 / 10.795			J,W	5
		27.9	.25				293	3 / CYL	0.0	0.0	2.0 / 10.795			K	5

**ADDITIONAL PROPERTIES   a) MODULUS OF RIGIDITY (GPa)   c) SHEAR WAVE VELOCITY (km/s)   e) SHORE SCLEROSCOPE HARDNESS   g) MODULUS OF RUPTURE (MPa)
b) COMPRESSIBILITY (10^{-6}/MPa)   d) IMPACT TOUGHNESS (m/m^2)   f) LONGITUDINAL WAVE VELOCITY (km/s)

ROCK TYPE: GRANITE	MECHANICAL PROPERTIES						TEST CONDITIONS								
NAME DESCRIPTION LOCATION	ρ (g/cm³)	(GPa)		C₀ (MPa)	T₀ (MPa)	ADDITIONAL PROPERTIES (**)	T (K)	No. TESTS / SHAPE	PRESS.: CONF./ PORE (MPa)	MOISTURE CONTENT (%)	SAMPLE L:D / LENGTH (cm)	SATURATION (%) / MEDIUM	LOAD RATE (MPa/s)	NOTES	REF.
Raymond Granite	2.64	42.1	.26	178.03		88.0[e]	293	/ CYL	0.0 / 0.0	0.0	2.0 / 11.43	0.0 /		C	1
		33.1		156.52		80.0[e]	293	/ CYL	0.0 /	0.30	2.0 / 11.43	24.2 / Water		C	1
Raymond Granite Dense, unfractured unweathered				147.49			293	6 / CYL	0.0 /		2.0 / 5.385		0.6894	C	2
				198.76			293	6 / CYL	0.0 /		2.0 / 8.484		0.6894	C	2
				179.50			293	9 / CYL	0.0 /		2.0 / 10.795		0.6894	C	2
				189.35			293	3 / TRI	0.0 /		1.5 / 11.43		0.6894	C	2
				179.84			293	24 / CYL	0.0 /		2.0 /		0.6894	C	2
Rose Granite		41.4	.28	308.00		101.0[e]	293	/ CYL	0.0 / 0.0	0.0	2.0 / 11.43			C	1
	2.64	48.3		242.22		93.0[e]	293	/ CYL	0.0 / 0.0	0.27	2.0 / 11.43	24.2 / Water		C	1
Rovnenskoye Gray Granite; USSR	2.69	68.60					291	/	/		/				19

**ADDITIONAL PROPERTIES
a) MODULUS OF RIGIDITY (GPa)
b) COMPRESSIBILITY (10^{-6}/MPa)
c) SHEAR WAVE VELOCITY (km/s)
d) IMPACT TOUGHNESS (m/m²)
e) SHORE SCLEROSCOPE HARDNESS
f) LONGITUDINAL WAVE VELOCITY (km/s)
f) MODULUS OF RUPTURE (MPa)

ROCK TYPE: GRANITE	MECHANICAL PROPERTIES						TEST CONDITIONS								
NAME DESCRIPTION LOCATION	ρ (g/cm³)	E (GPa)	ν	C_o (MPa)	T_o (MPa)	ADDITIONAL PROPERTIES (**)	T (K)	No. TESTS SHAPE	PRESS.: CONF./ PORE (MPa)	MOISTURE CONTENT (%)	SAMPLE L:D LENGTH (cm)	SATURATION (%) MEDIUM	LOAD RATE (MPa/s)	NOTES	REF.
Rovnenskoye Gray Granite; USSR	2.69	66.7					323								19
	2.69	63.7					373								19
	2.69	55.9					423								19
	2.69	51.0					473								19
	2.69	42.7					523								19
	2.69	35.8					573								19
	2.69	28.9					623								19
	2.69	26.0					673								19
	2.69	22.1					723								19
Rovnenskoye Granite Coarse grained USSR	2.68	88.8					291								19

**ADDITIONAL PROPERTIES a) MODULUS OF RIGIDITY (GPa) c) SHEAR WAVE VELOCITY (km/s) e) SHORE SCLEROSCOPE HARDNESS g) MODULUS OF RUPTURE (MPa)
           b) COMPRESSIBILITY (10^{-6}/MPa) d) IMPACT TOUGHNESS (m/m²) f) LONGITUDINAL WAVE VELOCITY (km/s)

ROCK TYPE: GRANITE	MECHANICAL PROPERTIES						TEST CONDITIONS							
NAME DESCRIPTION LOCATION	ρ (g/cm^3)	E (GPa)	ν	C_o (MPa)	T_o (MPa)	ADDITIONAL PROPERTIES (**)	T (K)	No. TESTS SHAPE	PRESS.: CONF./ PORE (MPa)	MOISTURE CONTENT (%)	SAMPLE L:D LENGTH (cm)	SATURATION (%) MEDIUM	LOAD RATE (MPa/s)	NOTES	REF.
Rovnenskoye Granite Coarse grained USSR	2.68	97.9					323								19
	2.68	85.8					373								19
	2.68	61.3					423								19
	2.68	51.0					473								19
	2.68	40.7					523								19
	2.68	34.8					573								19
	2.68	30.4					623								19
	2.68	21.5					673								19
	2.68	18.3					723								19
Rovnenskoye Granite Medium to fine grained USSR	2.68	64.7					291								19

**ADDITIONAL PROPERTIES
a) MODULUS OF RIGIDITY (GPa) c) SHEAR WAVE VELOCITY (km/s) e) SHORE SCLEROSCOPE HARDNESS g) MODULUS OF RUPTURE (MPa)
b) COMPRESSIBILITY (10^{-6}/MPa) d) IMPACT TOUGHNESS (m/m^2) f) LONGITUDINAL WAVE VELOCITY (km/s)

188

ROCK TYPE: GRANITE	MECHANICAL PROPERTIES						TEST CONDITIONS								
NAME DESCRIPTION LOCATION	ρ (g/cm^3)	E (GPa)	ν	C_o (MPa)	T_o (MPa)	ADDITIONAL PROPERTIES (**)	T (K)	No. TESTS / SHAPE	PRESS.: CONF./ PORE (MPa)	MOISTURE CONTENT (%)	SAMPLE L:D / LENGTH (cm)	SATURATION (%) / MEDIUM	LOAD RATE (MPa/s)	NOTES	REF.
Scotstown Granite USA				194.18			523								7
				188.29			573								7
Shartashskoye Granite Fine grained USSR	2.64	41.2					291								19
	2.64	40.2					323								19
	2.64	39.2					373								19
	2.64	38.1					423								19
	2.64	35.3					473								19
	2.64	32.4					523								19
	2.64	29.4					573								19
	2.64	27.9					623								19

**ADDITIONAL PROPERTIES
a) MODULUS OF RIGIDITY (GPa) c) SHEAR WAVE VELOCITY (km/s) e) SHORE SCLEROSCOPE HARDNESS g) MODULUS OF RUPTURE (MPa)
b) COMPRESSIBILITY (10^{-6}/MPa) d) IMPACT TOUGHNESS (m/m^2) f) LONGITUDINAL WAVE VELOCITY (km/s)

189

ROCK TYPE: GRANITE	MECHANICAL PROPERTIES						TEST CONDITIONS								
NAME DESCRIPTION LOCATION	ρ (g/cm^3)	E (GPa)	ν	C_o (MPa)	T_o (MPa)	ADDITIONAL PROPERTIES (**)	T (K)	No. TESTS / SHAPE	PRESS.: CONF./ PORE (MPa)	MOISTURE CONTENT (%)	SAMPLE L:D / LENGTH (cm)	SATURATION (%) / MEDIUM	LOAD RATE (MPa/s)	NOTES	REF.
Rovnenskoye Granite Medium to fine grained USSR	2.68	54.9					323								19
	2.68	49.0					373								19
	2.68	39.2					423								19
	2.68	33.3					473								19
	2.68	30.0					576								19
	2.68	27.0					623								19
	2.68	25.0					673								19
	2.68	22.1					723								19
Scotstown Granite USA				211.83			373								7
				200.06			473								7

**ADDITIONAL PROPERTIES
a) MODULUS OF RIGIDITY (GPa) c) SHEAR WAVE VELOCITY (km/s) e) SHORE SCLEROSCOPE HARDNESS g) MODULUS OF RUPTURE (MPa)
b) COMPRESSIBILITY (10^{-6}/MPa) d) IMPACT TOUGHNESS (m/m^2) f) LONGITUDINAL WAVE VELOCITY (km/s)

ROCK TYPE: MISC. GRANITIC	MECHANICAL PROPERTIES						TEST CONDITIONS								
NAME DESCRIPTION LOCATION	ρ (g/cm^3)	E (GPa)	ν	C_o (MPa)	T_o (MPa)	ADDITIONAL PROPERTIES (**)	T (K)	No. TESTS SHAPE	PRESS.: CONF./ PORE (MPa)	MOISTURE CONTENT (%)	SAMPLE L:D LENGTH (cm)	SATURATION (%) MEDIUM	LOAD RATE (MPa/s)	NOTES	REF.
Alpine Pegmatites Central Alps, Europe	2.61					1.79^c 2.66^f	293	3							27
Pegmatite; granitic Very coarse grain Star Lake, NY	2.59	61.6		213.70		22.8^a, 200.8^d 87.0^e, 4.90^f 22.1^g	298		0.0	0.0					10
Quartz Monzonite Coarse grain Butte Mines, MT				112.40		28.1^a 20.0^g	298	CYL	0.0	0.0	2.5 13.494			F	16
	2.75					185.0^d 65.0^e	298	CYL		0.0	1.0 5.3975				16
Quartz Monzonite Coarse grain Canada	2.65						298								7
Granite and Quartz Syenite; fine to medium grain; Star Lake, NY	2.62	66.9		275.10		283.5^d, 88.0^e 5.10^f, 20.7^g	298		0.0	0.0					10
Granite and Quartz Syenite; Lyon Mountain, NY	2.65	33.9		293.70		16.3^a, 551.0^d 95.0^e, 3.60^f	298		0.0	0.0					10
Meta-Rhyolite $\geq$ Quartz Porphyry Chloritic; MN	2.69			235.10		472.0^d, 68.0^e 7.60^g	298		0.0	0.0					10
Meta-Rhyolite $\geq$ Quartz Porphyry Soudan, MN	2.84	77.0		130.30		31.6^a, 512.0^d 5.20^f, 47.0^e 20.7^g	298		0.0	0.0					10
Rhyolite Fine grain Canada	2.64						298								7

**ADDITIONAL PROPERTIES a) MODULUS OF RIGIDITY (GPa) c) SHEAR WAVE VELOCITY (km/s) e) SHORE SCLEROSCOPE HARDNESS f) MODULUS OF RUPTURE (MPa)
b) COMPRESSIBILITY (10^{-6}/MPa) d) IMPACT TOUGHNESS (m/m^2) f) LONGITUDINAL WAVE VELOCITY (km/s)

ROCK TYPE: GRANODIORITE	MECHANICAL PROPERTIES						TEST CONDITIONS								
NAME DESCRIPTION LOCATION	ρ (g/cm^3)	E (GPa)	ν	C_o (MPa)	T_o (MPa)	ADDITIONAL PROPERTIES (**)	T (K)	No. TESTS SHAPE	PRESS.: CONF./ PORE (MPa)	MOISTURE CONTENT (%)	SAMPLE L:D LENGTH (cm)	SATURATION (%) MEDIUM	LOAD RATE (MPa/s)	NOTES	REF.
St. Cloud Grey Granodiorite; medium grain; St. Cloud, MN					6.97		298	30 CYL	0.0	0.0	2.0 5.08		.16 (10^{-5})		9
	2.72	18.4	.25			2.96^c 4.21^f	298	30 CYL	0.0	0.0	1.0 2.54				9
St. Cloud Granodiorite St. Cloud, MN	2.72						293			0.0				A	21

**ADDITIONAL PROPERTIES   a) MODULUS OF RIGIDITY (GPa)   c) SHEAR WAVE VELOCITY (km/s)   e) SHORE SCLEROSCOPE HARDNESS   f) MODULUS OF RUPTURE (MPa)
    b) COMPRESSIBILITY (10^{-6}/MPa)   d) IMPACT TOUGHNESS (m/m^2)   f) LONGITUDINAL WAVE VELOCITY (km/s)

ROCK TYPE: GRANODIORITE	MECHANICAL PROPERTIES						TEST CONDITIONS								
NAME DESCRIPTION LOCATION	ρ (g/cm^3)	E (GPa)	ν	C_o (MPa)	T_o (MPa)	ADDITIONAL PROPERTIES (**)	T (K)	No. TESTS / SHAPE	PRESS.: CONF./ PORE (MPa)	MOISTURE CONTENT (%)	SAMPLE L:D / LENGTH (cm)	SATURATION (%) / MEDIUM	LOAD RATE (MPa/s)	NOTES	REF.
Smolinskoye Granodiorite; Coarse grained; USSR	2.74	38.1					323								19
	2.74	37.8					373								19
	2.74	36.8					423								19
	2.74	36.1					473								19
	2.74	33.8					523								19
	2.74	32.4					573								19
	2.74	29.4					623								19
	2.74	27.5					673								19
	2.74	25.5					723								19
St. Cloud Grey Granodiorite; medium grain; St. Cloud, MN		70.8		282.00			298	30 / CYL	0.0	0.0	2.0 / 5.08		.10 (10^{-4})	J	9

**ADDITIONAL PROPERTIES   a) MODULUS OF RIGIDITY (GPa)   c) SHEAR WAVE VELOCITY (km/s)   e) SHORE SCLEROSCOPE HARDNESS   f) MODULUS OF RUPTURE (MPa)
                    b) COMPRESSIBILITY (10^{-6}/MPa)   d) IMPACT TOUGHNESS (m/m^2)   f) LONGITUDINAL WAVE VELOCITY (km/s)

ROCK TYPE: GRANODIORITE	MECHANICAL PROPERTIES						TEST CONDITIONS								
NAME DESCRIPTION LOCATION	ρ (g/cm^3)	E (GPa)	ν	C_o (MPa)	T_o (MPa)	ADDITIONAL PROPERTIES (**)	T (K)	No. TESTS / SHAPE	PRESS.: CONF./ PORE (MPa)	MOISTURE CONTENT (%)	SAMPLE L:D / LENGTH (cm)	SATURATION (%) / MEDIUM	LOAD RATE (MPa/s)	NOTES	REF.
Granodiorite Medium grained Canada	2.74						298								7
Finnsjon Granodiorite		82.5	.20	240.60	13.48		293	12 / CYL	0.0	0.0	2.5				3
Granodiorite Nevada Test Site NV		64.0	.31				293	/ CYL			2.0 / 2.54				18
		70.0	.29				293	/ CYL			2.0 / 2.54				18
Granodiorite Shocked by nuclear blast; NTS, NV		18.0	.45				293	/ CYL			2.0 / 2.54			N	18
		18.0	.45				293	/ CYL			2.0 / 2.54			N	18
		70.0	.29				293	/ CYL			2.0 / 2.54			N	18
Granodiorite Mechanically shocked NTS, NV		1.0	.50				293	/ CYL			2.0 / 2.54			O	18
		7.0	.29				293	/ CYL			2.0 / 2.54			O	18
Smolinskoye Granodiorite; Coarse grained; USSR	2.74	38.2					291								19

**ADDITIONAL PROPERTIES
a) MODULUS OF RIGIDITY (GPa) c) SHEAR WAVE VELOCITY (km/s) e) SHORE SCLEROSCOPE HARDNESS f) MODULUS OF RUPTURE (MPa)
b) COMPRESSIBILITY (10^{-6}/MPa) d) IMPACT TOUGHNESS (m/m^2) f) LONGITUDINAL WAVE VELOCITY (km/s)

194

ROCK TYPE: GRANITE	MECHANICAL PROPERTIES						TEST CONDITIONS							
NAME DESCRIPTION LOCATION	ρ (g/cm^3)	E (GPa)	ν	C_0 (MPa)	T_0 (MPa)	ADDITIONAL PROPERTIES (**)	T (K)	No. TESTS / SHAPE	PRESS.: CONF./ PORE (MPa)	MOISTURE CONTENT (%)	SAMPLE L:D / LENGTH (cm)	SATURATION (%) / MEDIUM	LOAD RATE (MPa/s)	NOTES	REF.
Westerly Granite Homogeneous Westerly, RI				253.00			298	CYL			1.33 / 1.27		.13 (10^{-3})	G	8
				379.00			298	CYL			1.33 / 1.27		.20	G	8
				470.00			298	CYL			1.33 / 1.27		.30 (10^4)	G	8
	2.65						298								8
Granite Woodstock Granite Quarry; Woodstock, MD	2.65	54.6		351.00		25.4^a, 271.0^d 98.0^e, 4.50^f 20.7^g	298		0.0	0.0					10
Granite Zuni Mt. Area Valencia Co., NM				193.10			293	CYL	0.0		2.5 / 5.715				6
		82.0	.27			5.40^f	293	CYL			12.0 / 25.4				6
	2.64						0	CYL			1.0 / 2.225			P	6
						547.24^d	293	CYL			1.0 / 2.225			P	6

**ADDITIONAL PROPERTIES a) MODULUS OF RIGIDITY (GPa) c) SHEAR WAVE VELOCITY (km/s) e) SHORE SCLEROSCOPE HARDNESS f) MODULUS OF RUPTURE (MPa)
b) COMPRESSIBILITY (10^{-6}/MPa) d) IMPACT TOUGHNESS (m/m^2) f) LONGITUDINAL WAVE VELOCITY (km/s)

195

ROCK TYPE: GRANITE	MECHANICAL PROPERTIES						TEST CONDITIONS								
NAME DESCRIPTION LOCATION	ρ (g/cm³)	E (GPa)	ν	C_o (MPa)	T_o (MPa)	ADDITIONAL PROPERTIES (**)	T (K)	No. TESTS / SHAPE	PRESS.: CONF./PORE (MPa)	MOISTURE CONTENT (%)	SAMPLE L:D / LENGTH (cm)	SATURATION (%) / MEDIUM	LOAD RATE (MPa/s)	NOTES	REF.
Granite Westerly, RI			.18			31.0[a] 2.08[b]	298								20
			.19			32.0[a] 1.95[b]	298		0.0						20
			.20			33.0[a] 1.84[b]	298		0.0						20
			.21			34.0[a] 1.71[b]	298		0.0						20
Westerly Granite						8.30[b] 2.69[c] 4.14[f]	298		0.0						23
Westerly Granite Quartz Monzonite						51.0[b] 1.00[c] 1.00[f]	1225		0.1						24
Westerly Granite Fine grain, equigranular Westerly, RI		49.9		233.00			298	30 / CYL	0.0	0.0	2.0 / 5.08		.10 (10⁻⁴)	J	9
					9.61	93.8[e]	298	30 / CYL	0.0	0.0	2.0 / 5.08		.16 (10⁻⁵)		9
	2.64	44.3	.21			2.71[c] 4.09[f]	298	30 / CYL	0.0	0.0	1.0 / 2.54			A	9
Westerly Granite Homogeneous Westerly, RI				253.00			298	CYL			1.33 / 1.27		.10 (10⁻⁵)	G	8

**ADDITIONAL PROPERTIES a) MODULUS OF RIGIDITY (GPa) c) SHEAR WAVE VELOCITY (km/s) e) SHORE SCLEROSCOPE HARDNESS f) MODULUS OF RUPTURE (MPa)
b) COMPRESSIBILITY (10^{-6}/MPa) d) IMPACT TOUGHNESS (m/m²) f) LONGITUDINAL WAVE VELOCITY (km/s)

ROCK TYPE: GRANITE	MECHANICAL PROPERTIES						TEST CONDITIONS								
NAME DESCRIPTION LOCATION	ρ (g/cm^3)	E (GPa)	ν	C_o (MPa)	T_o (MPa)	ADDITIONAL PROPERTIES (**)	T (K)	No. TESTS SHAPE	PRESS.: CONF./ PORE (MPa)	MOISTURE CONTENT (%)	SAMPLE L:D LENGTH (cm)	SATURATION (%) MEDIUM	LOAD RATE (MPa/s)	NOTES	REF.
Unaweep Granite Coarse grain Grand Junction, CO						303.7^d 37.0^e	298	 CYL		0.0	1.0 5.3975			F	16
Unaweep Granite Coarse grain, || to bed CO				161.30		22.8^g	298	0.0 CYL		0.0	2.5 13.494			F	16
		42.3			5.60	19.0^a 3.93^f	298	0.0 CYL		0.0	4.5 25.40			E,F	16
	2.73					173.2^d	298	 CYL		0.0				F	16
						44.0^e	298	 CYL		0.0	1.0 5.3975			F	16
Granite Westerly, RI			.06			20.0^a 5.64^b	298	0.0							20
			.11			24.0^a 3.62^b	298	0.0							20
			.15			28.0^a 2.66^b	298	0.0							20
			.17			29.0^a 2.37^b	298	0.0							20
			.18			30.0^a 2.18^b	298	0.0							20

**ADDITIONAL PROPERTIES
a) MODULUS OF RIGIDITY (GPa)
b) COMPRESSIBILITY (10^{-6}/MPa)
c) SHEAR WAVE VELOCITY (km/s)
d) IMPACT TOUGHNESS (m/m^2)
e) SHORE SCLEROSCOPE HARDNESS
f) LONGITUDINAL WAVE VELOCITY (km/s)
f) MODULUS OF RUPTURE (MPa)

197

ROCK TYPE: GRANITE	MECHANICAL PROPERTIES						TEST CONDITIONS							
NAME DESCRIPTION LOCATION	ρ (g/cm^3)	E (GPa)	ν	C_o (MPa)	T_o (MPa)	ADDITIONAL PROPERTIES (**)	T (K)	No. TESTS / SHAPE	PRESS.: CONF./ PORE (MPa)	MOISTURE CONTENT (%)	SAMPLE L:D / LENGTH (cm)	SATURATION (%) / MEDIUM	LOAD RATE (MPa/s)	NOTES	REF.
Unaweep Granite Coarse grain Grand Junction, CO		38.2	.002			19.1[a] 3.75[f]	298	CYL	0.0	0.0	4.5 25.40			F	16
		18.7	.08			17.9[g]	298	CYL	0.0	0.0	2.5 13.494			V,F	16
		27.2	.12			15.5[a] 3.17[f]	298	CYL	0.0	0.0	4.5 25.40			F	16
		29.2	.13			15.9[g]	298	CYL	0.0	0.0	2.5 13.494			V,F	16
		27.2	-.13				298	CYL	0.0	0.0	4.5 25.40			F	16
	2.67						298			0.0					16
	2.71						298			0.0					16
	1.60						298			0.0					16
						307.1[d] 59.0[e]	298	CYL		0.0	1.0 5.3975			F	16
						303.1[d] 53.0[e]	298	CYL		0.0	1.0 5.3975			F	16

**ADDITIONAL PROPERTIES
a) MODULUS OR RIGIDITY (GPa)
b) COMPRESSIBILITY (10^{-6}/MPa)
c) SHEAR WAVE VELOCITY (km/s)
d) IMPACT TOUGHNESS (m/m^2)
e) SHORE SCLEROSCOPE HARDNESS
f) LONGITUDINAL WAVE VELOCITY (km/s)
f) MODULUS OF RUPTURE (MPa)

198

ROCK TYPE: GRANITE	MECHANICAL PROPERTIES						TEST CONDITIONS								
NAME DESCRIPTION LOCATION	ρ (g/cm³)	E (GPa)	ν	C₀ (MPa)	T₀ (MPa)	ADDITIONAL PROPERTIES (**)	T (K)	No. TESTS / SHAPE	PRESS.: CONF./ PORE (MPa)	MOISTURE CONTENT (%)	SAMPLE L:D / LENGTH (cm)	SATURATION (%) / MEDIUM	LOAD RATE (MPa/s)	NOTES	REF.
Swenson Pink Granite; USA				143.18			573								7
Texas Granite				170.99			293	5 / CYL	0.0		2.0 / 10.909				4
Unaweep Granite Coarse grain Grand Junction, CO				175.80		16.5^g	298	/ CYL	0.0	0.0	2.5 / 13.494			E	16
				158.60		17.9^g	298	/ CYL	0.0	0.0	2.5 / 13.494			E	16
				174.40			298	/ CYL	0.0	0.0	2.5 / 13.494			E	16
					4.10		298	/ CYL	0.0	0.0	4.5 / 25.40			E	16
					3.60		298	/ CYL	0.0	0.0	4.5 / 25.40			E	16
					3.40		298	/ CYL	0.0	0.0	4.5 / 25.40			E	16
		27.2	.19			16.8^a 3.17^f	298	/ CYL	0.0	0.0	4.5 / 25.40			F	16
		21.3	.05			16.5^g	298	/ CYL	0.0	0.0	2.5 / 13.494			V,F	16

**ADDITIONAL PROPERTIES
a) MODULUS OF RIGIDITY (GPa) c) SHEAR WAVE VELOCITY (km/s) e) SHORE SCLEROSCOPE HARDNESS g) MODULUS OF RUPTURE (MPa)
b) COMPRESSIBILITY (10^{-6}/MPa) d) IMPACT TOUGHNESS (m/m²) f) LONGITUDINAL WAVE VELOCITY (km/s)

ROCK TYPE: GRANITE	MECHANICAL PROPERTIES						TEST CONDITIONS							
NAME DESCRIPTION LOCATION	ρ (g/cm^3)	E (GPa)	ν	C_o (MPa)	T_o (MPa)	ADDITIONAL PROPERTIES (**)	T (K)	No. TESTS — SHAPE	PRESS.: CONF./ PORE (MPa)	MOISTURE CONTENT (%)	SAMPLE L:D — LENGTH (cm)	SATURATION (%) — MEDIUM	LOAD RATE (MPa/s)	NOTES	REF.
Stripa Granite					14.96		293	12	0.0	0.0					3
		50.8	.13	148.00			463	6	0.0						3
	2.62					64.9^a 5.18^f	293	2 CYL							3
	2.61					65.2^a 5.24^f	293	2 CYL							3
	2.62					65.5^a 5.31^f	293	2 CYL							3
	2.62					65.7^a 5.38^f	293	2 CYL							3
	2.62					5.21^f	293	9 CYL							3
Swenson Pink Granite; USA				156.91			373								7
				150.05			473								7
				147.11			523								7

**ADDITIONAL PROPERTIES a) MODULUS OF RIGIDITY (GPa) c) SHEAR WAVE VELOCITY (km/s) e) SHORE SCLEROSCOPE HARDNESS f) MODULUS OF RUPTURE (MPa)
b) COMPRESSIBILITY (10^{-6}/MPa) d) IMPACT TOUGHNESS (m/m^2) f) LONGITUDINAL WAVE VELOCITY (km/s)

ROCK TYPE: GRANITE	MECHANICAL PROPERTIES						TEST CONDITIONS								
NAME DESCRIPTION LOCATION	ρ (g/cm^3)	E (GPa)	ν	C_o (MPa)	T_o (MPa)	ADDITIONAL PROPERTIES (**)	T (K)	No. TESTS / SHAPE	PRESS.: CONF./ PORE (MPa)	MOISTURE CONTENT (%)	SAMPLE L:D / LENGTH (cm)	SATURATION (%) / MEDIUM	LOAD RATE (MPa/s)	NOTES	REF.
Granite Stone Mountain, GA			.18			38.0[a] 1.72[b]	298		0.0						20
Stone Mountain Granite Even texture, medium grain	2.61			28.00			298		0.0						12
Stripa Granite		82.2		470.00			293	5	20.0	0.0					3
		83.2		530.00			293	5	30.0	0.0					3
		69.4		207.60			293	10	0.0						3
		71.2		208.20			323	8	0.0						3
		62.4		221.30			373	7	0.0						3
		57.2		205.50			423	6	0.0					D	3
		75.4		308.50			293	5	5.0	0.0					3
		77.2		372.00			293	5	10.0	0.0					3

**ADDITIONAL PROPERTIES
a) MODULUS OF RIGIDITY (GPa)
b) COMPRESSIBILITY (10^{-6}/MPa)
c) SHEAR WAVE VELOCITY (km/s)
d) IMPACT TOUGHNESS (m/m^2)
e) SHORE SCLEROSCOPE HARDNESS
f) LONGITUDINAL WAVE VELOCITY (km/s)
f) MODULUS OF RUPTURE (MPa)

ROCK TYPE: GRANITE	MECHANICAL PROPERTIES						TEST CONDITIONS									
NAME DESCRIPTION LOCATION	ρ (g/cm^3)	E (GPa)	ν	C_o (MPa)	T_o (MPa)	ADDITIONAL PROPERTIES (**)	T (K)	No. TESTS / SHAPE	PRESS.: CONF./ PORE (MPa)	MOISTURE CONTENT (%)	SAMPLE L:D / LENGTH (cm)	SATURATION (%) / MEDIUM	LOAD RATE (MPa/s)	NOTES	REF.
Shartashskoye Granite Medium grained USSR	2.64	19.1					673								19
	2.64	16.2					723								19
Granite Stone Mountain, GA			.06			16.0^a 7.18^b	298		0.0						20
			.05			24.0^a 5.03^b	298		0.0						20
			.13			29.0^a 2.83^b	298		0.0						20
			.14			31.0^a 2.45^b	298		0.0						20
			.16			33.0^a 2.19^b	298		0.0						20
			.16			35.0^a 2.03^b	298		0.0						20
			.16			36.0^a 1.92^b	298		0.0						20
			.17			37.0^a 1.85^b	298		0.0						20

**ADDITIONAL PROPERTIES
a) MODULUS OF RIGIDITY (GPa)
b) COMPRESSIBILITY (10^{-6}/MPa)
c) SHEAR WAVE VELOCITY (km/s)
d) IMPACT TOUGHNESS (m/m^2)
e) SHORE SCLEROSCOPE HARDNESS
f) LONGITUDINAL WAVE VELOCITY (km/s)
f) MODULUS OF RUPTURE (MPa)

ROCK TYPE: GRANITE	MECHANICAL PROPERTIES						TEST CONDITIONS								
NAME DESCRIPTION LOCATION	ρ (g/cm^3)	E (GPa)	ν	C_o (MPa)	T_o (MPa)	ADDITIONAL PROPERTIES (**)	T (K)	No. TESTS / SHAPE	PRESS.: CONF./ PORE (MPa)	MOISTURE CONTENT (%)	SAMPLE L:D / LENGTH (cm)	SATURATION (%) / MEDIUM	LOAD RATE (MPa/s)	NOTES	REF.
Shartashskoye Granite Fine grained USSR	2.64	26.5					673								19
	2.64	23.5					723								19
Shartashskoye Granite Medium grained USSR	2.64	31.9					291								19
	2.64	30.9					323								19
	2.64	29.4					373								19
	2.64	27.0					423								19
	2.64	26.0					473								19
	2.64	23.5					523								19
	2.64	22.6					573								19
	2.64	20.6					623								19

**ADDITIONAL PROPERTIES
a) MODULUS OF RIGIDITY (GPa)
b) COMPRESSIBILITY (10^{-6}/MPa)
c) SHEAR WAVE VELOCITY (km/s)
d) IMPACT TOUGHNESS (m/m^2)
e) SHORE SCLEROSCOPE HARDNESS
f) LONGITUDINAL WAVE VELOCITY (km/s)
f) MODULUS OF RUPTURE (MPa)

A.4 NOTES

A. Helium, mercury barometer method

B. Water wet sample

C. Model composition available

D. Partial failured edge spall

E. Failure strain approximate only

F. Geologic description available

G. Values estimated from graph

H. Point load test

I. Secant modulus at 50% failure

J. Tangent modulus, 50% ultimate strength

K. Axial Stress, 34.48 MPa

L. Axial stress 34.48 MPa, constrained modulus

M. Hydraulic conductivity value less than 1.0×10^{-10} m/s

N. Unknown stress level

O. Estimated stress, 3500 to 4000 MPa

P. The type of test is unknown for this data

Q. Stress level, 20.7 MPa

R. Stress level, 62.1 MPa

S. Deformation modulus, stress level, 20.7 MPa

T. Deformation modulus, stress level, 62.1 MPa

U. Unloading

V. Intermediate load, secant value

W. Stress level, 50% ultimate strength

X. Absorption, percent of dry weight

Y. Flash method

Z. Previous maximum temperature - 1000K

aa. In situ drill hole test

bb. Test on side of specimen

205

A.5 APPENDIX A REFERENCES

Influence of Water on Hardness, Strength and Compressibility of Rock," *Bulletin Association Engineering Geology*, Vol. 13, pp. 1-22.

2. Stephenson, D. E. and G. E. Triandafilidis, 1974. "Influence of Loading Rate on Rock Response," *Proceedings of the American Society of Civil Engineering*, Vol. 100, No. GT2, pp. 101-122.

3. Swan, G., 1977. *The Mechanical Properties of the Rocks in Stripa, Krakemala, Finnsjön, and Blekinge*, KBS TR 48, Stockholm, Sweden.

4. Brady, B. T., W. I. Duvall, and F. G. Horino, 1973. "An Experimental Determination of the True Uniaxial Stress-Strain Behavior of Brittle Rock," *Rock Mechanics*, Vol. 5, pp. 107-120.

5. Deere, D. U. and R. P. Miller, 1966. *Engineering Classification and Index Properties for Intact Rock*, Technical Report No. AFWL-TR-65-116, Air Force Weapons Laboratory.

6. Blair, B. E., 1955. "Physical Properties of Mine Rock. Part III.," *U.S. Bureau Mines Report of Investigation No. 5130*, Denver CO.

7. Geller, L. B., 1970. "A New Look at Thermal Rock Fracturing," Extract from *Transactions/Sec. American Institute of Mining and Metallurgy*, Vol. 79, pp. A133-A170.

8. Green, S. J. and R. D. Perkins, 1968. *Uniaxial Compression Tests at Strain Rates From 10^{-4}/sec. to 10^4/sec. on Three Geologic Materials*, Report No. MSL-68-6, General Motors Corporation, Materials and Structures Laboratory.

9. Krech, W. W., F. A. Henderson, and K. E. Hjelmstad, 1974. "A Standard Rock Suite for Rapid Excavation Research," *U.S. Bureau Mines Report of Investigation No. 7865*, Denver, CO.

APPENDIX A

REFERENCES

(Continued)

10. Windes, S. L., 1949. "Physical Properties of Mine Rock. Part I.," U.S. Bureau Mines Report of Investigation No. 4459, Denver, CO.

11. Janach, W., 1976. "The Role of Bulking in Brittle Failure of Rocks Under Rapid Compression," International Journal of Rock Mechanics and Mining Science, Vol. 13, pp. 177-186.

12. Schwartz, A., 1964. "Failure of Rock in the Triaxial Shear Test," Proceedings, 6th U.S. Symposium on Rock Mechanics, Rolla, MO, October, pp. 109-151.

13. Stowe, R. L., 1972. "Comparison of In-Situ and Laboratory Test Results on Granite," Transactions of the Society of Mining Engineers, Vol. 252, pp. 194-199.

14. Kranz, R. L. and C. H. Scholz, 1977. "Critical Dilatant Volume of Rocks at the Onset of Tertiary Creep," Journal of Geophysical Research, Vol. 82, pp. 4893-4898.

15. Lauriello, P. J. and Y. Chen, 1973. "Thermal Fracturing of Hard Rock," Journal of Applied Mechanics, Vol. 484, pp. 909-914.

16. Blair, B. E., 1956. "Physical Properties of Mine Rock. Part IV.," U.S. Bureau Mines Report of Investigation No. 5244, Denver, CO.

17. Stowe, R. L. and D. L. Ainsworth, 1968. "Effect of Rate of Loading on Strength and Young's Modulus of Elasticity of Rock," Proceedings, 10th U.S. Symposium on Rock Mechanics, Austin, TX, May, pp. 3-33.

18. Giardini, A. A., J. R. Lakner, D. R. Stephens, and H. D. Stromberg, 1968. "Triaxial Compression Data on Nuclear Explosion Shocked, Mechanically Shocked, and Normal Granodiorite from the Nevada Test Site," Journal of Geophysical Research, Vol. 73, pp. 1305-1320.

APPENDIX A

REFERENCES

(Continued)

19. Dmitriyev, A. P., L. S. Kuzyayev, and Y. I. Protasov, 1969. "Physical Properties of Rocks at High Temperatures," NASA Technical Translation No. NASA TT F-684.

20. Simmons, G. and W. F. Brace, 1965. "Comparison of Static and Dynamic Measurements of Compressibility of Rocks," Journal of Geophysical Research, Vol. 70, pp. 5649-5656.

21. Hanley, E. J., D. P. DeWitt, and R. F. Roy, 1978. "The Thermal Diffusivity of Eight Well-Characterized Rocks for the Temperature Range 300-1000 K," Engineering Geology, Vol. 12, pp. 31-47.

22. Richter, D. and G. Simmons, 1974. "Thermal Expansion Behavior of Igneous Rocks," International Journal of Rock Mechanics and Mining Science and Geomechanic Abstracts, Vol. 11, pp. 403-410.

23. Simmons, G. and A. Nur, 1968. "Granites: Relation of Properties In Situ to Laboratory Measurements," Science, Vol. 162, pp. 789-791.

24. Simmons, G., T. Todd, and W. Baldridge, 1975. "Toward a Quantitative Relationship Between Elastic Properties and Cracks in Low Porosity Rocks," American Journal of Science, Vol. 275, pp. 318-345.

25. Brace, W. F., J. B. Walsh, and W. T. Frangos, 1968. "Permeability of Granite under High Pressure," Journal of Geophysical Research, Vol. 73, pp. 2225-2236.

26. Cooper, H. W. and G. Simmons, 1977. "The Effect of Cracks on the Thermal Expansion of Rocks," Earth and Planetary Science Letters, Vol. 36, pp. 404-412.

27. Johnson, L. R. and H. R. Wenk, 1974. "Anisotropy of Physical Properties in Metamorphic Rocks," Tectonophysics, Vol. 23, pp. 79-98.

APPENDIX A

REFERENCES

(Concluded)

28. Jessop, A. M., P. B. Robertson, and T. J. Lewis, 1976. A Brief Summary of the Thermal Conductivity of Crystalline Rocks, Geothermal Service of Canada Internal Report 76-4, Department of Energy, Mines and Resources.

29. Ohle, E. L., 1951. "The Influence of Permeability on Ore Distribution in Limestone and Dolomite," Economic Geology, Vol. 46.

30. Carlsson, A. T. and T. Olsson, 1977. "Variations of Hydraulic Conductivity in Some Swedish Rock Types," Rockstore 77, Vol. 2, pp. 301-307.

31. Lindroth, D. P., 1974. "Thermal Diffusivity of Six Igneous Rocks at Elevated Temperatures and Reduced Pressures," U.S. Bureau Mines Report of Investigation No. 7954, Denver, CO.

32. Dames and Moore, 1978. "Baseline Rock Properties - Granite," Technical Support for GEIS: Radioactive Waste Isolation in Geologic Formations, Vol. 5, April.

APPENDIX B

SELECTION OF THE "EFFECTIVE" THERMAL CONDUCTIVITY

IN A DISPOSAL ROOM

APPENDIX B
LIST OF FIGURES

APPENDIX B

LIST OF TABLES

APPENDIX B

Heat transfer within a sealed disposal room before backfilling with crushed granite is a complex combination of conduction, radiation, and convection. Heat conduction and radiation can be modeled explicitly, although the highly nonlinear nature of radiative heat transfer significantly increases the time and expense of the near-field analyses. The approximation of free convection within a sealed disposal room is crude at best and must be based on very limited empirical data. However, since the disposal room is sealed after waste emplacement, the combined heat transfer processes simply enhance the heat transfer across the room, particularly from the room floor to the ceiling and walls. Consequently, the effects of conduction, radiation, and convection can be approximated by increasing the thermal conductivity of the air in the room to an "effective" value which simulates the enhanced heat transfer across the room due to the combined heat transfer modes. The subject of this appendix is the selection of the value for the "effective" thermal conductivity, k_e, of the air.

In this investigation, five different approximations for the medium in a disposal room were made that range from conduction through stagnant air to combined conduction-radiation. These five cases are summarized in Table B-1. Two values for the effective conductivity are included in these five cases along with an approximation based on the thermal properties of granite. The latter case was included to assess the impact of the disposal room on the near-field thermal response. The model of a CHLW disposal room with an areal thermal loading of 25 W/m^2 was used to perform the comparison of the five cases.

The results of this investigation are presented in Figure B-1 and Table B-2. The temperature difference between the floor and roof in Case A appears to greatly deviate from the other four cases. A large difference between the floor and roof temperatures is expected in Case A since stagnant air is a very effective insulator and heat conduction through stagnant air closely approximates a perfectly insulated boundary along the room periphery. Case B, which for heat transfer purposes considers the room to be granite, shows the difference in roof and floor temperature to be considerably less than in Case A. The roof and floor temperatures for Cases C and D are almost identical. This close agreement indicates that the change in thermal conductivity has only a minor influence after the effective thermal conductivity has exceeded a certain value. Finally, the roof and floor temperatures from Case E during most of the 100-year period

Table B-1. Five Heat Transfer Mediums in Disposal Room

Case	Disposal Room Description	Thermal Conductivity (W/m-K)	Specific Heat (J/kg-K)	Density (kg/m^3)
A	Stagnant Air	0.001	1003	1.3
B	Granite	2.52	809	2652
C	Effective Thermal Conductivity (k_e = 25,000 k_{air})	25.	1003	1.3
D	Effective Thermal Conductivity (k_e = 50,000 k_{air})	50.	1003	1.3
E	Stagnant Air with 1-D Radiation[a]	0.001	1003	1.3

(a) Radiative exchange between the floor and roof only.
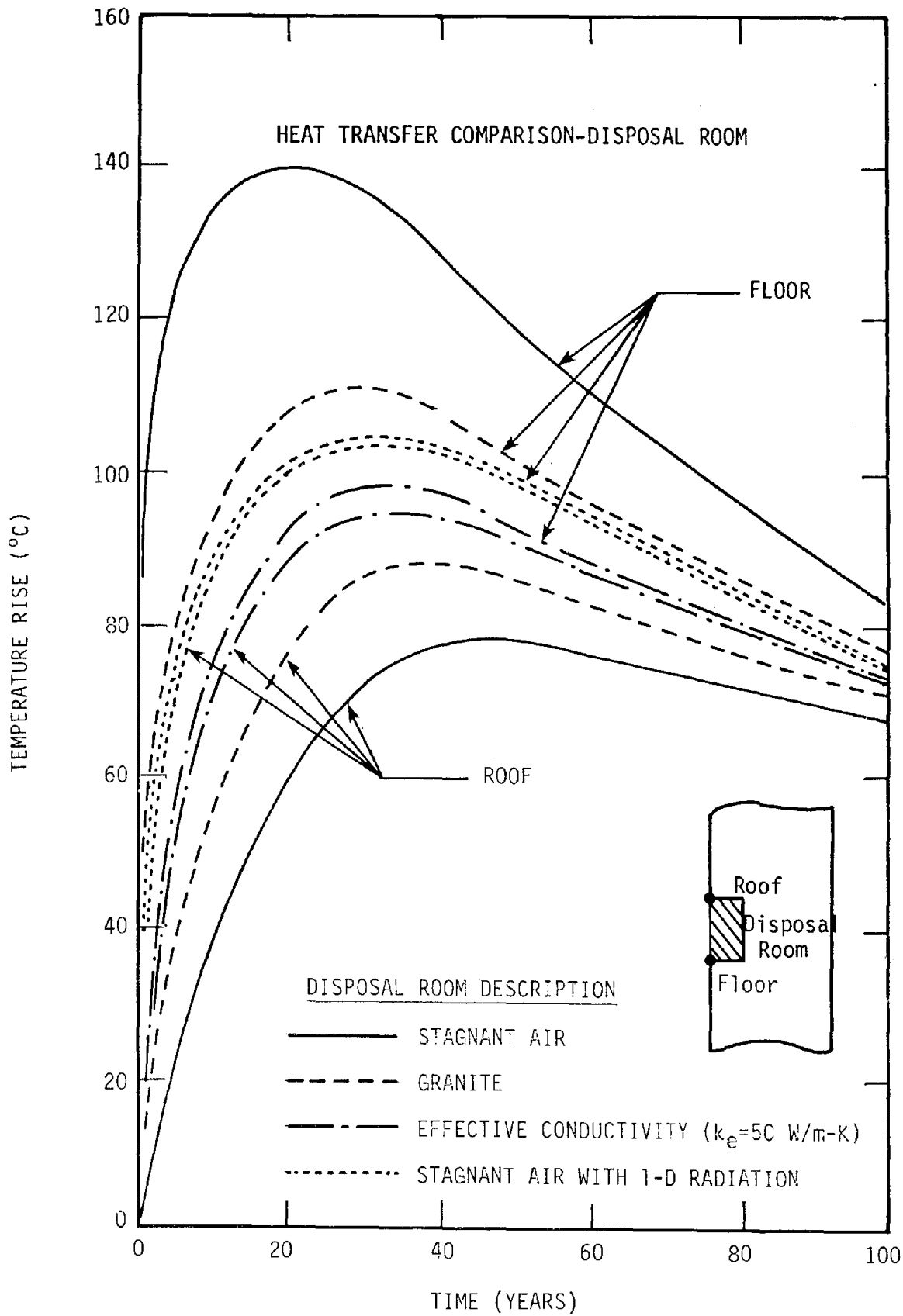
Figure B-1. Comparison of Temperatures at the Roof and Floor for Four Cases with Different Heat Transfer Mediums in the Disposal Room.

Table B-2. Temperature Rises (°C) for Five Different Heat Transfer
Mediums in Disposal Room

Time (Years)	Floor					Rib					Roof				
	A	B	C	D	E	A	B	C	D	E	A	B	C	D	E
1	86	47	29	27	46	11	15	24	24	11	1	8	22	23	41
5	124	80	59	57	73	43	48	54	54	43	19	36	52	53	69
15	139	103	87	85	96	75	78	83	83	75	51	68	81	82	94
25	139	110	97	96	104	88	90	94	94	88	67	82	92	93	101
40	128	108	99	98	103	93	94	97	97	93	78	88	96	96	102
55	114	100	92	92	95	89	90	91	91	88	77	85	90	91	94
70	103	92	87	87	89	85	85	86	86	84	76	82	86	86	88
100	83	77	74	73	75	73	73	73	73	72	68	71	73	73	74

Roof

Rib
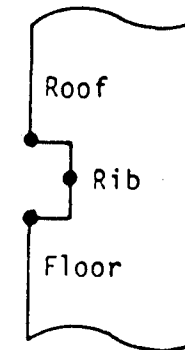
Floor

are approximately 5°C greater than either Case C or D. However, the rib temperatures for Case E during most of the 100-year period are approximately 5°C less than either Case C or D. Since the radiative exchange in Case E was one-dimensional (floor-roof exchange), two-dimensional modeling of radiation should increase the rib temperature and reduce the roof and floor temperatures. Consequently, two-dimensional modeling of the radiative exchange should agree more closely with the thermal behavior along the room periphery predicted in Cases C and D.

The computation of an "effective" thermal conductivity was performed by examining the difference between the floor and roof temperatures from Case E and estimating the total heat transfer across the room using the following relation:

$$q_{total} = q_{conduction} + q_{radiation} \tag{B-1}$$

$$q_{total} = -k_{air} \frac{\partial T}{\partial z} + \sigma (T_f^4 - T_r^4) \tag{B-2}$$

where:

q = heat flux (W/m^2)

k_{air} = thermal conductivity of air (0.001 W/m-K)

$\frac{\partial T}{\partial z}$ = vertical gradient of air temperature (K/m)

σ = Stefan-Boltzmann constant $(5.669 \times 10^{-8} \ W/m^2 - K^4)$

T_f = absolute temperature of floor (K)

T_r = absolute temperature of roof (K).

If the vertical gradient of air temperature is approximated as the difference between the roof and floor temperatures divided by the height of the room, Equation B-2 can be rewritten as follows:

$$q_{total} = k_{air} \frac{(T_f - T_r)}{L} + \sigma (T_f^4 - T_r^4) \tag{B-3}$$

where:

L = room height (7.0 m).

If an "effective" thermal conductivity is chosen such that the heat transfer across the room is equal to the total heat transfer given by Equation B-3 for the same floor and roof temperatures, k_e is given by the following equation:

$$k_e \frac{(T_f - T_r)}{L} = k_{air} \frac{(T_f - T_r)}{L} + \sigma (T_f^4 - T_r^4)$$

$$k_e = k_{air} + \sigma L (T_f^2 + T_r^2)(T_f + T_r). \tag{B-4}$$

The floor and roof temperatures for Case E (Table B-2) were evaluated to determine an effective thermal conductivity and a value of 75 W/m-K was selected to model the heat transfer through the disposal room before backfilling. This value is approximately 75,000 times the thermal conductivity of stagnant air. As previously discussed, the value could be lowered to values associated with Cases C and D without any appreciable change in room periphery temperature.

APPENDIX C

THE DEVELOPMENT OF A FINITE ELEMENT PROGRAM

TO MODEL COUPLED CONVECTIVE AND CONDUCTIVE HEAT TRANSFER

APPENDIX C
TABLE OF CONTENTS

APPENDIX C

LIST OF FIGURES

APPENDIX C
LIST OF FIGURES
(Concluded)

APPENDIX C
LIST OF TABLES

APPENDIX C

C.1 INTRODUCTION

This appendix reviews the theoretical considerations necessary to develop finite element program SPECTROM-55, which is capable of modeling heat transport in the liquid and solid phases of a ground-water flow system. The ultimate application of this particular program is to predict any perturbation of the regional hydrogeology in the vicinity of a nuclear waste repository. This application typically involves modeling both forced and free convection through a vertical cross section composed of multi-layered strata.

The program development is based principally on the Galerkin formulation of the coupled, partial differential equations governing hydrothermal transport in ground-water systems outlined by Mercer and Pinder [1974]. The convective transport term is incorporated into the heat transfer equation using techniques investigated by Hsu and Nickell [1974].

In the following sections, the governing equations and the methodology used to incorporate them into SPECTROM-55 are described. A series of examples that were used to validate the program are presented.

C.2 FORMULATION OF THE EQUATIONS

The porous medium is assumed to be a mixture of a solid phase and a liquid phase, and both phases are assumed to be continuous. Further, it is assumed that throughout time, a representative elementary volume is occupied simultaneously by both phases and that the volume is saturated. Also, the motion of the liquid phase is assumed to be relative to the solid phase. Based on these premises, two partial differential equations may be developed [Mercer, 1973]; one equation governs the motion of the liquid phase and the other describes the transport of heat in the liquid and solid phases. The equation of motion for the liquid phase in a nonisothermal, single-component, ground-water flow system may be written as:

$$\nabla \cdot \frac{\rho_\ell \overline{\overline{\kappa}}}{\mu} \cdot (\overline{\nabla} p - \rho_\ell \overline{g}) - (\rho_\ell \alpha_p + \theta \rho_0 \beta_p) \frac{\partial p}{\partial t} - \theta \rho_0 \beta_T \frac{\partial T}{\partial t} + q_h = 0 \qquad (C-1)$$

where:

ρ_ℓ = liquid density

$\overline{\overline{\kappa}}$ = intrinsic permeability tensor

μ = dynamic viscosity of liquid

p = pressure

$\overline{g}$ = gravitational vector

α_p = vertical compressibility of the liquid-solid mixture

θ = porosity

β_p = compressibility coefficient of liquid

β_T = coefficient of thermal volume expansion of liquid

T = temperature

q_h = volumetric time rate of supply of liquid mass.

Single and double bar overscores indicate vector and tensor quantities, respectively.

The heat transport equation for a porous medium containing only a liquid and solid phase may be written as:

$$\overline{\nabla} \cdot [\theta \, \overline{\overline{k}}_\ell + (1-\theta)\overline{\overline{k}}_s] \cdot \overline{\nabla}T - [\theta\rho_\ell c_{v\ell} + (1-\theta)\rho_s c_{vs}] \frac{\partial T}{\partial t}$$

$$-\theta\rho_\ell c_{v\ell}\overline{v}_r \cdot \overline{\nabla}T + Q + q_h c_{v\ell} (T-T_h) = 0 \qquad (C-2)$$

where:

$\overline{\overline{k}}_\ell$ = hydrodynamic thermal dispersion tensor of liquid

$\overline{\overline{k}}_s$ = thermal conductivity tensor of solid

$c_{v\ell}$ = specific heat capacity of liquid

c_{vs} = specific heat capacity of solid

ρ_s = solid density

$\overline{v}_r$ = velocity of liquid phase relative to solid phase

Q = volumetric heat generation rate of mixture

T_h = temperature of liquid mass source, q_h.

It is apparent from the preceding equations that the field variables the finite element program will determine are pressure (Equation C-1) and temperature (Equation C-2). Also, the liquid and solid phases are assumed to be in thermal equilibrium; that is, the liquid and solid phases are at the same temperature.

The following constitutive relationships are used in conjunction with Equations C-1 and C-2:

- The velocity is governed by Darcy's Law;

$$\bar{v}_r = \frac{\kappa}{\mu\theta} \cdot (\bar{\bar{\nabla}}_p - \rho_\ell \bar{g}). \tag{C-3}$$

- Viscosity is temperature dependent as follows;

$$\frac{1}{\mu_\ell} = \frac{1}{\mu_0} + \sum_{i=1}^{3} a_i T^i \tag{C-4}$$

where:

$$\mu_0 = 2.4945 \times 10^{-8} \frac{lb_f\text{-}hr}{ft^2}$$

$$a_1 = 1.5376 \times 10^6 \frac{ft^2}{lb_f\text{-}hr\text{-}°F}$$

$$a_2 = 6.9680 \times 10^3 \frac{ft^2}{lb_f\text{-}hr\text{-}°F^2}$$

$$a_3 = 7.6912 \frac{ft^2}{lb_f\text{-}hr\text{-}°F^3}$$

T = temperature °F (range 32°F to 570°F).

- Density is temperature and pressure dependent as follows;

$$\rho_\ell = \rho_0 + \rho_0\beta_T(T-T_0) + \rho_0\beta_p(P-P_0) \tag{C-5}$$

where the subscript zero denotes a reference value.

C.3 BOUNDARY CONDITIONS

Two types of boundary conditions may be applied to the equation of motion: isobaric and mass flux. The former condition specifies a constant pressure at a point and its implementation is a straightforward application of a Dirichlet-type boundary condition. The latter condition is a Neumann-type boundary and may be derived from the constitutive relation for velocity, viz:

$$\frac{\rho_\ell \overline{\overline{k}}}{\mu} \cdot \frac{\partial p}{\partial n} = [-\rho_\ell \overline{v} + \frac{\rho_\ell^2}{\mu} \overline{\overline{k}} \cdot \overline{g}] \cdot \hat{n} \tag{C-6}$$

where:

$\overline{v}$ = superficial velocity, $\theta\overline{v}_r$

$\hat{n}$ = unit vector normal to boundary

$\frac{\partial}{\partial n}$ = partial derivative with respect to normal direction.

Note that for an impermeable boundary, $\overline{v} \cdot \hat{n} = 0$, the preceding equation reduces to:

$$\frac{\partial p}{\partial n} = \rho_\ell \overline{g} \cdot \hat{n}. \tag{C-7}$$

Dirichlet-type and Neumann-type boundary conditions may similarly be applied to the heat transfer equation. The Dirichlet condition takes the form of an isothermal (constant temperature) boundary. The Neumann condition is once again an applied flux condition described by the following equation:

$$- [\theta\overline{\overline{k}}_\ell + (1-\theta)\overline{\overline{k}}_s] \cdot \frac{\partial T}{\partial n} = \overline{q} \cdot \hat{n} \tag{C-8}$$

which, in the case of insulated boundaries, reduces to:

$$\frac{\partial T}{\partial n} = 0. \tag{C-9}$$

In addition to these two conditions, a third type of surface condition, the convective boundary, may be applied to the heat transfer equation. This condition is another flux-type boundary, where the heat flux is defined as follows:

$$q = h(T_e - T) \tag{C-10}$$

h = convective heat transfer coefficient

T_e = ambient temperature outside surface.

C.4 FINITE ELEMENT METHODOLOGY

An examination of the governing Equations C-1 and C-2 and the constitutive relations reveals the complexity of the coupling between the equation of motion and the heat transfer equation. The equation of motion is coupled to the temperature distribution both explicitly through the $\frac{\partial T}{\partial t}$ term and implicitly through the temperature dependence of liquid density and viscosity. The heat transfer equation is coupled to the pressure distribution principally by the convective transport term, $\theta \rho_\ell c_{v\ell} v_r \cdot \nabla T$, and secondarily by the dependence of density on pressure (if the liquid phase is assumed compressible). Further, a degree of nonlinearity is introduced into the equation of motion by the dependence of density on pressure and into the heat transfer equation by the temperature dependence of both density and viscosity.

Clearly, an iterative approach is appropriate if the nonlinearities within each equation are to be accounted for. To solve both the equation of motion and the heat transfer equation simultaneously is not an attractive prospect. As a consequence of the preceding reasoning, the following solution methodology is adopted at each time step:

● Solve the equation of motion using temperatures and pressures from the previous time step.

- Solve the heat transfer equation using the pressures and velocities just calculated and the temperatures from the last time step.

- Repeat this alternating solution technique using the pressure, temperature, and velocity distributions calculated in the previous iteration to update the current iteration.

- After convergence of both the pressure and the temperature distributions to stationary values, proceed to the next time step.

The methodology outlined above is implemented within the framework of an existing conduction heat transfer program that was based on a solution method described by Wilson and Nickell [1966]. In the investigation by Wilson and Nickell, a variational principle was applied to the following partial differential equation which governs transient heat conduction:

$$\overline{\nabla} \cdot \overline{\overline{k}} \cdot \overline{\nabla} T - \rho c \frac{\partial T}{\partial t} + q = 0. \tag{C-11}$$

The first variation of Equation C-11 yields a set of linear equations to be solved for the nodal point temperatures of the finite element model as a function of time. In SPECTROM-55, the finite element model uses eight-noded, isoparametric elements exclusively.

Noting the similarity between Equation C-11 and the equation of motion (Equation C-1) and the heat transfer equation (Equation C-2), it is clear that many of the variables in the three equations are analogous. The analogies are shown in detail in Table C-1.

The identification of these analogous variables points out an efficient method of structuring the finite element program. By the selection of the appropriate grouping of variables depending on whether pressure or temperature is being solved, the same subroutines may be used to assemble and solve the required matrices and vectors for either field variable. A similar set of analogies and method of approach can be applied to the boundary conditions outlined in Section C-3.

Table C-1. Analogous Variables Between the Solution of Conduction Heat Transfer Outlined by Wilson and Nickell [1966] and the Equations Governing Hydrothermal Transport in a Ground-water Flow System

Term	Conduction Heat Transfer (Equation C-11)	Equation of Motion (Equation C-1)	Heat Transfer Equation (Equation C-2)
Field Variable	T	p	T
Conductivity	$\overline{\overline{k}}$	$\dfrac{\rho_\ell \overline{\overline{K}}}{\mu}$	$\theta \overline{\overline{k}}_\ell + (1-\theta)\overline{\overline{k}}_s$
Capacitance	ρc	$\rho_\ell \alpha_p + \theta \rho_0 \beta_p$	$\theta \rho_\ell c_{v\ell} + (1-\theta)\rho_s c_{vs}$
Load	q	$q_h - \theta \rho_0 \beta_T \dfrac{\partial T}{\partial t}$ $- \overline{\nabla} \cdot \dfrac{\rho_\ell \overline{\overline{K}}}{\mu} \cdot \rho_\ell \overline{g}$	$Q + q_h c_{v\ell}(T-T_h)$

A remark concerning the time derivative of temperature in the equation of motion is warranted. This term is approximated by the first backward-difference expression for the first derivative, viz:

$$\frac{\partial T}{\partial t} = \frac{T_t - T_{t-\Delta t}}{\Delta t} . \tag{C-12}$$

The only term in the equations governing hydrothermal transport in a ground-water flow system not included in Table C-1 and unparalleled in the conduction heat transfer equation (Equation C-11) is the convective transport term, $\theta \rho_\ell c_{v\ell} \overline{V}_r \cdot \overline{\nabla} T$, in the heat transfer equation (Equation C-2). The following section is devoted to the incorporation of this term into the finite element program.

C.5 INCORPORATION OF THE CONVECTIVE TRANSPORT TERM

The treatment of the convective transport term, $\theta \rho_\ell c_{v\ell} \bar{v}_r \cdot \bar{\nabla} T$, in coupled convective and conductive heat transfer analysis by finite element methods was thoroughly investigated by Hsu and Nickell [1974]. All the methods outlined in that investigation involved the formation of an additional system conductivity matrix, $\bar{\bar{k}}_v$, which shall be referred to in this appendix as the convectivity matrix. The system convectivity matrix is the sum of all the elemental convectivity matrices in the system, viz:

$$\bar{\bar{k}}_v = \sum_m \bar{\bar{k}}_v^m \qquad (C-13)$$

where a subscript or superscript m refers to an elemental quantity. The elemental convectivity matrix is defined by the following equation:

$$\bar{\bar{k}}_v^m = \int_{\Psi_m} \theta \rho_\ell c_{v\ell} \bar{N}_m^T \cdot \bar{v}_m \cdot \bar{\bar{B}}_m \, dV \qquad (C-14)$$

where $\bar{N}_m$ is the assumed polynomial shape function vector, $\bar{\bar{B}}_m$ is the spatial differentiation of $\bar{N}_m$, and Ψ_m indicates integration over the elemental volume.

Several alternatives are available for including the convectivity matrix into the system of linear equations that will be solved for nodal temperatures. The most apparent is simply adding the convectivity matrix to the familiar conductivity matrix. The primary drawback to this approach lies in the fact that the convectivity matrix is unsymmetric, whereas the conductivity matrix is symmetric. Therefore, a more complex and time-consuming matrix solution technique must be used to solve the banded, unsymmetric matrix that results. Also, the memory required to store the matrix is doubled.

An alternative to this approach is to multiply the convectivity matrix by an appropriate temperature field and treat the resultant vector as an additional load or flux. The temperature field from the previous time step could be used as an initial estimate of the appropriate field and this estimate can be improved by iteration. This method does not alter the conductivity matrix and, hence, preserves its symmetry. However, it requires an additional iterative procedure which is time-consuming. Also, as the ratio of the convective heat transfer to conductive heat transfer becomes significant, the iterative solution becomes unstable.

During the course of development of finite element program SPECTROM-55, both of the aforementioned techniques were tried. Both techniques were satisfactory for many problems and both yielded accurate results. However, the inherent instability of the iterative technique limited its application and made it less general than the unsymmetric method. Also, the difference between the solution time required to iterate to convergence and to solve the unsymmetric matrix was inconsequential for most transient problems. This same conclusion was reached by Hsu and Nickell [1974] during their investigations.

Consequently, the iterative treatment of the convectivity matrix was disgarded in favor of solving the unsymmetric convectivity-conductivity matrix. The resultant finite element program requires somewhat more memory in terms of both program length and matrix storage but consistently yields stable, accurate results in approximately the same processor time.

C.6 VALIDATION OF FINITE ELEMENT PROGRAM SPECTROM-55

In this section, four of the examples used to validate finite element program SPECTROM-55 are described. These examples not only demonstrate the accuracy of the program but also illustrate its range of application. The first two examples are simple, uncoupled problems. The first involves conduction heat transfer only ($v = 0$), and the second shows the program's capability to predict velocities in porous media. The third example involves combined forced convection-conduction heat transfer. The problem is coupled in one direction; that is, the heat transfer equation depends on the velocity distribution but the velocity distribution is independent of the temperature field. The fourth example qualitatively illustrates the program's capability to model natural convection. This problem is coupled in both directions (the velocity distribution depends on the temperature field and vice versa).

All four examples are two-dimensional (x-y) problems, where the y-direction is vertical and gravity acts in the negative y-direction. Further, all the examples involve a homogeneous, isotropic solid phase composed of a single material. The properties of the solid phase are listed below.

$$\overline{\overline{k}}_s = 1.5 \, \overline{\overline{I}} \, \text{Btu/hr-ft-}°F$$

$$c_{vs} = 0.2 \, \text{Btu/lb}_m\text{-}°F$$

$$\rho_s = 170 \text{ lb}_m/\text{ft}^3$$

$$Q = 0.0 \text{ Btu/ft}^3$$

$$\overline{\overline{\kappa}} = 1.0 \times 10^{-10} \text{ I ft}^2$$

$$\theta = 0.15$$

$$\alpha_p = 0.0$$

$$q_h = 0.0 \text{ lb}_m/\text{hr}$$

where:

  I = Identity matrix.

All the properties of the solid phase are assumed to be temperature independent.

The properties of water are used for the liquid phase. These properties are listed below.

$$\overline{\overline{k}}_\ell = 0.35 \text{ I Btu/hr-ft-}°\text{F}$$

$$c_{v\ell} = 1.0 \text{ Btu/lb}_m\text{-}°\text{F}$$

$$\rho_o = 62.46 \text{ lb}_m/\text{ft}^3$$

$$\beta_T = \begin{cases} 0.0 & \text{Problems 1, 2, 3} \\ -0.001/°\text{F} & \text{Problem 4} \end{cases}$$

$$T_o = 60°\text{F}$$

$$\beta_p = 0.0$$

$$\mu = \mu_o = 6.42 \times 10^{-9} \text{ lb}_f\text{-hr/ft}^2.$$

As shown above, the water is assumed to be incompressible and its viscosity is independent of temperature.

The finite element mesh used in Examples 1 and 3 is illustrated in Figure C-1; the meshes used in Examples 2 and 4 are shown in Figures C-2 and C-3, respectively. Note that eight-noded, isoparametric elements are utilized in all the problems.
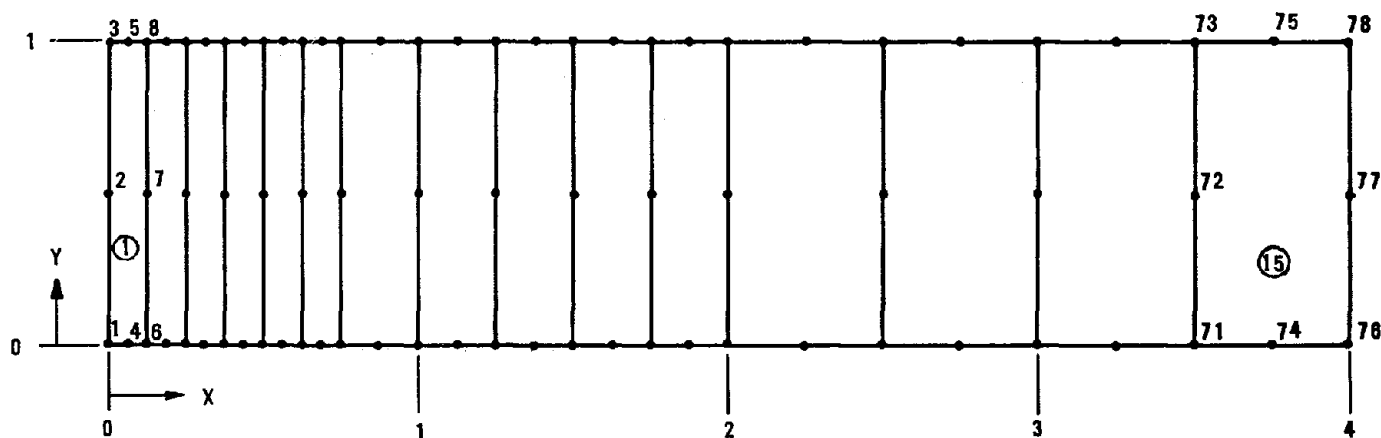
Figure C-1. Finite Element Mesh Used in Examples 1 and 3.
Dimensions are in Feet.
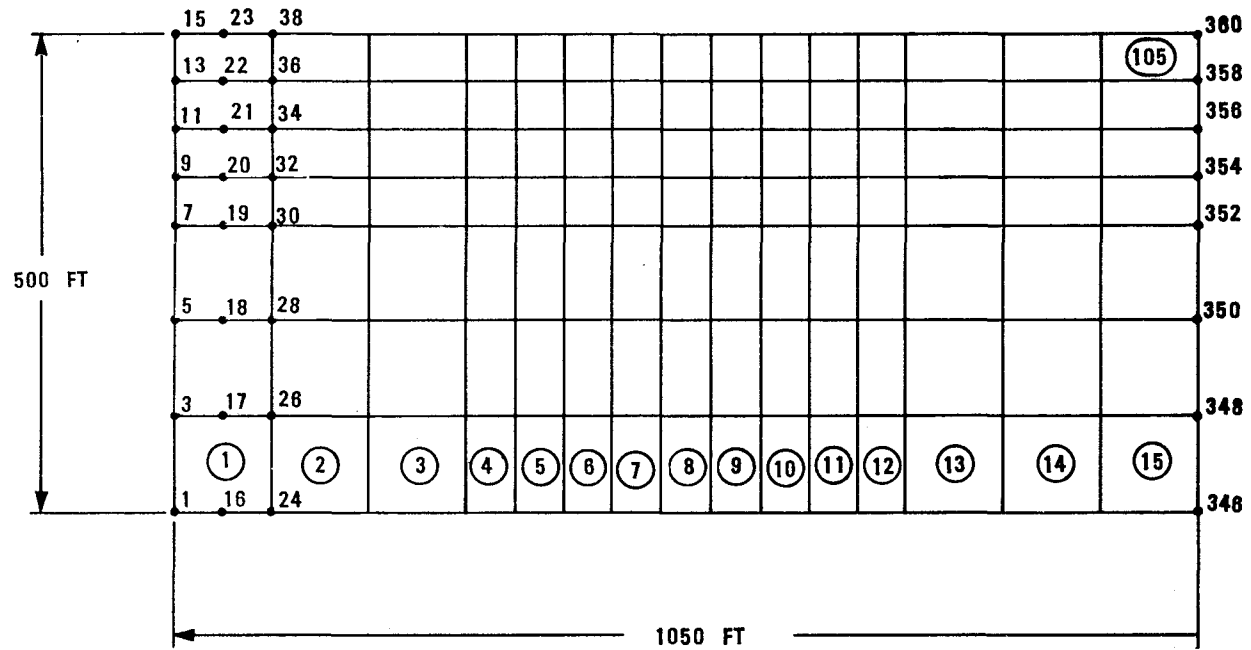
Figure C-2.   Finite Element Mesh Used in Example 2.
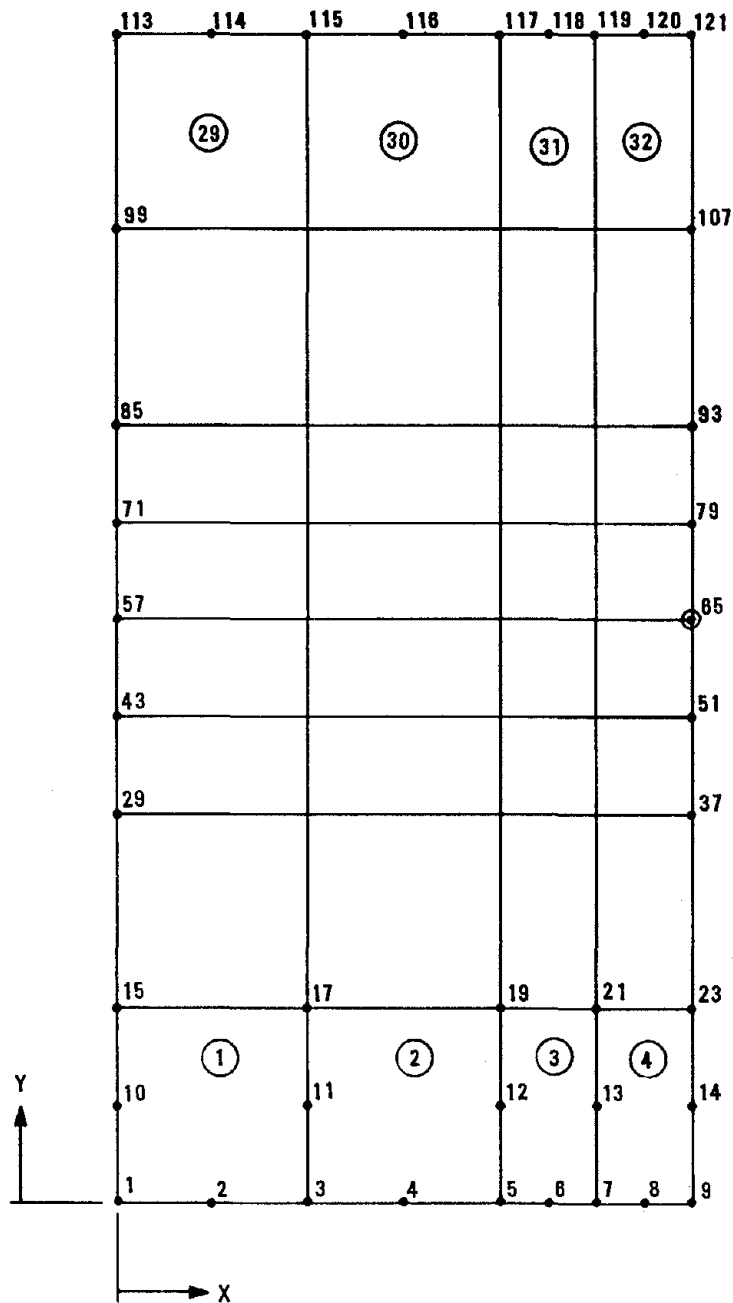
Figure C-3. Finite Element Mesh Used in Example 4.

C.6.1. Example 1. Transient Heat Conduction Analysis

Consider a semi-infinite body composed of a porous medium. The liquid phase is static and its density does not depend on temperature or pressure ($\beta_T = \beta_p = 0$). Initially the body is at a uniform temperature of 60°F. At $t = 0$, the surface of the body ($x = 0$) is raised to a temperature of 160°F and maintained at this temperature.

This example is essentially a one-dimensional transient conduction problem with the properties slightly modified to account for the fact that the conducting medium is a mixture. The governing equation, boundary conditions, and initial conditions of this problem are:

$$\alpha_m \frac{\partial^2 T}{\partial x^2} = \frac{\partial T}{\partial t} \tag{C-15a}$$

$$T(0,t) = T_1 \tag{C-15b}$$

$$T(\infty,t) = T(x,0) = T_0 \tag{C-15c}$$

where:

$$\alpha_m = \frac{\theta k_\ell + (1-\theta)k_s}{\theta \rho_0 c_{v\ell} + (1-\theta)\rho_s c_{vs}} \;,\; \text{a mixture thermal diffusivity.}$$

The analytical solution to this problem is reported in many sources, including Carslaw and Jaeger [1959], and it is described by the following equation:

$$\frac{T - T_0}{T_1 - T_0} = \text{erfc} \left(\frac{x}{2\sqrt{\alpha_m t}}\right). \tag{C-16}$$

Since the liquid phase is static, the pressure distribution is simply the hydrostatic solution,

$$\frac{\partial p}{\partial x} = 0 \tag{C-17a}$$

$$\frac{\partial p}{\partial y} = -\rho_0 g. \tag{C-17b}$$

The mesh used to model Example 1 is shown in Figure C-1 and the corresponding thermal boundary conditions are shown in Figure C-4. Although the example involves a semi-infinite body, the finite element model must be truncated to a finite length, L, which is beyond the influence of the elevated temperature boundary at x = 0 throughout the time domain of interest. In this case, L = 4 feet was arbitrarily selected; this length is adequate for the modeling period of ten hours. For the equation of motion, the boundaries were all modeled as impermeable surfaces and a hydrostatic pressure distribution was initially applied.

Figure C-5 illustrates the close agreement between the finite element solution and the analytical solution of the transient temperature distribution.

C.6.2 Example 2. Steady-State Velocity Distribution Around Base of Impermeable Dam

Consider an impermeable dam located between two bodies of water as illustrated in Figure C-6. Since the water depths in the two bodies are not equal, water will flow between them through the permeable ground beneath the dam. Example 2 involves predicting the steady-state pressure and velocity distribution in the permeable sub-surface. The temperature of the two bodies of water and the underlying ground is assumed to be uniform, and hence, no heat transfer occurs.

Figure C-2 shows the finite element mesh used to model this example. The applicable boundary conditions are illustrated in Figure C-7. The left, bottom, and right boundaries are assumed to be far enough from the principle flow field that they may be considered impermeable. The central section of the top boundary represents the impermeable base of the dam. The left and right sides of the top boundary are the bottoms of the two bodies of water and are therefore considered constant head (pressure) surfaces.

Figure C-8 shows lines of equipotential predicted in the porous material below the two bodies of water and the base of dam. Potential is defined by the following equation:

PERFECTLY INSULATED

ISOTHERMAL T = 160°F

$T_{t=0}$ = 60°F

ISOTHERMAL T = 60°F
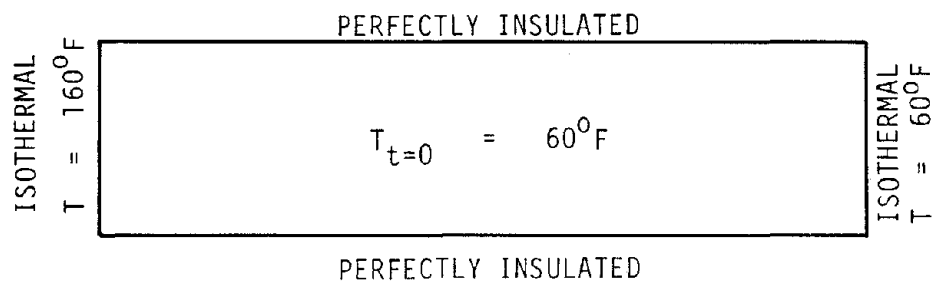
PERFECTLY INSULATED

Figure C-4. Initial and Boundary Conditions Applied to Heat Transfer Equation in Example 1.
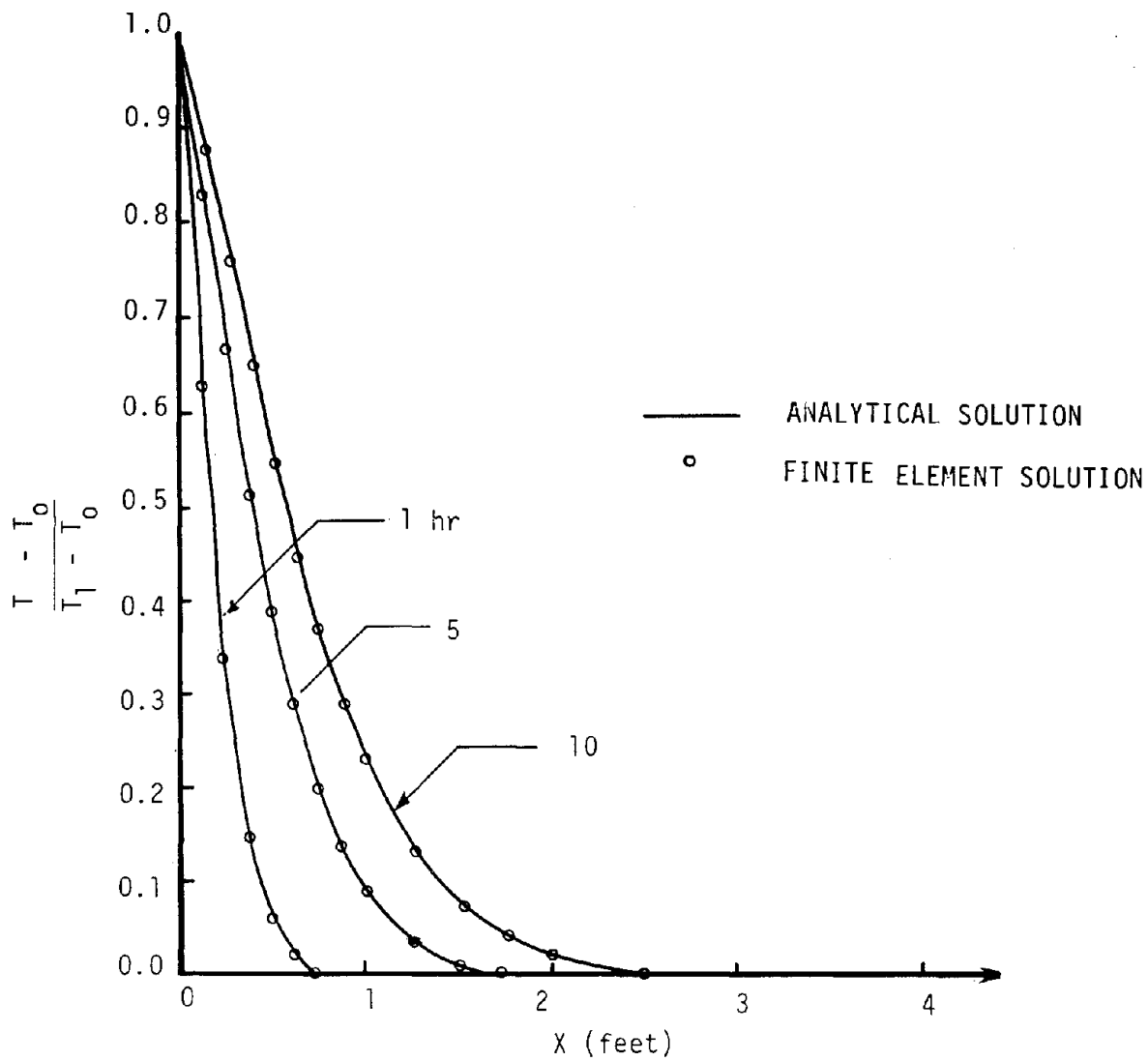
Figure C-5. Comparison of Finite Element Solution to Analytical
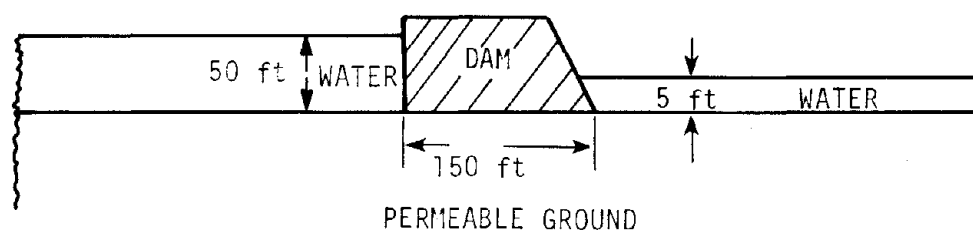Solution of Transient Heat Conduction Example 1.

Figure C-6.   Physical Representation of Example 2, Flow Around
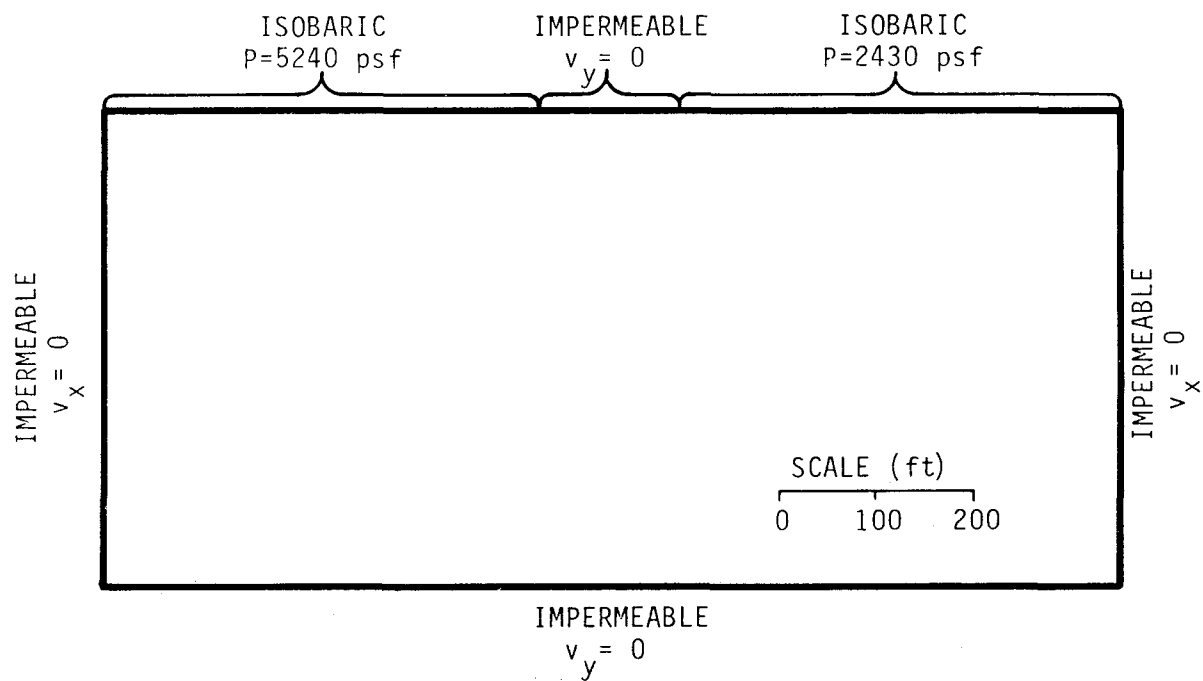   the Base of an Impermeable Base.   NOT TO SCALE.

ISOBARIC
P=5240 psf

IMPERMEABLE
$v_y = 0$

ISOBARIC
P=2430 psf

IMPERMEABLE
$v_x = 0$

IMPERMEABLE
$v_x = 0$

SCALE (ft)

0   100   200

IMPERMEABLE
$v_y = 0$

Figure C-7.   Boundary Conditions Applied to Equation of Motion
in Example 2.
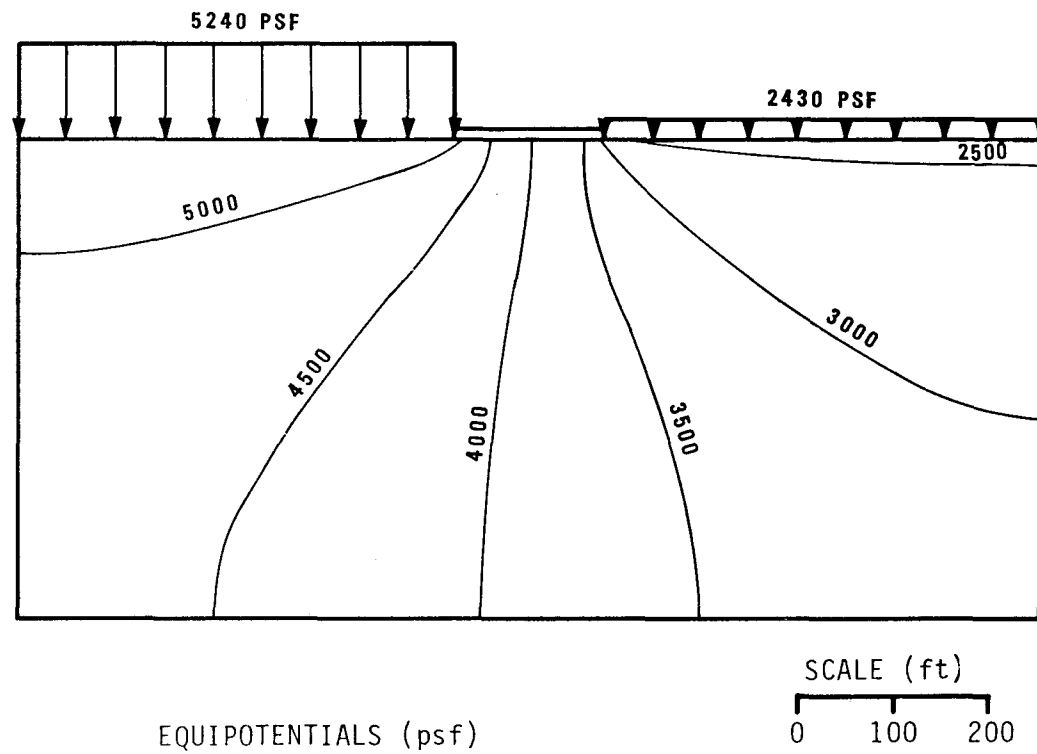
Figure C-8. Equipotentials in Porous Medium Below Base of an
Impermeable Dam Separating Two Bodies of Water.

$$\phi = p - \rho_0 gd \qquad\qquad\qquad \text{(C-18)}$$

where:

ϕ = potential

p = pressure

ρ_0 = density of liquid

g = gravitational constant

d = depth below surface of porous material.

These equipotentials closely resemble those shown by Bear [1972] for this porous media flow problem. The resultant velocity distribution is shown in Figure C-9.

C.6.3 Example 3. Coupled Conduction and Forced Convection Heat Transfer

Consider a semi-infinite body composed of a porous medium. Liquid is flowing into the exposed surface and through the body at a constant velocity. The superficial velocity at the surface is $v_x = \theta\, v_{rx} = 0.1$ ft/hr, where v_{rx} is the x-component of the pore velocity. Initially the body is at a uniform temperature of 60°F. At t = 0, the surface of the body (x = 0) is raised to a temperature of 160°F and maintained at this temperature.

This example is similar to the transient conduction problem (Example 1) except for the addition of convective transport. The governing equation, boundary conditions, and initial conditions of this problem are:

$$\frac{\partial T}{\partial t} + U\,\frac{\partial T}{\partial x} = \frac{\partial}{\partial x}\left(\alpha_m\,\frac{\partial T}{\partial x}\right) \qquad\qquad \text{(C-19a)}$$

$$T(0,t) = T_1 \qquad\qquad\qquad \text{(C-19b)}$$

$$T(\infty,t) = T_0 \qquad\qquad\qquad \text{(C-19c)}$$

where:

$$U = \frac{\rho_0 c_{v\ell} v_x}{\theta \rho_0 c_{v\ell} + (1-\theta)\,\rho_s c_{vs}}$$
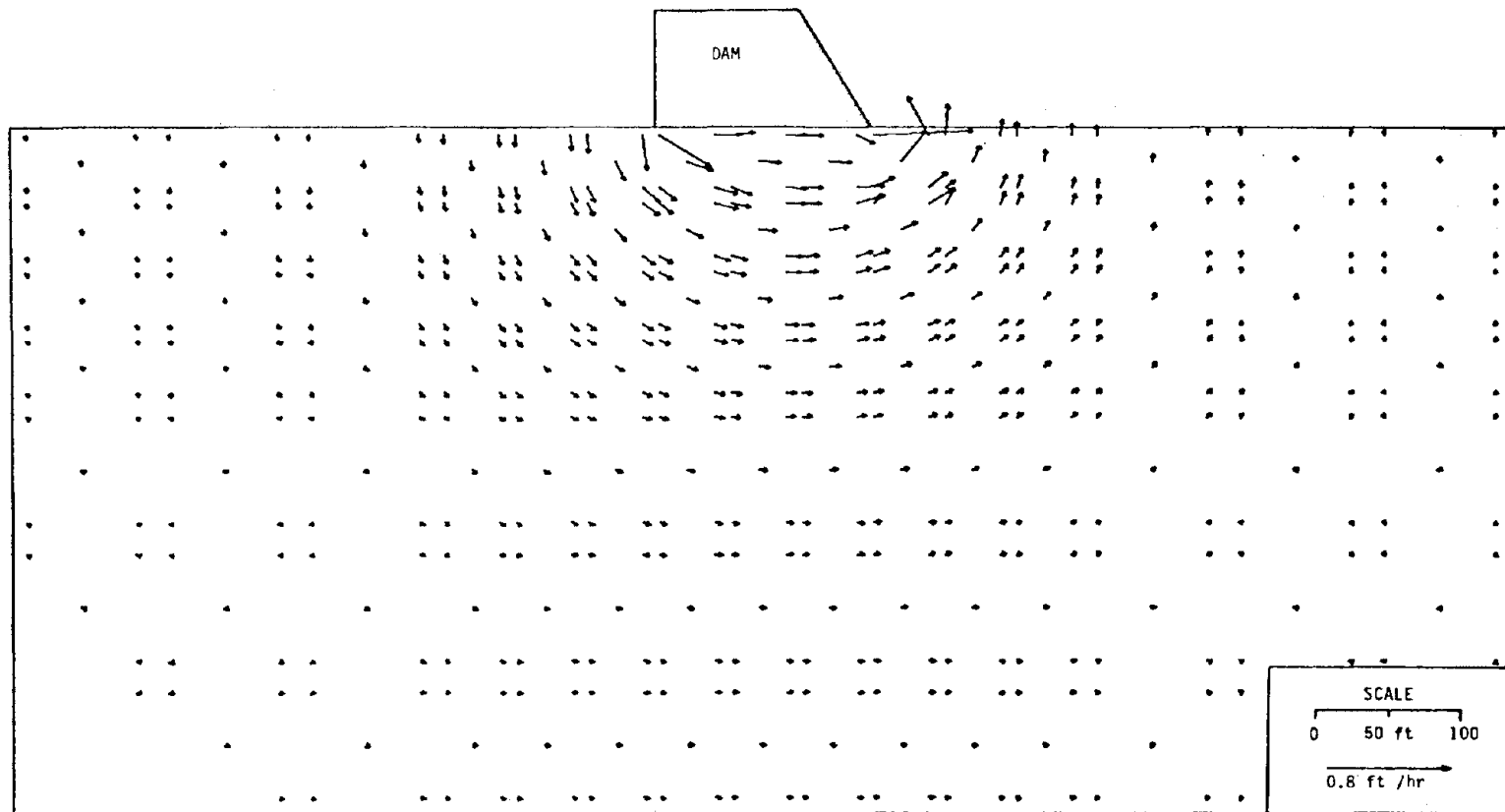
Figure C-9. Superficial Velocity ($\bar{v} = \theta \bar{v}_r$) in Porous Media Below an Impermeable Dam Separating Two Bodies of Water.

$$\alpha_m = \frac{\theta \; k_\ell + (1-\theta) \; k_s}{\theta \rho_0 c_{v\ell} + (1-\theta) \; \rho_s c_{vs}}$$

The analytical solution to this problem is shown in the literature by Zienkiewicz and Taylor [1971], and it is described by the following equation:

$$\frac{T - T_0}{T_1 - T_0} = \left[\frac{1}{2} \; erfc \; \left(\frac{x - UT}{2\sqrt{\alpha_m t}} \right) + exp \left(\frac{xU}{\alpha_m} \right) erfc \; \left(\frac{x+UT}{2\sqrt{\alpha_m t}} \right) \right] . \qquad \text{(C-20)}$$

Note that if $V_x = 0$, this problem is equivalent to the transient heat conduction problem in Example 1, and Equation C-20 will reduce to the corresponding solution (Equation C-16) when U = 0.

Since the flow is horizontal, the pressure gradient can be predicted from Equation C-3. Hence, the gradient of pressure should be given by the following equation:

$$\left\{ \begin{array}{c} \dfrac{\partial p}{\partial x} \\[3mm] \dfrac{\partial p}{\partial y} \end{array} \right\} = \left\{ \begin{array}{c} \dfrac{-\mu_\ell V_x}{k_h} \\[3mm] -\rho_0 g \end{array} \right\} . \qquad \text{(C-21)}$$

The mesh used to model Example 3 is shown in Figure C-1 and the corresponding boundary conditions for temperature and pressure are shown in Figure C-10. Although the example involves a semi-infinite body, the finite element model must be truncated to finite length, L, which is beyond the influence of the elevated temperature boundary at x = 0 throughout the time domain of interest. In this case, L = 4 feet was arbitrarily chosen; this length is adequate for the modeling period of ten hours.

A comparison of the finite element solution and the analytical solution of this problem is shown in Figure C-11. The finite element solution slightly underpredicted the temperatures near the surface and slightly overpredicted the temperatures at larger depths. The latter result may be a consequence of the truncation of the semi-infinite body to a finite length. Nonetheless, the maximum error between the two solutions was approximately 3 percent.
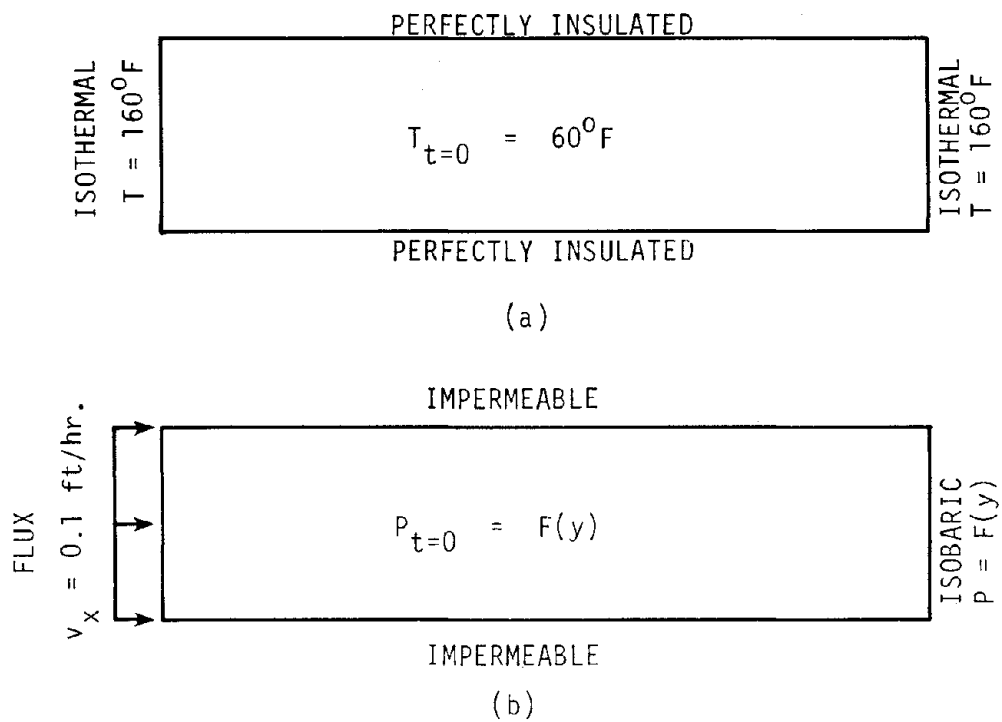
PERFECTLY INSULATED

ISOTHERMAL
T = 160°F

$T_{t=0}$ = 60°F

ISOTHERMAL
T = 160°F

PERFECTLY INSULATED

(a)

IMPERMEABLE

FLUX
v_x = 0.1 ft/hr.

$P_{t=0}$ = F(y)

ISOBARIC
P = F(y)

IMPERMEABLE

(b)

Figure C-10.   Initial and Boundary Conditions Applied to Heat
               Transfer Equation (a) and Equation of Motion (b)
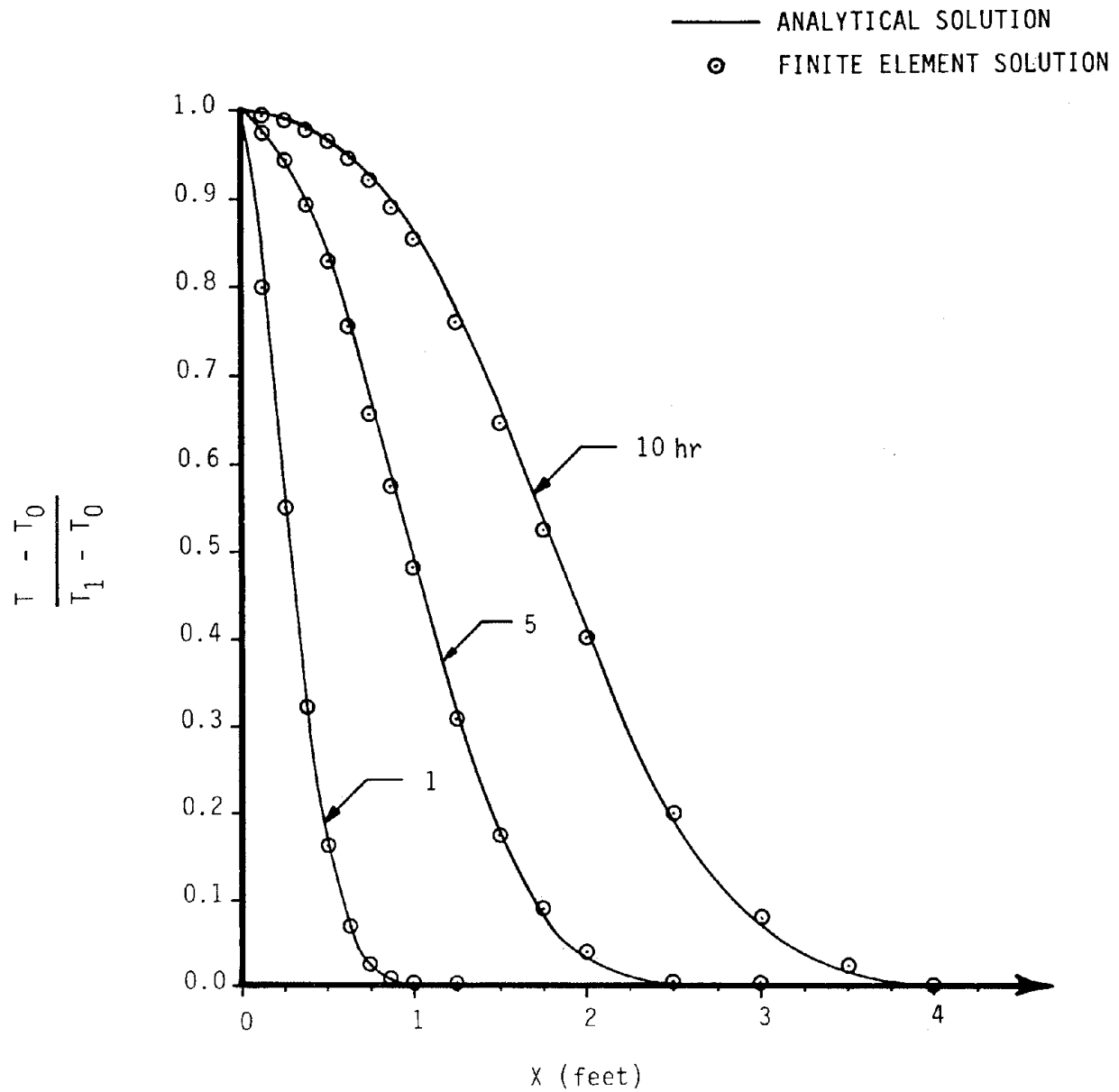   in Example 3.   F(y) = 2000 - 62.46 y psf.

Figure C-11. Comparison of Finite Element Solution to Analytical Solution of Coupled Convection-Conduction Example 3. $v_x = 0.1$ ft/hr

C.6.4 Example 4. Transient-Free Convection Analysis

Consider an infinite body composed of a porous medium with a straight wire passing horizontally through it. Initially the temperature of the entire body is 60°F and at t = 0, the wire is instantaneously heated to a temperature 160°F and maintained at this temperature.

For the finite element model of this example, a vertical section, 3-foot square and perpendicular to the wire, was selected. The wire was modeled as an isothermal node at the center of the section. Since the section is symmetric about a vertical plane parallel to the wire, only the left hand side of the section was modeled. The boundary conditions applied to the finite element model are shown in Figure C-12 and the finite element mesh is shown in Figure C-3. It should be noted that the finite dimensions of the model limit the time domain which may be accurately modeled since the boundary conditions will influence the solution at later times. The size of the model chosen for this example is adequate for a modeling period of about ten hours.

The development of the convection cells is illustrated in Figure C-13. The shape of the cells and their growth pattern agree qualitatively with the physical situation. The influence of the heat transfer due to free convection is shown in Figure C-14. This figure shows the ratio of the temperature predicted for this example to the temperatures predicted for the equivalent conduction problem. As anticipated, the motion of the fluid carries heat into the porous medium above the point that is maintained at an elevated temperature. In turn, cool fluid is swept into the region below the hot point. Hence, the temperatures in the region above the hot point are slightly higher than the conduction solution predicts and the temperatures in the region below the hot point are slightly lower.
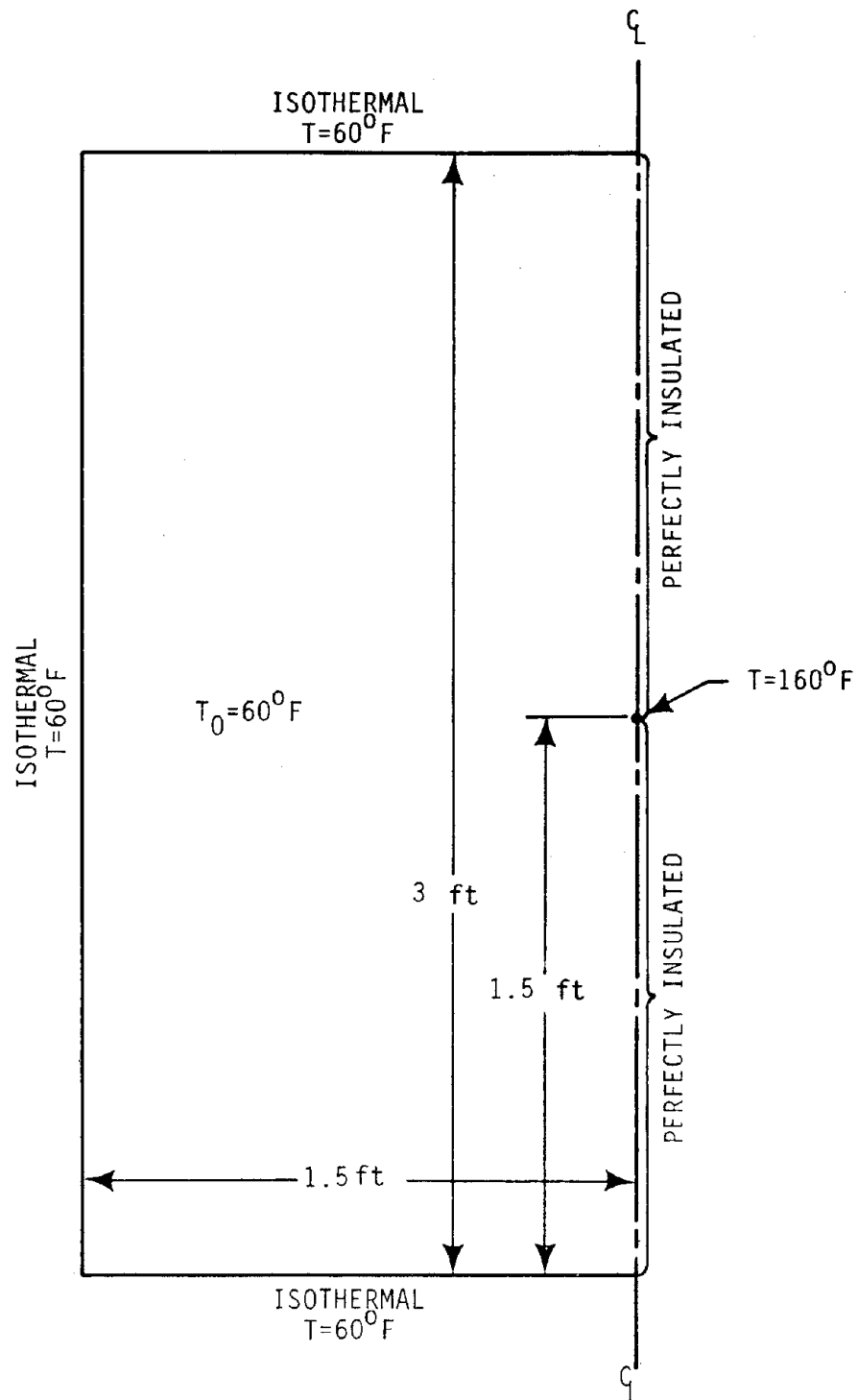
Figure C-12. Initial and Boundary Conditions Applied to
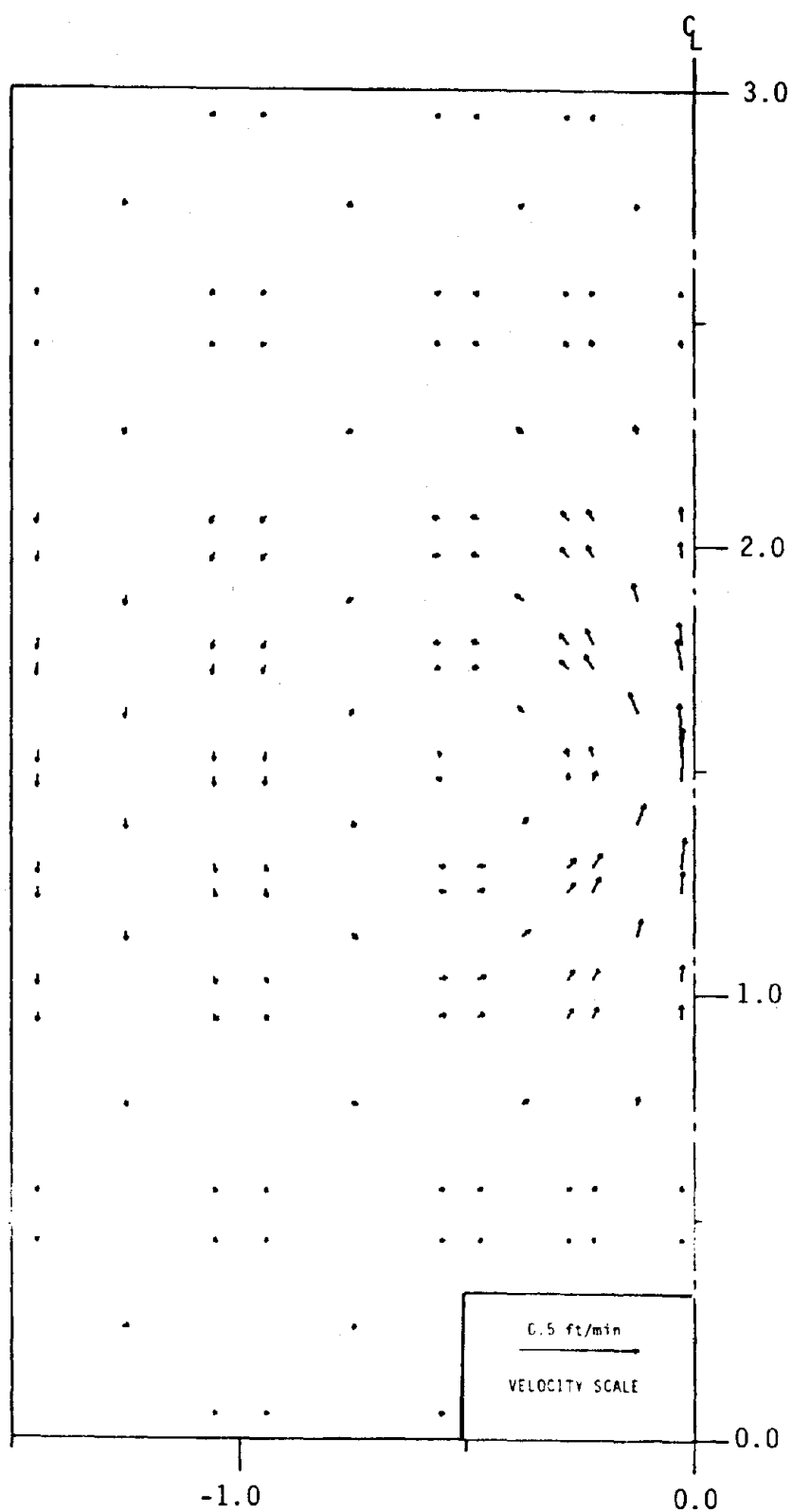Heat Transfer Equation in Example 4.

Figure C-13. Superficial Velocity Distribution ($\overline{v} = \theta\overline{v}_r$) in Free Convection Example 4 at t = 9 hours. Dimensions are in Feet.
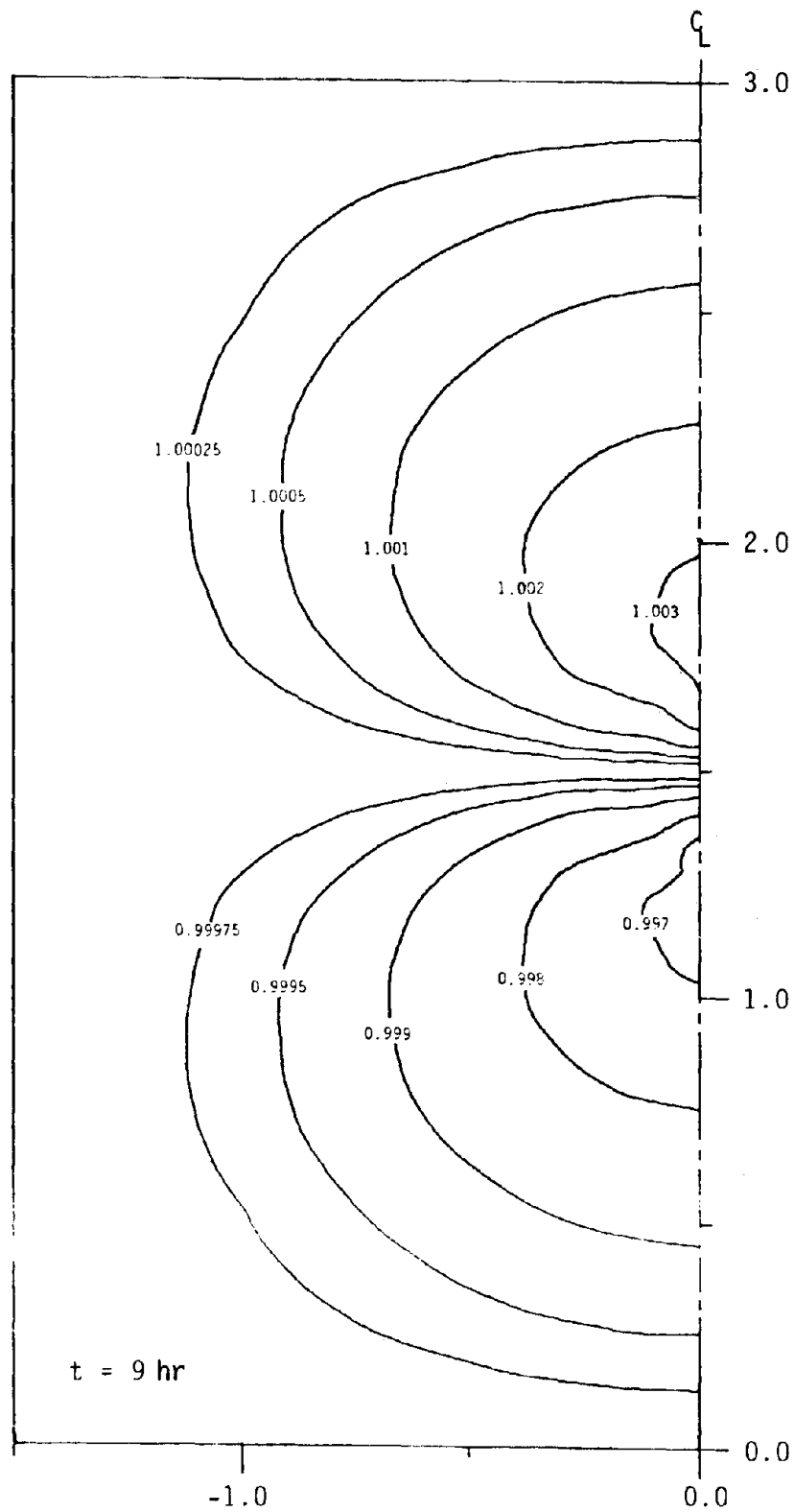
Figure C-14. Ratio of Temperatures Predicted in Free Convection
Example 4 to Temperatures Predicted in Equivalent
Conduction Problem. Dimensions are in Feet.

C.7 APPENDIX C REFERENCES

Bear, J., 1972. _Dynamics of Fluids in Porous Media_, American Elsevier Publishing Co.

Carslaw, H. S. and J. C. Jaeger, 1959. _Conduction of Heat in Solids_, Oxford University Press.

Hsu, M. B. and R. E. Nickell, 1974. "Coupled Convective and Conductive Heat Transfer by Finite Element Methods," _Finite Element Methods in Flow Problems_, University of Alabama in Huntsville Press.

Mercer, J. W., 1973. "Finite Element Approach to the Modeling of Hydrothermal Systems," Ph.D Thesis, University of Illinois, Urbana, IL.

Mercer, J. W. and G. F. Pinder, 1974. "Finite Element Analysis of Hydrothermal Systems," _Finite Element Methods in Flow Problems_, University of Alabama in Huntsville Press.

Wilson, E. L. and R. E. Nickell, 1966. "Application of the Finite Element Method to Heat Conduction Analysis," _Nuclear Engineering and Design_, Vol. 4, pp. 276-286.

Zienkiewicz, O. C. and C. Taylor, 1971. "Weighted Residual Processes in F.E.M. with Particular Reference to Some Transient and Coupled Problems," _Lecture Notes_, NATO Advanced Study Institute on Finite Element Methods in Continuum Mechanics.

APPENDIX D

DOSE RATE CALCULATIONS BY SCIENCE APPLICATIONS, INC.

APPENDIX D

This appendix contains correspondence from Mr. L. D. Rickertsen, Science Applications, Inc. of Oak Ridge, TN. The correspondence contains the results of dose rate calculations performed by Science Applications, Inc. for SF, CHLW, and DHLW canisters in the reference granitic repository defined in this report. The method of calculation is described in the letter dated May 9, 1980. However, the dose rate data included in this letter were found to be incorrect and a second set of calculations were performed. Details of the correction and a revised set of calculations (including DHLW) are in the letter dated July 17, 1980.

A couple notes regarding the data contained in these letters are appropriate. The dose rates in these letters are referred to as "KERMA rate". In the context of a canister emplaced in a backfilled drillhole in granitic rock, the terms KERMA and absorbed dose are essentially synonomous. Also, the initial thermal power assumed for the three waste types in these calculations were 550, 2160, and 310 W per canister for SF, CHLW, and DHLW, respectively. Because of the unacceptable very-near-field thermal response predicted for a 2100 W CHLW canister in granite, the canister thermal loading of CHLW was lowered in subsequent analyses by diluting the waste with more glass (the canister dimensions were not changed). The dose rates for a CHLW canister with the thermal loading changed in this manner are approximately proportional to the canister thermal loading. Consequently, for a 1 kW CHLW canister, the dose rates are approximately 1/2.16 of the rates shown in the letters in this appendix.

The authors of this report sincerely appreciate the assistance of Mr. L. D. Rickertsen and Science Applications, Inc. in providing these data.

Preceding page blank

May 9, 1980

John Osnes
RE/SPEC Inc.
P. O. Box 725
Rapid City, SD   57709

Dear John:

Recently we sent you the results of calculations for the energy
absorption rate of the rock in a granite repository. Calculations
were made for both spent fuel (SF) and high-level waste (HLW) canisters
with waste emplaced in the repository 10 years after discharge from the
reactor. The fission product density assumed for the HLW was selected
such that the canister thermal load at emplacement would be 2.16 kW.
The SF canister selected contained a single PWR spent fuel assembly.
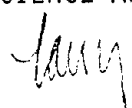
All calculations were performed with the one-dimensional discrete
ordinates code, ANISN (W.W. Engle, Jr. "A User's Manual for ANISN -
A One Dimensional Discrete Ordinates Transport Code with Anisotropic
Scattering", UCND-K-1693, 1967) and only gamma radiation was considered
(previous work has shown the neutron component to be insignificant - for
example, see Y/OWI/TM-36/22). The quantity calculated is the kinetic
energy release to matter (KERMA) which describes the kinetic energy
transferred from the indirectly ionizing radiation to the charged
particles liberated within a volume element. Away from material inter-
faces the KERMA rate differs insignificantly from the material dose
rate.

The granite composition used in the calculations is given in Table 1.
The mass and energy adsorption coefficients corresponding to these
components and provided by the Radiation Shielding Information Center
were used for the granite KERMA response functions. The backfill around
the 0.3 m diameter canister was chosen to have a 0.1 meter thickness and
a 31% void fraction. The KERMA rates resulting from these calculations
are given in Tables 2 and 3.

If you have any questions concerning these calculations, please do not
hesitate to ask. We hope this information is of use to you.

Sincerely,

SCIENCE APPLICATIONS, INC.

Larry D. Rickertsen

cc: G. Raines, ONWI

Table 1.

Composition Assumed for Granite Repository Host Rock

Component	% by Weight
SiO_2	71.5
Al_2O_3	14.0
Fe_2O_3	1.5
FeO	1.4
MgO	0.6
CaO	1.6
Na_2O	3.4
K_2O	4.3
Water + MnO	1.7
H_2O	0.8
TiO_2	0.4
P_2O_5	0.2
MnO	0.1
TOTAL	99.9

TABLE 2   HLW GRANITE KERMA RATE (RAD/HR)

Distance

(m)	10 YR	20 YR	40 YR	70 YR	100 YR
20.7	1.31 (5)*	3.08 (4)	2.95 (4)	1.40 (4)	7.01 (3)
21.5	1.21 (5)	2.84 (4)	2.72 (4)	1.30 (4)	6.48 (3)
22.4	1.09 (5)	2.56 (4)	2.45 (4)	1.17 (4)	5.83 (3)
23.3	9.88 (4)	2.32 (4)	2.22 (4)	1.06 (4)	5.27 (3)
24.1	8.91 (4)	2.09 (4)	2.00 (4)	9.50 (3)	4.75 (3)
25.0	8.04 (4)	1.89 (4)	1.80 (4)	8.58 (3)	4.29 (3)
25.9	7.09 (4)	1.66 (4)	1.59 (4)	7.54 (3)	3.77 (3)
26.8	6.04 (4)	1.42 (4)	1.35 (4)	6.14 (3)	3.20 (3)
27.1	5.11 (4)	1.20 (4)	1.14 (4)	5.41 (3)	2.70 (3)
28.6	4.26 (4)	9.96 (3)	9.95 (3)	4.49 (3)	2.24 (3)
29.5	3.49 (4)	8.16 (3)	7.76 (3)	3.67 (3)	1.83 (3)
30.5	2.66 (4)	6.19 (3)	5.88 (3)	2.76 (3)	1.38 (3)

* Read 1.31(5) as 1.31×10^5

TABLE 3   SF GRANITE KERMA RATE (RAD/HR)

Distance (m)	10 YR	20 YR	40 YR	70 YR	100 YR
20.7	5.12 (3)	2.80 (3)	1.62 (3)	7.96 (2)	3.96 (2)
21.6	4.72 (3)	2.58 (3)	7.33 (2)	7.33 (2)	3.65 (2)
22.4	4.27 (3)	2.33 (3)	1.36 (3)	6.62 (2)	3.29 (2)
23.3	3.87 (3)	2.12 (3)	1.23 (3)	6.00 (2)	2.99 (2)
24.1	3.50 (3)	1.91 (3)	1.12 (3)	5.42 (2)	2.70 (2)
25.0	3.17 (3)	1.74 (3)	1.01 (3)	4.90 (2)	2.43 (2)
25.9	2.81 (3)	1.53 (3)	8.87 (2)	4.32 (2)	2.15 (2)
26.8	2.41 (3)	1.31 (3)	7.59 (2)	3.69 (2)	1.84 (2)
27.7	2.05 (3)	1.11 (3)	6.43 (2)	3.13 (2)	1.56 (2)
28.6	1.72 (3)	9.33 (2)	5.37 (2)	2.61 (2)	1.30 (2)
29.6	1.42 (3)	7.69 (2)	4.41 (2)	2.14 (2)	1.07 (2)
30.5	1.10 (3)	5.90 (2)	3.37 (2)	1.63 (2)	8.12 (1)

July 17, 1980

John Osnes
RB/SPEC, Inc.
P. O. Box 725
Rapid City, SD   57709

Dear John,

Earlier we sent you the results of calculations for the dose rate to
the rock and backfill in a grantie repository (reference the letter
of May 9   ). Those calculations for HLW are not correct and we are
including the corrected curves here.

The calculations for the dose take into account a 0.662 MeV gamma ray
from the chain decay of Cs-137 which makes a major contribution for
20-year old HLW. Unfortunately, because the ORIGEN runs include this
gamma ray both in the description of Cs-137 and its daughter Ba-137m,
the contribution was included twice. This double-counting has now
been corrected in the present results. In addition all other possibilities
for double-counting have been investigated and the present curves contain
only a single contribution from each decay.

We appreciate the help of Neil Bibler and Dick Lynch in helping to point
out the possible discrepancy in the earlier results. We hope these
results are useful to you.

Sincerely,

SCIENCE APPLICATIONS, INC.

Larry D. Rickertsen
Division Manager

cc: N. Bibler
     R. Lynch
     G. Raines

LDR/jl

Predicted Dose Rates for Granite Repositories*

HLW

r(cm)	10 yr-old waste	20 yr-old	40 yr-old	70 yr-old	100 yr-old
0.2074E+02	105717.0000	25904.0332	17531.8496	8320.1992	4166.0430
0.2157E+02	97647.0000	23885.5371	16164.9590	7725.8994	3851.0637
0.2244E+02	87963.0000	21530.6250	14560.3496	6953.3096	3464.7688
0.2328E+02	79731.6016	19512.1289	13193.4590	5978.6577	3131.9609
0.2413E+02	71903.6953	17577.7363	11885.9990	5645.8496	2822.9248
0.2498E+02	64882.7969	15895.6572	10697.3994	5099.0938	2549.5469
0.2586E+02	57216.2969	13961.2646	9449.3691	4481.0220	2240.5110
0.2679E+02	48742.8008	11942.7686	8023.0498	3649.0017	1901.7599
0.2771E+02	41237.6992	10092.4805	6775.0195	3215.1628	1604.6100
0.2864E+02	34378.1992	8395.6826	5913.2847	2668.4070	1331.2319
0.2956E+02	28164.2988	6862.8867	4611.7676	2181.0808	1087.5690
0.3049E+02	21466.1992	5206.0381	3494.4839	1640.2679	820.1340

Spent Fuel

r(cm)	10 yr-old	20 yr-old	40 yr old	70 yr-old	100 yr-old
0.2074E+02	4131.8398	2346.2427	962.7659	473.0628	235.3420
0.2157E+02	3809.0398	2161.8950	892.6385	436.2162	217.5130
0.2244E+02	3445.8899	1960.7886	808.2480	393.4266	196.1190
0.2328E+02	3123.0898	1776.4410	730.9890	356.5800	178.2900
0.2413E+02	2924.5000	1600.4728	665.6160	322.1106	160.4610
0.2498E+02	2558.1899	1458.0223	600.2430	291.2070	145.0092
0.2586E+02	2267.6699	1292.0541	527.7384	256.7376	125.9916
0.2679E+02	1944.8700	1097.7064	451.6680	219.8910	109.3512
0.2771E+02	1654.3500	930.1177	382.7292	186.6102	92.7108
0.2864E+02	1388.0399	782.6395	319.7334	155.7066	77.2590
0.2956E+02	1145.9399	645.2167	262.6806	127.1902	63.5901
0.3049E+02	837.7000	494.3869	200.8734	96.8709	48.2572

GRANITE KERMA RATES - DHLW

DISTANCE FROM CENTER OF CAN (CM.)	KERMA RATES (RADS/HR)				
	5 YRS.	15 YRS.	40 YRS.	75 YRS.	100 YRS.
0.34670E+02	0.30093E+04	0.16452E+04	0.89542E+03	0.39421E+03	0.22458E+03
0.35410E+02	0.28448E+04	0.15568E+04	0.84745E+03	0.37851E+03	0.21255E+03
0.36150E+02	0.26178E+04	0.14317E+04	0.77922E+03	0.34803E+03	0.19543E+03
0.36890E+02	0.24175E+04	0.13214E+04	0.71910E+03	0.32119E+03	0.18036E+03
0.37630E+02	0.22244E+04	0.12147E+04	0.66099E+03	0.29522E+03	0.16578E+03
0.38495E+02	0.19827E+04	0.10811E+04	0.58816E+03	0.26269E+03	0.14752E+03
0.39465E+02	0.16981E+04	0.92382E+03	0.50238E+03	0.22437E+03	0.12600E+03
0.40475E+02	0.14524E+04	0.78811E+03	0.42840E+03	0.19133E+03	0.10744E+03
0.41465E+02	0.12406E+04	0.67130E+03	0.36475E+03	0.16290E+03	0.91477E+02
0.42455E+02	0.10594E+04	0.57163E+03	0.31045E+03	0.13865E+03	0.77858E+02
0.43446E+02	0.90399E+03	0.48630E+03	0.26399E+03	0.11789E+03	0.66203E+02
0.44436E+02	0.77130E+03	0.41363E+03	0.22443E+03	0.10022E+03	0.56282E+02
0.45426E+02	0.65772E+03	0.35156E+03	0.19066E+03	0.85142E+02	0.47812E+02
0.46416E+02	0.56081E+03	0.29875E+03	0.16194E+03	0.72312E+02	0.40607E+02
0.47406E+02	0.47796E+03	0.25372E+03	0.13745E+03	0.61379E+02	0.34467E+02
0.48396E+02	0.40730E+03	0.21543E+03	0.11665E+03	0.52085E+02	0.29249E+02
0.49386E+02	0.34696E+03	0.18283E+03	0.98936E+02	0.44176E+02	0.24807E+02
0.50376E+02	0.29552E+03	0.15513E+03	0.83895E+02	0.37459E+02	0.21035E+02
0.51366E+02	0.25163E+03	0.13156E+03	0.71107E+02	0.31748E+02	0.17828E+02
0.52356E+02	0.21435E+03	0.11155E+03	0.60252E+02	0.26901E+02	0.15106E+02
0.53347E+02	0.18235E+03	0.94546E+02	0.51034E+02	0.22784E+02	0.12795E+02
0.54337E+02	0.15519E+03	0.80115E+02	0.43215E+02	0.19293E+02	0.10834E+02
0.55327E+02	0.13205E+03	0.67863E+02	0.36580E+02	0.16330E+02	0.91703E+01
0.56317E+02	0.11235E+03	0.57471E+02	0.30956E+02	0.13819E+02	0.77600E+01
0.57307E+02	0.95572E+02	0.48655E+02	0.26188E+02	0.11690E+02	0.65645E+01
0.58297E+02	0.81293E+02	0.41183E+02	0.22149E+02	0.98867E+01	0.55519E+01
0.59287E+02	0.69139E+02	0.34848E+02	0.18727E+02	0.83590E+01	0.46940E+01
0.60277E+02	0.58796E+02	0.29481E+02	0.15830E+02	0.70655E+01	0.39676E+01
0.61267E+02	0.49999E+02	0.24935E+02	0.13378E+02	0.59707E+01	0.33528E+01
0.62257E+02	0.42515E+02	0.21086E+02	0.11303E+02	0.50443E+01	0.28326E+01
0.63248E+02	0.36149E+02	0.17827E+02	0.95471E+01	0.42606E+01	0.23925E+01
0.64238E+02	0.30736E+02	0.15068E+02	0.80623E+01	0.35978E+01	0.20203E+01
0.65228E+02	0.26133E+02	0.12734E+02	0.68070E+01	0.30374E+01	0.17056E+01
0.66218E+02	0.22219E+02	0.10760E+02	0.57459E+01	0.25638E+01	0.14397E+01
0.67208E+02	0.18892E+02	0.90899E+01	0.48492E+01	0.21636E+01	0.12149E+01
0.68198E+02	0.16064E+02	0.76779E+01	0.40916E+01	0.18254E+01	0.10251E+01
0.69188E+02	0.13659E+02	0.64842E+01	0.34517E+01	0.15399E+01	0.86470E+00
0.70178E+02	0.11615E+02	0.54753E+01	0.29114E+01	0.12987E+01	0.72929E+00
0.71168E+02	0.98781E+01	0.46227E+01	0.24552E+01	0.10951E+01	0.61497E+00
0.72158E+02	0.84015E+01	0.39022E+01	0.20701E+01	0.92330E+00	0.51847E+00
0.73149E+02	0.71463E+01	0.32937E+01	0.17451E+01	0.77830E+00	0.43705E+00
0.74139E+02	0.60794E+01	0.27797E+01	0.14709E+01	0.65597E+00	0.36835E+00
0.75129E+02	0.51725E+01	0.23457E+01	0.12396E+01	0.55277E+00	0.31040E+00
0.76119E+02	0.44015E+01	0.19792E+01	0.10445E+01	0.46574E+00	0.26153E+00
0.77109E+02	0.37461E+01	0.16698E+01	0.87998E+00	0.39235E+00	0.22032E+00
0.78099E+02	0.31888E+01	0.14088E+01	0.74127E+00	0.33048E+00	0.18557E+00
0.79089E+02	0.27150E+01	0.11882E+01	0.62434E+00	0.27832E+00	0.15629E+00
0.80079E+02	0.23121E+01	0.10022E+01	0.52579E+00	0.23436E+00	0.13160E+00
0.81069E+02	0.19695E+01	0.84522E+00	0.44273E+00	0.19733E+00	0.11081E+00
0.82059E+02	0.16780E+01	0.71279E+00	0.37275E+00	0.16612E+00	0.93262E-01
0.83050E+02	0.14301E+01	0.60107E+00	0.31379E+00	0.13983E+00	0.78520E-01
0.84040E+02	0.12191E+01	0.50682E+00	0.26413E+00	0.11769E+00	0.66085E-01
0.85030E+02	0.10395E+01	0.42733E+00	0.22230E+00	0.99039E-01	0.55614E-01
0.86020E+02	0.88672E-00	0.36029E+00	0.18708E+00	0.83337E-01	0.46797E-01

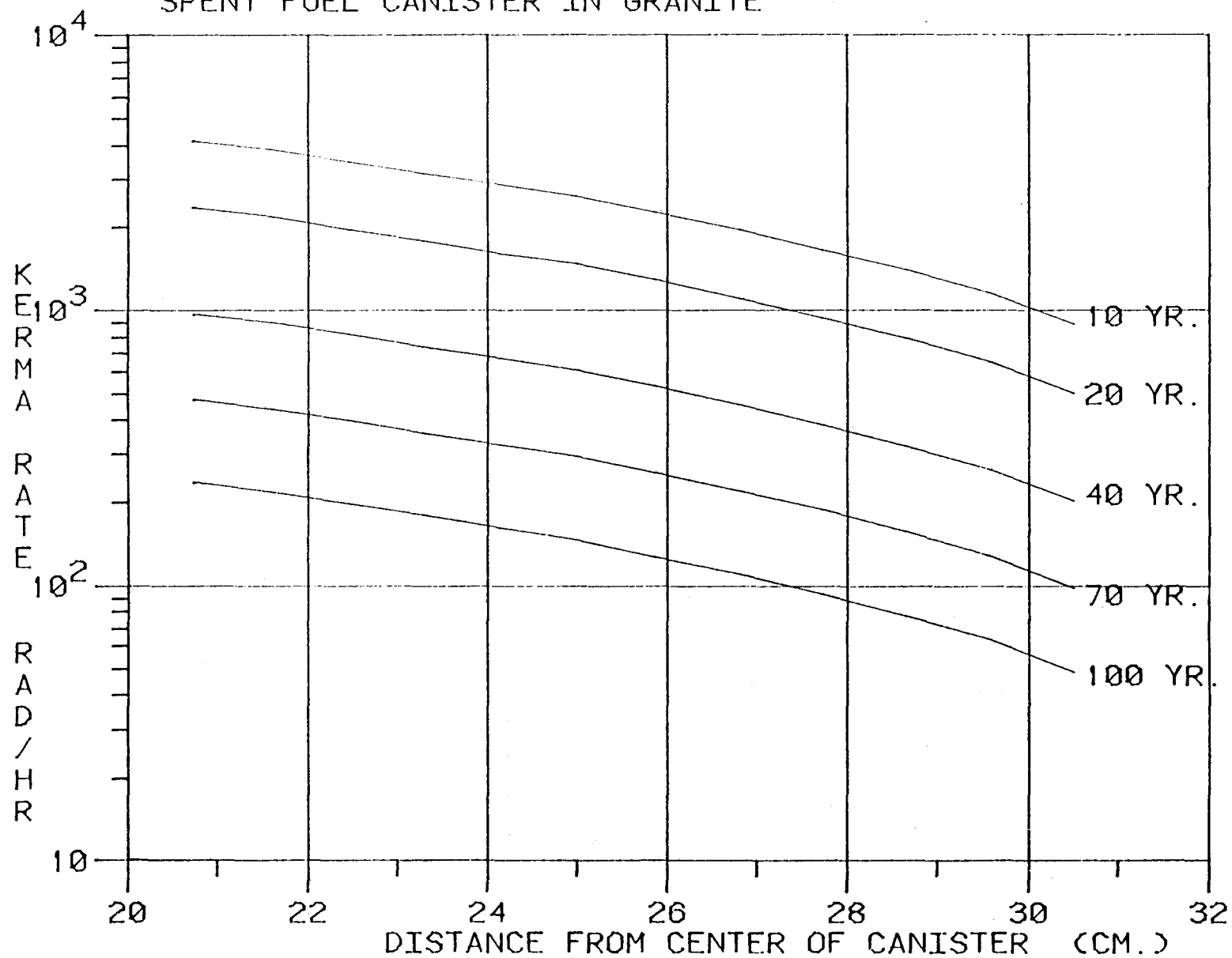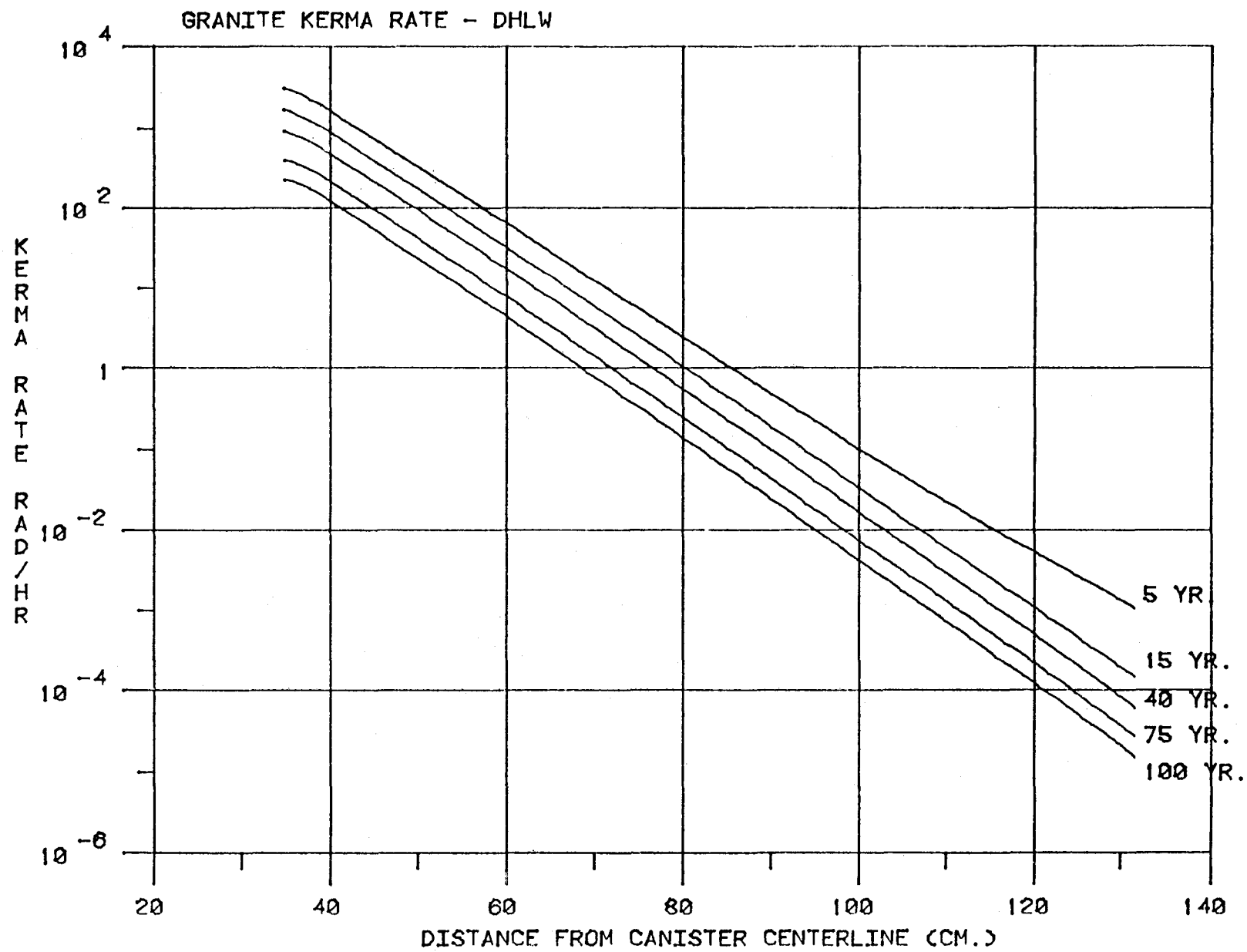|					
0.87010E+02	0.75061E-00	0.30376E+00	0.15742E+00	0.70116E-01	0.39373E-01
0.88000E+02	0.64582E-00	0.25608E+00	0.13245E+00	0.58986E-01	0.33123E-01
0.88990E+02	0.55146E-00	0.21588E+00	0.11142E+00	0.49618E-01	0.27862E-01
0.89980E+02	0.47107E-00	0.18199E+00	0.93732E-01	0.41734E-01	0.23435E-01
0.90970E+02	0.10256E-00	0.15341E+00	0.78840E-01	0.35099E-01	0.19709E-01
0.91960E+02	0.34415E-00	0.12932E+00	0.66308E-01	0.29515E-01	0.16574E-01
0.92951E+02	0.29434E-00	0.10901E+00	0.55764E-01	0.24818E-01	0.13936E-01
0.93941E+02	0.25186E-00	0.91888E-01	0.46892E-01	0.20867E-01	0.11717E-01
0.94931E+02	0.21561E-00	0.77456E-01	0.39429E-01	0.17543E-01	0.98508E-02
0.95921E+02	0.18466E-00	0.65290E-01	0.33150E-01	0.14747E-01	0.82808E-02
0.96911E+02	0.15624E-00	0.55036E-01	0.27870E-01	0.12396E-01	0.69605E-02
0.97901E+02	0.13567E-00	0.46393E-01	0.23426E-01	0.10419E-01	0.58503E-02
0.98891E+02	0.11636E-00	0.39106E-01	0.19694E-01	0.87561E-02	0.49168E-02
0.99881E+02	0.99886E-01	0.32968E-01	0.16553E-01	0.73583E-02	0.41318E-02
0.10087E+03	0.85779E-01	0.27793E-01	0.13912E-01	0.61832E-02	0.34720E-02
0.10186E+03	0.73706E-01	0.23430E-01	0.11692E-01	0.51954E-02	0.29173E-02
0.10285E+03	0.63371E-01	0.19754E-01	0.98253E-02	0.43651E-02	0.24511E-02
0.10384E+03	0.54518E-01	0.16654E-01	0.82562E-02	0.36671E-02	0.20592E-02
0.10483E+03	0.46931E-01	0.14042E-01	0.69373E-02	0.30807E-02	0.17298E-02
0.10582E+03	0.40426E-01	0.11841E-01	0.58288E-02	0.25878E-02	0.14531E-02
0.10681E+03	0.34844E-01	0.99846E-02	0.48971E-02	0.21736E-02	0.12205E-02
0.10780E+03	0.30054E-01	0.84201E-02	0.41141E-02	0.18256E-02	0.10251E-02
0.10879E+03	0.25939E-01	0.71012E-02	0.34561E-02	0.15332E-02	0.86094E-03
0.10978E+03	0.22404E-01	0.59894E-02	0.29033E-02	0.12876E-02	0.72302E-03
0.11077E+03	0.19363E-01	0.50521E-02	0.24387E-02	0.10813E-02	0.60716E-03
0.11176E+03	0.16746E-01	0.42618E-02	0.20484E-02	0.90794E-03	0.50982E-03
0.11275E+03	0.14494E-01	0.35955E-02	0.17204E-02	0.76235E-03	0.42807E-03
0.11374E+03	0.12553E-01	0.30336E-02	0.14449E-02	0.64007E-03	0.35941E-03
0.11473E+03	0.10879E-01	0.25598E-02	0.12135E-02	0.53738E-03	0.30175E-03
0.11572E+03	0.94360E-02	0.21602E-02	0.10191E-02	0.45112E-03	0.25331E-03
0.11671E+03	0.81897E-02	0.18232E-02	0.85575E-03	0.37869E-03	0.21264E-03
0.11770E+03	0.71130E-02	0.15389E-02	0.71857E-03	0.31787E-03	0.17849E-03
0.11869E+03	0.61822E-02	0.12991E-02	0.60334E-03	0.26680E-03	0.14981E-03
0.11968E+03	0.53774E-02	0.10968E-02	0.50656E-03	0.22391E-03	0.12573E-03
0.12067E+03	0.46801E-02	0.92602E-03	0.42526E-03	0.18790E-03	0.10551E-03
0.12166E+03	0.40757E-02	0.78190E-03	0.35698E-03	0.15766E-03	0.88530E-04
0.12265E+03	0.35516E-02	0.66024E-03	0.29961E-03	0.13227E-03	0.74272E-04
0.12364E+03	0.30966E-02	0.55751E-03	0.25142E-03	0.11094E-03	0.62296E-04
0.12463E+03	0.27012E-02	0.47074E-03	0.21092E-03	0.93028E-04	0.52239E-04
0.12562E+03	0.23572E-02	0.39740E-03	0.17689E-03	0.77979E-04	0.43788E-04
0.12661E+03	0.20576E-02	0.33540E-03	0.14826E-03	0.65334E-04	0.36668E-04
0.12760E+03	0.17962E-02	0.28293E-03	0.12421E-03	0.54697E-04	0.30715E-04
0.12859E+03	0.15679E-02	0.23852E-03	0.10395E-03	0.45752E-04	0.25692E-04
0.12958E+03	0.13681E-02	0.20081E-03	0.86865E-04	0.38210E-04	0.21457E-04
0.13057E+03	0.11927E-02	0.16882E-03	0.72462E-04	0.31855E-04	0.17889E-04
0.13156E+03	0.10381E-02	0.14151E-03	0.60248E-04	0.26469E-04	0.14865E-04

HLW CANISTER IN GRANITE

KERMA RATE RAD/HR (y-axis)

DISTANCE FROM CENTERLINE OF CANISTER (CM.) (x-axis)

10 YR.
20 YR.
40 YR.
70 YR.
100 YR.
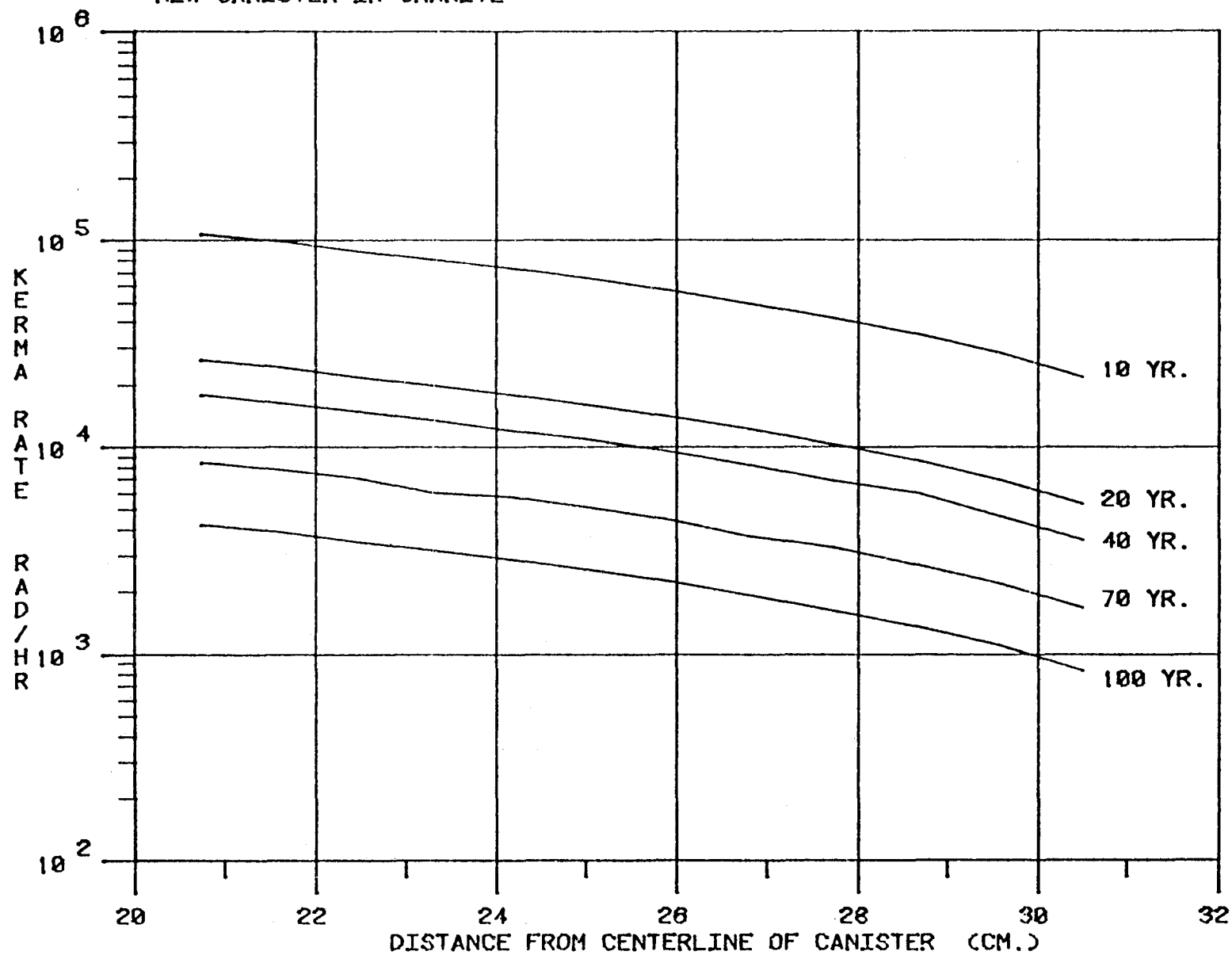
SPENT FUEL CANISTER IN GRANITE

KERMA RATE RAD/HR (y-axis, values 10^4, 10^3, 10^2, 10)

DISTANCE FROM CENTER OF CANISTER (CM.)

10 YR.
20 YR.
40 YR.
70 YR.
100 YR.

GRANITE KERMA RATE – DHLW

KERMA RATE RAD/HR (y-axis)

DISTANCE FROM CANISTER CENTERLINE (CM.) (x-axis)

5 YR.
15 YR.
40 YR.
75 YR.
100 YR.

268

APPENDIX E   LIST OF ABBREVIATIONS

ASTM	American Society for Testing and Materials
ATL	areal thermal loading
BMI	Battelle Memorial Institute
CHLW	commercial high-level waste
CRWN	Civilian Radioactive Waste Management Program
DHLW	defense high-level waste
DOE	U. S. Department of Energy
ERE	expected repository environments
FC	flow condition
FEM	finite element mesh
FF	far field
HLW	high-level waste
ICB	Interface Control Boards
NF	near field
NWTS	National Waste Terminal Storage program
OCRD	Office of Crystalline Repository Development
PWR	pressurized water reactor
RRC-IWG	Reference Repository Conditions - Interface Working Group
SF	spent fuel
VNF	very near field

DISTRIBUTION LIST

ACRES AMERICAN INC
A. S. BURGESS
ROBERT H. CURTIS
R. STRUBLE
AEROSPACE CORP
PETER J. ALEXANDRO
BARRETT R. FRITZ
AGBABIAN ASSOCIATES
CHRISTOPHER M. ST JOHN
ALABAMA DEPT OF ENERGY
CAMERON MCDONALD
ALABAMA STATE GEOLOGICAL SURVEY
THORNTON L. NEATHERY
AMERICAN EMBASSY - SWEDEN
ANALYSIS AND TECHNOLOGY INC
T. MAZOUR
APPLIED MECHANICS INC
GRAHAM G. MUSTOE
ARGONNE NATIONAL LABORATORY
DAVID F. FENSTER
DOUGLAS F. HAMBLEY
WYMAN HARRISON
J. HOWARD KITTEL
MARTIN SEITZ
MARTIN J. STEINDLER
STEVE Y. TSAI
ARINC RESEARCH CORP
H. P. HIMPLER
ARIZONA PUBLIC SERVICE COMPANY
HENRY W. RILEY, JR.
ARKANSAS GEOLOGICAL COMMISSION
WILLIAM V. BUSH
NORMAN F. WILLIAMS
ARTHUR D. LITTLE INC
AVIVA BRECHER
CHARLES R. HADLOCK
ATKINS RESEARCH & DEVELOPMENT - UNITED KINGDOM
T. W. BROYD
ATOMIC ENERGY CONSULTANTS
DONALD G. ANDERSON
ATOMIC ENERGY CONTROL BOARD - CANADA
KEN SHULTZ
ATOMIC ENERGY OF CANADA LTD
T. CHAN
M. O. LUKE
ROBERT B. LYON
ALEX MAYMAN
ANN QUINN
F. P. SARGENT
ATOMIC ENERGY RESEARCH ESTABLISHMENT - UNITED KINGDOM
D. P. HODGKINSON
ATOMIC INDUSTRIAL FORUM INC
EMANUEL GORDON
AUSTRALIAN ATOMIC ENERGY COMMISSION
BATTELLE COLUMBUS DIVISION
JOHN T. MCGINNIS
JEFFREY L. MEANS
NEIL E. MILLER
STEPHEN NICOLOSI
BATTELLE MEMORIAL INSTITUTE
JAMES DUGUID
BE INC
K. J. ANDERSON
BECHTEL GROUP INC
TOM S. BAER
LESLIE J. JARDINE
R. C. LOVINGTON

T. R. MONGAN
U. YOUNG PARK
RICHARD J. TOSETTI
CHING LIU WU
BELGISCHE GEOLOGISCHE DIENST - BELGIUM
NOEL VANDENBERGHE
BENDIX FIELD ENGINEERING CORP
ARCH GIRDLEY
CHARLES A. JONES
DONALD LIVINGSTON
MICHAEL H. MOBLEY
JOHN C. PACER
BERKELEY GEOSCIENCES/HYDROTECHNIQUE ASSOCIATES
BRIAN KANEHIRO
BHABHA ATOMIC RESEARCH CENTRE - INDIA
V. SUKUMORAN
BLACK & VEATCH
M. JOHN ROBINSON
BLUE RIDGE ENVIRONMENTAL DEFENSE COMMITTEE
WILLIAM B. T. MOCK
BOEING ENGINEERING AND CONSTRUCTION COMPANY
R. B. CAIRNS
BRIGHAM YOUNG UNIVERSITY
HAROLD B. LEE LIBRARY
WILLIAM M. TIMMINS
BRITISH GEOLOGICAL SURVEY
DAVID MICHAEL MCCANN
BROOKHAVEN NATIONAL LABORATORY
M. S. DAVIS
P. W. LEVY
CLAUDIO PESCATORE
PETER SOO
HELEN TODOSOW (2)
BROOME COMMUNITY COLLEGE
BRUCE OLDFIELD
BUNDESANSTALT FUR GEOWISSENSCHAFTEN UND ROHSTOFFE - W. GERMANY
MICHAEL LANGER
HELMUT VENZLAFF
BUNDESMINISTERIUM FUR FORSCHUNG UND TECHNOLOGIE - W. GERMANY
ROLF-PETER RANDL
BUREAU DE RECHERCHES GEOLOGIQUES ET MINIERES - FRANCE
BERNARD FEUGA
PIERRE F. PEAUDECERF
BURNS AND ROE INDUSTRIAL SERVICES CORP
JOHN PIRRO
BUTLER UNIVERSITY
PAUL VAN DER HEIJDE
C.F.H.F.
BILL DUESING
C.N.A. UNDERGROUND CONSTRUCTION CONSULTANTS
D. H. YARDLEY
CALIFORNIA ASSEMBLY COMMITTEE ON NATURAL RESOURCES
GENE VARANINI
CALIFORNIA DEPT OF CONSERVATION
PERRY AMIMITO
CALIFORNIA INSTITUTE OF TECHNOLOGY
LEON T. SILVER
CAPITAL UNIVERSITY
VICTOR M. SHOWALTER
CAYUGA LAKE CONSERVATION ASSOCIATION INC
D. S. KIEFER

CENTER FOR SPACE RESEARCH - NOAA
MICHAEL R. HELFERT
CENTRE D INFORMATIQUE GEOLOGIQUE - FRANCE
GHISLAIN DEMARSILY
CENTRO ATOMICO BARILOCHE
M. AUDERO
CHALMERS UNIVERSITY OF TECHNOLOGY - SWEDEN
BERT ALLARD
CHEVRON OIL FIELD RESEARCH COMPANY
BJORN PAULSSON
CITIZENS FOR A BETTER ENVIRONMENT
JOANNA HOELSCHER
CITY OF MONTICELLO
RICHARD TERRY
CLARK COUNTY
EARL SMITH
CLEVELAND CLIFFS IRON COMPANY
HENRY V. GREENWOOD
CLIFFS ENGINEERING INC
GARY D. AHO
COLORADO GEOLOGIC INC
MIKE E. BRAZIE
COLORADO GEOLOGICAL SURVEY
JOHN W. ROLD
COLORADO SCHOOL OF MINES
W. HUSTRULID
DONALD LANGMUIR
COLUMBIA UNIVERSITY
M. ASHRAF MAHTAB
COMISION NACIONAL DE ENERGIA ATOMICA - ARGENTINA
CAMILO PAGANINI
COMMISSION OF THE EUROPEAN COMMUNITIES
ALDO CRICCHIO
CONGRESSIONAL INFORMATION SERVICE
LINDLEY C. MCGREW
CONNECTICUT DEPT OF ENVIRONMENTAL PROTECTION
KEVIN MCCARTHY
CONNECTICUT GEOLOGICAL AND NATURAL HISTORY SURVEY
RALPH S. LEWIS
CONNECTICUT GOVERNORS OFFICE
MARY M. HART
CONNECTICUT HOUSE OF REPRESENTATIVES
DAVID LAVINE
CONNECTICUT NATURAL RESOURCES CENTER
HUGO F. THOMAS
CONNECTICUT STATE DEPT OF HEALTH SERVICES
MARGERY A. COHEN
CONROY ENGINEERING
PETER CONROY
COPPE/UFRJ
LUIZ OLIVEIRA
CORNELL UNIVERSITY
ARTHUR L. BLOOM
FRED H. KULHAWY
ROBERT POHL
CORTLAND COUNTY HEALTH DEPT
J. V. FEUSS
D.R.E.
KARL J. ANANIA
DAMES & MOORE
RON KEAR
JEFFREY KEATON
CHARLES R. LEWIS

Preceding page blank

LES SKOSKI
YU CHIEN YUAN
DAN L. WARD INC
DAN L. WARD
DAPPOLONIA CONSULTING ENGINEERS INC
LISA K. DONOHUE
ABBY FORREST
AMINA HAMDY
PETER C. KELSALL
CARL E. SCHUBERT
**DAWCON MANAGEMENT CONSULTING
SERVICE**
DAVID A. WEBSTER
DEAF SMITH COUNTY LIBRARY
DELAWARE CUSTOM MATERIEL INC
HOWARD NOVITCH
DELAWARE GEOLOGICAL SURVEY
ROBERT R. JORDAN
**DEPT OF ENERGY, MINES AND RESOURCES -
CANADA**
A. S. JUDGE
DICKINSON-IRON DISTRICT HEALTH DEPT
RONALD MATONICH
DISASTER PREPAREDNESS
TIMOTHY M. LEE
DISPOSAL SAFETY INC.
BENJAMIN ROSS
DIXON ASSOCIATES
J. DONALD DIXON
DUNN GEOSCIENCE CORP
WILLIAM E. CUTCLIFFE
DYNATECH R/D COMPANY
STEPHEN E. SMITH
E.I. DU PONT DE NEMOURS & CO
D. H. TURNO
**E.L.H. PUBLICATIONS - THE RADIOACTIVE
EXCHANGE**
HELMINSKI & WILKEN
E.R. JOHNSON ASSOCIATES INC
E. R. JOHNSON
G. L. JOHNSON
EAL CORP
LEON LEVENTHAL
EARTH SCIENCE AND ENGINEERING INC
LOU BLANCK
EARTH SCIENCES CONSULTANTS INC
HARRY L. CROUSE
EAST COMPANY INC
RAYMOND PEREZ
EAST TENNESSEE STATE UNIVERSITY
ALBERT F. IGLAR
VAY A. RODMAN
EBASCO SERVICES INC
ZUBAIR SALEEM
RAYMOND H. SHUM
ECOLOGY & ENVIRONMENT INC
MICHAEL BENNER
ECOLOGY CENTER OF LOUISIANA
ROSS VINCENT
EDISON ELECTRIC INSTITUTE
R. E. L. STANFORD
EDS NUCLEAR INC
C. SUNDARARAJAN
EG & G IDAHO INC
SCOTT HIRSCHBERGER
GEORGE B. LEVIN
ROBERT M. NEILSON, JR.
**EIDG INSTITUT FUER REAKTORFORSCHUNG -
SWITZERLAND**
BIBLIOTHEK
**ELEKTRIZITAETS-GES. LAUFENBURG -
SWITZERLAND**
H. N. PATAK

ENERCOR INC
JOHN RODOSEVICH
ENERGY RESEARCH GROUP INC
MARC GOLDSMITH
ENGINEERS INTERNATIONAL INC
V. RAJARAM
ENVIROLOGIC SYSTEMS INC
JIM V. ROUSE
ENVIRONMENT CANADA
CLAUDE BARRAUD
ENVIRONMENTAL POLICY INSTITUTE
DAVID M. BERICK
ENVIROSPHERE COMPANY
ROGER G. ANDERSON
K. E. LIND-HOWE
EXXON NUCLEAR COMPANY INC
GERALD L. RITTER
EXXON NUCLEAR IDAHO COMPANY INC
NATHAN A. CHIPMAN
ROGER N. HENRY
GARY WAYMIRE
FENIX & SCISSON INC
JOSE A. MACHADO
CHARLENE U. SPARKMAN
FERRIS STATE COLLEGE
MICHAEL E. ELLS
FINLAND TECH RESEARCH CENTRE
MARGIT SNELLMAN
FLORIDA INSTITUTE OF TECHNOLOGY
JOSEPH A. ANGELO, JR.
FLORIDA POWER & LIGHT COMPANY
JAMES R. TOMONTO
FLORIDA STATE UNIVERSITY
JOSEPH F. DONOGHUE
FLUOR ENGINEERS & CONSTRUCTORS INC
RAYMOND J. DUGAL
FOSTER-MILLER ASSOCIATES INC
NORBERT PAAS
FOUNDATION SCIENCES INC
LOU BATTAMS
FREIE UNIVERSITAET BERLIN
HANSKARL BRUEHL
FRIENDS OF THE EARTH
RENEE PARSONS
FUTURE RESOURCES ASSOCIATES INC
ROBERT J. BUDNITZ
GARTNER LEE ASSOCIATES LTD - CANADA
ROBERT E. J. LEECH
GENERAL ATOMIC COMPANY
ROBERT M. BURGOYNE
MICHAEL STAMATELATOS
GENERAL COURT OF MASSACHUSETTS
TIMOTHY J. BURKE
GEO/RESOURCE CONSULTANTS INC
ALVIN K. JOE, JR.
GEOLOGICAL SURVEY OF CANADA
JEFFREY HUME
PAVEL KURFURST
LIBRARY
JOHN SCOTT
GEOLOGICAL SURVEY OF IRELAND
MICHAEL D. MAX
GEOLOGICAL SURVEY OF NORWAY
SIGURD HUSEBY
GEORGIA GEOLOGICAL SURVEY
WILLIAM H. MCLEMORE
GEORGIA INSTITUTE OF TECHNOLOGY
MELVIN W. CARTER
GEOFFREY G. EICHHOLZ
ALFRED SCHNEIDER
CHARLES E. WEAVER
GEOSTOCK - FRANCE
R. BARLIER

GEOTECHNICAL ENGINEERS INC
RONALD C. HIRSCHFELD
GEOTHERMAL ENERGY INSTITUTE
DONALD F. X. FINN
GEOTRANS
JAMES MERCER
**GESELLSCHAFT F. STRAHLEN U.
UMWELTFORSCHUNG M.B.H. - W.
GERMANY**
WOLFGANG BODE
NORBERT FOCKWER
HANS W. LEVI
H. MOSER
GILBERT/COMMONWEALTH
JERRY L. ELLIS
GOLDER ASSOCIATES
DONALD M. CALDWELL
MELISSA MATSON
J. W. VOSS
GOLDER ASSOCIATES - CANADA
CLEMENT M. K. YUEN
GRAND COUNTY PUBLIC LIBRARY
GREAT LAKES ENERGY ALLIANCE
MARY P. SINCLAIR
**GREAT LAKES ENVIRONMENTAL STUDY
CENTERS**
DOUGLAS R. ZULLO
GSE NUCLEAR
MOHSEN NIROOMAND-RAD
**GTC GEOLOGIC TESTING CONSULTANTS LTD -
CANADA**
JOHN F. PICKENS
GULF INTERSTATE ENGINEERING
THOMAS J. HILL
GULF STATES UTILITIES COMPANY
E. LINN DRAPER
GUSTAVSON ASSOCIATES
RICHARD M. WINAR
H & R TECHNICAL ASSOCIATES INC
WILLIAM R. RHYNE
H-TECH LABORATORIES INC
BRUCE HARTENBAUM
**HAHN-MEITNER-INSTITUT FUR
KERNFORSCHUNG BERLIN**
KLAUS ECKART MAASS
HALEY AND ALDRICH INC
JANICE HIGHT
**HANFORD ENGINEERING DEVELOPMENT
LABORATORY**
ROBERT EINZIGER
W. E. ROAKE
HART-CROWSER AND ASSOCIATES
MICHAEL BAILEY
HARVARD UNIVERSITY
CHARLES W. BURNHAM
DADE W. MOELLER
RAYMOND SIEVER
HIGH PLAINS WATER DISTRICT
A. WAYNE WYATT
HITACHI WORKS, HITACHI LTD
MAKOTO KIKUCHI
HOUGH-NORWOOD HEALTH CARE CENTER
GEORGE H. BROWN, M.D.
IDAHO BUREAU OF MINES AND GEOLOGY
EARL H. BENNETT
ILLINOIS DEPT OF NUCLEAR SAFETY
TERRY R. LASH
MILTON ZUKOR
ILLINOIS STATE GEOLOGICAL SURVEY
KEROS CARTWRIGHT
MORRIS W. LEIGHTON

IMPERIAL COLLEGE OF SCIENCE AND
TECHNOLOGY - ENGLAND
B. K. ATKINSON
INDIANA GEOLOGICAL SURVEY
MAURICE BIGGS
INDIANA UNIVERSITY
HAYDN H. MURRAY
INDUSTRIAL POWER COMPANY LTD -
FINLAND
VEIJO RYHANEN
JUKKA-PEKKA SALO
INSTITUT FUR TIEFLAGERUNG - W. GERMANY
WERNT BREWITZ
KLAUS KUHN
E. R. SOLTER
INSTITUTE FOR CHEMICAL TECHNOLOGY - W.
GERMANY
REINHARD ODOJ
INSTITUTE OF GEOLOGICAL SCIENCES -
ENGLAND
STEPHEN THOMAS HORSEMAN
INSTITUTE OF RADIATION PROTECTION -
FINLAND
KAI JAKOBSSON
ESKO RUOKOLA
INTER/FACE ASSOCIATES INC
RON GINGERICH
INTERA ENVIRONMENTAL CONSULTANTS INC
F. J. PEARSON, JR.
LARRY RICKERTSEN
ROBERT WILEMS
INTERNATIONAL ATOMIC ENERGY AGENCY -
AUSTRIA
FRANK A. OHARA
INTERNATIONAL ENERGY ASSOCIATES LTD
BLYTHE K. LYONS
INTERNATIONAL ENGINEERING COMPANY
INC
MAX ZASLAWSKY
INTERNATIONAL RESEARCH AND
EVALUATION
R. DANFORD
INTERNATIONAL SALT COMPANY
JOHN VOIGT
IOWA STATE COMMERCE COMMISSION
IOWA STATE UNIVERSITY
MARTIN C. EDELSON
BERNARD I. SPINRAD
IRAD-GAGE
JAMES H. VEZINA
IRT CORP
J. STOKES
ISMES - ITALY
F. GERA
ISTITUTO SPERIMENTALE MODELLI E
STRUTTURE S.P.A. - ITALY
NEIL A. CHAPMAN
ITASCA CONSULTING GROUP, INC.
ROGER HART
J.F.T. AGAPITO & ASSOCIATES INC
MICHAEL P. HARDY
J.L. MAGRUDER & ASSOCIATES
J. L. MAGRUDER
JAPAN ATOMIC ENERGY RESEARCH INSTITUTE
TARO ITO
HARUTO NAKAMURA
JAY L. SMITH COMPANY INC
JAY L. SMITH
JGC CORPORATION - JAPAN
MASAHIKO MAKINO
JOHNS HOPKINS UNIVERSITY
JARED L. COHON

JOINT STUDY COMMITTEE ON ENERGY
T. W. EDWARDS, JR.
JORDAN GORRILL ASSOCIATES
JOHN D. TEWHEY
KAISER ENGINEERS INC
W. J. DODSON
H. L. JULIEN
KALAMAZOO COLLEGE
RALPH M. DEAL
KANSAS DEPT OF HEALTH AND
ENVIRONMENT
GERALD W. ALLEN
KARNBRANSLESAKERHET - SWEDEN
LARS B. NILSSON
KBHW RADIO
BRUCE CHRISTOPHERSON
KELLER WREATH ASSOCIATES
FRANK WREATH
KERNFORSCHUNGSZENTRUM KARLSRUHE
GMBH - W. GERMANY
K. D. CLOSS
R. KOESTER
KERNFORSCHUNGSZENTRUM UND
UNIVERSITAT
GERHARD ONDRACEK
KETTERING FOUNDATION
ESTUS SMITH
KIHN ASSOCIATES
HARRY KIHN
KIMBERLY MECHANICAL CONSULTANTS
KENNETH CROMWELL
KLM ENGINEERING INC
B. GEORGE KNIAZEWYCZ
KOREA INSTITUTE OF ENERGY AND
RESOURCES (KIER)
CHOO SEUNG HWAN
CHONG SU KIM
KRSP RADIO
DAN BAMMES
KUTV-TV
ROBERT LOY
KYOTO UNIVERSITY - JAPAN
YORITERU INOUE
LACHEL HANSEN & ASSOCIATES INC
DOUGLAS E. HANSEN
LAKE SUPERIOR REGION RADIOACTIVE
WASTE PROJECT
C. DIXON
LAW ENGINEERING TESTING COMPANY
JAMES L. GRANT
LAWRENCE BERKELEY LABORATORY
JOHN A. APPS
EUGENE BINNALL
NORMAN M. EDELSTEIN
M. S. KING
E. MAJER
ROBIN SPENCER
CHIN FU TSANG
J. WANG
PAUL A. WITHERSPOON
LAWRENCE LIVERMORE NATIONAL
LABORATORY
LYNDEN B. BALLOU
TED BUTKOVICH
DAE H. CHUNG
EDNA M. DIDWELL
HUGH HEARD
FRANCOIS E. HEUZE
DANA ISHERWOOD
DONALD D. JACKSON
NAI-HSIEN MAO
THOMAS E. MCKONE

WILLIAM J. OCONNELL
ABELARDO RAMIREZ
LAWRENCE D. RAMSPOTT (2)
R. N. SCHOCK
TECHNICAL INFORMATION DEPARTMENT
L-53
RICHARD THORPE
RICHARD VAN KONYNENBURG
WASTE PACKAGE TASK LIBRARY
DALE G. WILDER
JESSE L. YOW, JR.
LEAGUE OPPOSING SITE SELECTION
LINDA S. TAYLOR
LEHIGH UNIVERSITY
D. R. SIMPSON
LIBRARY OF MICHIGAN
RICHARD J. HATHAWAY
LOCKHEED ENGINEERING & MANAGEMENT
COMPANY
STEVE NACHT
LOS ALAMOS NATIONAL LABORATORY
DONALD W. BROWN
ERNEST A. BRYANT
P. L. BUSSOLINI
B. CROWE
BRUCE R. ERDAL
WAYNE R. HANSEN
CLAUDE HERRICK
W. C. MYERS
DONALD T. OAKLEY
K. K. S. PILLAY
ROBERT E. RIECKER
KURT WOLFSBERG
LOS ALAMOS TECHNICAL ASSOCIATES INC
R. J. KINGSBURY
LOUISIANA GEOLOGICAL SURVEY
CHARLES G. GROAT
LOUISIANA TECHNICAL UNIVERSITY
LIBRARY
R. H. THOMPSON
LOWENBERG ASSOCIATES
HOMER LOWENBERG
M.J. OCONNOR & ASSOCIATES LTD
M. J. OCONNOR
MAINE BUREAU OF HEALTH
DONALD C. HOXIE
MAINE GEOLOGICAL SURVEY
WALTER A. ANDERSON, PH.D.
MAINE STATE PLANNING OFFICE
RICHARD D. KELLY JR.
MAINE STATE SENATE
JUDY KANY
MARQUETTE COUNTY HEALTH DEPT
ALAN R. BUDINGER
MARQUETTE COUNTY PLANNING
COMMISSION
JAMES KIPPOLA
MARYLAND DEPT OF HEALTH & MENTAL
HYGIENE
MAX EISENBERG
MARYLAND DEPT OF HEALTH AND MENTAL
HYGIENE
WILLIAM M. EICHBAUM
MARYLAND DEPT OF NATURAL RESOURCES
THOMAS MAGETTE
CHRIS ZABAWA
MARYLAND GEOLOGICAL SURVEY
KENNETH N. WEAVER
MASSACHUSETTS DEPT OF ENVIRONMENTAL
QUALITY ENGINEERING
JOSEPH A. SINNOTT

MASSACHUSETTS HOUSE OF REPRESENTATIVES
WILLIAM ROBINSON
MASSACHUSETTS INSTITUTE OF TECHNOLOGY
W. F. BRACE
JOHN DEUTCH
RICHARD K. LESTER
MARSHA LEVINE
DANIEL METLAY
MASSACHUSETTS RADIATION CONTROL PROGRAM
ROBERT HALLISEY
MASSACHUSETTS STATE SENATE
CAROL C. AMICK
MATERIALS RESEARCH LABORATORY LTD - CANADA
S. SINGH
MATH SCIENCES RESEARCH STATION
MARTIN & ELAINE WALTER
MCMASTER UNIVERSITY - CANADA
L. W. SHEMILT
MELLEN GEOLOGICAL ASSOCIATES INC
FREDERIC F. MELLEN
MEMBERS OF THE GENERAL PUBLIC
R. H. BECK
LOUISE BECKER
W. E. BENSON
JAMES BOYD
THOMAS G. BRADFORD
ROGER H. BROOKS
HAZEL CHAPMAN, PH.D.
LAWRENCE CHASE, PH.D.
YVONNE C. CONDELL
STEVE CONEWAY
M. VAL DALTON
RICHARD DAVIES
GERALD A. DRAKE, M.D.
CHARLES S. DUNN
JEAN EARDLEY
THAUMAS P. EHR
WARREN EISTER
MICHAEL A. FATLA
SHIRLEY M. GIFFORD
MICHAEL J. GILBERT
HARRY D. GOODE
DOUGLAS H. GREENLEE
KENNETH GUSCOTT
C. F. HAJEK
A. M. HALE
STEPHEN B. HARPER
JOSEPH M. HENNIGAN
VIRGINIA HOMME
DOROTHY HUSEBY
KENNETH S. JOHNSON
HELEN B. KENNY
SCOTT KRAMER
THOMAS H. LANGEVIN
HARRY E. LEGRAND
LINDA LEHMAN
A. ALAN MOGHISSI
RAYMOND MOHR
F. L. MOLESKI
BARBARA MORRA
LAWRENCE G. PETERSON
CAROLINE PETTI
SHAILER S. PHILBRICK
RUS PURCELL
MARTIN RATHKE
TOM & MARY REES
PETER J. SABATINI, JR.
OWEN SEVERANCE

PAUL SHEWMON
HARRY W. SMEDES
NORMAN C. SMITH
PATRICIA SNYDER
GLENN W. STEWART
M. J. SZULINSKI
A. E. WASSERBACH
JIMMY L. WHITE
RICHARD J. WILLIS
SUSAN D. WILTSHIRE
LINDA WITTKOPF
STEPHEN G. ZEMBA
MEMORIAL UNIVERSITY OF NEWFOUNDLAND
JOHN E. GALE
MENOMINEE INDIAN TRIBE OF WISCONSIN
STEVEN L. DODGE
MICHAEL BAKER, JR. INC
C. J. TOUHILL
MICHIGAN CENTER FOR ENVIRONMENTAL HEALTH SCIENCES
JOHN L. HESSE
MICHIGAN DEPT OF NATURAL RESOURCES
DAN E. REED
R. THOMAS SEGALL
MICHIGAN DEPT OF PUBLIC HEALTH
ARTHUR W. BLOOMER
GEORGE W. BRUCHMANN
ERIC SCHWING
MICHIGAN ENVIRONMENTAL PROTECTION COMMITTEE
DAVE CHAPMAN
MICHIGAN GEOLOGICAL SURVEY
ROBERT C. REED
MICHIGAN PUBLIC SERVICE COMMISSION
RON CALLEN
MICHIGAN STATE CHAMBER OF COMMERCE
GEORGE GRAFF
MICHIGAN STATE SENATE
PENNY ANCEL
MICHIGAN STATE UNIVERSITY
BILL COOPER
WILLIAM C. TAYLOR
BRUCE W. WILKINSON
MICHIGAN TECHNOLOGICAL UNIVERSITY
ROBERT PATTERSON
MICHIGAN UNITED CONSERVATION CLUBS
WAYNE SCHMIDT
MIDWESTERN CONFERENCE OF THE COUNCIL OF STATE GOVERNMENTS
JAMES BOWHAY
MINNESOTA AUDUBON COUNCIL
VIRGINIA K. BLACK
MINNESOTA DEPT OF ENERGY AND DEVELOPMENT
MINNESOTA DEPT OF HEALTH
ALICE T. DOLEZAL HENNIGAN
MINNESOTA DEPT OF NATURAL RESOURCES
TOM BALCOM
MINNESOTA ENVIRONMENTAL QUALITY BOARD
TOM KALITOWSKI
GREGG LARSON
RICHARD PATON
MINNESOTA GEOLOGICAL SURVEY
MATT S. WALTON
MINNESOTA GOVERNORS TASK FORCE ON HIGH-LEVEL RADIOACTIVE WASTE
MINNESOTA HEADWATERS REGIONAL DEVELOPMENT COMMISSION
MINNESOTA STATE SENATE
CONRAD VEGA

MISSISSIPPI ATTORNEY GENERALS OFFICE
MACK CAMERON
MISSISSIPPI BUREAU OF GEOLOGY
MICHAEL B. E. BOGRAD
MISSISSIPPI CITIZENS AGAINST NUCLEAR DISPOSAL
STANLEY DEAN FLINT
MISSISSIPPI DEPT OF ENERGY AND TRANSPORTATION
RONALD J. FORSYTHE (3)
MISSISSIPPI DEPT OF NATURAL RESOURCES
CURTIS W. STOVER
MISSISSIPPI HOUSE OF REPRESENTATIVES
MACK MCINNIS
MISSISSIPPI STATE BOARD OF HEALTH
EDDIE S. FUENTE
MISSISSIPPI STATE HOUSE OF REPRESENTATIVES
HILLMAN TEROME FRAZIER
MITRE CORP
LESTER A. ETTLINGER
MITSUBISHI METAL CORP
TATSUO ARIMA
MOAB NUCLEAR WASTE INFORMATION OFFICE
MICHAELENE PENDLETON (2)
MOBAY CHEMICAL CORP
KENNETH H. HASHIMOTO
MONTANA BUREAU OF MINES AND GEOLOGY
EDWARD C. BINGLER
MONTICELLO NUCLEAR WASTE INFORMATION OFFICE
CARL EISEMANN (2)
MORRISON-KNUDSEN COMPANY INC
SERGI KAMINSKY
STEPHANIE NICHOLS
NAGRA - SWITZERLAND
HANS ISSLER
CHARLES MCCOMBIE
NATIONAL ACADEMY OF SCIENCES
JOHN T. HOLLOWAY
HAROLD L. JAMES
NATIONAL AERONAUTICS AND SPACE ADMINISTRATION
MICHAEL ZOLENSKY
NATIONAL BOARD FOR SPENT NUCLEAR FUEL, KARNBRANSLENAMDEN - SWEDEN
NILS RYDELL
NATIONAL BUREAU OF STANDARDS
RILEY M. CHUNG
NATIONAL HYDROLOGY RESEARCH INSTITUTE - CANADA
DENNIS J. BOTTOMLEY
K. U. WEYER
NATIONAL PARKS & CONSERVATION ASSOCIATION
TERRI MARTIN
NATIONAL SCIENCE FOUNDATION
ROYAL E. ROSTENBACH
NATIONAL WILDLIFE FEDERATION
MARK VAN PUTTEN
NATURAL RESOURCES DEFENSE COUNCIL
THOMAS B. COCHRAN
NAVAL WEAPONS STATION EARLE
GENNARO MELLIS
NEW ENGLAND NUCLEAR CORP
KERRY BENNERT
CHARLES B. KILLIAN
NEW HAMPSHIRE GOVERNORS ENERGY OFFICE
DENNIS HEBERT

NEW HAMPSHIRE OFFICE OF STATE PLANNING
  DAVID G. SCOTT
NEW JERSEY DEPT OF ENVIRONMENTAL
  PROTECTION
  JEANETTE ENG
NEW JERSEY GEOLOGICAL SURVEY
  FRANK J. MARKEWICZ
NEW JERSEY INSTITUTE OF TECHNOLOGY
  BEN STEVENSON
NEW MEXICO BUREAU OF MINES AND
  MINERAL RESOURCES
  FRANK E. KOTTLOWSKI
NEW MEXICO ENVIRONMENTAL EVALUATION
  GROUP
  ROBERT H. NEILL
NEW YORK DEPT OF HEALTH
  DAVID AXELROD, M.D.
NEW YORK ENERGY RESEARCH &
  DEVELOPMENT AUTHORITY
  JOHN P. SPATH (8)
NEW YORK GEOLOGICAL SURVEY
  ROBERT H. FAKUNDINY
NEW YORK STATE ASSEMBLY
  STANLEY FINK
  MAURICE D. HINCHEY
  ANGELO ORAZIO
NEW YORK STATE ATTORNEY GENERALS
  OFFICE
  EZRA I. BIALIK
NEW YORK STATE DEPT OF ENVIRONMENTAL
  CONSERVATION
  PAUL MERGES
NEW YORK STATE ENERGY RESEARCH AND
  DEVELOPMENT AUTHORITY
  JOHN C. DEMPSEY
NEW YORK STATE ENVIRONMENTAL
  FACILITIES CORP
  PICKETT T. SIMPSON
NEW YORK STATE GEOLOGICAL SURVEY
  JAMES R. ALBANESE
  ROBERT H. FICKIES
NEW YORK STATE HEALTH DEPT
  JOHN MATUSZEK
NEW YORK STATE PUBLIC SERVICE
  COMMISSION
  FRED HAAG
NEW YORK STATE SENATE
  DALE M. VOLKER
NEW YORK STATE SENATE RESEARCH SERVICE
  DAVID WHITEHEAD
NEYER, TISEO, & HINDO LTD
  KAI R. HINDO
NORTH CAROLINA CONSERVATION
  COUNCIL
  JANE SHARP
NORTH CAROLINA DEPT OF NATURAL
  RESOURCES & COMMUNITY DEVELOPMENT
  STEPHEN G. CONRAD
NORTH CAROLINA STATE SENATE
  J. R. ALLSBROOK
NORTH CAROLINA STATE UNIVERSITY
  M. KIMBERLEY
NORTH CENTRAL WISCONSIN REGIONAL
  PLANNING COMMISSION
  ARNO WILLIAM HAERING, JR.
NORTH DAKOTA GEOLOGICAL SURVEY
  DON L. HALVORSON
NORTH DAKOTA STATE UNIVERSITY
  JOHN M. HALSTEAD
NORTH ILLINOIS UNIVERSITY
  B. VON ZELLEN

NORTHEAST UTILITIES SERVICE COMPANY
  PATRICIA ANN OCONNELL
NORTHERN MICHIGAN UNIVERSITY
  GAIL D. GRIFFITH
  MAIN LIBRARY
  JON L. SAARI
NORTHERN STATE POWER COMPANY
  BILL HEANEY
NORTHWEST REGIONAL PLANNING
  COMMISSION
  MARK J. MUELLER
NORTHWESTERN UNIVERSITY
  BERNARD J. WOOD
NTR GOVERNMENT SERVICES
  THOMAS V. REYNOLDS
NUCLEAIRE HYDRO LTD
  JOHN WILLIAM KENNY, III
NUCLEAR ASSURANCE CORP
  JOHN V. HOUSTON
  JEAN RION
NUCLEAR ENERGY AGENCY/OECD - FRANCE
  ANTHONY MULLER
NUS CORP
  W. G. BELTER
  RODNEY J. DAVIS
  N. BARRIE MCLEOD
  BARRY N. NAFT
  DOUGLAS D. ORVIS
  YONG M. PARK
NUTECH ENGINEERS INC
  GARRISON KOST
  ALFRED SUGARMAN
NWT CORP
  W. L. PEARL
OAK RIDGE NATIONAL LABORATORY
  CARLOS E. BAMBERGER
  J. O. BLOMEKE
  H. C. CLAIBORNE
  ALLEN G. CROFF
  LESLIE R. DOLE
  CATHY S. FORE
  DAVID C. KOCHER
  T. F. LOMENICK
  ELLEN D. SMITH
  STEPHEN S. STOW
OKLAHOMA GEOLOGICAL SURVEY
  CHARLES J. MANKIN
OKLAHOMA STATE DEPT OF HEALTH
  R. L. CRAIG
ONTARIO HYDRO - CANADA
  R. W. BARNES
  J. A. CHADHA
  K. A. CORNELL
  C. F. LEE
  R. C. OBERTH
ONTARIO MINISTRY OF THE ENVIRONMENT -
  CANADA
  JAAK VIIRLAND
ONTARIO RESEARCH FOUNDATION -
  CANADA
  LYDIA M. LUCKEVICH
ORANGE COUNTY COMMUNITY COLLEGE
  LAWRENCE E. OBRIEN
OREGON DEPT OF ENERGY
  DONALD W. GODARD
OREGON STATE UNIVERSITY
  JOHN C. RINGLE
ORGANISATION FOR ECONOMIC
  COOPERATION AND DEVELOPMENT -
  FRANCE
  PETER D. JOHNSTON
OTHA INC
  JOSEPH A. LIEBERMAN

PACIFIC NORTHWEST LABORATORY
  W. F. BONNER
  DON J. BRADLEY
  JOHN B. BROWN
  H. C. BURKHOLDER
  JOHN B. BURNHAM
  T. D. CHIKALLA
  L. L. CLARK
  HARVEY DOVE
  FLOYD N. HODGES
  J. H. JARRETT
  CHARLES T. KINCAID
  MAX R. KREITER
  DONALD E. LARSON
  J. E. MENDEL
  J. M. RUSIN
  R. JEFF SERNE
  CARL UNRUH
  R. E. WESTERMAN
  J. H. WESTSIK, JR.
PARSONS BRINCKERHOFF QUADE &
  DOUGLAS INC
  T. R. KUESEL
  ROBERT PRIETO
  MARK E. STEINER
PARSONS-REDPATH
  BRUNO LORAN
PB-KBB INC
  JUDITH G. HACKNEY
PENBERTHY ELECTROMELT INTERNATIONAL
  INC
  LARRY PENBERTHY
PENNSYLVANIA DEPT OF ENVIRONMENTAL
  RESOURCES
  THOMAS M. GERUSKY
PENNSYLVANIA STATE UNIVERSITY
  MARY BARNES
  MICHAEL GRUTZECK
  DELLA M. ROY
  WILLIAM B. WHITE
PENNSYLVANIA TOPOGRAPHIC &
  GEOLOGICAL SURVEY
  ARTHUR A. SOCOLOW
PHILADELPHIA ELECTRIC COMPANY
  JOHN J. TUCKER
PHYSIKALISCH-TECHNISCHE BUNDESANSTALT
  - W. GERMANY
  HORST SCHNEIDER
PIRGIM
  RICHARD LEVICK
POBERESKIN INC.
  MEYER POBERESKIN
POINT BEACH NUCLEAR PLANT
  JAMES J. ZACH
POLLUTION AND ENVIRONMENTAL
  PROBLEMS
  CATHERINE QUIGG
PRESEARCH INC
  RHONNIE L. SMITH
PRIVATE CITIZEN
  JANET R. REMUS
PSE & G
  JOHN J. MOLNER
PUBLIC SERVICE INDIANA
  ROBERT S. WEGENG
PURDUE UNIVERSITY
  PAUL S. LYKOUDIS
RADIAN CORP
  BARBARA MAXEY
RADIATION PROTECTION COUNCIL
  TERI L. VIERIMA

RADIOACTIVE WASTE PROJECT/MINNESOTA
PUBLIC INTEREST RESEARCH FOUNDATION
  BARBARA J. JOHNSON
RALPH M. PARSONS COMPANY
  JERROLD A. HAGEL
RE/SPEC INC
  GARY D. CALLAHAN
  WILLIAM C. MCCLAIN
RED ROCK 4-WHEELERS
  GEORGE SCHULTZ
RENSSELAER POLYTECHNIC INSTITUTE
  BRIAN BAYLY
RESEARCH AND PRODUCTIVITY COUNCIL -
CANADA
  D. ABBOTT
RESOURCE SYSTEMS INSTITUTE
  KIRK R. SMITH
RHODE ISLAND GOVERNORS ENERGY OFFICE
  BRUCE VILD
RHODE ISLAND GOVERNORS OFFICE
  JOHN A. IVEY
RIO ALGOM CORP
  DUANE MATLOCK
RISO NATIONAL LABORATORY - DENMARK
  LARS CARLSEN
ROCHESTER POST-BULLETIN
  BRUCE MAXWELL
ROCKWELL HANFORD OPERATIONS
  RONALD C. ARNETT
  JAMES L. ASH
  HARRY BABAD
  G. S. BARNEY
  L. R. FITCH
  R. J. GIMERA
  KUNSOO KIM
  KARL M. LA RUE
  STEVEN J. PHILLIPS
  MICHAEL J. SMITH
  RICHARD T. WILDE
ROCKWELL INTERNATIONAL ENERGY SYSTEMS
GROUP
  HARRY PEARLMAN
  LAWRENCE J. SMITH
ROGERS & ASSOCIATES ENGINEERING CORP
  ARTHUR A. SUTHERLAND
ROGERS, GOLDEN & HALPERN
  JACK A. HALPERN
RONALD M. HAYS & ASSOCIATES
  RONALD M. HAYS
ROY F. WESTON INC
  MARTIN HANSON
  WILLIAM IVES
  RONALD MACDONALD
  MICHAEL V. MELLINGER
  SAM PANNO
  JILL RUSPI
  DOUGLAS W. TONKAY
  LAWRENCE A. WHITE
ROYAL INSTITUTE OF TECHNOLOGY -
SWEDEN
  IVARS NERETNIEKS
  ROGER THUNVIK
RPC INC
  JAMES VANCE
S.E. LOGAN & ASSOCIATES INC
  STANLEY E. LOGAN
S.M. STOLLER CORP
  ROBERT W. KUPP
SAFE ENERGY COALITION
  JENNIFER PUNTENNEY

SALT LAKE CITY TRIBUNE
  JIM WOOLF
SAN DIEGO GAS & ELECTRIC COMPANY
  LOUIS BERNATH
SAN JOSE STATE UNIVERSITY SCHOOL OF
ENGINEERING
  R. N. ANDERSON
SANDIA NATIONAL LABORATORIES
  G. C. ALLEN
  KEN BEALL
  MARGARET S. CHU
  JOE A. FERNANDEZ
  THOMAS O. HUNTER
  J. KEITH JOHNSTONE
  A. R. LAPPIN
  R. W. LYNCH
  MARTIN A. MOLECKE
  JAMES T. NEAL
  E. J. NOWAK
  NESTOR R. ORTIZ
  SCOTT SINNOCK
  A. W. SNYDER
  LYNN D. TYLER
  WOLFGANG WAWERSIK
  WENDELL D. WEART
  WIPP CENTRAL FILES
SANTA FE SHAFT DRILLING CO
  ROBERT J. PLISKA
SARGENT & LUNDY ENGINEERS
  LAWRENCE L. HOLISH
SAVANNAH RIVER LABORATORY
  E. J. HENNELLY
  CAROL JANTZEN
  I. WENDELL MARINE
  WILLIAM R. MCDONELL
  DONALD ORTH
SCANDPOWER INC
  DAN POMEROY
SCIAKY BROTHERS
  JOHN C. JASPER
SCIENCE APPLICATIONS INC
  JEFFREY ARBITAL
  JERRY J. COHEN
  NADIA DAYEM
  BARRY DIAL
  MICHAEL B. GROSS
  JAMES E. HAMMELMAN
  DEAN C. KAUL
  DAVID H. LESTER
  PETER E. MCGRATH
  JOHN E. MOSIER
  HOWARD PRATT
  MICHAEL E. SPAETH
  M. D. VOEGELE
  KRISHAN K. WAHI
  ROBERT A. YODER
SCRIPPS INSTITUTE OF OCEANOGRAPHY
(A-015)
  HUBERT STAUDIGEL
SENATE RESEARCH SERVICE
  DAVID WHITEHEAD
SENECA COUNTY DEPT OF PLANNING &
DEVELOPMENT
SERATA GEOMECHANICS INC
  FRANK TSAI
SHANNON & WILSON INC
  HARVEY W. PARKER
SHIMIZU CONSTRUCTION COMPANY LTD
  JUNJI TAKAGI
SHIMIZU CONSTRUCTION COMPANY LTD -
JAPAN
  JUN SHIMADA

SIERRA CLUB
  MARVIN RESNIKOFF
SIERRA CLUB - COLORADO OPEN SPACE
COUNCIL
  ROY YOUNG
SIERRA CLUB LEGAL DEFENSE FUND
  H. ANTHONY RUCHEL
SIERRA GEOPHYSICS INC
  DAVID M. HADLEY
SKBF/KBS - SWEDEN
  C. THEGERSTROM
SOGO TECHNOLOGY INC
  TIO C. CHEN
SOKAOGON CHIPPEWA COMMUNITY
  ARLYN ACKLEY
SOUTH CAROLINA GEOLOGICAL SURVEY
  NORMAN K. OLSON
SOUTH CAROLINA GOVERNORS DIVISION OF
ENERGY POLICY
  WILLIAM NEWBERRY
SOUTH CAROLINA GOVERNORS OFFICE
  TRISH JERMAN
  JOHN J. STUCKER
SOUTH DAKOTA GEOLOGICAL SURVEY
  RICHARD BRETZ
SOUTH DAKOTA OFFICE OF ENERGY POLICY
  STEVEN M. WEGMAN
SOUTH DAKOTA SCHOOL OF MINES AND
TECHNOLOGY
  CANER ZANBAK
SOUTHERN STATES ENERGY BOARD
  J. F. CLARK
  NANCY KAISER
SOUTHWEST RESEARCH AND INFORMATION
CENTER
  DON HANCOCK
  ALISON P. MONROE
SPRING CREEK RANCH
  DALTON RED BRANGUS
SRI INTERNATIONAL (PS 285)
  DIGBY MACDONALD
ST & E TECHNICAL SERVICES INC
  STANLEY M. KLAINER
ST. JOSEPH COLLEGE
  CLAIRE MARKHAM
STANFORD UNIVERSITY
  KONRAD B. KRAUSKOPF
  GEORGE A. PARKS
  IRWIN REMSON
STATE UNIVERSITY OF NEW YORK AT
BINGHAMTON
  FRANCIS T. WU
STATE UNIVERSITY OF NEW YORK COLLEGE AT
CORTLAND
  JAMES E. BUGH
STAUFFER CHEMICAL COMPANY
  RANDY L BASS.BASSETT
STEARNS-ROGER SERVICES INC
  VERYL ESCHEN
STONE & WEBSTER ENGINEERING CORP
  ARLENE C. PORT
STUDSVIK ENERGITEKNIK AB - SWEDEN
  AKE HULTGREN
  OVE LANDSTROM
  ROLF SJOBLOM
SWANSON ENVIRONMENTAL INC
  PETER G. COLLINS
SWEDISH GEOLOGICAL
  LIBRARY
  KAJ AHLBOM
  LEIF CARLSSON

SWISS FEDERAL NUCLEAR SAFETY DEPT
  SABYASACHI CHAKRABORTY
SWISS FEDERAL OFFICE OF ENERGY
  U. NIEDERER
SYRACUSE UNIVERSITY
  WALTER MEYER
SYSTEMS SCIENCE AND SOFTWARE
  PETER LAGUS
T.M. GATES INC
  TODD M. GATES
TECHNICAL INFORMATION PROJECT
  DONALD PAY
TECHNICAL RESEARCH CENTRE OF FINLAND
  SILJA RUMMUKAINEN
  KARI SAARI
  SEPPO VUORI
TEKNEKRON RESEARCH INC
  DOUGLAS K. VOGT
TELEDYNE PIPE
  TOBY A. MAPLES
TERRA TEK INC
  KHOSROW BAKHTAR
  DANIEL D. BUSH
TERRAFORM ENGINEERS INC
  FRANCIS S. KENDORSKI
TERRAMETRICS INC
  HOWARD B. DUTRO
TEXAS A & M UNIVERSITY
  JOHN HANDIN
  EARL HOSKINS
  STEVE MURDOCK
  GARY ROBBINS
  JAMES E. RUSSELL
TEXAS BUREAU gF ECONOMIC GEOLOGY
  WILLIAM L. FISHER
TEXAS GOVERNORS OFFICE
  R. DANIEL SMITH
THE ANALYTIC SCIENCES CORP
  JOHN W. BARTLETT
  CHARLES M. KOPLIK
THE BENHAM GROUP
  KEN SENOUR
THE EARTH TECHNOLOGY CORP
  FRED A. DONATH (2)
  JOSEPH G. GIBSON
  DAN MELCHIOR
  JAMES R. MILLER
  FIA VITAR
  MATI WERNER
  KENNETH L. WILSON
THE NORWEGIAN GEOTECHNICAL INSTITUTE
  NICK BARTON
THOMSEN ASSOCIATES
  C. T. GAYNOR, II
TIMES-PICAYUNE
  MARK SCHLEIFSTEIN
TIOGA COUNTY PLANNING BOARD
  THOMAS A. COOKINGHAM
TRANSNUCLEAR INC
  BILL R. TEER
TUN ISMAIL ATOMIC RESEARCH CENTRE
  (PUSPATI)
  SAMSURDIN BIN AHAMAD
U.H.D.E. - W. GERMANY
  FRANK STEINBRUNN
U.S. BUREAU OF LAND MANAGEMENT
  LYNN JACKSON
U.S. DEPT OF COMMERCE
  PETER A. RONA
U.S. DEPT OF ENERGY

CHED BRADLEY
R. COOPERSTEIN
LAWRENCE H. HARMON
ROGER MAYES
CARL NEWTON
DAVID SCHWELLER
JAMES TURI
U.S. DEPT OF ENERGY - ALBUQUERQUE
  OPERATIONS OFFICE
  R. LOWERY
  DORNER T. SCHUELER
U.S. DEPT OF ENERGY - CHICAGO
  OPERATIONS OFFICE
  VICKI ALSPAUGH-PROUTY
  NURI BULUT
  DUANE DAY
  GARY C. MARSHALL
  ERIC J. MOTZ
  PUBLIC READING ROOM
  R. SELBY
U.S. DEPT OF ENERGY - CRYSTALLINE
  REPOSITORY PROJECT OFFICE
  SALLY A. MANN
U.S. DEPT OF ENERGY - CRYSTALLINE ROCK
  PROJECT OFFICE
  STEVEN A. SILBERGLEID
U.S. DEPT OF ENERGY - DIVISION OF WASTE
  REPOSITORY DEPLOYMENT
  JEFF SMILEY
U.S. DEPT OF ENERGY - GEOLOGIC
  REPOSITORY DIVISION
  J. W. BENNETT
  C. R. COOLEY (2)
  JIM FIORE
  MARK W. FREI
  RALPH STEIN
U.S. DEPT OF ENERGY - HEADQUARTERS
  PUBLIC READING ROOM
  HENRY F. WALTER
U.S. DEPT OF ENERGY - IDAHO OPERATIONS
  OFFICE
  M. BARAINCA
  JAMES F. LEONARD
  PUBLIC READING ROOM
U.S. DEPT OF ENERGY - NEVADA OPERATIONS
  OFFICE
  PUBLIC READING ROOM
U.S. DEPT OF ENERGY - NUCLEAR WASTE
  POLICY ACT OFFICE
  ROBERT M. ROSSELLI
U.S. DEPT OF ENERGY - OAK RIDGE
  OPERATIONS OFFICE
  PUBLIC READING ROOM
U.S. DEPT OF ENERGY - OFFICE OF BASIC
  ENERGY SCIENCES
  MARK W. WITTELS
U.S. DEPT OF ENERGY - OFFICE OF CIVILIAN
  RADIOACTIVE WASTE MANAGEMENT
  JANIE SHAHEEN
U.S. DEPT OF ENERGY - OFFICE OF DEFENSE
  WASTE AND BYPRODUCTS
  G. K. OERTEL
U.S. DEPT OF ENERGY - OFFICE OF ENERGY
  RESEARCH
  FRANK J. WOBBER
U.S. DEPT OF ENERGY - OFFICE OF PROJECT
  AND FACILITIES MANAGEMENT
  D. L. HARTMAN
U.S. DEPT OF ENERGY - OSTI (317)
U.S. DEPT OF ENERGY - RICHLAND
  OPERATIONS OFFICE
  J. SCHREIBER

U.S. DEPT OF ENERGY - SAN FRANCISCO
  OPERATIONS OFFICE
  ENERGY RESOURCES CENTER
  LEN LANNI
  PUBLIC READING ROOM
U.S. DEPT OF ENERGY - SAVANNAH RIVER
  OPERATIONS OFFICE
  T. B. HINDMAN
U.S. DEPT OF ENERGY - WEST VALLEY PROJECT
  OFFICE
  W. H. HANNUM
U.S. DEPT OF LABOR
  ALEX G. SCIULLI
  KELVIN K. WU
U.S. DEPT OF THE INTERIOR
  PAUL A. HSIEH
U.S. ENVIRONMENTAL PROTECTION AGENCY
  DIVISION OF CRITERIA & STANDARDS
  DONALD HUNTER
  JAMES NEIHEISEL
U.S. ENVIRONMENTAL PROTECTION AGENCY
  - REGION II
  JOYCE FELDMAN
U.S. GENERAL ACCOUNTING OFFICE
  WILLIAM DAVID BROOKS
  CHARLES D. MOSHER
U.S. GEOLOGICAL SURVEY
  VIRGINIA M. GLANZMAN
  GERHARD W. LEO
  JACOB RUBIN
U.S. GEOLOGICAL SURVEY - COLUMBUS
  A. M. LA SALA, JR.
U.S. GEOLOGICAL SURVEY - DENVER
  JESS M. CLEVELAND
  W. SCOTT KEYS
  RAYMOND D. WATTS
  ROBERT A. ZIELINSKI
U.S. GEOLOGICAL SURVEY - JACKSON
  GARALD G. PARKER, JR.
U.S. GEOLOGICAL SURVEY - MENLO PARK
  JOHN BREDEHOEFT
  J. BYERLEE
  MICHAEL CLYNNE
U.S. GEOLOGICAL SURVEY - RESTON
  I-MING CHOU
  NEIL PLUMMER
  JOHN ROBERTSON
  EDWIN ROEDDER
  EUGENE H. ROSEBOOM, JR.
  DAVID B. STEWART
  NEWELL J. TRASK, JR.
U.S. HOUSE OF REPRESENTATIVES
  LES ASPIN
  B. JEANINE HULL
U.S. HOUSE SUBCOMMITTEE ON ENERGY AND
  THE ENVIRONMENT
  MORRIS K. UDALL
U.S. NATIONAL PARK SERVICE
  THOMAS C. WYLIE
U.S. NUCLEAR REGULATORY COMMISSION
  J. CALVIN BELOTE
  LEON BERATAN
  GEORGE BIRCHARD
  R. BOYLE
  FAITH N. BRENNEMAN
  KIEN C. CHANG
  EILEEN CHEN
  PATRICIA A. COMELLA
  ENRICO F. CONTI
  F. ROBERT COOK

SWISS FEDERAL NUCLEAR SAFETY DEPT
  SABYASACHI CHAKRABORTY
SWISS FEDERAL OFFICE OF ENERGY
  U. NIEDERER
SYRACUSE UNIVERSITY
  WALTER MEYER
SYSTEMS SCIENCE AND SOFTWARE
  PETER LAGUS
T.M. GATES INC
  TODD M. GATES
TECHNICAL INFORMATION PROJECT
  DONALD PAY
TECHNICAL RESEARCH CENTRE OF FINLAND
  SILJA RUMMUKAINEN
  KARI SAARI
  SEPPO VUORI
TEKNEKRON RESEARCH INC
  DOUGLAS K. VOGT
TELEDYNE PIPE
  TOBY A. MAPLES
TERRA TEK INC
  KHOSROW BAKHTAR
  DANIEL D. BUSH
TERRAFORM ENGINEERS INC
  FRANCIS S. KENDORSKI
TERRAMETRICS INC
  HOWARD B. DUTRO
TEXAS A & M UNIVERSITY
  JOHN HANDIN
  EARL HOSKINS
  STEVE MURDOCK
  GARY ROBBINS
  JAMES E. RUSSELL
TEXAS BUREAU gF ECONOMIC GEOLOGY
  WILLIAM L. FISHER
TEXAS GOVERNORS OFFICE
  R. DANIEL SMITH
THE ANALYTIC SCIENCES CORP
  JOHN W. BARTLETT
  CHARLES M. KOPLIK
THE BENHAM GROUP
  KEN SENOUR
THE EARTH TECHNOLOGY CORP
  FRED A. DONATH (2)
  JOSEPH G. GIBSON
  DAN MELCHIOR
  JAMES R. MILLER
  FIA VITAR
  MATT WERNER
  KENNETH I. WILSON
THE NORWEGIAN GEOTECHNICAL INSTITUTE
  NICK BARTON
THOMSEN ASSOCIATES
  C. T. GAYNOR, II
TIMES-PICAYUNE
  MARK SCHLEIFSTEIN
TIOGA COUNTY PLANNING BOARD
  THOMAS A. COOKINGHAM
TRANSNUCLEAR INC
  BILL R. TEER
TUN ISMAIL ATOMIC RESEARCH CENTRE
  (PUSPATI)
  SAMSURDIN BIN AHAMAD
U.H.D.E. - W. GERMANY
  FRANK STEINBRUNN
U.S. BUREAU OF LAND MANAGEMENT
  LYNN JACKSON
U.S. DEPT OF COMMERCE
  PETER A. RONA
U.S. DEPT OF ENERGY

CHED BRADLEY
R. COOPERSTEIN
LAWRENCE H. HARMON
ROGER MAYES
CARL NEWTON
DAVID SCHWELLER
JAMES TURI
U.S. DEPT OF ENERGY - ALBUQUERQUE
  OPERATIONS OFFICE
  R. LOWERY
  DORNER T. SCHUELER
U.S. DEPT OF ENERGY - CHICAGO
  OPERATIONS OFFICE
  VICKI ALSPAUGH-PROUTY
  NURI BULUT
  DUANE DAY
  GARY C. MARSHALL
  ERIC J. MOTZ
  PUBLIC READING ROOM
  R. SELBY
U.S. DEPT OF ENERGY - CRYSTALLINE
  REPOSITORY PROJECT OFFICE
  SALLY A. MANN
U.S. DEPT OF ENERGY - CRYSTALLINE ROCK
  PROJECT OFFICE
  STEVEN A. SILBERGLEID
U.S. DEPT OF ENERGY - DIVISION OF WASTE
  REPOSITORY DEPLOYMENT
  JEFF SMILEY
U.S. DEPT OF ENERGY - GEOLOGIC
  REPOSITORY DIVISION
  J. W. BENNETT
  C. R. COOLEY (2)
  JIM FIORE
  MARK W. FREI
  RALPH STEIN
U.S. DEPT OF ENERGY - HEADQUARTERS
  PUBLIC READING ROOM
  HENRY F. WALTER
U.S. DEPT OF ENERGY - IDAHO OPERATIONS
  OFFICE
  M. BARAINCA
  JAMES F. LEONARD
  PUBLIC READING ROOM
U.S. DEPT OF ENERGY - NEVADA OPERATIONS
  OFFICE
  PUBLIC READING ROOM
U.S. DEPT OF ENERGY - NUCLEAR WASTE
  POLICY ACT OFFICE
  ROBERT M. ROSSELLI
U.S. DEPT OF ENERGY - OAK RIDGE
  OPERATIONS OFFICE
  PUBLIC READING ROOM
U.S. DEPT OF ENERGY - OFFICE OF BASIC
  ENERGY SCIENCES
  MARK W. WITTELS
U.S. DEPT OF ENERGY - OFFICE OF CIVILIAN
  RADIOACTIVE WASTE MANAGEMENT
  JANIE SHAHEEN
U.S. DEPT OF ENERGY - OFFICE OF DEFENSE
  WASTE AND BYPRODUCTS
  G. K. OERTEL
U.S. DEPT OF ENERGY - OFFICE OF ENERGY
  RESEARCH
  FRANK J. WOBBER
U.S. DEPT OF ENERGY - OFFICE OF PROJECT
  AND FACILITIES MANAGEMENT
  D. L. HARTMAN
U.S. DEPT OF ENERGY - OSTI (317)
U.S. DEPT OF ENERGY - RICHLAND
  OPERATIONS OFFICE
  J. SCHREIBER

U.S. DEPT OF ENERGY - SAN FRANCISCO
  OPERATIONS OFFICE
  ENERGY RESOURCES CENTER
  LEN LANNI
  PUBLIC READING ROOM
U.S. DEPT OF ENERGY - SAVANNAH RIVER
  OPERATIONS OFFICE
  T. B. HINDMAN
U.S. DEPT OF ENERGY - WEST VALLEY PROJECT
  OFFICE
  W. H. HANNUM
U.S. DEPT OF LABOR
  ALEX G. SCIULLI
  KELVIN K. WU
U.S. DEPT OF THE INTERIOR
  PAUL A. HSIEH
U.S. ENVIRONMENTAL PROTECTION AGENCY
  DIVISION OF CRITERIA & STANDARDS
  DONALD HUNTER
  JAMES NEIHEISEL
U.S. ENVIRONMENTAL PROTECTION AGENCY
  - REGION II
  JOYCE FELDMAN
U.S. GENERAL ACCOUNTING OFFICE
  WILLIAM DAVID BROOKS
  CHARLES D. MOSHER
U.S. GEOLOGICAL SURVEY
  VIRGINIA M. GLANZMAN
  GERHARD W. LEO
  JACOB RUBIN
U.S. GEOLOGICAL SURVEY - COLUMBUS
  A. M. LA SALA, JR.
U.S. GEOLOGICAL SURVEY - DENVER
  JESS M. CLEVELAND
  W. SCOTT KEYS
  RAYMOND D. WATTS
  ROBERT A. ZIELINSKI
U.S. GEOLOGICAL SURVEY - JACKSON
  GARALD G. PARKER, JR.
U.S. GEOLOGICAL SURVEY - MENLO PARK
  JOHN BREDEHOEFT
  J. BYERLEE
  MICHAEL CLYNNE
U.S. GEOLOGICAL SURVEY - RESTON
  I-MING CHOU
  NEIL PLUMMER
  JOHN ROBERTSON
  EDWIN ROEDDER
  EUGENE H. ROSEBOOM, JR.
  DAVID B. STEWART
  NEWELL J. TRASK, JR.
U.S. HOUSE OF REPRESENTATIVES
  LES ASPIN
  B. JEANINE HULL
U.S. HOUSE SUBCOMMITTEE ON ENERGY AND
  THE ENVIRONMENT
  MORRIS K. UDALL
U.S. NATIONAL PARK SERVICE
  THOMAS C. WYLIE
U.S. NUCLEAR REGULATORY COMMISSION
  J. CALVIN BELOTE
  LEON BERATAN
  GEORGE BIRCHARD
  R. BOYLE
  FAITH N. BRENNEMAN
  KIEN C. CHANG
  EILEEN CHEN
  PATRICIA A. COMELLA
  ENRICO F. CONTI
  F. ROBERT COOK

PAUL F. GOLDBERG
CLYDE JUPITER
PHILIP S. JUSTUS
KYO KIM
WILLIAM D. LILLEY
MARK J. LOGSDON
DONNA R. MATTSON
JOHN C. MCKINLEY
THOMAS J. NICHOLSON
EDWARD OCONNELL
JAY E. RHODERICK
R. JOHN STARMER
NANCY STILL
MICHAEL WEBER
KRISTIN B. WESTBROOK
EVERETT A. WICK
ROBERT J. WRIGHT
UNION CARBIDE CORP
DENNIS J. FENNELLY
JOHN D. SHERMAN
UNION OF CONCERNED SCIENTISTS
MICHAEL FADEN
GORDON THOMPSON
**UNITED KINGDOM DEPT OF THE
ENVIRONMENT**
F. S. FEATES
UNITED NORTHERN SPORTSMEN
JANINE HELMER
UNIVERSITY OF AKRON
LORETTA J. COLE
UNIVERSITY OF ALBERTA - CANADA
F. W. SCHWARTZ
UNIVERSITY OF ARIZONA
JAAK DAEMEN
STANLEY N. DAVIS
I. W. FARMER
AMITAVA GHOSH
JAMES G. MCCRAY
SHLOMO P. NEUMAN
ROY G. POST
**UNIVERSITY OF BRITISH COLUMBIA -
CANADA**
CRAIG FORSTER
R. ALLAN FREEZE
UNIVERSITY OF CALIFORNIA AT BERKELEY
NEVILLE G. W. COOK
RICHARD E. GOODMAN
TODD LAPORTE
THOMAS H. PIGFORD
UNIVERSITY OF CALIFORNIA AT LOS ANGELES
D. OKRENT
KRIS PRESTON
UNIVERSITY OF CALIFORNIA AT RIVERSIDE
LEWIS COHEN
UNIVERSITY OF CINCINNATI
ATTILA KILINC
UNIVERSITY OF DELAWARE
FRANK A. KULACKI
UNIVERSITY OF FLORIDA
DAVID E. CLARK
DOLORES C. JENKINS
M. J. OHANIAN
UNIVERSITY OF HAWAII AT MANOA
DAVID EPP
**UNIVERSITY OF ILLINOIS AT URBANA -
CHAMPAIGN**
DANIEL F. HANG
ALBERT J. MACHIELS
MAGDI RAGHE

UNIVERSITY OF LOWELL
JAMES R. SHEFF
UNIVERSITY OF LULEA - SWEDEN
SVEN KNUTSSON
OVE STEPHANSSON
UNIVERSITY OF MARYLAND
AMERICAN NUCLEAR SOCIETY
MARVIN ROUSH
UNIVERSITY OF MICHIGAN
WILLIAM KERR
RICHARD C. PORTER
UNIVERSITY OF MINNESOTA
CHARLES FAIRHURST
DONALD GILLIS
RAYMOND STERLING
J. K. TYLKO
UNIVERSITY OF MISSOURI AT COLUMBIA
W. D. KELLER
UNIVERSITY OF MISSOURI AT KANSAS CITY
EDWIN D. GOEBEL
SYED E. HASAN
UNIVERSITY OF MISSOURI AT ROLLA
ALLEN W. HATHEWAY
ARVIND KUMAR
NICK TSOULFANIDIS
UNIVERSITY OF NEVADA AT RENO
BECKY WEIMER-MCMILLION
UNIVERSITY OF NEW MEXICO
HAROLD M. ANDERSON
DOUGLAS G. BROOKINS
RODNEY C. EWING
UNIVERSITY OF OKLAHOMA
DANIEL T. BOATRIGHT
UNIVERSITY OF OTTAWA - CANADA
TUNCER OREN
UNIVERSITY OF PITTSBURGH
B. L. COHEN
UNIVERSITY OF RHODE ISLAND
EDWARD P. LAINE
UNIVERSITY OF SOUTHERN MISSISSIPPI
JAMES W. PINSON
DANIEL A. SUNDEEN
GARY C. WILDMAN
UNIVERSITY OF SOUTHWESTERN LOUISIANA
RICHARD U. BIRDSEYE
**UNIVERSITY OF TENNESSEE AT
CHATTANOOGA**
HABTE G. CHURNET
UNIVERSITY OF TEXAS AT AUSTIN
BUREAU OF ECONOMIC GEOLOGY
EARNEST F. GLOYNA
JOE O. LEDBETTER
UNIVERSITY OF TEXAS AT SAN ANTONIO
DONALD R. LEWIS
UNIVERSITY OF TOKYO - JAPAN
RYOHEI KIYOSE
UNIVERSITY OF TOLEDO
DON STIERMAN
UNIVERSITY OF TORONTO - CANADA
R. M. STESKY
UNIVERSITY OF UTAH
MARRIOTT LIBRARY
UNIVERSITY OF UTAH RESEARCH INSTITUTE
LIBRARY
DUNCAN FOLEY
UNIVERSITY OF WASHINGTON
CHRISTOPHER J. EARLE
KAI N. LEE
M. A. ROBKIN

UNIVERSITY OF WATERLOO - CANADA
PETER FRITZ
F. SYKES
UNIVERSITY OF WISCONSIN
RICHARD BARROWS
B. C. HAIMSON
PHILIP A. HELMKE
UNIVERSITY OF WISCONSIN AT MILWAUKEE
HOWARD PINCUS
UNIVERSITY OF WISCONSIN CENTER
LIBRARY - DOCUMENTS
**UPPER PENINSULA ENVIRONMENTAL
COALITION**
DAVE BACH
URS-BERGER
TONY MORGAN
**URS/JOHN A. BLUME & ASSOCIATES,
ENGINEERS**
ANDREW B. CUNNINGHAM
USAID/CAIRO EQYPT
DAVID SNOW
**UTAH DIVISION OF ENVIRONMENTAL
HEALTH**
MARV H. MAXELL
UTAH DIVISION OF OIL, GAS & MINING
SALLY J. KEFER
UTAH ENERGY OFFICE
ROD MILLAR
UTAH GEOLOGICAL AND MINERAL SURVEY
BILL LUND
MAGE YONETANI
UTAH MULTIPLE USE ADVISORY COUNCIL
DIXIE BARKER BARKSDALE
**UTAH SOUTHEASTERN DISTRICT HEALTH
DEPARTMENT**
ROBERT L. FURLOW
UTAH STATE GEOLOGIC TASK FORCE
DAVID D. TILLSON
UTAH STATE UNIVERSITY
DEPT OF GEOLOGY 07
UTILITY DATA INSTITUTE
FRED YOST
VANDERBILT UNIVERSITY
FRANK L. PARKER
VEPCO
B. H. WAKEMAN
VERMONT DEPT OF HEALTH
RAY MCCANDLESS
**VERMONT DEPT OF WATER RESOURCES AND
ENVIRONMENTAL ENGINEERING**
CHARLES A. RATTE
VERMONT STATE NUCLEAR ADVISORY PANEL
VIRGINIA CALLAN
VERMONT STATE SENATE
JOHN HOWLAND
JOHN HOWLAND
VIRGINIA DEPT OF HEALTH
WILLIAM F. GILLEY
ROBERT G. WICKLINE
VIRGINIA DIVISION OF MINERAL RESOURCES
ROBERT C. MILICI
VIRGINIA HOUSE OF DELEGATES
A. VICTOR THOMAS
VIRGINIA MILITARY INSTITUTE
HENRY D. SCHREIBER
**VIRGINIA POLYTECHNICAL INSTITUTE AND
STATE UNIVERSITY**
GARY L. DOWNEY
VIRGINIA SOLID WASTE COMMISSION
BARBARA M. WRENN
**WASHINGTON DEPT OF SOCIAL AND HEALTH
SERVICES**
T. STRONG

WASHINGTON HOUSE OF REPRESENTATIVES
  RAY ISAACSON
WASHINGTON STATE DEPT OF ECOLOGY
  DAVID W. STEVENS
WASHINGTON STATE UNIVERSITY
  NACHHATTER S. BRAR
WATER AND AIR RESOURCE COMMITTEE
  ROBERT MCALISTER
WEST CENTRAL WISCONSIN REGIONAL
  PLANNING COMMISSION
  DAVID G. LENNANDER
WEST DADE REGIONAL LIBRARY
  LOURDES BLANCO LOPEZ
WEST MICHIGAN ENVIRONMENTAL ACTION
  COUNCIL
  FRANK RUSWICK, JR.
WEST VALLEY NUCLEAR SERVICES COMPANY
  INC
  CHRIS CHAPMAN
  ERICH J. MAYER
WESTERN MICHIGAN UNIVERSITY
  ROBERT KAUFMAN
  W. THOMAS STRAW
WESTERN STATE COLLEGE
  FRED R. PECK

WESTERN UPPER PENINSULA CHAPTER
  PERCY R. SMITH
WESTINGHOUSE ELECTRIC CORP
  GEORGE V. B. HALL
  JAMES H. SALING
  JAMES R. SCHORNHOUST
WILDLIFE UNLIMITED INC
  ROBERT L. BAKER
WILLIAM BEAUMONT HOSPITAL
  NORMAN H. HORWITZ
WISCONSIN DEPT OF NATURAL RESOURCES
  DUWAYNE F. GEBKEN
WISCONSIN DIVISION OF STATE ENERGY
  ROBERT HALSTEAD
WISCONSIN GEOLOGICAL AND NATURAL
  HISTORY SURVEY
  MICHAEL G. MUDREY, JR.
  MEREDITH E. OSTROM
WISCONSIN PUBLIC SERVICE CORP
  PAUL WOZNIAK
WISCONSIN RADIOACTIVE WASTE REVIEW
  BOARD
  JIM KLEINHANS
  JAME SCHAEFER

WISCONSIN STATE ASSEMBLY
  TOMMY THOMPSON
WISCONSIN STATE SENATE
  JOSEPH STROHL
WONALANCET OUTDOOR CLUB
  W. S. RANDALL
WOODS ROBERTSON ASSOCIATES - CANADA
WOODWARD-CLYDE CONSULTANTS
  F. R. CONWELL (2)
  ASHOK PATWARDHAN
  WESTERN REGION LIBRARY
WP-SYSTEM AB - SWEDEN
  IVAR SAGEFORS
WRIGHT STATE UNIVERSITY
  MICHAEL FARRELL
WYOMING GEOLOGICAL SURVEY
  JAMES C. CASE
YALE UNIVERSITY
  G. R. HOLEMAN
  BRIAN SKINNER